Development of a 3D *in vitro* model to study lung pathophysiology

Inaugural-Dissertation
to obtain the academic degree
Doctor rerum naturalium (Dr. rer. nat.)

submitted to the Department of Biology, Chemistry, Pharmacy
of Freie Universität Berlin

by

ANNE KIRSTIN EICHHORST

2021

The data and findings of this work were obtained from April 2017 till April 2020 at the Institute of Pharmacy, Department of Pharmacology and Toxicology, at the Freie Universität Berlin under the supervision of **Prof. Dr. Sarah Hedtrich.**

1. Reviewer: **Prof. Dr. Sarah Hedtrich**
   Current address: University of British Columbia
   Faculty of Pharmaceutical Sciences
   2405 Wesbrook Mall
   Vancouver, BC V6T 1Z3, Canada

2. Reviewer: **Prof. Dr. Burkhard Kleuser**
   Freie Universität Berlin
   Institut für Pharmazie
   Königin-Luise-Straße 2+4
   14195 Berlin, Deutschland

Date of disputation: 17.11.2021

Nothing in life is to be feared, it is only to be understood.
Now is the time to understand more, so that we may fear less.

Marie Curie

Part of this thesis has already been published:

Charbaji, R., M. Kar, L. E. Theune, J. Bergueiro, **A. Eichhorst**, L. Navarro, P. Graff, F. Stumpff, M. Calderón and S. Hedtrich (2021). "Design and Testing of Efficient Mucus-Penetrating Nanogels-Pitfalls of Preclinical Testing and Lessons Learned, small, *John Wiley & Sons, Ltd,* DOI: 10.1002/smll.202007963

All figures and text passages based on this publication were marked with the specific source. Experimental work and other contributions of co-authors were also clearly indicated.

Summary

The comparison between the animal and human body in preclinical research is still hampered. Despite of data and acquired knowledge of several studies, differences of physiological behaviour were inclined towards using animal models remain as the standard in preclinical studies, the need of alternative test models is still in demand. Especially because human airway differs a lot to rodent's airway.

My work is based on the development of human 3D bronchial epithelium models to provide a test matrix for further studies as infection or use of new therapeutical treatments. My work presented a 3D bronchial tissue based on primary human epithelial cells and embedded primary human lung fibroblast in a collagen matrix. It formed a 3D compartment and contained all characteristics of a bronchial epithelium and presented a great comparison to naïve lung tissue, based on proof of histology by detecting ciliated cells, goblet cells with high mucus production, basal cell monolayer and even measured cilia movement. Nevertheless, the model with a self-assembled extracellular matrix and vascularized system provides an even more complex setting, first trails were recognized. The 3D model offered a great basic setup and enables more complex improvements, as well as implementing immune cells for future projects.

The work exhibited ability to infect the *in vitro* model with Influenza A virus and showed innate immune responses of host cells. Virus inhibiting effects of the neuraminidase inhibitor Zanamivir were measured at gene and protein level. Even new therapeutical options were tested as Qß-capsid.

In vivo like properties challenged drug delivery and provided a realistic setting. In the study I tested novel delivery systems as degradable nanogels. I showed successful delivery of charged and non-charged nanogels with etanercept. The hypothesize worked, that disulphide-containing biodegradable nanogels were able to penetrate mucus glycoproteins, to approach epithelial cells by passing through thick mucus layers. Other particles charged with Curcumin were tested. Also, lipid nanoparticles to transfect epithelial cells, to direct to new fields of genetical therapies. The study presented Cystic Fibrosis (CF) model based on CF patient's bronchial epithelial cells. New approaches of genetical therapy can be tested on CF model.

The *in vitro* bronchial epithelium model enables to study infections, smart delivery systems and novel therapies in *in vivo* like environment.

Zusammenfassung

Die Übertragung von gesammelten Daten aus präklinischen Studien, die am Tier stattfanden, auf den menschlichen Organismus ist stark erschwert. Obwohl zahlreiche Ergebnisse und erworbenes Wissen von verschiedenen Studien vorhanden sind, die Unterschiede im physiologischen Verhalten beschreiben. Obgleich das Tiermodel als Standard in präklinischen Studien verbleibt, sind an dieser Stelle dennoch alternative Testmodelle gefragt. Da besonders der humane Respirationstrakt sich sehr zu dem eines Nagetiers stark unterscheidet.

Meine Arbeit beruht auf der Entwicklung eines human basierten 3D Bronchialepithelium Models, welches eine Testmatrix für weitere Studien, wie für Infektionsversuche oder neue therapeutische Anwendungen, bietet. Dieses 3D Bronchialepithel Model basiert auf primären humanen bronchial Epithelzellen und primären Lungenfibroblasten, die in einer Kollagenmatrix eingebettet sind. Ein 3D Kompartiment wurde gebildet. Dieses beinhaltet alle charakteristischen Eigenschaften vom bronchialen Epithelium und stellt einen großartigen Vergleich zu nativem Lungengewebe dar. Dies wird durch den histologischen Nachweis von Kinozilien-tragenden Zellen, Becherzellen mit einer starken Mukusproduktion und einschichtigen Basalzellen ermöglicht. Einen noch komplexeren Aufbau stellt ein Model mit einer selbst organisierten extrazellulären Matrix und einem vaskularisierten System dar. Hierzu wurden die ersten Versuche bereits durchgeführt. 3D Modelle bieten einen grundlegenden Aufbau und ermöglichen, wie zum Beispiel durch das Implementieren von Immunzellen, noch mehr Komplexität.

Die Arbeit zeigt die Möglichkeit, das *in vitro* Model mit dem Modellvirus Influenza A zu infizieren und ebenso die Immunantwort der Wirtszelle zu aktivieren. Virus inhibitorische Effekte des Neuraminidase Hemmers Zanamivir konnten auf Gen- und Proteinebene nachgewiesen werden. Zusätzlich wurden auch neue Therapiemöglichkeiten wie die Anwendung des Qß-Kapsids getestet.

In vivo Bedingungen sind herausfordernd für die Medikamentenverabreichung, die Bedingungen sind darstellbar in dem *in vitro* Model. In der Studie wurden neue Wirkstoffapplikationssysteme wie abbaubare Nanogele getestet. Es wird eine erfolgreiche Verabreichung von beladenen und unbeladenen Nanogelen mit Etanercept gezeigt. Die Hypothese, dass Disulfid haltige bioabbaubare Nanogele Mucuglycoproteine penetrieren können, wurde bestätigt. Die Nanogele waren fähig die Mukusschicht zu passieren und die Epithelzellen zu erreichen. Ähnliches wurde bei Curcumin beladene Partikel beobachtet, die ebenso die Epithelzellen erreichten.

Um sich neuen Bereichen wie der Gentherapie zu zuwenden, wurden zur Transfektion von Epithelzellen Lipidnanopartikel verwendet. Neue Herangehensweisen der Gentherapie können im in vitro Model getestet werden, wie an dem neuartigen *in vitro* Model der monogenetischen Erkrankung Zystische Fibrose, das in der Studie präsentiert wird. Es basiert auf Bronchialepithelzellen von Patienten.

Das *in vitro* bronchial Epithelium Model ermöglicht Testungen von Infektionen, moderner Medikament Transportsysteme und neuartige Therapien in einem *in vivo* ähnlichem Umfeld.

Table of content

List of Abbreviations

2D	two dimensional
3D	three dimensional
Acetyl.	acetylated
ENaC	epithelial sodium channel
CA	Canada
CF	Cystic fibrosis
CFTR	Cystic fibrosis transmembrane conductance regulator
cfu	Colony forming unit
cDNA	Complementary desoxyribonucleic acid
Ct	cycle threshold
DAMP	danger associated molecular pattern
DAPI	4´6-Diamidin-2-phenylindol
DE	Germany
DMSO	Dimethyl sulfoxide
DNA	desoxyribonucleic acid
DNase	Deoxyribonuclease
dNTPs	Deoxyribonucleoside triphosphate
DOPC	1,2-(cis, cis-9,12-octadecadienoyl)-sn-glycero-3-phosphocholine
DOPE	1,2-dioleoyl-sn-glycero-3-phosphoethanolamine
DSPC	1,2-distearoyl-sn-glycero-3-phosphocholine
DSPG	di-stearoyl-phosphatidylglycerol
EDTA	Ethylenediaminetetraacetic acid
ELISA	enzyme-linked immunosorbent assay
et al.	And others
ES	Egg sphingomyelin
F	France
FCS	fetal calf serum

GM-CSF	granulocyte macrophage-colony stimulating factor
HA	Hemagglutinin
HBSS	Hanks buffered saline solution
HRP	horse reddish peroxidase
IAV	Influenza A Virus
IFN	Interferon
IFNAR	Interferon-α/β Rezeptor
Ig	Immunoglobulin
IL	Interleukin
IV	Influenza virus
JPN	Japan
LDH	Lactate dehydrogenase
LNPs	lipid-based nanoparticles
LPS	Lipopolysaccharide
MDCK	Madin-Darby Canine Kidney
MEM	Minimal essential medium
MOI	multiplicity of infection
mRNA	Messenger ribonucleic acid
MyD88	myeloid differentiation primary response protein 88
NA	Neuraminidase
NFκB	nuclear factor κ B
NL	Netherlands
p. i.	post infection
PAMP	pathogen-associated molecular pattern
A/Panama/1999/2007	Influenza A virus/country of origin Panama/ molecule number 1999/occurred in 2007
PBS	phosphate buffered saline
PCR	polymerase chain reaction
PFA	Paraformaldehyde

pfu	Plaque forming unit
p^x	passage
qRT-PCR	quantitative real time PCR
RNA	ribonucleic acid
rpm	rounds per minute
RT	Room temperature
RT	Reverse transcription
SEM	standard error of the mean
Taq Polymerase	Thermostable DNA polymerase I
TLR	Toll-like-Receptor
TNFα	Tumor necrosis factor α
TMB	3,3',5,5-tetramethylbenzidine
TPCK	(Toluene sulfonyl)-L-phenylalanyl Chloromethyl Ketone
UK	United Kingdom
USA	United States of America
WHO	World Health Organization

List of figures

List of tables

List of contributions

Publication and contribution

Original articles

Charbaji, R., M. Kar, L. E. Theune, J. Bergueiro, **A. Eichhorst**, L. Navarro, P. Graff, F. Stumpff, M. Calderón and S. Hedtrich (2021). "Design and Testing of Efficient Mucus-Penetrating Nanogels-Pitfalls of Preclinical Testing and Lessons Learned. small, *John Wiley & Sons, Ltd,* DOI: 10.1002/smll.202007963

Conferences

A Eichhorst, M Mieth, S Kaessmeyer, S Hippenstiel, A Hocke, S Hedtrich, *Development and characterization of a human-based bronchial epithelium model for infection studies,* Poster presentation, LIVe LIVe 2018 – Lung In Vitro event for innovative and predictive models, Nice, France, July 2018

A Eichhorst, M Mieth, S Kaessmeyer, S Hippenstiel, A Hocke, S Hedtrich, *Development and characterization of a human-based bronchial epithelium model for infection studies,* Poster presentation, Tag der Pharmazie, Freie Universität Berlin, Germany, July 2018

A Eichhorst, M Mieth, S Kaessmeyer, S Hippenstiel, A Hocke, S Hedtrich, *Development and characterization of a human-based bronchial epithelium model for infection studies,* Poster presentation, CSPS/CC-CRS 2019 CONFERENCE, Vancouver, Canada, May 2019

Stiepnds and Grants

Fellowship Nanoscale, Freie Universität Berlin, Germany, April - December 2017

Fellowship Dr. Hilmer Stiftung, Zur Förderung der Forschung auf pharmazeutischem Gebiet, Frankfurt, Germany, January 2018 - December 2019

Travel Grant by Women's Representative (Frauenförderung des Fachbereichs BCP) of Freie Universität Berlin for LIVe 2018 – Lung In Vitro event for innovative and predictive models, Nice, France, July 2018

International fellowship by Bayer Foundation, Otto Bayer Fellowships in Drug Discovery, Leverkusen, Germany, February - April 2020

1. Introduction

1.1 Physiology and anatomy of the human lung

1.1.1 Upper Airway

The main function of our respiratory organs is gas exchange; to extract oxygen out of the atmosphere by inhaling and providing it to our cells, and to remove the side product (carbon dioxide) from our body. This controls the acid-base balance in the blood vessels and is essential for the human body. Besides breathing, the respiration organs are the first contact area in-between environment and the inside of the body. This special location requires the development of important defending structures and strategies. The entrance forms the nasal and oral cavity, continues to the pharynx, which is build up from the naso- oro- and hypopharynx and ends with the larynx to connect with the trachea, the beginning of the lower airway (**figure 1**) (Ronald Miller 2014). The nose is the external respiratory organ. The nose acts as a filter, preventing particles in the airstream from entering the body (Sahin-Yilmaz and Naclerio 2011). A similar task is performed by the oropharynx during breathing through the mouth, as it shields the deeper areas. In the nasal cavity entrance, nasal hair is present as well, to filter bigger particles (Swift and Kesavanathan 1996). The nasal cavity exhibits a multilayered squamous tissue and the lining of the epithelial cells starts as pseudostratified columnar epithelial tissue and continues down the whole bronchial tree (Scherzad, Hagen et al. 2019). Major functions of the conducting zone are passing air in and out to the respiratory tissue, trapping pathogens and debris, warming and humidify the air and also involved in swallowing and speech (Pierce and Worsnop 1999).

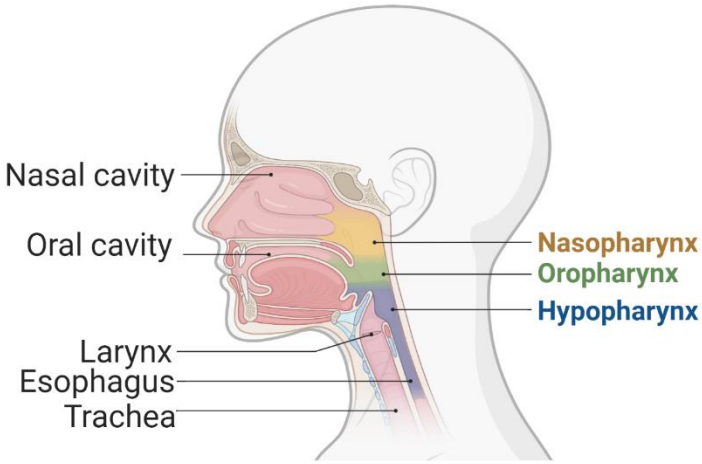

Figure 1. Upper airway of a human. The nasal and oral cavity forms the entrance of the upper airways. The Nasopharynx connects the nasal cavity and the oropharynx, both entry points get connected. Subsequently the hypopharynx follows, to the side the Larynx is located, the source of vocal, it goes down to the trachea and the esophagus. Created with BioRender.com.

1.1.2 Lower Airway

The lung itself is a paired organ and is divided into the right and left lung. The right lung has a bigger volume than the left lung and contains three lobes. The left lung has two lobes and the cardiac notch (Chaudhry R. 2020), It is pyramid shaped organ and locates in the thoracic cavity (French 2009). It is embedded by the intercostal muscles and below by the diaphragm, which are the necessary muscles for the action of in- and exhalation. The *pleura visceralis* covers the lung and the *pleura parietalis* covers the inside of the chest cavity (Charalampidis, Youroukou et al. 2015). In-between the two pleura surfaces is the essential pleural space, it creates a pressure gradient and which protects against collapsing and gives space for expanding of the lung during inhalation. It builds a pleura cavity as a flexible skin which aids the lung for optimal friction during breathing. A fluid covers the pleura surfaces to enable gliding in the thoracic cavity (Charalampidis, Youroukou et al. 2015).

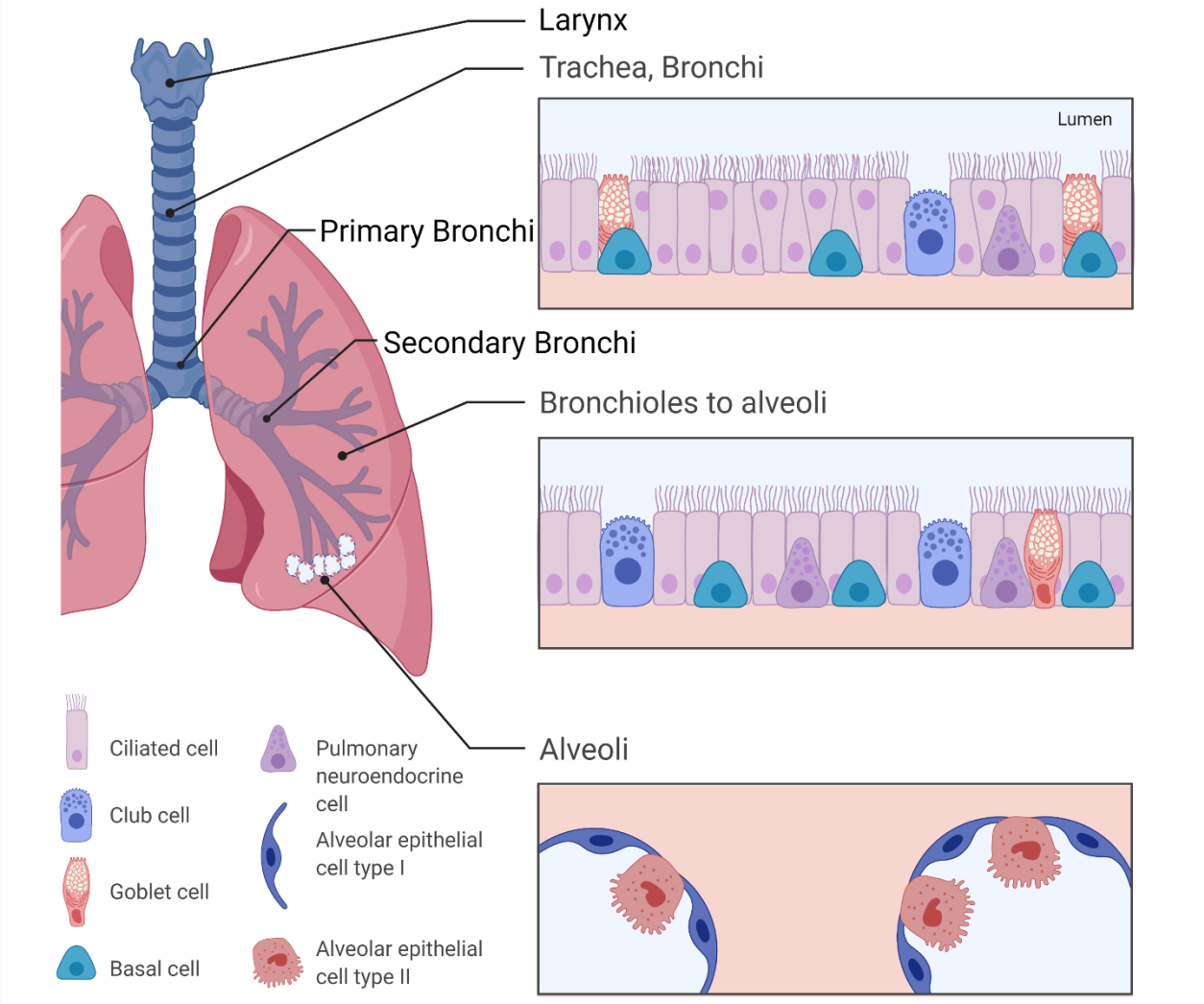

Figure 2. Lower airway of a human. The larynx and the trachea are the connectors to the lower airway in the human body. The traches divide at the primary bronchus, into the left and right part. At the secondary bronchus, the bronchial tree divides again and continues. The final units are bronchioles, which turn into alveoli where the gas exchange takes place. The tissue is lined by predominately ciliated cells, as well as goblet cells and neuroendocrine and club cells. All are connected a monolayer of basal cells. In the bronchioles area, more club cells are contained in the epithelial surface. In the alveolar area there are two cell types; alveolar epithelial cell type I and alveolar epithelial cell type II. Created with BioRender.com.

The beginning of the lower airway tract derives from the upper airway. The entrance is the larynx and is connected to the trachea, which branches into the primary bronchi and is followed by the secondary bronchi (**figure 2**) (BéruBé, Prytherch et al. 2010). It builds the bronchial tree down to the bronchiole. The trachea and primary bronchi are predominately lined with ciliated cells. These cells have 5 µm long cilia on the surface, directed into the luminal side. Besides these cells, goblet cells occur at a ratio of one per six ciliated cells (French 2009). Goblet cells appear in a cup-form, secret mucin, and thereby form a mucosal layer for protection (Dao DPD 2020). These cell types work together to form the muco-ciliary clearance, whereby pathogens or particles can be trapped in the mucus and sent out by the cilia movement. Non-ciliated columnar microvilli cells and immune cells such as resident dendritic cells, natural killer cells, innate lymphoid cells, T-cells are found in the lower airway as well (Condon, Sawyer et al. 2011, Qin, Liu et al. 2012, LeMessurier, Tiwary et al. 2020). Underneath the columnar cells is a monolayer formed of basal cells, these are precursor cells of ciliated and goblet cells (French 2009). Pulmonary neuroendocrine cells occur at less than 1% of cells in the respiratory tissue (Kobayashi and Tata 2018).

In the terminal bronchioles, club cells add to the number of non-ciliated cells (French 2009). Club cells are columnar or cuboidal shaped, and secret surfactant proteins and protective proteins such as SCGB1A1 (uteroglobin), which forms part of the lining fluid. They are progenitor cells of goblet and ciliated cells (Reid, Sutanto et al. 2019). The terminal area contains bronchioalveolar stem cells (BASCs), which can become club cells or alveolar cells. This stem cell property plays an important role in the transition area from terminal bronchioles to alveoli (Kim, Jackson et al. 2005, Hogan, Barkauskas et al. 2014). The alveolar sac builds the terminal ends, which contains alveoli, where the gas exchange takes place and named respiratory tissue. Alveolar tissue contains two types of alveolar epithelial cell type 1 and type 2 (Guillot, Nathan et al. 2013). Alveolar macrophages are present in alveolar tissue as a part of the cellular immune response as phagocytosis and detection of pathogens, activating cells by cytokines and antigen presentation (Hussell and Bell 2014).

The lungs are complex and essential organ of human body. Small disbalance caused by infection or other disease can easily disrupt physiological conditions and impacts human health immense.

1.2 Threats and diseases of the human lung

1.2.1 Influenza A virus

1.2.1.1 Influenza A infections and therapeutic approaches

Influenza is a common and serious viral respiratory infection with limited therapeutic options, which can be fatal (Gao, Yao et al. 2016). The influenza virus has been one of the major causes of lung infections with a high rate of morbidity and mortality (Troeger, Blacker et al. 2019). The need for a successful therapy is in demand yet is faced with difficulties due to the huge genetic variety of the virus and the specificity needed for each target application.

1.2.1.2 The Influenza virus

The Influenza A virus itself belongs to the genera of the family *Orthomyxoviridae.* They all share eight segmented negative-strand viral ribonucleic acids (RNAs) as their genome and a lipid bilayer as an outer envelope (Fauquet 2008). The family includes four different virus types as alpha, beta, gamma, and delta influenza virus, better known as Influenza A, B, C and D respectively. This distinction is based on the various nucleoproteins of the viruses. Type A, B, C affect humans, type D is considered to have the potential to do so. Moreover, type A and B are the most severe types (Zambon 1999, Hause, Ducatez et al. 2013, Peteranderl, Herold et al. 2016).

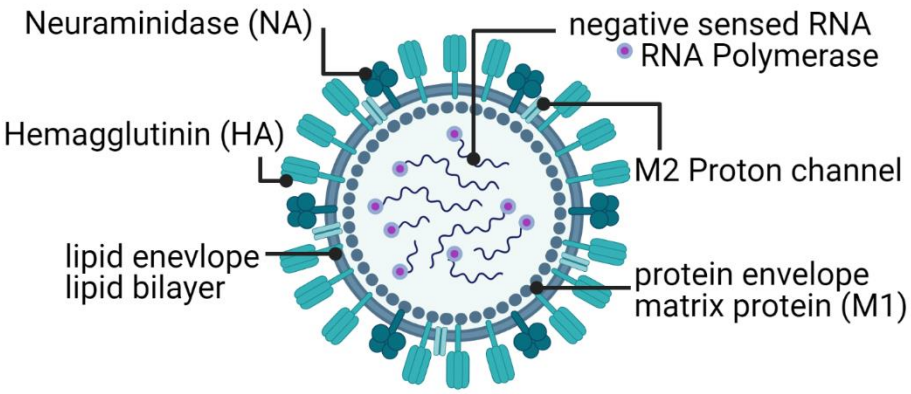

Figure 3. Influenza A virus. Virus enveloped by a lipid bilayer and an interior protein layer. Surface proteins such as Haemagglutinin allow binding to the host cell. The Neuraminidase cleaves the new virus from the host cell. M2 enables the release of the viral RNA into the host cell by passing protons. Inside eight, single stranded RNAs, negative sensed contain in the influenza virus.

The subtype classification of influenza viruses is based on the virus surface proteins, specifically on the composition of hemagglutinin (HA, H) and neuraminidase (NA, N). HA is the receptor that docks on the host epithelial cell sialic acid and enables the virus to enter by membrane fusion. The NA is the enzyme that releases the newly produced virus out of the host cell; it cleaves the connection of the hemagglutinin and the host sialic acid (Cohen, Zhang et al. 2013). Both are main responsible infection targets and HA addresses the B-cell immunity for antibody production. The full nomenclature is based on several pieces of information about the virus; a virus is named by the class, the type, the country of origin, the isolate number and when it first appeared, for instance H3N2 (A/Panama/2007/1999) (Fauquet 2008).

The subdivision into serotypes is based on the antibody response. HA has 18 and NA has 11 subtypes (Tong, Zhu et al. 2013), they change frequently by mutation and recombination, which is why they are a challenge to our immune system (Bouvier and Palese 2008). So far just H 1, 2, 3 and N 1, 2 have caused a relevant infection in the human body, specifically A/H1N1, A/H2N2, A/H3N2 (Peteranderl, Herold et al. 2016). Also, avian-origin influenza virus H5N1, H7N9 infected hundreds of people, but were not as dangerous as the others so far due to the low rate of transmission in humans (Gambotto, Barratt-Boyes et al. 2008, Gao, Cao et al. 2013). In comparison, Influenza B is not divided into subtypes, just two different lines; the Yamagata and Victoria line have been circulating for years (Biere, Bauer et al. 2010) and are both responsible for the seasonal flu.

An important aspect is the subtype of HA, as this determines in which part of the bronchial tract the virus binds, and therefore which species are affected (Couceiro, Paulson et al. 1993, Ibricevic, Pekosz et al. 2006, de Graaf and Fouchier 2014). The virus attaches to sialic acid (SA) and different types of SA 2-3 and SA 2-6 bindings occur in the human body. SA 2-3 is predominantly distributed in the lower airway and SA 2-6 in the upper airway (de Graaf and Fouchier 2014). Avian-origin virus predominantly affects the lower airway, whereas human-origin virus targets the upper airway (Matrosovich, Matrosovich et al. 2004, Matrosovich, Matrosovich et al. 2007). The location of binding plays an important role for the transmission of the virus as well (Saunders-Hastings and Krewski 2016). These aspects are important factors for the severity and danger of the virus, which has led to the hypothesis that if the upper airway is affected, a transmission is more likely to result than when binding occurs in the lower airway (van Riel, den Bakker et al. 2010). Additionally, the weather conditions are an important factor. The epidemic peak in winter is caused by different reasons; the cold and rainy weather conditions cause people stay indoors more, where the transmission from person to person becomes easier (Goldmann 2000).

Furthermore, increased relative humidity, for example during rainy weather, increases the stability of aerosols, which contains virus particle enclosed in droplets (Marr, Tang et al. 2019). Additionally, cold and dry air has a positive effect on the remaining aerosol as well, as shown in an animal trial (Lowen, Mubareka et al. 2007), enhancing airborne transmission. This hypothesis also helps explain the low flotation in tropical countries (Viboud, Alonso et al. 2006, Alonso, Viboud et al. 2007). More arguments are a higher vitality status of the hosts during summer season, which relies on Vitamin D storage, caused by an increased UV radiation (Adams and Hewison 2008, McDevitt, Rudnick et al. 2012). Other hypotheses even include travel, which is more relevant during cold seasons (Grais, Ellis et al. 2004).

1.2.1.3 Historical background of influenza infections

The viral threat by influenza to humanity was scientifically documented for the first time in 1580 (Potter 2001). Even earlier, historical records indicate the occurrence of influenza back to 412 BC by early Greek writings from Hippocrates (Pappas, Kiriaze et al. 2008). During the last century, the world witnessed the most lethal pandemic situation caused by an influenza virus, the Spanish flu (H1N1). The outbreak caused 27 to 100 million deaths around the globe (Morens and Fauci 2007). Earlier presumptions suspected that a bacterium caused the infection outbreak, but clarity came 1932 by the first isolation of the virus itself (Smith, Andrewes et al. 1933, Smith, Andrewes et al. 1935, Bazin 2011). It was followed by more pandemic outbreaks caused by the Influenza Virus, the Asian flu (1957-1958), Hong Kong flu (1968-1969) and 2009 flu pandemic (2009-2010). The date of occurrence and severity of the coming threat is uncertain. Currently the world is still suffering of the seasonal outbreak of the influenza virus.

The seasonal flu, which is mainly at an epidemic level, causes a fatality rate of < 0.1 (Paget, Spreeuwenberg et al. 2019). In comparison to the previously mentioned pandemics, it has a lower fatality rate, but is still harmful for the population and there is a need for effective therapies. Immunization is the most promising strategy. The first investigation into an influenza vaccine started in the mid-1930s. Initially, vaccines were monovalent preparations, i.e. they protected against one strain of the influenza virus (Barberis, Myles et al. 2016). The development of the influenza vaccine improved greatly in the past decades, and today the seasonal vaccine is quadrivalent, providing protection against four different virus strains (Mosnier, Launay et al. 2018). Nevertheless, the greatest difficulty is the fast mutation rate of the influenza virus, which impedes the development of a universal vaccine. During a single replication and translation process of virus RNA in a host cell, reading failures occur. As the virus lacks the proof-reading mechanisms

required to correct these errors (Cheung, Watson et al. 2014), they lead to permanent antigenic shifts of the virus (Westgeest, Russell et al. 2014). Vaccine protection often does not last longer than a few years because of the virus gene variation. However, every year the World Health Organization (WHO) predicts which virus strains are likely to circulate in the following flu season, one year ahead of the seasonal outbreak (Klimov, Garten et al. 2012, Barr, Russell et al. 2014). The pharmaceutical industry needs a year for production to provide millions of vaccines. The WHO recommends two different vaccines combinations per year, because there are two different flu seasons on the globe: in the northern hemisphere from November to March and in the southern hemisphere from May to September. Recently the FDA approved a high-dose quadrivalent vaccine for people over 65 years of age, to induce an increased immune response and thereby provide better protection against the seasonal flu (Grohskopf, Alyanak et al. 2020).

1.2.1.4 Influenza virus reproduction in the host cell

A closer look at the replication process explains the high mutation rate. As already mentioned, hemagglutinin binds to glycoconjugates with sialic ends. The binding triggers endocytosis, where the virus becomes enclosed in an endosome (**figure 5**). The virus activates the M2 channel to let protons pass to the virus inside and lower the pH (Rust, Lakadamyali et al. 2004). This triggers a structural change of hemagglutinin to fuse proteins, that mediates the fusion of the endosome (White, Helenius et al. 1982). Through the pH change, proteins and RNAs become detached, which is part of the uncoating process. It results in the RNAs and associated proteins being released into the cytosol of the host cell (Martin and Helenius 1991). The nucleoproteins cover the RNA strands and recruit the binding of alpha importin (Wang, Palese et al. 1997). The α-importin binds to ß-importin and it directs the RNA to the nucleoplasm through the nuclear pores (Martin and Helenius 1991).

Once inside the nucleus, the RNA replication process can proceed. RNA segments are ‘minus’ (-) RNAs. These are noncoding strands which need to be transcribed into positive strands before being used for protein translation. If the viral RNA is replicated without modification it is referred to as complimentary RNA (‘cRNA’) (Pflug, Lukarska et al. 2017). The viral RNA can also be transcribed into mRNA by viral polymerase. This transcription is started through ‘cap-snatching’, in which the host cell RNA is used as the 5’ cap for mRNA synthesis. The produced RNA receives a poly-A tail and 5’ cap to protect the strand against degradation (Pflug, Lukarska et al. 2017).

The mRNA leaves the nuclei through the cell pores. In the cytosol, host ribosomes translate the RNAs into proteins (Yángüez and Nieto 2011). The proteins are packaged into endosomes at the

Golgi apparatus, creating a new virus which gets released from the host cell to infect more host cells. Because of the absence of RNA proofreading enzymes, the RNA-dependent RNA polymerase that copies the viral genome makes an error roughly every 10 thousand nucleotides, which is the approximate length of the influenza viral RNA (Steinhauer, Domingo et al. 1992). That means the new virus copies are mainly mutants, and this is the cause for antigenic drift. A slow change of the surface proteins is the reason for a changing immune response to the antigen in the human body (Wang, Taaffe et al. 2006). A homologous recombination happens when two viruses infect one host cell during the replication process, but it plays a minor role in the human influenza A evolution and drives the mutation rate (Boni, Zhou et al. 2008). The faulty process of the virus replication leads to a rapid change of the presenting antigens which allows it to overcome appropriated protective immunity.

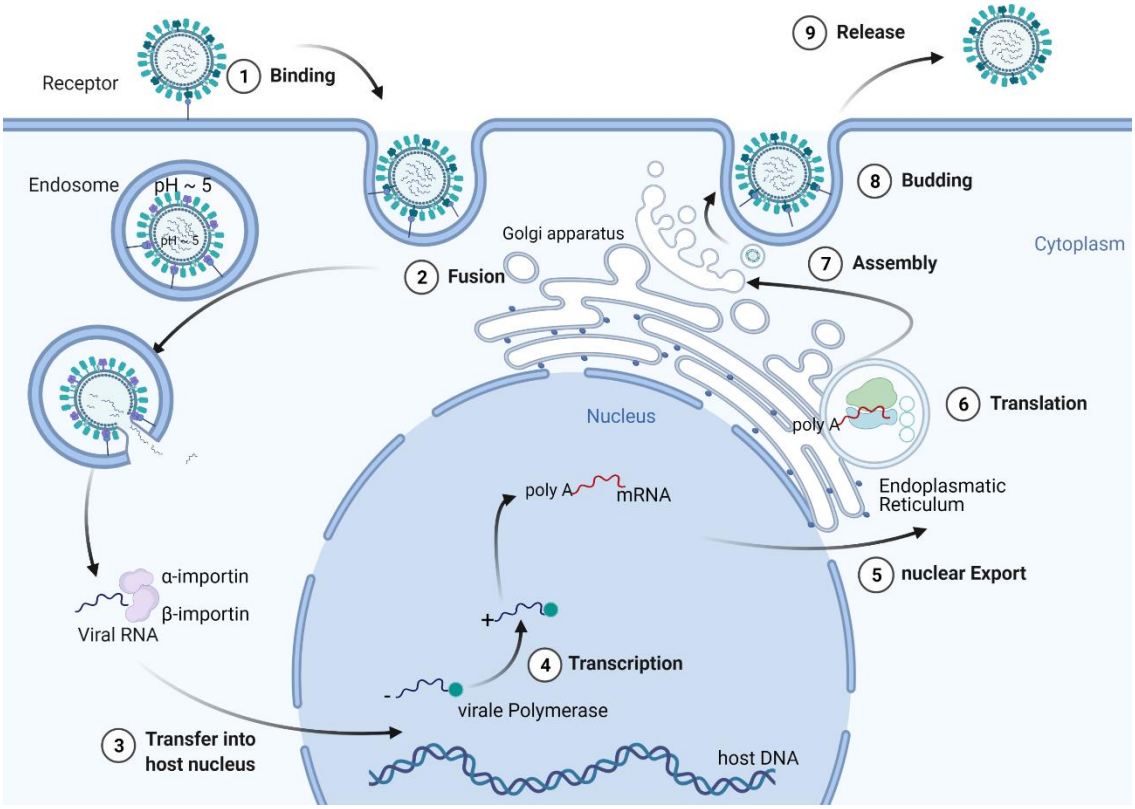

Figure 4. Influenza virus reproduction in a host cell. The virus binds with HA at sialic receptor on host cell surface (1). By endocytosis, a fusion (2) of the virus takes place. Inside the endosome the pH is around 5. When M2 activates, protons pass inside the virus and lower the pH to 5 there too, thereby triggering a confirmation change of haemagglutinin and fusion with the endosome layer, which releases the viral RNA. Viral RNA binds to α-importin, it connects to ß-importin and imports the viral RNA inside the nucleus (3). Transcription to + sensed RNA is the first step by the viral polymerase (4). A poly-A tail is attached to the viral RNA and developed to mRNA. The nuclear export of mRNA occurs through pores in the nucleus (5). Translation is performed by ribosomes in the ER (6) and assembly of the virus happens at the Golgi apparatus, where the virus is packaged into an endosome (7). The new virus endosome buds at the host cell surface (8) and is released by enzymatic cleavage of NA to infect more cells (9).

Mutations enables viruses to infect new species as well, which is referred to as ‘zoonotic overlap’ (Mostafa, Abdelwhab et al. 2018). The seasonal infections or pandemics are mainly caused by the IAV strains H1N1 and H2N3, which circulate in humans. Almost all IAVs occur in the aquatic bird reservoir, for example H5N1, H5N6, H6N1, H7N9 etc., which are also called avian influenza virus. When species cross from birds to mammals/humans, infections and fatality can occur (Parry 2013). This poses the danger of a pandemic and is one reason for the challenging treatment of the seasonal flu.

1.2.1.5 Host immune response to influenza

Typical symptoms of an influenza infection appear abruptly and are characterized by fever, myalgia, malaise, and loss of appetite. Potential symptoms are an unproductive cough, vomiting, diarrhea, runny nose, or sore throat (Monto, Gravenstein et al. 2000). The infection lasts for 5 – 7 days. These physical symptoms are the result of the biochemical actions provoked by the virus infection. Interferons (IFNs) play a central role in this, as they induce primary reactions during a viral attack. IFNs are a subgroup of cytokines and are classified into three types. Type I is IFN-α, β, δ, ε, κ, ω and τ, type II is IFN-γ and type III is IFN-λ, some have additional further subtypes. The type arises from the receptor binding. IFN type I and III are the lead components of a viral defense (Chen, Zhang et al. 2016). The first activated genes are IFN-β-1 and IFN-α, followed by IFN-λ.

However, to start IFN synthesis, the virus needs to be recognized by the host cell. Human cells have the ability to detect non-self-molecules because of pattern recognition receptors (PRRs) on the host cells or even on innate immune cells, such as the retinoic acid-inducible gene-I protein (RIG-I) (Cao 2016). They are able to detect pathogen associated molecular patterns (PAMPS) (Medzhitov and Janeway Jr 1998), e.g. single stranded viral RNA. Some outside and internal parts of the host membrane contain Toll like receptors (TLR). Through TLR activation, signals are transduced to their cytoplasmic Toll like interleukin receptor, causing genetic induction for protein transcription of interferons. TLRs react to specific PAMPS. Relevant for IAV are TLR 3, 7 and 8, located at the inside of endosomes and lysosomes, as these recognize nucleic acid PAMPs (Kawai and Akira 2010).

TLR 3 recognizes unidentified RNAs of phagocytosed infected cells. It transmits the pathway by a Toll-Interleukin receptor domain (Schulz, Diebold et al. 2005), it directs nuclear factor kB (NF-kB), activating protein 1 and regulatory factor 3 and results in inducing IFN-ß (Hiscott, Lin et al. 2006).

Single stranded RNA is sensed by TLR 7 and TLR 8, together with the adapter molecule myeloid differentiation primary response protein 88 (MyD88) (Lund, Alexopoulou et al. 2004). They associate with kinases as the interleukin-1 receptor–associated kinases IRAK1 and IRAK4, and the tumor necrosis factor receptor–associated factor 6 (TRAF6). As a complex, they activate IFN regulatory factor 7 (IRF7), NF-kB and activating protein 1. The translocation of the transcription factors into the nucleus activates the genome transcription of IFN and proinflammatory cytokines (Lund, Alexopoulou et al. 2004).

Released IFNs target the type I or III IFN receptor, IFN I interacts with the IFN-α/ß-receptor and IFN III with IFN-λ-receptor (de Weerd, Samarajiwa et al. 2007, Miknis, Magracheva et al. 2010). For IFN-α/ß-receptor, it contains two subunits IFN-A receptor 1 (IFNAR1) and IFNAR2 (Jaks, Gavutis et al. 2007). IFN-λ-receptor subunits are heterodimeric as well, it contains IFN-λR1 and IL-10R2 (Gad, Dellgren et al. 2009, Miknis, Magracheva et al. 2010). Following the receptor confirmation change, the subunits dimerize, kinase Janus-activated kinase 1 (JAK1) and tyrosine kinase 2 (TYK2) associate with the receptor (Lavoie, Kalie et al. 2011). IFN-λ-receptor associates with JAK1 and JAK2. Through autophosphorylation of the ligands the signal transducers and activators of transcription 1 and 2 (STAT1 and STAT2) dimerize (Rawlings, Rosler et al. 2004). The phosphorylated STAT1-STAT2 bids with IFN regulatory factor 9 (IRF9) complex and form IFN-stimulated gene factor 3 (ISGF3). It translocates to the nucleus and binds to deoxyribonucleic acid (DNA) regulatory sequences, containing IFN-stimulated response elements (Schneider, Chevillotte et al. 2014). The resulting stimulation leads to the transcription of more than hundred IFN-stimulated genes, whose concerted action lead to the generation of an ‘‘antiviral state’’(Randall and Goodbourn 2008). IFN-stimulated genes restrict the viral entrance into host cells, by e. g. cell membrane alteration as cell adhesion and curvatures (Brass, Huang et al. 2009). Additionally, through the IFN-stimulated genes antiviral host factors such as tetherin becomes expressed to suppress the virus export to the surface (Evans, Serra-Moreno et al. 2010). Natural killer cells become activated as well (Lee, Rao et al. 2000, Paolini, Bernardini et al. 2015).

1.2.1.6 Medical treatment of influenza

Though medical options exist for influenza treatment, there is a need for improved efficacy of therapies. Antiviral therapies against influenza are limited to either M2-membraneprotein-/Endonuclease-inhibitors or Neuraminidase targeting therapies. Current medicines do not attack the virus itself to eliminate it; infected cells stay attacked but the infection is halted. This means that the treatment is most effective if started early of even in prophylactic use. A therapy can

shorten the duration of illness to less than 0.5 – 1.5 d of the infection time of 6.6 – 7 d, if used 48h after the first symptoms (Jefferson, Jones et al. 2014)

Medical substance group	Medical substance	Target	Mechanism of action
M2 inhibitor	Amantadine Rimantadine	M2-membran protein	Inhibit M2, protons do not enter, results in no release of viral RNA
Neuraminidase inhibitor	Oseltamivir Zanamivir	Neuraminidase	Block the release of new produced viruses

Table 1. Influenza available medicine treatments

M2-membraneprotein inhibitor therapies

M2-membraneprotein inhibitors (M2 inhibitor) block the ion channels of the virus. Protons of the lysosome cannot enter the virus and therefore the virus envelope stays stable. It is effective against IAV but not against IBV. IBV contain a BM2 channel, which differs structurally to M2 (Mould, Paterson et al. 2003). Common M2 inhibitors are Amantadine and Rimantadine. Usage is associated with strong side effects such as nausea, loss of appetite and effects on the central nervous system (Lehnert, Pletz et al. 2016). The main concern is the high risk of developing resistance and the passing on of resistant virus (Monto 2003). Therefore, M2 inhibitors are not first line treatment.

Neuraminidase targeting therapies

Several drug therapies target the surface enzyme Neuraminidase, as it plays a role in releasing new replicated viruses from the host cell, to infect more cells. NAIs are effective with both IAVs and IBVs. Oseltamivir and Zanamivir are two Neuraminidase inhibitors (NAIs)(von Itzstein, Wu et al. 1993). Oseltamivir is an oral prodrug; the activated drug is Oseltamivir decarboxylate. Zanamivir is an inhaled drug, because of its zwitterion structure. The polar chemical structure hampers the oral bioavailability, reducing it to 2 % in contrast to the inhaled bioavailability of 4 – 17 % (National Center for Biotechnology Information 2020, 12, 21). Nevertheless, Oseltamivir has side effects such as headache, nausea, and vertigo. Therapy with Zanamivir has been known to cause eczema. In a pandemic situation, the intake of NAIs for 16 weeks can be used as a prophylactical treatment (Anekthananon, Pukrittayakamee et al. 2013). The drug of first choice depends on the sensitivity of the circulating virus strains. For instance, the influenza strain H1N1 from 2007/2008 showed a resistance of 98 % to Oseltamivir, because of a single amino acid substitution. This is in contrast to the following year, where Oseltamivir succeeded to 100 % against the pandemic H1N1 virus (Adam, Angie et al. 2009). The emerge of the virus strain is unpredictable, it results of rapid mutations and gene drifts. Different antiviral strategies are necessary.

Zanamivir, also known as Relenza, is currently on the market as produced by GlaxoSmithKline (GSK). The recommended dose is to inhale twice 5 mg or once 10 mg per day for 5 days. In the bronchial tract, it acts as a sialic acid analogue. The newly produced virus gets released via cleaving the sialic acid residues bound from glycoconjugates of the infected epithelial cell by the virus-produced neuraminidase. Mimicking the target of the sialidase inhibits the spread of the virus

in the human body. Zanamivir (4-guanidino-2,4-dideoxy-2,3dehydro-N-acetylneuraminic acid) was identified as a successful inhibitor after testing many candidates (von Itzstein, Wu et al. 1993). The FDA approved Zanamivir for the therapy of Influenza A and B in 2006. Preclinical trials in *in vitro* cultures showed IC50 by around 0.33 nM to13 nM Zanamivir concentrations (Ferraris, Kessler et al. 2005, Memoli, Hrabal et al. 2010, Okomo-Adhiambo, Sleeman et al. 2013). In these tests, throat swabs of influenza patients were collected and tested on MDCK cell culture and were treated by the new neuraminidase inhibitor (Ferraris, Kessler et al. 2005).

1.2.2 Monogenetic diseases in the lung as Cystic fibrosis

Besides pulmonary viral infections, non-viral diseases like cystic fibrosis can lead to pulmonal disfunction, and these patients in turn can develop pulmonary infections. Cystic fibrosis (CF) is a lethal, inherited, autosomal recessive disorder where a genetic mutation occurs in the Cystic Fibrosis Conductance Transport Regulator (CFTR). When mutated, the mucus viscosity is significant increased, and the mucus transport is impaired, thereby more mucus accumulates in the lumen (**figure 6**). CFTR is highly expressed in the lung and other organs as pancreas, intestine, *vas deferens* and sweat glands (Kerem, Rommens et al. 1989, Rommens, Iannuzzi et al. 1989). The channel exchanges the anions chloride and bicarbonate, and controls muco-ciliary clearance (Stoltz, Meyerholz et al. 2015). In those with CF, decreased chloride secretion and increased sodium absorption is observed, and this disfunction causes insufficiently hydrated mucus (Saint-Criq and Gray 2017). The absent or impaired CFTR channel increases the function of the epithelial Na^+ channel (ENaC) (Berdiev, Qadri et al. 2009). ENaC normally regulates homeostasis by absorbing Na^+ ions into the cell, whereas in CF patients ENaC is hyperactive to decompensate for CFTR disfunction. However, this induces even more water to follows the osmotic gradient, causing further dehydration of the airway mucus (Boucher 1994, Mall and Galietta 2015). The channel locations are in the apical membrane of the epithelial cells and are the contact point to the lumen.

Patients suffer from muco-obstruction and are prone to severe lung infections which are often the cause for the reduced life expectancy of about 40 years (Elborn 2016). The thick mucus layer serves as pathogen trap, however the low movement, caused by the viscosity, does not allow a protective transport out of the airway. Germs chronically colonize the CF patient’s airways, eradication mainly fails. (Whiteley, Bangera et al. 2001). The chronic infections mainly account for the morbidity and mortality of CF patients (Lyczak, Cannon et al. 2002).

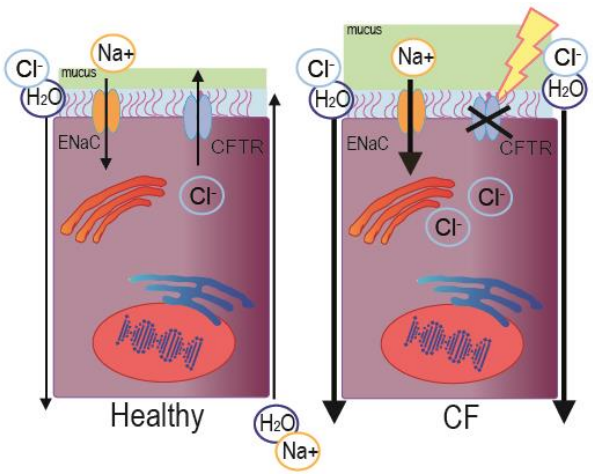

Figure 5. A healthy and a CF pulmonary epithelial cell. The healthy cell (left) shows a functional CFTR channel, CFTR exports Cl^- ions to the lumen and ENaC transports Na^+ ions into the cell. Water, Na^+ and Cl^- exchange to the lumen and back through intercellular paths. The CF cell (right) shows decreased Cl^- secretion because of the dysfunctional CFTR, ENaC gets hyperactive to compensate CFTR. In turn, water and Cl^- ions flow to the cytosol side. This results in dehydrated mucus, which is difficult to move by muco-ciliary clearance.

The basic CF therapy is symptom based, and includes mucolytics and broncho dilatators sometimes in combination with glucocorticoids and antibiotics. Applied as mucus thinners is hypertonic saline (3 %, 3,5 % and up to 7 %) which dilutes the mucus by inhalation when water strains to the lumen and hydrates the mucus. Another enhancer belongs to the group Dornase alfa. A recombinant human deoxyribonuclease I (rhDNase) (MacConnachie 1998), it cleaves extracellular DNA from leucocytes which accumulates in the lung sputum caused by infections. By hydrolysis of the neutrophil DNA it reduces the sticky viscosity of the airway phlegm (Amin, Subbarao et al. 2011, Konstan and Ratjen 2012).

Other targets are ß2-receptors, as the lungs dilate after inhalation of ß2 sympathomimetics (Ziebach, Pietsch-Breitfeld et al. 2001, Hordvik, Sammut et al. 2002, Halfhide, Evans et al. 2005). The bronchus dilatation can also be useful as a pretreatment for applying other medication such as antibiotics. Upon dilation, subsequent medication can reach lower parts of the lung (Brand 2000). Together with inhaled glucocorticoids, they are used to suppress the immune reaction. Cochrane reviews do not present much effective evidence of this combined drug treatment (Balfour-Lynn, Welch et al. 2019).

Besides the previously discussed symptom-based therapies, there are limited targeted therapeutic options currently available. They address the CFTR directly. These are channel modulators, such as correctors, potentiators and stabilizers, as Ivacaftor, combined with other modulators as Lumacaftor, Tezacaftor and Elexacaftor. Ivacaftor alone potentiates the channel so that more ions pass through, (Van Goor, Hadida et al. 2009, 2012). Lumacaftor corrects the protein folding, resulting in a stabilized transporter (Boyle, Bell et al. 2014). Tezacaftor itself supports the trafficking of misfolded proteins, allowing more functional transporters at the membrane surface (Kirby 2018). The youngest approved medication (approved in August 2020) combines Tezacaftor, Elexacaftor and Ivacaftor. Elexacaftor functions as a corrector (Middleton, Mall et al. 2019). In general, the combined medications were mainly developed for the most common mutation ΔF508 (phenylalanine 508 (Phe508del), ~90 % of all CF cases worldwide). The therapeutics sound quite promising, but not every drug can be utilized by all patients, because of the high variety of CFTR gene mutations (Castellani, Cuppens et al. 2008). In clinical settings, applied CFTR modulators show an increase of only up to 10 % measured by the lung function (Heijerman, McKone et al. 2019), lower than hoped.

Currently, CF cannot be cured and the available treatment options focus on a symptomatic treatment. All these reviewed therapeutic options impact positively the patient survival, decrease

morbidity and lethality. However, patients still suffer greatly and have limited quality of life, particularly those affected by orphan mutations.

With the discovery of CRISPR-Cas, a highly promising treatment option for CF patients emerged. Monogenic diseases such as cystic fibrosis are the ideal candidates for gene therapy using CRISPR-Cas. A successful result will pave the way for the establishment of new therapeutic options to correct CF-associated mutations aiming for a cure for CF. This technique offers an individual therapy, ideal for CF's high mutation diversity that requires highly specific treatments. This therapy would enable an improved life quality and life expectancy for patients.

However, a major obstacle for gene therapy is the delivery of CRISPR-Cas to the target cells in the lung. Here, mucus and cilia movement hamper the delivery as described in the previous section on the delivery of nanogels. In CF, the delivery is even more difficult due to the highly viscous mucus. Hence, sophisticated delivery strategies are needed to allow local application of cell transfection. Currently, viral delivery systems and electroporation are most frequently used, however, these techniques have clear limitations and cannot readily be applied in vivo (Hida, Lai et al. 2011). Hence, non-viral delivery systems such as lipid-based nanoparticles are needed to aim for an *in situ* correction of disease-causing mutations. Lipid nanoparticles (LNPs) are one of the most advanced delivery systems and might promise successful and safe delivery for genetical tools as CRISPR-Cas to target cells, such as those needed to treat cystic fibrosis patients.

1.3 Delivery systems for lung therapeutics as Nanogels and Lipid Nanoparticles

Major administration route for most lung therapeutics is drug inhalation. It has the advantage above orally delivered drugs, because they function in systematic pathways in our organism. This causes side effects, which can range from mild to severe symptoms. For patients with combination therapy, drug interactions can appear. The ideas of addressing the point of action directly, and additionally to enclose the drug in smart delivery system that induced fewer side effects, have been in favor in drug development for years and even promote patient compliance. It allows a lower drug dose and is less harming in a systematical path.

These advantages are very convincing, and a lot of investigations succeeded even for chronic diseases where long-term uptake of drugs are unavoidable e. g. the therapy of asthma bronchial (Rau 2005). The topical use of inhaling drugs addresses the target directly as ß-sympathomimetics, in asthma bronchial. Inhaled application also reduces side effects when glucocorticoids are used to suppress inflammation (Dahl 2006).

Inhaled application of drugs is made challenging by the structure and function of the lungs. The human lung surface and the cilia are covered with thick mucus layers, which is part of the immune system and one of the first defense barriers to protect our body. Lung mucus is produced mainly by goblet cells and submucosal glands (Ostedgaard, Price et al. 2020). Collected mucin granule is generated in vesicles and stored in cells until secretion (Adler, Tuvim et al. 2013). It contains a complex combination of mucins, glycoproteins, ions, lipids and immune factors as IgA, transferrin, lysozyme and defensins (Singh, Parsek et al. 2002, Thornton and Sheehan 2004). Mucins are glycoproteins, they hold typically an amino- and carboxy-terminal. The ends are partwise glycosylated and abundant with thiolated proteins such as cysteine and glutathione. Cysteine and Glutathione have a characteristic thiol group (R-SH), which can easily form disulfide bridges (R-S-S-R) and connect single monomers, mainly performed in the *Endoplasmic reticulum*. More polymerization follows in the Golgi apparatus, as well the O-glycosylation (Adler, Tuvim et al. 2013). The construct of formed polymeric mucins builds a sticky colloid system. These characteristics form the perfect trap for bacteria, fungal or foreign bodies, to protect our bodies from infections.

The genes MUC2, MUC19, MUC5B and MUC5AC are mucin genes expressed in a human lung, MUC5AC and MUC5B predominate (de Sousa and David 2006). MUC5AC is mucin produced by goblet cells, MUC5B is a mucin of submucosal glands (Wickström, Davies et al. 1998). The

polymers are homotopic, the single monomers just bind the other monomer of the group (Thornton, Rousseau et al. 2008). Through noncovalent bindings, the homotopic polymers crosslink like a network with each other (Thornton, Rousseau et al. 2008). Water binds through the glycan terminus. Only 1.5 - 2.5 % of a healthy mucus are solid components, this proportion of solids and liquids forms a hydrogel (Hill, Vasquez et al. 2014). This density is perfect to trap pathogens, but consequently, drug delivery system such as particles or simple nanogels get stuck as well. The mucus, together with ciliated cells, forms the muco-ciliary clearance; a synergistic protective power. It is the main innate defense mechanism of the respiratory system (Bustamante-Marin and Ostrowski 2017).

For decades, labs have been studying effective drug targeting systems. Approaches distinguish between mucoadhesive and mucus penetrating particles (Lai, Wang et al. 2009). Each type can be beneficial for different treatments and it primarily depends on the target area. The idea of mucoadhesive particles is to keep the drug at the target location for as long as possible, to prolong the therapeutical effect. For example, antibiotic vaginal suppositories to treat an infection target the vaginal flora environment (Rossi, Bonferoni et al. 2014). Mucoadhesive enhancers can be polymers such as polyacrylic acid, sodium carboxymethylcellulose, hyaluronic acid, chitosan etc. Their properties are high viscosity, abundant mucin interactions as covalent and polar bonds (Boddupalli, Mohammed et al. 2010).

To allow a therapy to reach the epithelial cells, smart drug formulation is necessary. Muco-penetration is necessary as these cells are below the mucus layer. For instance, muco-penetration is essential in gene-therapy to treat CF cells (Hida, Lai et al. 2011). Here, as few mucus interactions as possible are in favor. Also, features are applied such as mimicked virus surface properties. Viruses have a highly charged surface, which provides a hydrophilic charge and lowers the hydrophobic mucus interactions. This technique has allowed viruses to avoid the mucus adhesive interactions for many centuries (Olmsted, Padgett et al. 2001, Olmsted, Padgett et al. 2001). Similar features were observed in proteins as well e. g. in antibodies as IgA to be able to operate in a mucus environment (Saltzman, Radomsky et al. 1994). An added PEG-layer offers a mimicked advantage and enhances the passage by creating a hydrophilic shell (Lai, O'Hanlon et al. 2007).

The lab of Marcelo Calderón has developed degradable nanogels. The idea is based on minimizing the interactions of nanoparticles and surface to allow muco-penetration. The nanogels contain dendritic polyethylene glycol (dPEG) with disulfide bonds as a controlled drug delivery

system. The nanogels were polymerized with poly-N-isopropylacrylamide (PNIPAM) and poly-N-isopropylmethacrylamide (PNIPMAM). The hypothesis is that by forming disulfide bridges with the mucin proteins which are containing thiol to disentangle the mucus layers. I have tested disulphide-containing biodegradable nanogels, PNIPMAM-(S-S)-dPG nanogels and as control non-degradable nanogels PNIPMAM-dPG and the same set loaded nanogels with Etanercept on the bronchial epithelium model. For fluorescence analysis all nanogels were labeled with Rhodamine-B.

Another delivery system are lipid nanoparticles (LNPs). These days, they are one of the most advanced formulations for delivery. LNPs are applied e. g. in gene therapy. For RNAi gene therapy (Onpattro®), first approved gene therapy by FDA in 2018 (Akinc, Maier et al. 2019). Their LNP system has been shown to transfect large molecules into the intracellular environment of target cells. The LNP system is composed of 4 lipid constituents - cationic lipid, also called “helper lipid” (e.g. distearolyphosphatidycholine or DSPC), cholesterol, PEG-lipids and siRNA (Kulkarni, Witzigmann et al. 2019). Cationic lipids are pH-sensitive components that enhance the loading and encapsulation process. PEG-lipids influence the particle size and the transfection rate success (Heyes, Hall et al. 2006). ApoE is well-known lipoprotein involved in lipo-metabolism in our bodies. ApoE’s main function is to interact with the low-density lipoprotein-receptor (LDL-R) for leading to endocytose of the LNP(Yao, Gordon et al. 2016). Its feature is used to support uptake for e. g. LNP enveloped siRNA into cell. LNPs are a promising tool for further genetical therapies as e. g. delivery of CRISPR Cas to treat or even cure monogenetic diseases as Cystic Fibrosis.

1.4 Drug development

New drug candidates are tested every day, with the aim of improving the life quality of patients and prolonging our lives. There is a long process of testing and evaluation before a newly-discovered substance becomes a final drug which released on the market and available for use in therapy. Drug discovery takes 12 years on average, and this process carries immense costs (Van Norman 2016). Despite the duration and cost, this stringent development path exists for our safety.

The first step in the process is ‘early target discovery’ or ‘target to hit’, which describes the search for an addressable object for a medical substance (Paul, Mytelka et al. 2010). To identify molecules that can be targeted to treat specific diseases, biochemical processes need to be studied in-depth and all major consequences of the disease should be identified on cell level. Information about the symptoms enhance the chances of finding a target of interest. Receptors and enzymes are common targets, with the goal of the drug compound being to inhibit or to increase their action.

A promising target is helpful, but it is crucial to subsequently discover a substance that can act upon this target as a new active agent, the ‘hit to lead’. These are often found through high throughput screening of possible fitting substances for the target. With each round of testing, possible active substances are eliminated until only a few possible candidates are left. Computational chemistry (‘*in silico* tests’) can be used to increase the chances of drug discovery and optimization (Brogi, Ramalho et al. 2020). Before moving on to the second step, these candidates agents are validated and improved. Chemical optimization is used to modulate and improve the active agent, such as attaching functional groups e. g. to increase the affinity to the target (Krall, da Cruz et al. 2016).

The second step is where proof of concept is tested in *in vitro* and *in vivo* models, to evaluate pharmacology (a proven improvement of the state of the relevant disease) and toxicology (it must not harm the test subject or show toxic effects). As an *in vivo* model, rodents are often used, and non-human primates can be used in final stages (Watson and Platt 2012). There is a long process of testing and evaluation before a newly-discovered substance becomes a final drug on the market and available for use in therapy.

The drug is not given to humans until the third step, the clinical development. This is subdivided into three phases. During Phase one, also named ‘first-in-human’ is made up of a small amount

of healthy people. Studying the pharmaceutical effect in a human body and to find the right dosage are necessary to confirm that the substance is safe (USA 2018). During Phase two, the drug is applied to patients and the number of probands number increased (100-300) (Sanne, Piliero et al. 2003, Van Norman 2016). In Phase three, the number of patients is increased to several thousands, allowing the safety and efficacy of the drug to be thoroughly evaluated in a diverse population (Lara, Douillard et al. 2011). Different hospitals all over the world participate in these studies (Teicher 2013). Upon successful testing, the drug can receive the approval of a local medicine agency, such as the Food and Drug Administration (FDA) or European Medicines Agency (EMA) to release the product to the market. The data collection and observation of medical reports that persists after release forms the last step of new therapeutics (Van Norman 2016).

1.4.1 Alternatives to animal testing in preclinical research

Preclinical research is an immensely important stage. Preclinical research evaluates safe candidates by testing toxicology, pharmacokinetics and pharmacodynamics. (ICH M3(R2) Non-clinical safety studies for the conduct of human clinical trials for pharmaceuticals). Though these essential points are covered, efficacy is lost in the translation from animal to human. During the clinical phase, approximately 90% of compounds fail drug approval (Despina G. Contopoulos-Ioannidis 2003, Seok, Warren et al. 2013, Hay, Thomas et al. 2014), for example in cancer research (Kola and Landis 2004, Sharpless and DePinho 2006). Data shows that animal research results struggle to predict the action in the human body and can lead to harmful or misleading medical solutions (Martić-Kehl, Schibli et al. 2012, Akhtar 2015). Reversely, promising candidates can be excluded too early if they do not show efficiency in an animal, when they might have worked in a human.

An animal model is only used if it is ethically inappropriate to test in humans, but is that the only solution? The animals used for pulmonary research are rodents such as mice, rats, hamsters, genuine pigs, also equids are tested (Barrios 2008, Peake and Pinkerton 2015, Carrington, Jordan et al. 2018, Rosen, Chanson et al. 2018). Pulmonary research is particularly challenged by the translation from an animal to a human body. The airway anatomy and physiology of rodent and human differs immensely, yet animal models are still exceedingly present in preclinical research; the length of the bronchial tree, angle of the trachea and bronchos connections, several points of the airway architecture is dissimilar in comparison to the human lung (Peake and Pinkerton 2015). Rodents and equids have alveolar ducts, whereas primates (as well as cats and dogs) have respiratory bronchiole locates between the terminal bronchiole and alveoli (Peake and Pinkerton

2015). Anatomy plays an important role in studying pathogenesis, requiring careful attention to inter-species differences.

Airway diseases such as bronchial asthma are uniquely human diseases, as broncho constriction does not occur in mice (Bates, Rincon et al. 2009). Only cats and equines next to humans and non-human primate exhibit eosinophilic bronchitis, which is one essential symptom of asthma (Herszberg, Ramos-Barbón et al. 2006, Williams and Roman 2016). Nonhuman primates exhibit almost all asthma bronchial symptoms which can be observed in a human (Coffman and Hessel 2005). Testing non-human primates is more challenging, not only in terms of ethical considerations but also in terms of cost; very few institutes house and test these species. On the other hand, it is important to keep in mind the high cost of exploring treatments that showed falsely promising results due to the use of a rodent model (Chatfield and Morton 2018).

Limits of animal models occur in infection studies as well. There are two shortcomings of using mouse models to study infection of the airways. First, disease related host-pathogen-interactions may differ, taking other routes of infection or not causing infection at all. Secondly, upon infection, rodents and humans may show very different symptoms, especially against bacteria or virus contagions (Swearengen 2018, Muñoz-Fontela, Dowling et al. 2020).

Human lungs contain a complex tissue physiology. Various specific cell types as ciliated, club and goblet cells among others line the airway surface in a multidimensional system. The architecture is difficult to rebuild. It represents the difficulty of studying this essential organ and to translate the observations from an animal model to a human. For instance, there is a need for a bronchial epithelial *in vitro* model as a test matrix for infections, rather than relying on mice models. Specifically, the wild type of the influenza A virus (IAV) infection is not even infectious in mice and causes different symptoms (Bouvier 2015), yet remains the most frequent used animal model for infection testing. A human based model is more promising to improve exploration quality.

Influenza is an infectious RNA virus transmitted disease, it contagious the human air way and causes mild symptoms from a runny nose to fever and severe respiratory distress (Suarez 2016, Denney and Ho 2018). Influenza infections are mainly rely on the sialic acid receptor with an alpha 2,6 linkage to galactose, as this is the entering target for the virus into the human lung. In human tracheal and bronchial tissue, it is highly attendant (Shinya, Ebina et al. 2006, van Riel, Munster et al. 2007). In mice the receptor differs by an alpha 2,3 binding (Ibricevic, Pekosz et al. 2006, Glaser, Conenello et al. 2007), which may explain why mice generally do not get infected by

human isolated viruses (Bouvier and Lowen 2010). Just adopted viruses offer a chance for infection.

Typical symptoms (such as fever) are present in mice, instead hypothermia can be reported. In humans, damage in the upper airway is typical, whereas in mice lower airway damage is more likely to occur (Belser, Lu et al. 2007, Belser, Wadford et al. 2010). The lower cost of mice studies, easy to care and the high number of animals are offering robust data and are still leading to use this animal model (Bouvier 2015).

Transgenic mice are a promising tool, though developing new transgenic models can be time-consuming. A recent example is the pandemic situation in 2020 caused by COVID-19, which relies, for entering the airway, on the receptor ACE-2, which is missing in mice (Bao, Deng et al. 2020). A humanized ACE2 mouse was developed in 2002 in response to the SARS-2 outbreak (McCray, Pewe et al. 2007), and is related to COVID-19. Unfortunately, through loss of interest, labs stopped working with this humanized mice, which means the production of the test animal needs even more time until the demand of researching labs is met (Callaway 2020). Time became an important factor for a generation who never faced a crisis as severe as a pandemic before.

Monogenetic diseases are caused by a single gene disorder and is characteristic for their inheritance in family generations (O'Neal and Knowles 2018). These days monogenetic diseases are an interesting and promising research field, especially these days with genetical tools as CRISPR. Difficulties also occur when studying monogenetic diseases, as we do not find the same genetic problems in animals. For instance, the complex lungs of humans have submucosal glands, which are important for diseases as Cystic Fibrosis (CF) (Rosen, Chanson et al. 2018). In contrast, in mice airway histology, the glands are present in different tissue parts than in humans. Submucosal glands produce the essential mucin MUC5B, one of the predominant mucins in human mucus (Wickström, Davies et al. 1998, Bonser and Erle 2019). Studies showed that MUC5B has a huge impact of the antibacterial defense during infections (Ostedgaard, Price et al. 2020). A similar problem is the secretory cell type which differs in between the species as well. Even genetic knock-outs in mice can show different observations to human studies. A CFTR mice, knock-out mice of a not functional transmembrane conductance regulator gene to study cystic fibrosis, does not present the classical spontaneous developed lung infection (Guilbault, Saeed et al. 2007), one of the most urgent points to study CF. Instead, mice with targeted overexpression of the epithelial sodium channel (ENaC) receptor were developed to create a similar picture of muco-obstructive and infective pathology as in CF patients (Mall, Grubb et al. 2004). Though this

was a great improvement for studying CF in general, especially today when the medicine is trying to get closer to find paths to gene therapy, the mice becomes even more difficult to study. Bigger mammals as ferret and pig seem to be most reliable knock out animals for studying Cystic Fibrosis. Both show the most similarities of physiology and cellular anatomy to humans (Rosen, Chanson et al. 2018). However, raising large transgenic mammals raises a far more complex ethical question, as well needing a long amount of time to achieve the modification, more work to maintain breeding, a special facility for housing and, finally, high costs. To improve genetic therapy research and to close the gap of translation to produce successful therapies, human based models are necessary.

1.4.2 Human-based *in vitro* models in pulmonary research

Many alternative models for studying the human airway now exist; a two-dimensional (2D) model, bioreactor, printed or not printed three-dimensional (3D) model, tissue sample as an *ex vivo* model, organoid or organ on a chip (**figure 6**). These alternative options will be briefly discussed below.

The 2D model involves growing cells on a solid surface as plastic or glass and culture a monolayer of cells (Kapałczyńska, Kolenda et al. 2018). The method is one of the oldest and has contributed greatly to our understanding of the cell and interactions with pathogens in earlier times (Medzhitov and Janeway 1997, Hurley and McCormick 2003). Advantages of 2D cultures are low costs, established handling and to perform functional tests as toxicity assays. However, 2D cultures contain a single cell type cultured in a monolayer, it does not represent an *in vivo* tissue (Fontoura, Viezzer et al. 2020). Cell monolayer does not enable cell polarity and thereby inhibits cell differentiation (Breslin and O'Driscoll 2013). Missing cell functionality (enable by cell differentiation) leads to absent secreted proteins for cell-cell communication, which play an important role for natural cell mechanisms as in apoptosis (Song, Najjar et al. 2014). Additionally, in 2D cultures different gene expression and gene splicing was found (Anczuków, Akerman et al. 2015, Fontoura, Viezzer et al. 2020), it makes comparison difficult. Nonetheless, it is obvious that these limitations hamper the translation to *in vivo* tissue and the usage of 2D model regarding stimuli responses, cell function studies or even drug metabolism trials. (Edmondson, Broglie et al. 2014, Galarza, Kim et al. 2019).

A 3D model provides a high complexity and bridges the missing aspects by co-cultivating different cell types. The set-up enables a three-dimensional growth, which is greatly comparable to tissue of origin in a human body (Knight and Przyborski 2015, Marrazzo, Maccari et al. 2016). Cell-cell

interaction studies, detailed molecular signal observations and transcriptional profile studies are also possible (Lee, Lilly et al. 2009, Pezzulo, Starner et al. 2011). By providing a scaffold or a trans-well with applying a matrix (e. g. hydrogel or collagen) and by using different methods as manual pipetting or even 3D printing, enables the cells to grow vertically (Steinke, Gross et al. 2014, Marrazzo, Maccari et al. 2016, Wang, Zhang et al. 2018). These 3D models can be seeded on a microfluid device, such as a chip, that facilitates the interaction with different 3D tissues and can be built up from organ on a chip to a desired “human on the chip” setting (Rossi, Manfrin et al. 2018, Schimek, Frentzel et al. 2020). Microfluid chambers work with micro tissue construction and are fully automatic for standardized throughput also for new drug responses and interactions (Delamarche, Tonna et al. 2013). 3D culture models all exhibit an air liquid interface, which enables the epithelial cell layer to have direct contact with the environment. This is important, as CO_2/O_2 and additional differentiation medium leads to the cell differentiation into characteristic epithelial cells. It mimics the muco-ciliary clearance, where the surface is exposed to the outside and facilitates interactions as pathogen infection, gas exposure or even inhaled drug studies e. g. for delivery (Lai, O'Hanlon et al. 2007, Müller, Riediker et al. 2010, Lenz, Karg et al. 2013, Chandorkar, Posch et al. 2017).

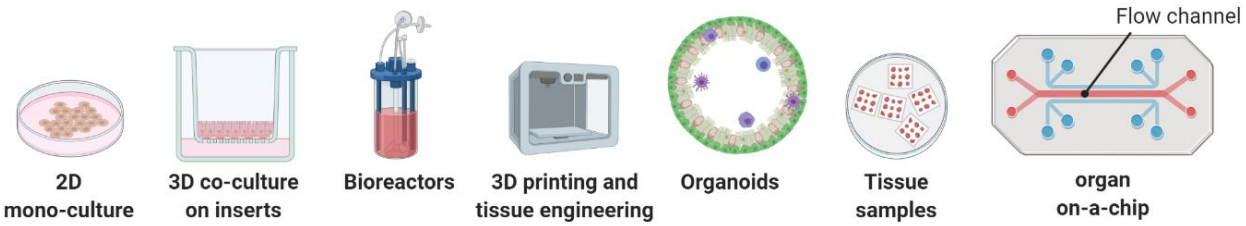

Figure 6. Tissue culture and engineering platforms for testing. An overview of non-animal test models, (left-to-right): 2D monoculture of cells. 3D co-culture on inserts, one or more different cell types can be seeded on the insert and cultured at air liquid interface conditions. A bioreactor provides a permanent perfused set up and can cultivate 3D structures. In 3D printed models, like a 3D co-culture model, cells get automatically seeded into the model structure by a bioprinter. Organoids are self-organized and autonomously build 3D tissue structures in small spheroids. Tissue samples are small biopsy samples collected from human tissue, which provide all native tissue features. An organ on a chip allows several 3D cultures models to interact with each other and are connected through a flow channels, to study more than one organ at a time to provide an even more realistic model. Created with BioRender.com.

Bioreactors provide an environment of a precise control over media transfer rates, shear stress, gas exchange (pO2, pCO2), constant level of pH and nutrients. It can be applied in a big scale and in a micro scale. It offers a long-term culture and produces 3D constructs (Nichols, Niles et al. 2014). A great advantage is a high throughput, especially for toxicity tests, macro scales even offers a perfusion for transplants (Law, Liau et al. 2016).

Also, tissue samples can be collected during a surgery, e. g. when a part of healthy tissue is attached to tumorous tissue and gets taken out as well (Fatykhova, Rabes et al. 2015, Hocke, Suttorp et al. 2017). These tissues can be used to create *ex vivo* models, grown from the human lung. Because this sample received all normal tissue features during development, this test set-up has great advantages over more artificial models (Fatykhova, Rabes et al. 2015). The disadvantages of this technique are that the collected sample location depends on the surgery, and a full exclusion of neoplastic, tumor cells is difficult.

Another novel alternative are organoids. This model is self-organized and builds an autonomous system from a homogenous cell population and forms a multicellular 3D *in vitro* spheroid (Sasai 2013). Organoids are derived from stem cells; from induced pluripotent or adult stem cells (Huch and Koo 2015). Induced pluripotent stem cells mimic the embryonic growth, and all kind of organs can be developed from that source (Klimanskaya, Kimbrel et al. 2020). In contrast, adult or tissue stem cells stay conditioned to the tissue of origin and keep the ability of differentiation and renewing (Lancaster and Huch 2019). The properties of organoids derived from stem cells mimic a great comparable *in vivo* equivalent, ideal for glandular tissue, also for stratified tissue as bronchial tissue, but the asked question need to be considered, because it is a one organ system by itself. Additionally, organoids cannot provide a multilayer morphology by coculturing different cell types so far, as e. g. fibroblasts and epithelial cells (Barkauskas, Chung et al. 2017). For 2D and 3D models stem cells can be also used, other common cells are primary cells and cell lines. Stem cells relate higher costs and a daily care (Miller, Dye et al. 2019).

Besides the type of test model chosen, the specific cells used within that model is of importance cell lines are immortalized cells which proliferate indefinitely due to mutation of cellular senescence, these are often collected from tumor tissue such as A549 derived from lung cancer alveolar cells (Smith 1977). Another cell line is Calu-3, it is collected form bronchial epithelial submucosal glands (Shen, Finkbeiner et al. 1994). 16HBE14o- or BEAS-2B cell lines are derived from bronchial epithelium transformed by a retrovirus (Amstad, Reddel et al. 1988). Handling of cell lines is considered straightforward and as a low-cost investment, because the continued

passaging and genotypical similarities. However, the loss of cellular characteristics such as differentiating patterns is reason to doubt the result reliability (Stewart, Torr et al. 2012). Difficulties in observing the transit of biomolecules or transport of particles for delivery trials are noticeable, because of a reduced barrier function (Forbes, Shah et al. 2003). As well as a genetic alteration, this changes the functionality of the cells and influences metabolic aspects (Boei, Vermeulen et al. 2017). All these arguments are reason to avoid data collection by use of cell lines during preclinical trials, as this can easily lead to wrong assumptions (Pan, Kumar et al. 2009).

Primary airway cells can be collected by biopsies, transplant programs, nasal brushing or bought in frozen vials from providing companies. The life span is finite, inter- and intra-donor variation are challenging for interpreting and characterizing the data, but primary cells feature the hold of cellular senescence and natural behavior as observed as *in vivo* (Stewart, Torr et al. 2012). Another advantage is for studying diseases, primary cells can be obtained directly from patients and even provide the opportunity of personalized medicine.

In comparison all types of cells and models have their own advantage and disadvantages, the asked question and the aim of research is central in choosing the model and the cell type. In conclusion, for preclinical tests as alternatives to animal trials, primary human cells or even stem cells are the best choice as their *in vivo* like characteristics provide a natural environment similar to the human body. They are difficult to access, require more work to maintain and come at a higher cost for the lab, but are essential for reliable studies.

2. Thesis Aim

My thesis is motivated by the need for a more realistic alternative test model for studying bronchial tissue behaviors in preclinical trials. These human-based models offer more promising study observations by bridging the gap of translating from an animal model to a human body. Animal models are still the gold standard in clinical research, even though the airway anatomy and physiology of rodents and human differs immensely. Additionally, host-pathogen-interactions are not fully understood and show differing characteristics in human and animal tissue.

Hence, my thesis aims to develop an *in vitro* model of bronchial epithelium tissue, exclusively based on primary human bronchial cells as a full–thickness model. It opens up many new options as a test matrix for developing a better understanding of human lung infections and diseases, as well as testing and developing new therapy options.

The model was used for an infectious trial with influenza A virus. A method was established to infect the *in vitro* model with H3N2 (Panama/2007/1999 (PANIII)). To analyze the behavior of the bronchial epithelial tissue on gene and protein level and to study the impact of inhibitors to observe comparisons to *in vivo* studies.

Another part of my project was to develop a human based CF bronchial epithelium model. A human-based CF model may help to overcome the therapeutical shortage and allows studying of the disease and novel therapeutic approaches in a more realistic setting. For the diseased model CF bronchial epithelial cells from patients were used. The cells hold the homozygotic ΔF508 mutation. We predict that a human-based CF model will benefit the studying of the disease and novel therapeutic approaches as genetic therapy.

An additional task was to test different delivery systems as degradable nanogels, curcumin charged particles and LNP compositions as for their ability to overcome the mucociliary barrier in the healthy models. Transfection efficacy was tested with high content screening and imaging analysis. Sadly, tests were prematurely interrupted by the pandemic situation of COVID-19 and the lockdown rules imposed locally by the federal government.

3. Materials

3.1 Reagents

Acrylamide/Bis Lösung 19:1, 40 % (v/v)	Carl Roth, Karlsruhe, DE
Agar 100	Agar Scientific, Stansted, Great Britain, UK
Alcian Blue	Sigma-Aldrich, Munich, DE
Amphotericin B (250 µg/ml)	Sigma-Aldrich, Munich, DE
Avicel RC-581	FMC BioPolymer
α-Nuclear red	Sigma-Aldrich, Munich, DE
Bovine Serum Albumin 30 %, steril	Sigma-Aldrich, Munich, DE
Bovines Serum Albumin, fraction V, >96 %	Sigma-Aldrich, Munich, DE
BEGM Media and Bullet Kit	Lonza, Basel, CH
Bovine Collagen I	Cellsystems, Troisdorf, DE
cacodylic acid sodium salt trihydrate,	Carl Roth, Karlsruhe, DE
Crystal violet	Carl Roth, Karlsruhe, DE
DDSA	Scientific, Stansted, Great Britain, UK
DEAE-Dextran	Sigma-Aldrich, Munich, DE
DMEM 2, low Glucose, Glutamax	ThermoFisher SCIENTIFIC, Waltham, USA
DMEM 1, high Glucose	Sigma-Aldrich, Munich, DE
DNase	Sigma-Aldrich, Munich, DE
Dimethyl sulfoxide (DMSO)	Sigma-Aldrich, Munich, DE
Disodium hydrogenphosphate (pro analysi)	Merck, Darmstadt, DE
Dispase II	Roche Diagnostics, Mannheim, DE
Dithiothreitol (DTT)	Carl Roth, Karlsruhe, DE
DMP 30	Agar Scientific, Stansted, Great Britain, UK
Dulbecco's Phosphate-Buffered saline Solution (PBS) w Ca^{2+}/ Mg^{2+} (1x)	ThermoFisher SCIENTIFIC, Waltham, USA

Dulbecco's Phosphate-Buffered saline Solution (PBS) w/o Ca^{2+} /Mg^{2+} (1x)	ThermoFisher SCIENTIFIC, Waltham, USA
Endothelial Cell Medium (EGM-2)	Lonza, Basel, CH
Eosin G	Carl Roth, Karlsruhe, DE
Ethanol absolute	Carl Roth, Karlsruhe, DE
Ethanol 96 %	Erkel AHK, Berlin, DE
Formaldehyde solution (37 %)	Sigma-Aldrich, Munich, DE
Formalin	Carl Roth, Karlsruhe, DE
FCS	Biochrom, Berlin, DE
Goat serum	Dianova, Hamburg, DE
Gentamycin (50 mg/ml)	Sigma-Aldrich, Munich, DE
Hematoxylin	Carl Roth, Karlsruhe, DE
HBSS	ThermoFisher SCIENTIFIC, Waltham, USA
Heparin	STEMCELL Technologies, Vancouver, CA
Human Placental Collagen Type VI	Sigma-Aldrich, Munich, Germany
Hydrocortisone	STEMCELL Technologies, Vancouver, CA
Karnovsky's fixative	Merck Eurolab, Darmstadt, DE
L-Glutamine	Sigma-Aldrich, Munich, DE
Methanol	Carl Roth, Karlsruhe, DE
Milk powder	Carl Roth, Karlsruhe, DE
Minimal Essential Medium (MEM)	ThermoFisher SCIENTIFIC, Waltham, USA
MNA	Agar Scientific, Stansted, Great Britain, UK
Sodium hydrogen carbonate (Na_2HCO_3)	Merck, Darmstadt, DE
Sodium dodecyl sulfate (SDS)	Carl Roth, Karlsruhe, DE
Nickle grids	Agar Scientific, Stansted, Great Britain, UK
Nitrogen (liquid)	Air Liquide, Paris, F
Osmium tetroxide (1 %)	Chempur, Karlsruhe, DE

Paraffin	Carl Roth, Karlsruhe, DE
Paraformaldehyde (PFA)	Carl Roth, Karlsruhe, DE
Penicillin-Streptomycin-solution (100 x, 10.000 U/mL Penicillin, 10 mg/mL Streptomycin)	Sigma-Aldrich, Munich, DE
NHLFb	Epithelix, Geneva, CH
NHBEC	Epithelix, Geneva, CH
Phosphate Buffered Saline (PBS)	Sigma-Aldrich, Munich, DE
PneumaCult Ex Plus	STEMCELL Technologies, Vancouver, CA
Ponceau S	Sigma-Aldrich, Munich, DE
Roti® - Histofix	Carl Roth, Karlsruhe, DE
Roti® - Histokit	Carl Roth, Karlsruhe, DE
Roti® - Histol	Carl Roth, Karlsruhe, DE
Protease XIV	Sigma-Aldrich, Munich, DE
siRNA (GFP-tagged)	IDT, San Jose, California, USA
Sodium chloride (NaCl)	Sigma-Aldrich, Munich, DE
Sodium hydroxide (NaOH)	Sigma-Aldrich, Munich, DE
TEMED	Carl Roth, Karlsruhe, DE
Tissue Freezing Medium	Leica Biosystems, Nussloch, DE
Tris buffer	Carl Roth, Karlsruhe, DE
Trypsin/EDTA	Sigma-Aldrich, Munich, DE
Triton-X-100	Carl Roth, Karlsruhe, DE
Tween-20	Carl Roth, Karlsruhe, DE
Xylol	Carl Roth, Karlsruhe, DE

3.2 Cell culture Media

Fibroblast Basal Medium (FBM)	DMEM supplemented: 1 % L-glutamine
Fibroblast Growth Medium (FGM)	FBM supplemented: 7.5 % FBS
PneumaCult™ Ex Plus Medium	PneumaCult Ex Plus Basal Medium supplemented: 2 % PneumaCult™ 50 x Supplement
PneumaCult™-ALI Medium	PneumaCult™-ALI Basal Medium supplemented: 10 % PneumaCult™-ALI Medium 10x Supplement 1 % PneumaCult™-ALI Maintenance 100 x Supplement 0.2 % Hydrocortisone 0.5 % Heparin
Airway Epithelial Cell Growth Medium Kit, defined	0.3 % Supplement I, II, III
Endothelial Basal Medium Cell (EBM2)	EBM supplemented: EGM-2 MV Bullet Kit
DMEM 2	DMEM, low Glucose, Glutamax Supplemented
DMEM^{+}	DMEM supplemented: 7.5 % FCS 1 % L-glutamine

3.3 Kits

CytoTox-ONE™ Homogeneous Membrane Integrity Assay Kit	Promega, Madison, Wisconsin, USA
DyLight™ Microscale Antibody Labeling Kit	Novus Biological brand, Littleton, Colorado, USA
EKU03199 ELISA Kit Club Cell Protein (CC16), precoated ELISA	Biomatik, Cambridge, Canada
Human IL-29 (IFN lambda 1) uncoated ELISA	Invitrogen, ThermoFisher SCIENTIFIC, Waltham, USA
Human IL-1ß, uncoated ELISA	ThermoFisher SCIENTIFIC, Waltham, USA
RNase-free DNase Set (50)	Qiagen, Germantown USA
VeriKine-HSTM Human Interferon beta-1 (IFN-ß1) TCM, uncoated ELISA Kit	pbl ASSAY SCIENCE, Piscataway, USA

3.4 Antibodies

Antibody	Marker	Isotype	Clone	IF	WB	Company
Acetyl. tubulin	Cilia at bronchial epithelial cells	Mouse IgG_{2b}	Monoclonal 6-11-B1	1:100	-	Sigma-Aldrich, Munich, DE
CFTR	CF trans-membrane conductance regulator, transmembrane protein	Mouse IgG_{2a}	Monoclonal (24-1)	1:100	1:500	Bio-Techne, Wiesbaden, DE
CD31	EC identification	Mouse	clone JC70A	1:50	-	DAKO, Glostrup, DK
ETN	Etanercept	IgG_1	monoclonal (2C11)	1:1000	-	Abcam, Cambridge, UK
Influenza A	IAV	goat	polyclonal	1:30	-	Bio-Rad, UK
Ki67	Nuclear protein, associated with cell proliferation	mouse IgG	monoclonal (Ki67-P)	1:200	-	Dianovo, Hamburg, DE
MUC5AC	Mucin protein, produced by airway epithelial cells	mouse IgG1	monoclonal (CLH2)	1:400	-	Merck, Darmstadt, DE
PAN-Cytokeratin (4, 5, 6, 8, 10, 13, 18)	Cytokeratin	Mouse IgG1	monoclonal	1:100	-	Santa Cruz Biotechnology
UG	Protein secreted by Club Cells (CC16)	rabbit	polyclonal	1:400	-	Abcam, Cambridge, UK
vWF	EC surface protein	rabbit IgG	polyclonal	1:50	-	Abcam, Cambridge, UK
ZO-1	Tight junctions Protein	rabbit IgG	polyclonal	1:100	-	ThermoFisher, Waltham, USA
Alexa Fluor®488	Secondary antibody	rabbit IgG	polyclonal	1:400	-	Abcam, Cambridge, UK
Alexa Fluor®594	Secondary antibody	Mouse IgG	polyclonal	1:400	-	Abcam, Cambridge, UK
DyLight™488	Secondary antibody	Goat IgG	polyclonal	1:30	-	ThermoFisher, Waltham, USA

Table 2. Antibodies

3.5 Software

Adobe Illustrator	Adobe Inc., San Jose, CA, USA
Biorender (free trial version)	Biorender, Toronto, ON, CAN
GraphPad Prism	GraphPad Software, La Jolla, CA, USA
Microsoft Word	Microsoft, Albuquerque, NM, USA
Microsoft Excel	Microsoft, Albuquerque, NM, USA
Photoshop	Adobe Inc., San Jose, CA, USA

3.6 Consumables

Blotting Pads	VWR, Pennsylvania, USA
Cell Culture Inserts Falcon ® (3 µm pore size)	Corning, Amsterdam, NL
Cell Culture Inserts Falcon ® (0.4 µm pore size)	Corning, Amsterdam, NL
Cell culture inserts – 0.4 µm membrane (Corning 3460 Transwell, CLR, 12 mm, TCT)	Corning, Amsterdam, NL
Cell Culture flasks (25 cm^2, 75 cm^2, 1550 cm^2)	TPP, Melbourn, UK
Cell strainer (70 µm pore size)	BD, Franklin Lakes, NJ, USA
Centrifuge tubes (15, 50 ml)	Sarstedt, Nürnbrecht, DE
Cover slips	Carl Roth, Karlsruhe, DE
Cryo vial	Almeco, Esbjerg N, DK
Embedding molds	Sigma-Aldrich, Munich, DE
Forceps	Carl Roth, Karlsruhe, DE
Mr.Frosty™	ThermoFisher SCIENTIFIC, Waltham, USA
Multiwell cell culture plates (6, 12, 96-well)	VWR, Pennsylvania, USA
Nitrocellulose membrane	Bio-Rad, Munich, DE
Nitril gloves	Hansa-Trading HTH, Hamburg, DE
Parafilm	Carl Roth, Karlsruhe, DE
Pipette tips (10, 100, 1000 µl)	Sarstedt, Nürnbrecht, DE
Pipette tips with filter (10, 100, 1000 µl)	Sarstedt, Nürnbrecht, DE

Polylysine slides	Carl Roth, Karlsruhe, DE
Scalpels	Carl Roth, Karlsruhe, DE
Serological pipettes (5, 10, 25 ml)	Sarstedt, Nürnbrecht, DE
Syringe	Carl Roth, Karlsruhe, DE
Syringe Filter (0.45 µm)	Sarstedt, Nürnbrecht, DE
Tissue culture dish	TPP, Trasadingen, CH
Tissue culture test plate (6-well)	TPP, Trasadingen, CH

3.7 Devices

Autoclave V Series	Systec, Wettenberg, DE
Balance XS205 dualRange	Mettler-Toledo, Giessen, DE
Centrifuge, Eppendorf Centrifuge 5415 C	Eppendorf AG, Hamburg, DE
Centrifuge, Megafuge 1.0 R	Heraeus, Hanau, DE
CO_2 Incubator	Heraeus, Hanau, DE
CO_2 -free Incubator	Heraeus, Hanau, DE
Confocal microscope	Carl Zeiss, Jena, DE
Cryotome Leica CM1510 S	Leica Biosystems, Nussloch, DE
Digital camera, EOS 1000D	Canon, Tokyo, JPN
Electron microscope, EM109.	Zeiss, Jena, DE
Fluorescence microscope BZ-8000	Keyence, Neu-Isenburg, DE
FLUOstar Optima	BMG Labtech, Ortenberg, DE
LaminAir HB 2472	Heraeus, Hanau, DE
Lab dancer (mini-table vortex)	Avantor (vwr), Radnor, USA
LightCycler® 480 Instrument II	Roche, Basel, Switzerland
light microscope	Olympus CX21, Olympus, Stuttgart, DE
Magnetic mixer D-6011	Neolab Migge GmbH, Heidelberg, DE
Megafuge with swing-off rotor	Thermo Fisher Scientific, Waltham, UK
Microtome	Zeiss, Oberkochen, DE
Micro scale MC5	Sartorius Lab Instruments, Göttingen, DE
Mini-orbital shaker MT52	IKA® Werke GmbH & Co KG, Staufen, DE
Mini-Protean® TetraCell- Electrophorese chamber	Bio-Rad, Munich, DE

Mini centrifuge	Corning, Amsterdam, NL
Microscope, phase contrast Axiovert 135	Carl Zeiss, Jena, DE
Micro scales HM−300	A&D Instruments, Abingdon, UK
Mini-PROTEAN Tetra System	Bio-Rad, Munich, DE
Multiskan™ FC Micro titer plates-Photometer	Thermo Fisher Scientific, Waltham, UK
NanoDrop 2000/2000c Spectrophotometer	Thermo Fisher Scientific, Waltham, UK
Neubauer cell counting chamber	Carl Zeiss, Jena, DE
Peristaltic pump	Heidolph, Schwabach, DE
Peristaltic pump, pump head C4	Heidolph, Schwabach, DE
Peristaltic pump, Cassette small	Heidolph, Schwabach, DE
Pump tube, Tygon®, with 3 plugs, R-3603, Ø-I: 0,25 mm, Ø-A: 2,05 mm, wall thickness: 0,90 mm	Heidolph, Schwabach, DE
Pump tube, PharMed®, with 3 plugs, Ø-I: 0,25 mm, Ø-A: 2,05 mm, wall thickness: 0,90 mm	Heidolph, Schwabach, DE
pH meter 766	Knick, Berlin, DE
Pipettes (10, 100, 1000 µl)	Eppendorf, Hamburg, DE
Plate shaker	Neolab Migge GmbH, Heidelberg, DE
PXi/PXi Touch gel imaging system	Syngene, Cambridge, UK
Tissue-Tek VIP®	Sakura Finetek Europe B.V., Alphen aan den Rijn, NL
Trans-Blot Turbo Blotting System	BioRad, Munich, DE
Rotating water bath SW 23	Julabo, Seelbach, DE
Perfusion plate REINNERVATE®, Alvetex® Scaffold	Reinnervate, Durham, UK
Ultramicrotome, Reichert UltracutS	Leica Microsystems, Wetzlar, DE
Vacuum pump	MerckMillipore, Darmstadt, DE
Vortex 2 Genie	Scientific Industries,
balance 440-33	KERN, Balingen, DE
Water bath	Memmert GmbH, Büchenach, DE

4. Methods:

4.1 Cell culture

Isolation of normal human bronchial epithelial cells (NHBEC)

The Charité received two human lungs from USA. Normal human bronchial epithelial cells (NHBEC) were isolated from trachea, primary and secondary bronchos. The study was approved by the ethics committee at the Charité-Universitätsmedizin Berlin, Germany (projects EA2/079/13).

First the cell culture flasks were precoated with Collagen. 50 mg human placental Collagen Type VI (Sigma-Aldrich, Darmstadt, DE) was mixed with 83,3 ml dH2O and 167 µl glacial acetic acid. The solution was heated up in a water bath by 37 °C, then collagen was placed for 15 min on a stove by 37 °C, a magnetic mixer enhanced the dissolving process (stock 10 x). Afterwards a 1:10 dilution with dH2O and sterile filtration followed (pore size 0,22 µm). For pre-coating, a 7 ml collagen solution was pipetted in T75 flasks and were incubated for 18 h at room temperature (RT).

At day one of the isolation process, the lung was cut and divided into pieces of trachea and bronchi. Trachea and main bronchi were cleared from fat and other tissue parts, while started from proximal to distal. The isolated bronchial branches were cut into 5-10 cm pieces. Additional lung tissue was removed with a scalpel. All parts were washed in phosphate buffered saline (PBS) (Sigma-Aldrich, Munich, DE). The bronchial branches were opened length wise and were cut into 1-2 cm pieces and were washed three times in wash medium (minimal essential medium (MEM), 1 % L-Glutamine, 0.01 % Penicillin/Streptomycin (Pen/Strep)). Afterwards, pieces were transferred into 50 ml tubes, which were filled with 30 ml washing medium (1:10) to reach an end volume of 40 ml. A solution of 0.4 ml Protease/DNase (1 % protease XIV with 0,01 % DNase dissolved in PBS) was added for 36 hours at 4 °C on a rotating incubator (50-60 revolutions per minute (rpm)).

At day three the protocol continued, the 50 ml tube was emptied onto a petri dish (diameter, 150 mm) In the following, the protease was neutralized with MEM (10 % fetal calf serum (FCS). With a scalpel the inside of the bronchial walls were scraped softly (4-5 times). The solution was collected in a 50 ml tube and bronchi pieces were washed with PBS several times and washing-PBS was collected to the 50 ml tubes. The solution was filtered throw a cell strainer in a new 50 ml tube. Then the tubes were centrifuged (1250 rpm, 5 min, 4°C) and the cells were washed with

PBS. Later the cells were counted with a Neubauer counting chamber. The cells were seeded with an amount of 4 x 10^6 NHBEC in the precoated T75 cell flasks, which were pre-washed with PBS. 12 ml of bronchial epithelial growth medium (BEGM) (Lonza, Basel, CH) were added to each T75 cell flask. The cells were cultivated in an incubator (37 °C, 80 % relative humidity, CO_2 5 %) conditions and the medium was changed every second day. The ells grew to 70 % confluency. Then cells were treated with 2 ml Trypsin (0.25 % ethylenediaminetetraacetic acid (EDTA) 1 mM) each T75 cell culture flask for 5 minutes, gentle hand claps at the flask surface helped the detaching process. The process was stopped with 8 ml Hanks´ balanced salt solution (HBSS) (ThermoFisher SCIENTIFIC, Waltham, USA) and 25 % FCS. The solution was passed in a 50 ml tube and centrifuged (1250 rpm, 5 minutes, 4°C). Cells were washed with PBS and counted. 75 x 10^4 NHBEC were dissolved in tissue freezing medium (60 % BEGM, 30 % FCS, 10 % DMSO), 1.8 ml total volume were pipetted into a cryotube, each tube was passed into Mr. Frosty™ freezing container to -80 °C for 24 h. The day after all the tubes were transferred to a nitrogen tank.

Isolation of human skin fibroblasts

For the first trials I used normal human skin fibroblasts (NHDF), which were later replaced with normal human bronchial lung fibroblasts (NHLFb).

Juvenile foreskin was used as specimen to isolate primary (NHDF) (approved by the ethics committee of the Charité-Universitätsmedizin Berlin, Germany, EA1/081/13) using standard protocols. Specimen from donors who did not exceeded age of 10 was used. The specimen was washed three to five times with PBS in a cell culture dish. All fat tissue was detached with a scalpel from the tissue. It was cut into 3 mm pieces by using the scalpel and forceps. Small, cleaned pieces were placed in a second cell culture dish, epidermis upwards and dermis was touching the dish. Dispase working solution (1.2 U/ml) was pipetted on the tissue surface, to detach epidermis from dermis (2.8 ml/cell culture dish). Afterwards cell culture dish was closed, sealed with parafilm, and stored at 4 °C for 18-20 hours. Later the epidermis was able to be stripped off. Dermal pieces were placed upside down in a 6-well plate. For 30 minutes RT dermal pieces attached the plate surface. 1.5 ml fibroblasts growth medium (FGM) were pipetted softly into the well, the dermal pieces sticked onto the surface. The plate was incubated by 37 °C, 80 % humidity, 5 % CO_2. NHDF were growing out of the tissue pieces on the well surface. Every second day the medium was changed softly. Cells were reaching a confluency of 70 % (about 7 days later). Cells were

detached while incubation with 0.5 ml Trypsin (0.25 % EDTA 1 mM) for 5-10 minutes, the enzyme reaction was stopped with 5 ml FGM. Cells were centrifuged (1250 rpm, 5 minutes, RT), washed with PBS and cultured in T25 or T75 cell culture flasks, depending on the pellet size. NHDF (P^0) were cultured to a confluency of 70 %, while changing FGM every second day. Later cells were detached with Trypsin, stopped with FGM, washed with PBS again and counted by using the Neubauer counting chamber. 2.5 x 10^6 cells were reseeded into a T75 tissue flask. The culture process continued till passage 3 (p^3), after cells were detached, stopped, and counted again, 1.25 x 10^6 were diluted in freezing medium (FGM 90 %, DMSO 10 %). The freezing process was performed according to freezing NHBECs.

4.2 Generation of a human-based bronchial epithelium model

The first trials were performed with NHDF, later NHLFb (Epithelix, Geneva, CH) was used. Additionally, NHBEC isolated from the human lung received from United States of America (USA), bought NHBEC from Epithelix (Geneva, Switzerland) and from STEMCELLTechnologies (Vancouver, CAN) and were used for *in vitro* model cultivation.

Primary human lung fibroblasts (Epithelix, Geneva, CH) were cultivated in fibroblast growth medium (Dulbecco's Modified Eagle Medium, 7,5 % fetal calf serum and 5 % L-Glutamine (Sigma-Aldrich, Darmstadt, DE)). Primary NHBEC (Epithelix, Geneva, CH) p^2 were cultivated in bronchial epithelial growth medium (PneumaCult Ex Plus, STEMCELL Technologies, Vancouver, CAN). First, 64.300 NHLFb (p^4) were embedded in bovine collagen I (Cellsystems, Troisdorf, DE) to mimic the matrix of the bronchial epithelium into 12-well inserts. The Collagen was mixed with HBSS, it contained phenol red. Both mixed together, they showed a yellow color, because it indicated an acidic pH about 0.9. It was necessary to titrate the mixture to a red violet color, pH 6.4 with NaOH 2 M, otherwise the fibroblasts did not survive. After titrating the right pH resuspended fibroblasts in fetal bovine serum (FBS) were added to the collagen mix. The proportion was about 1:1:8 (FBS: HBSS: Collagen). 268 µl collagen mix is added to one insert. The plate stays for one hour at RT. Later, one hour of incubation follows in a CO_2 free incubator. Afterwards PneumaCult-Ex Plus Medium is added, 550 µl beneath and 900 µl above the insert. The medium adjusted the correct pH of the collagen matrix, it incubated for 2 hours in 95 % humidity, 5 % CO_2 incubator. 9x10^5 NHBEC were added on top of the matrix, after removing the apical medium. 24 hours later, the entire construct was lifted to the air-liquid interface. The

bronchial epithelium model was then cultured for 21 days in PneumaCult™-ALI Medium (ALI medium) (STEMCELL Technologies, Vancouver, CAN). Medium was changed every second day, a volume of 550 µl was used for each well. To remove excessive mucus, the models were rinsed gently with PBS in the third week of cultivation, on cultivation day 18. At day 21 the bronchial epithelium model was ready for further experiments.

Alternative ECM matrices

The lab of Prof. Dr. Andreas Kurtz, Charité - Universitätsmedizin Berlin, Brandenburg-Berlin Center for Regenerative Therapies (BCRT), produced hydrogel of human lung matrix. The hydrogel was obtained from a human lung from a deceased patient at the Heart Center Berlin, Germany (approved by the ethics committee of the Charité-Universitätsmedizin Berlin, Germany, (project: EA2/079/13)).

The following protocol was performed by the lab of Prof. Dr. Andreas Kurtz. First the lung pieces were decellularized, while lung pieces were placed in 0.1 % sodium dodecyl sulfate (4 h, at RT). Then incubated in 350 IU/ml DNase1 (2 h, at RT) and sterilized in PBS (supplemented with 100 U/mL penicillin and 100 µg/ml streptomycin) for 2 hours. Next, lyophilization of ECM was performed, afterwards ECM powder was redissolved in a pepsin solution of 1 mg/ml (pH 2.0; prepared in 0.01 M hydrochloric acid (HCl)) to obtain a final ECM concentration of 10 mg/ml. The digested ECM solution was then neutralized with 10x PBS (pH 7.4) and 0.1 M NaOH (Hiller, Berg et al. 2018).

The ECM hydrogel was used, instead of bovine collagen 1 according to the human-based bronchial epithelium model protocol. Additionally, different hydrogel dilutions were applied, the hydrogel got mixed with human collagen (Sigma-Aldrich, Munich, DE), 1:100, 1:20, 1:10 and 1:3. The control was pure human collagen with NHLFb. The NHLFb were embedded in the specific mixture of hydrogel and hydrogel/human collagen mixture and it was cultivated for 14 days submerse, 550 µl basal and 200 µl FGM apical.

Self-synthesized ECM with ascorbic acid

NHLFb were stimulated to produce self-synthesized ECM by cell medium with supplemented ascorbic acid. For the first step, some 12-well inserts where precoated with diluted human

collagen. Human collagen (Sigma-Aldrich, Munich, DE) (3 mg/ml) was diluted to 0.1 mg/ml with sterile water. 43 µl of the diluted collagen were pipetted on the insert surface, once apical and once apical and basal. Inserts were dried for 2 hours by room temperature and afterwards rinsed with FGM. Followed, by seeding 1 million NHLFb in 214 µl FGM and were placed into the incubator. 24 hours later, medium was changed to FGM (supplemented with 0.1 % Ascorbic acid). The NHLFb were cultivated submersed for 7 days with FGM + 0.1 % Ascorbic acid, medium was changed every second day. Later, $9x10^5$ NHBEC cells were seeded on top and was cultivated for 21 days according to the human-based bronchial epithelium model.

Human based bronchial epithelial *in vitro* model cultivation with Teflon® ring support

A Teflon® ring (polytetrafluoroethylene) with a diameter of 1 cm, built by the FU Berlin workshop, led by the Physics department, was used to support the cultivation of the bronchial epithelium model. Different approaches were applied. The procedure of preparing the fibroblast and collagen matrix mix was performed according to the human-based bronchial epithelium model protocol. In the following the ring was placed on top of the collagen matrix, after it was soaked with FGM and the pH of the collagen and embedded NHLFb was adjusted. For all model trials the 9×10^5 NHBEC cells (in 900 µl PneumaCult-Ex Plus Medium) were seeded inside the ring, which laid on top of the model base.

In case of model A, 24 hours later the airlift was implemented, and the model was cultured for 21 d. For model B, it was cultured for 7 days submersed and 14 days at an air liquid interface conditions. Model C was cultured 7 days submersed and after performing the airlift the support ring was removed. All models were cultured under incubator conditions and the medium was refreshed every second day.

Human based bronchial epithelial *in vitro* model placed in dynamic system

The model was built and cultured according to the human-based bronchial epithelium model protocol for the first 7 days. At day 8, models were placed in a 6-well perfusion plate (Reinnervate, Durham, UK). In collaboration with the group of Prof. Jens Kurreck from the TU Berlin, his student Alexander Mensch printed a 12-well adapter out of high temp resin cartridge (Formlabs Inc., Moerdijk, NL), to hold a 12-well inserts in a 6-well plate, to assure an air liquid interface. The model

culture continued for 7 days under medium perfusion conditions. The flow rate was 150 µl/min, according to the inspiring publication (Chandorkar, Posch et al. 2017). All settings of the dynamic system were set by Patrick Graff. He used a peristaltic pump with a C4 pump head and a small cassette (Heidolph, Schwabach, DE). He installed a tube system with tubes from type Tygon® and PharMed® (Heidolph, Schwabach, DE) to connect the medium reservoir and the plate. The model was cultured under incubator conditions, the pump was placed outside of the incubator and the tube's out- and input were sealed with parafilm. After 14 days in total the experiment was stopped, and the models were fixed in PFA.

.

Model modulation by testing different inserts, medium, collagen batches, NHBEC sources.

In these trials all models were built according to human-based bronchial epithelium model protocol. Inserts, bovine collagen I batches, model culture medium and NHBEC donors were tested. Two different types of inserts were used, one with 0.4 µm and general used insert with 3.0 µm pore size (Corning, Amsterdam, NL). Two bovine collagen I batches were used for fibroblast collagen base. Different types of a cell culture medium was applied in the models such as, MucilAir™ Culture Medium (Epithelix, Geneva, CH) and established medium PneumaCult™-ALI Medium (STEMCELLTechnologies, Vancouver, CAN). Three NHBEC cell donors were cultivated, self-isolated NHBEC from USA lung, NHBEC (STEMCELLTechnologies, Vancouver, CAN) and NHBEC (Epithelix, Geneva, CH).

Human based vascularized bronchial epithelial *in vitro* model

NHLFb were cultured in 100 % $DMEM^+$ in cell culture flask (2500 cells/cm²). The medium was changed after every 1-2 days to 75 % $DMEM^+$ + 25 % Endothelial Cell Growth Basal Medium 2 (EBM2). Two, three days later, medium was changed to 50 % $DMEM^+$ + 50 % EBM2. After two more days 12-well plates with 12-well inserts (0.4 µm pore size) were used for following model cultivation. Trypsinized NHLFb were centrifuged (5 min/1000 rpm), wash with PBS and centrifuged again (5 min/1000 rpm). 2800 NHLFb were seeded on 0.4 µm pore size inserts (2500 cells/cm^2 growth area) in 500 µl (50 % $DMEM^+$ + 50 % EBM2) into the well. 1500 µl (50 % $DMEM^+$ + 50 % EBM2) were added to the basal side of the well. The next day 5.000-10.000 lung endothelial cells (LECs) /cm² were cultivated in pre-coated tissue flasks (w/ Porcine Gelatin Type A). The medium was changed the next day and afterwards every 3-4^{th} days and were not washed with PBS. LECs

were cultured to confluency of 80 %, then trypsinized with Trypsin reagent pack. LECs were centrifuged, counted, and got resuspended in 50 % DMEM$^+$ + 50 % EBM2. The amount of 11.200 LECs/500 µl were seeded on top of NHLFbs in the inserts (10.000 ECs/cm²). The medium was changed every 2-3 days with 50 % DMEM$^+$ + 50 % EBM2: 1500 µl into the well + 500 µl onto the top of co-culture. NHLFb and LEC were cocultured for 18 days.

NHBEC were defrosted on day 13-14 of the co-culture of NHLFb and LEC. NHBEC were cultured in in PneumaCult Ex Plus (STEMCELL Technologies, Vancouver, CAN) 7.5 x 10^5 NHBEC were seeded T75 culture flask by using 12 ml of PneumaCult Ex Plus. The medium was changed the next day, afterwards every second day. NHBEC were seeded on the 19th day co-culture. Following trypsinization, centrifuging steps and cell count. 0.9 x 10^6 NHBEC on top of the co-culture (900 µl/insert). An airlift was performed 24 hours after seeding NHBECs. The basal medium was replaced with 550 µl of 50 % PneumaCult Ex Plus + 50 % (50 % DMEM$^+$ + 50 % EBM2). The medium was changed every second day (550 µl of 50 % PneumaCult Ex Plus + 50% (50 % DMEM$^+$ + 50 % EBM2). The model was cultivated for 21 days.

4.3 Histology

To analyze model histology, models were embedded in paraffin, performed by the institute of Veterinary Pathology of Freie Universität Berlin under the supervision of Prof. Dr. Joachim Gruber.

After 21 days of model cultivation, the models were collected. The first step cell medium was aspirated from the cell culture plate and then the second step was followed by pipetting apically 100 µl of 4 % PFA to model surface. With forceps, the insert was taken out from cell culture plate, scalpel was used to cut the insert membrane off the insert and the model was collected in a small glass tube filled with 4 % PFA and stored at 4 °C.

Later, it was sent to Prof. Dr. Joachim Gruber's lab. They performed the model embedding into paraffin with Tissue-Tek VIP® (Sakura Finetek Europe B.V., Alphen aan den Rijn, NL), following the procedure in **table 3**, then I got back the paraffin block.

For sectioning paraffin embedded tissue samples microtome (Zeiss, Oberkochen, DE) was used. Tissue sections were cut to 0.5 µm – 1 µm thickness and were collected in water bath at 40-50 °C on object slide. For drying object slides with tissue sections were placed in CO_2 free incubator at 37 °C overnight.

For experiments with nanoparticles tissues were collected as described in previous part and were embedded into Tissue Freezing Medium (Leica Microsystems, Wetzlar, DE), shock frozen in liquid N_2 and stored at -80 °C. At the cryotome (Leica Microsystems, Wetzlar, DE) vertical sectioning of frozen models was performed (7 µm) and collected on object slide and dried at RT.

Solution	Application period [min]
Formalin	60
Water	50
70 % Ethanol	50
80 % Ethanol	50
96 % Ethanol	50
96 % Ethanol	50
100 % Ethanol	50
100 % Ethanol	50
Xylol	50
Xylol	50
Paraffin	50
Paraffin	50
Paraffin	60
Paraffin	60

Table 3. Technical procedure of model embedding into paraffin

Hematoxylin & Eosin (HE) staining

The method is about visualizing cellular morphology of tissue sections. The process is pH dependent, Hematoxylin stains basophilic structures blue/purple as the nuclei and Eosin colors acidophilic structures red/pinkish as cytoplasm.

Procedure of dewaxing, hydration and H&E staining is followed in **table 4**. All slides were dried under the hood. At least one drop of Roti®-Histokit mounting medium was added and was covered with coverslip. The cryosections immediately used after drying and were fixated with 4 % PFA for 5 minutes. Followed by diving the slides in dH_2O for 30 sec, the staining method was continued

as described in **table 4**. Histology of bronchial epithelial sections was analyzed using the microscope BZ-8000 (Keyence, Neu-Isenburg, DE).

	Solution	Application period [min]
Deparaffinization and hydration	Roti®-Histol I	5
	Roti®-Histol II	5
	100 % Ethanol	5
	95 % Ethanol	5
	90 % Ethanol	5
	80 % Ethanol	5
	60 % Ethanol	5
	50 % Ethanol	5
	dH_2O	dipped
H&E staining	Double dH_2O	0.5
	Mayer's Hematoxylin	5 (agitated)
	Tap H_2O	5
	Eosin Y (plus 1 drop Acetic Acid)	0.5
	96 % Ethanol I	2
	96 % Ethanol II	2
	100 % Ethanol I	2
	100 % Ethanol II	2
	Roti®-Histol I	2
	Roti®-Histol II	2

Table 4. Technical procedure of deparaffinization, hydration and H&E staining

Alcian Blue staining

For studying the morphology and containment of mucus produced by the bronchial epithelium models an Alcian blue staining was performed. Alcian blue stained acidic surfaces as acidic polysaccharides such as glycosaminoglycans to blue green color, contained in mucus produced by goblet cells. Nuclei was stained by α-Nuclear to pink reddish color.

Tissue sections were prepared as in **table 4**, deparaffinization and hydrating process, Alcian blue was applied for 30 minutes to stain the tissue sections. Subsequently to several washing steps, counter staining with α-Nuclear red was performed for 5 minutes. Sections were mounted and analyzed as mentioned before.

4.3.1 Immunofluorescence analysis

Immunofluorescence staining visualizes proteins by using a fluorescence microscope for analyses. The technique is used primarily on microbiological samples, to detect the location of specific proteins. The method itself uses specific antibodies which bind to the desired epitope on antigen (target). Primary antibody conjugates to desired epitope and secondary antibody, which is a fluorophore-tagged antibody binds to the primary antibody to build a complex, thus increasing the fluorescent signal during microscopy.

For paraffin embedded tissue sections an antigen retrieval was performed after section hydration (**table 4**). Sections were incubated in citrate buffer (10 mM, pH 6) at 95 °C for 20 minutes. After cooling down, the object slides were washed in PBS for 5 minutes. The tissue section was permeabilized with PBS (supplemented with 1 % Triton X) for 10 minutes. Next, the slides were washed in a washing buffer for 5 minutes (0.02 M PBS, pH 7.2-7.4 + 0.0025 % BSA + 0.025 % Tween 20). Then the tissue sections were blocked with goat serum (1:20) for 30 minutes at RT. Later, the slides were washed with washing buffer. Then the incubation of primary antibody was continued. Desired target antibody was diluted with washing buffer according to **3.4 Antibody**, it contains all antibody dilutions. 400 µl of antibody dilution was pipetted on top of tissue sections and was incubated overnight at 4 °C. Later, the slides were washed three times with a washing buffer, each for 5 minutes. The secondary antibody was mixed accordingly to **3.4 Antibody** and was pipetted on top of tissue sections (400 µl/slide) and incubated for one hour at RT. Afterwards, slides were washed in washing buffer three times. Afterwards, they were washed in PBS for 5 minutes and 1 dip in dH_2O. The object slides were dried, but tissue sections remained wet. The tissue section was stained with DAPI mounting medium and covered with glass cover slide. For

drying the slides were stored at 4 °C for 24 hours. Histology of bronchial epithelial sections was analyzed with microscope BZ-8000 (Keyence, Neu-Isenburg, DE).

For analyzing infection trials with IAV, Influenza A antibody got linked to the chromophore before application by using DyLight™ Microscale Antibody Labeling Kit. The labeling process was performed by following the kit handbook. Primary antibody was diluted in Borat buffer (0.76 M) and PBS to a protein concentration 1 mg/ml in 0.05 M Borat buffer. The antibody dilution was mixed with the Dylight reagent and incubated in the dark at RT for 1 hour, here the protein was labeled. In the following the protein was purified by running through a column. First, the column was loaded with resin, later labeled antibody mix was loaded and collected in tube by using centrifuge (3200 rpm for 45 seconds). The applied antibody was diluted to 1:30 in washing buffer and ready to use.

The tissue section staining was continued according to the previous part. Continuing the full model staining, the model remained in the insert. It was washed with PBS and with 4 % PFA fixed and washed again with PBS three times, each for 5 minutes. Then the model was stained with the antibody (**3.4 Antibodies**) dilution as described before and stayed for the whole procedure in the insert.

Histology of bronchial epithelial sections and full model post IAV infection was analyzed using the confocal microscope (Carl Zeiss, Jena, Germany) by Prof. Dr. Andreas Hocke's lab (Charité, Pneumology and Infectiology, Berlin, Germany). Prof. Dr. Andreas Hocke and Dr. Katja Hönzke performed the confocal analysis.

4.3.2 Transmission electron microscopy (TEM) analysis

TEM visualizes cell compartments with electron transmission. The technique is based on atom density, high atom density is difficult to transmit because the lower the density, the higher is the electron transmission.

The following experiment was performed by Sabine Kaessmeyer (Department of Veterinary Medicine, Institute of Veterinary Anatomy, Freie Universität Berlin) and the method was taken from *R. Balansin Rigon (2018)* and summarized below (Balansin Rigon, Kaessmeyer et al. 2018).

For sample preparation the models were washed with 0.1 M cacodylate buffer (cacodylic acid sodium salt trihydrate, Roth, Karlsruhe, DE) and fixed in Karnovsky's fixative (Merck Eurolab,

Darmstadt, DE) for 1 h at 4 °C. After model fixation, 1 % osmium tetroxide (Chempur, Karlsruhe, DE) in 0.1 M sodium cacodylate buffer was used to postfix the model for 1 hour. Next, samples passed a gradual ethanol series for sample dehydration. The model fixation was performed by embedding sample in a composition of Agar 100 (epoxy resin), DDSA (softener), MNA (hardener), and DMP 30 (catalyst) (all: Agar Scientific, Stansted, Great Britain, UK). Polymerization followed at 45 °C and 55 °C, each for 24 hours. Model was cut into tissue sections (0.5 µm) with an ultramicrotome Reichert UltracutS (Leica Microsystems, Wetzlar, DE) and stained with modified Richardson solution at 80 °C for 45 s. Analysis of tissue sections was performed using a light microscope (Olympus CX21, Olympus, Stuttgart, DE). Later, ultrathin sections were cut to a 70 nm thickness with the UltracutS. Sections were mounted on nickel grids (Agar Scientific, Stansted, Great Britain, UK). Samples were examined to detect the occurrence of ciliated cell structures, goblet vesicles, cell–cell contacts, cell organelles, and cell shapes as well as to analyze ECM organization, distribution, and differentiation using an EM109 electron microscope (Zeiss, Jena, DE). The histology and ultrastructural investigation of the bronchial epithelium model was confirmed by TEM. Photographs were taken and processed using an Adobe Photoshop Program (Adobe System, Unterschleissheim, DE).

4.3.3 Influenza infection at the bronchial epithelium model

Bronchial epithelium model was infected with influenza virus H3N2 (pathogen Panama/2007/1999 (PANIII)) at day 21 of model cultivation. For model preparation 550 µl ALI medium was exchanged with 550 µl ALI medium (without supplemented hydrocortisone) at 24 hours pre infection. At the infection day, virus dilution was prepared freshly. For virus dilution preparation virus H3N2 (pathogen Panama/2007/1999 (PANIII)) stock solution (19.9 x 10^6 PFU/ml) (PFU = plaque forming units) was diluted in PBS to the desired multiplicities of infection (MOI) 0.01. Different MOIs were tested in first trial MOI 1, 0.1 and 0.01. Each model was infected apically with virus dilution (25 µl). Followed by virus incubation for 45 minutes at room temperature. Cell culture plate with models remained under laminar air flow working bench and was shaken every 5-10 minutes. After incubation models were rinsed apically with 150 µl PBS to aspirated model surface. This was timepoint zero. At 2 hours post infection first Zanamivir treatment followed, 13 µl of Zanamivir dilution (Zanamivir in PBS; 0.1, 100 and 1000 nM Zanamivir) was pipetted apically at model surface. At 8 hours post infection, the first sample was collected. The models were rinsed apically

with 150 µl PBS for 5 minutes. The collected sample was diluted to 250 µl, 250 µl sample was aliquoted in several tubes. Apically collected samples were used for plaque assay and enzyme-linked immunosorbent assay (ELISA). The medium sample was collected as well, for mass spectrometry (MS) analysis and ELISA. The medium was replaced with the same volume of fresh ALI medium. While testing Zanamivir concentration in medium, medium was not replaced, timepoints were 2, 8 and 48 hours post treatment. In general, the treatment followed every 12 hours (two times per day). Sample collection took place 8, 16, 24, 48 and 96 hours post infection.

4.4 Analysis

4.4.1 Plaque Assay

To quantify infective influenza virus activity a plaque assay was executed. The idea of the method is that is the virus infects a cell and a cell lysis follows, normally virus moves free to infect the neighbor cells, instead Avicel mix medium was used. It has a high viscosity and keeps the virus stick to its infected cell. The destroyed cell detaches from the plate surface. For visualizing the result, all cells get stained by crystal violet, the detached cell forms a circle and is unstained, called plaque. Through sample dilution and plaque calculating, a virus replication can be computed.

Assay samples were collected 8 hours, 16 hours, 24 hours, 48 hours and 96 hours post infection. Here, samples were collected by rinsing model surface with 150 µl PBS for 5 minutes (apical sample). Samples were diluted to 250 µl PBS, aliquoted and stored by -80 °C. For all time points a serial dilution was prepared in a 96-well plate from 10^{-1} to 10^{-10} in PBS^{++} (0.006 %, 30 % BSA). MDCK cells were cultivated in 12-well plates till cell confluence. The diluted supernatants were pipetted on MDCK cells before cells were washed twice with PBS. Virus dilution (150 µl) incubated for 45 minutes at room temperature and were softly shaken every 10 minutes. Then wells were rinsed with PBS two times afterwards. For cultivation 1 ml Avicel mix medium (for 10 ml: 4.86 ml Avicel medium, 4.86 ml 2 x MEM, 66.7 µl BSA-Stock, 100 µl $NaHCO_3$-Stock, Dextran-Stock) was added and were placed for 48 hours in an incubator (37 °C, 5 % CO_2). In the final step cells were rinsed with PBS twice and stained with crystal violet to visualize plaques.

Avicel Suspension (2.5 %) for 500 ml:

12.5 g	Avicel
500 ml	dH_2O

2 hours on a magnet mixer, highest level.
suspension: milky, white
steril autoclaved (115 °C, 101 kDa, 10 min)

MEM-Medium (2 x) for 500 ml:

9.53 g	MEM
2.2 g	$NaHCO_3$
500 ml	dH_2O

MEM mixed with 80 % dH_2O on a magnet mixer, highest level. Powder solved, $NaHCO_3$ was added. PH was titrated with HCl to pH 7.2. Medium placed into measuring cylinder, volume filled up to 500 ml. Sterile filtration in sterile bench (pH=7).

Crystal violet solution (staining solution)

Solution A		Solution B	
20 % 6 mg	EtOH Crystal Violet	10 %	Formaldehyde
Solution A + B (1:10) were mixed under a hut.			

Table 5. Crystal violet solution

$NaHCO_3$-Stock (5 % w/v)

2 % $NaHCO_3$ dH_2O solved,
sterile filtration in sterile bench.

Dextran-Stock (1 % w/v)

1 % Dextran dH_2O solved,
sterile filtration in sterile bench.

TPCK Trypsin-Stock (0.1 mg/ml)

5 mg Trypsin solved in 5 ml dH_2O (for injection) solved.

BSA-Stock (30 % w/v)

BSA was ready to use.

4.4.2 LDH Assay

Lactate dehydrogenase (LDH) Assay investigates cell damage. LDH is a common cell enzyme and has a high stability. If cell harming takes place, it is detected in cell plasma/serum. In nanogels application, basal medium sample was collected, 6 hours post infection. As positive control, one model was treated with 10 % Triton X for 3 hours, as negative control medium sample was collected of uninfected and untreated model. For analyzing samples, the CytoTox-ONE™ Homogeneous Membrane Integrity Assay Kit (Promega, Madison, Wisconsin, USA) was used and fluorometric measured. Samples were mixed with lactate and NAD+, the LDH release reacts with both to pyruvate and $NADH+H^+$. Resazurin was added as substrate and reacts with $NADH+H^+$ and forms Resorufin, it is detectable with a 384-well fluorometer. The intensity correlates with the amount of tracked protein.

4.4.3 MTT Assay

The cell viability was measured by MTT Assay, a colorimetric assay. NAD(P)H-dependent cellular oxidoreductase enzymes is addressed to reflect the number of viable cells. This enzyme reduces tetrazolium (MTT: 3-(4,5-dimethylthiazol-2-yl)-2,5-diphenyltetrazolium bromide) to formazan, which shows a purple color. Damaged cells contain a low number of this enzyme, a color reaction is quite little.

At 8 hours, 24 hours, 36 hours, 48 hours and 96 hours post infection, models were treated with MTT. MTT solution of 0.5 mg/ml in PneumaCult™-ALI Medium was prepared. At specific time point basal medium of the bronchial epithelium model was replaced with MTT solution and incubated with MTT solution for 4 hours, 37 °C, 5 % CO_2. For every timepoint the model for positive control and as negative control was treated identically. Positive control model was treated with 10 % Triton X for 3 hours and negative control was uninfected and untreated model. Later, models were collected and stored in a tube with acid isopropanol (500 µl, Isopropanol = 0.04 N HCl), vortexed and incubated for 4 hours in the dark, to extract formazan. To measure the result, sample was pipetted in 96-well to measure formazan by 520-570 nm with a microplate reader.

4.4.4 Enzyme linked immunosorbent assay (ELISA)

Enzyme linked immunosorbent assay (ELISA) is an immune assay. Target macromolecule is immobilized by binding at an antibody connected to 96-well plate. It complexed with a second antibody which is linked to an enzyme. The enzyme activates a color reaction which can be measured and quantify the target molecule amount. Culture medium sample of the trans well (basal side) and apical samples of the bronchial epithelium model were collected. For testing apical protein release, surface was washed with PBS for 5 minutes and was collected. The CC16 protein was tested in apical and basal samples using precoated ELISA Kit (Biomatik, Cambridge, CAN). For the following proteins apical sample was analyzed. IFN-ß-1 was quantified by using the VeriKine-HSTM Human Interferon beta TCM ELISA Kit (pbl ASSAY SCIENCE, USA), IFN-λ-1 was tested with the Human IFN-λ-1 uncoated ELISA Kit (ThermoFisher SCIENTIFIC, Waltham, USA). Human IL-1β tested with uncoated ELISA Kit (ThermoFisher SCIENTIFIC, Waltham, USA). Uncoated ELISA Kit, the 96-well plate was pre-coated with capture antibody overnight. Other Kits were ready to use. Analyses were proceeded by following the manufacture handbook. Applied standard and samples bound to the capture antibody which connected to the well-surface. A second antibody, which is horseradish peroxidase (HRP) linked attached as well to the target, a complex was formed. By adding 3,3',5,5'-tetramethylbenzidine (TMB) the visual reaction started, it oxidated by HRP and showed detectable signals, intensity correlated with the amount of tracked protein. To quantify the signal a micro plate reader was used with a 450 +/- 10 nm filter.

4.4.5 Real time polymerase chain reaction (RT-PCR) – Array

Method is based on the polymerase chain reaction (PCR) and is combined with a spectrofluorometer, which measures continuously the signal of intercalated SYBR Green during the whole process (real time). It monitors the CT (cycle threshold) values to calculate changes in gene expression.

First step was the total RNA isolation. Here, the collected model was placed into 500 µl Trizol by using the hut and was stored by -80 °C. The day of PCR performance, sample thawed on ice. Tubes were centrifuged by 1000 RPM. Supernatant discarded in Trizol trash and 500 µl EtOH were added, vortexed and transferred into RNase free tube. For detection, the gRNase-free DNase Set (50) Qiagen Set was used and according to manufacturer's handbook the isolation was proceed. Sample was pipetted on tube column and centrifuged at 8000 RPM, to let the RNA

bind on the column. 400 µl washing AW1 buffer was added to the column and centrifuged at 8000 RPM. Next, 400 µl of the washing AW2 buffer were added and centrifuged at 8000 RPM. Then the mini column transferred on a fresh tube, 400 µl Elute was added and centrifuged at 8000 RPM to collect the RNA. Pure nucleic acid was collected in vial.

Nanodrop was used to check RNA amount, by using 1.5 µl purified RNA. The cDNA preparation from purified RNA was performed with RT^2 First Strand Kit (Qiagen, Hilden, DE). Then, cDNA and RT^2 SYBR Green Master were mixed (includes already dNTPs, Primer, DNA Transcriptase).

A customer prepared plate was used, Custom RT^2 Profiler PCR Array (Qiagen, Hilden, DE) (**table 4**) and the cDNA and Master mix was aliquoted into the plate. Later, the experiment was run with the LightCycler 480 II (Roche, Darmstadt, Germany). mRNA expression data were normalized to GAPDH and analyzed by using the 2−ΔΔCT method.

PCR Cycler settings

Cycle conditions

Cycle	Duration	Temperature	
1 x	10 min	95 °C	HotStart DNA *Taq* Polymerase is activated by this heating step
1 x	15 sec.	95 °C	Perform fluorescence data collection
45 x	1 min	60 °C	

Heating ramp rate 1.5 °C/sec

96-Well Plate or 100-Well Disc Custom PCR Array Template	number	Gene Symbol	Gene Reference Sequence	
	1	IFN-α1	NM_024013.2	
	2	IFN-α2	NM_000605.3	
	3	IFN-α4	NM_021068.2	
	4	IFN-α5	NM_002169.2	
	5	IFN-α6	NM_021002.2	
	6	IFN-α7	NM_021057.2	
	7	IFN-α8	NM_002170.3	
	8	IFN-α10	NM_002171.2	
	9	IFN-α13	NM_006900.3	
	10	IFN-α14	NM_002172.2	
	11	IFN-α16	NM_002173.2	
	12	IFN-α17	NM_021268.2	
	13	IFN-α21	NM_002175.2	
	14	IFN-β-1	NM_002176.3	
	15	IFNω-1	NM_002177.1	
	16	IFN-ε	NM_176891.4	
	17	IFN-γ	NM_000619.2	
	18	IFN-λ1	NM_172140.1	
	19	IFN-λ2	NM_172138.1	
	20	IFN-λ3	NM_172139.2	
	21	IFN-λ4	NM_001276254.2	
	22	DDX58	NM_014314.4	
	23	IRF7	NM_001572.5	
	24	IFIT1	NM_001548.5	
	25	OAS1	NM_016816.4	
	26	BST2	NM_004335.4	
	27	MX1	NM_001144925.2	
	28	GAPDH	NM_002046	Housekeeping gene
	29	ACTB	NM_001101	
	30	HGDC	SA_00105	Human genomic DNA Ctrl

	31	RTC	SA_00104	Reverse Transcriptase Ctrl
	32	PPC	SA_00103	Positive PCR Ctrl

Table 6. 96-Well Plate or 100-Well Disc Custom PCR Array Template

4.4.6 Analysis of Zanamivir via Mass Spectroscopy

For quantification of Zanamivir in the basal medium of the bronchial epithelium model, I cooperated with Dr. Jan Joseph, who performed the analysis by Mass spectrometry at Freie Universität Berlin.

The samples were separated in Merck SeQuant ZIC-HILIC columns (100 mm x 2.1 mm, 3.5 µm) at 30 °C with an Agilent Infinity 1290 II liquid chromatography system and injected on an Agilent 6495 triple quadrupole with attached Jet Stream source (Agilent). Elution from the column at a constant flow rate of 0.500 ml/min with gradient mixture of solvent A (10 mM NH_4Ac in water) and solvent B (absolute Acetonitrile) was performed as follows: 70 % B for 0.5 minutes to 60 % B in 0.1 minutes for 0.9 minutes, to 70 % B at 1.6 minutes, 2.4 minutes hold, 1 minutes post-time. Standard source parameters for Zanamivir detection were stablished by injection of 1µL of 1 µg/ml Zanamivir in ACN/H2O (50/50, v/v) prior to analysis of our experiments. The following optimized parameters were chosen: Gas temperature of 120 °C and flow of 15 l/min, nebulizer at 40 psi, sheath gas temperature of 390 °C and flow of 12 l/min, capillary at 2000 V, 0 V at the nozzle, and HPRF and LPRF 130 V and 80 V, respectively. Zanamivir was quantified by multiple reaction monitoring (MRM) transition of precursor ions analyzed in positive polarity and fragmented with 20, 32 and 70 units of collision energy.

To detect Zanamivir tracks in the basal medium, all samples had to be cleaned by cartridges (Oasis® HLB Cartridge 1 cc/10 mg, Waters, Frankfurt am Main, DE). For a better quantification, Oseltamivir Carboxylate (4R-(acetylamino)-5S-amino-3R-(1-ethylpropoxy)-1-cyclohexene-1-carboxylic acid) (Cayman Chemical, Michigan, USA) as an internal standard was applied to all samples. Followed by the sample preparation 5 µl Oseltamivir Carboxylate (0.1 ng/ml) was added and to support the liberation of Zanamivir a base milieu was adjusted by adding 5 µl NH_3 (5 %). To proceed with the purification the cartridges were placed in a vacuum chamber of 5 Hg, the pump was started by applying the solvent and that the cartridges never went dry. First, the cartridges were conditioned with 100 µl MeOH and equilibrated with 100 µl H_2O (deionized water).

Next, the sample got loaded and after it was washed with 100 µl H2O (deionized water plus 25 % MeOH) and run through and at last for eluted out the sample 100 µl MeOH were added. Collected samples were evaporated by 80 °C and 1-2 bar of N_2. The sample got reconstituted in ACN/H_2O (50/50, V/V). A 96 well plate was loaded with the standard and all samples to run the Mass spectroscopy.

4.4.7 Model treated with nanogels

The bronchial epithelium models were treated with degradable and non-degradable NGs. 17 µl NGs were applied apically to the model. The treatment duration was 3 hours and 6 hours, models were placed in incubator for incubation. Later, models were fixed by preserving them in tissue freezing medium. Before, models were cut off the inserts with a scalpel and transferred in a small plastic box for freezing. The plastic box was filled with tissue freezing medium, 20 % of volume. Then, the model was added and a second layer of tissue freezing medium was applied to cover full model. The plastic box was placed into liquid nitrogen for a few minutes with the help of using forceps to freeze model. The box was wrapped with aluminum foil and stored by -80 °C. 24 hours later cryo-sectioning was performed on a cryotome, tissue sections were cut to a thickness of 10 µm and collected on an object slide. For the tissue fixation, models had to be dried at RT and then for one minute fixed in PFA at RT. Followed by counterstaining of DAPI and cover slides covered object slide and transferred in fridge for minimum 24 hours for drying. After drying slides were ready for fluorescence-based analysis.

Degradable nanogels	**Non-degradable nanogels**
PNIPMAM-(S-S) -dPG (labelled with RhodB) c (nanogel) 10 mg/ml	PNIPMAM-dPG (labelled with RhodB) c (nanogel) 10 mg/ml
PNIPMAM-(S-S) -dPG c (nanogel) 10 mg/ml c (ETN) 0.7 mg/ml	PNIPMAM-dPG (labelled with RhodB) c (Nanogel) 10 mg/ml c (ETN) 0.67 mg/ml
Negative control	
ETN diluted in PBS c (ETN) 0.7 mg/ml	

Table 7. Nanogel compositions

4.4.8 NHBEC transfection with LNPs

1.3 x 10^3 NHBEC per well were seeded in 96-well micro titer plate for a fluorescence-based assay, in Pneuma Cult Ex Plus for 24 hours, cells were cultured by incubator conditions to confluency of 70 %. For transfecting NHBEC different LNPs were used: DSPC (1,2-distearoyl-sn-glycero-3-phosphocholine), DOPC (1,2-(cis, cis-9,12-octadecadienoyl)-sn-glycero-3-phosphocholine), DOPE (1,2-dioleoyl-sn-glycero-3-phosphoethanolamine), ES (egg sphingomyelin) and DSGP (di-stearoyl-phosphatidylglycerol). They were combined with different amounts of PEG (0.5, 1.5, 5 %) and siRNA (0.1, 0.3, 1 µg/ml) and all were combined with and without ApoE.

LNP dilution	**siRNA dilution**
20 µl LNP + 30 µl acetate buffer	1.23 µl siRNA + 498.77 acetate buffer

Stock solution of each LNP

1275 µl media (Pneuma Cult Ex Plus) + 11.7 µl LNP dilution

LNP solution (final)

w/o ApoE (0.5 %)			w ApoE (0.5 %)		
5 % PEG **+** 0.1 % siRNA 0.3 % siRNA 1.0 % siRNA	1.5 % PEG **+** 0.1 % siRNA 0.3 % siRNA 1.0 % siRNA	0.5 % PEG **+** 0.1 % siRNA 0.3 % siRNA 1.0 % siRNA	5 % PEG **+** 0.1 % siRNA 0.3 % siRNA 1.0 % siRNA	1.5 % PEG **+** 0.1 % siRNA 0.3 % siRNA 1.0 % siRNA	0.5 % PEG **+** 0.1 % siRNA 0.3 % siRNA 1.0 % siRNA
+ DSPC DOPC DOPE ES DSGP					

Table 8. LNP solution composition

Samples were run in triplicates and as negative control wells were treated with PBS. The plate was aspirated and washed twice with PBS, then cells were treated with one of the final LNP solution (100 µl) for 24 hours. The next day the plate was aspirated and washed three times. All cells were fixes in 3 % PFA for 30 minutes. To assess the transfection efficacy high content screening was used, the cell nuclei was counterstained with Hoechst 33324 (1:2000 in PBS). The dye was incubated for 10 minutes, all wells were aspirated and washed three times with PBS. Plate was wrapped in aluminum foil and stored in a fridge till analyzing with a Cellomics Array Scan VTI (Thermo Scientific).

4.4.9 Curcumin application to model

The curcumin solution was synthesized by the lab of Prof. Dr. Shyh-Dar Li, who works in targeted drug delivery and nanomedicine at the UBC, Vancouver Canada. I received a curcumin solution in a desired composition (**table 7**). Curcumin was apically applied to bronchial epithelium models, with a volume of 17 µl. The model was collected 6 hours and 24 hours post curcumin application. Later, model fixation was done by preserving them in tissue freezing medium. Models were cut off the inserts with a scalpel and transferred in small plastic box for freezing. The plastic box was filled with tissue freezing medium, 20 % of volume. Then, the model was added and a second layer of tissue freezing medium was applied to cover the full model. The plastic box was placed into liquid nitrogen for a few minutes by using forceps to freeze the model. The plastic box was wrapped with aluminum foil and stored by -80 °C. 24 hours later cryo-sectioning was performed on a cryotome, tissue sections were cut to a thickness of 10 µm and collected on an object slide. For the tissue fixation, models had to be dried at RT and then for one minute fixed in PFA at RT. Followed by counterstaining of DAPI and the slides were closed with cover slip and dried in the fridge for minimum 24 hours. After drying slides were ready for fluorescence-based analysis.

Curcumin solution composition:

		[mmol/l]	[mg/ml]
First trial	Curcumin	0.065	0.024
	Tween80	0.943	1.234
	Cholesterol	2.734	1.057
Second trial	Additional fluorescent marker:		
	DiE (Ex 549, Em 565)	0.038	0.035

Table 9. Curcumin solution composition

The particle size is 71.5 nm, PDI 0.09 in HBS (pH 7.4)

5. Results

5.1 Development of the human based bronchial epithelial *in vitro* model

Alternatives to animal models in preclinical trials as the human based 3D *in vitro* model has highlighted the need due ethical reasons along with the distinct difference in the anatomy and physiology of animals and humans, which had led to different results. This has been recognized in previously collected data from preclinical to clinical studies by the translation from animal to human. The motivation of developing the bronchial epithelium model is to reduce this gap. Primary, it is about establishing the human based bronchial epithelium model. Guiding reference was established by the method to cultivate human based full thickness the skin *in vitro* model (Küchler, Henkes et al. 2011, Hönzke, Wallmeyer et al. 2016, Löwa, Vogt et al. 2018). Different parameters were tested to find perfect conditions to cultivate *in vivo* like bronchial epithelium model. Model cultivation was divided into five steps (**figure 7**): A) embedding fibroblasts in collagen matrix, B) submerged with cell medium, C) seeded NHBEC on collagen matrix submersed in culture medium, D) airlift performed, E) cell differentiation during model cultivation. Several tests were performed to find ideal culture conditions.

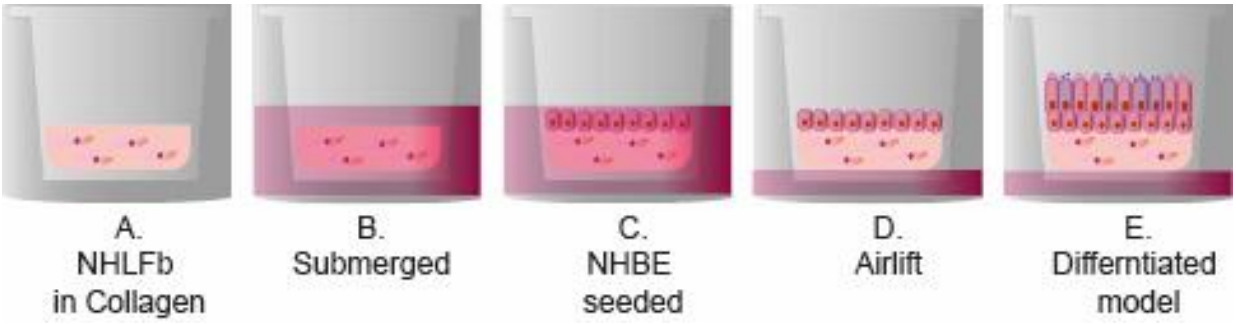

Figure 7. Human based bronchial epithelium model development. Step A, NHLFb embedded in bovine collagen 1, incubated for 2 hours in a CO2 free incubator. B, Collagen matrix got submerged with FGM for 2 hours by incubator conditions. C, NHBE cells seeded on the collagen surface, medium change to PeumaCult-ExPlus medium, for 24 hours under submerged conditions. D, 24 hours later the airlift got performed and medium change to ALI medium, the differentiation process took place for 21 days, E.

Some changes from the skin model protocol were already established; half the volume of collagen mix 268 µl instead of 536 µl and double the number of fibroblasts 64.000 instead of 32.000 were used. Followed by testing the NHBEC number, timepoint for airlift performance and cultivation duration. These parameters were expected to influence cell differentiation and morphology of bronchial epithelium model. Skin fibroblasts in the passage 4 (p^4) and NHBEC p^2 were used for model cultivation. For testing epithelial cell number 1 x 10^5, 5 x 10^5 and 9 x 10^5 NHBEC were trialed. The model with 1 x 10^5 NHBEC, airlift was performed 72 hours post seeding and models with 5 x 10^5 and 9 x 10^5 NHBEC airlift was performed 24 hours post seeding. All models were cultivated 14 and 21 days in an incubator (37 °C, 5 % CO_2). Tissues were H&E stained and immune stained against MUC5AC, mucus protein that indicates goblet cells (Thornton, Rousseau et al. 2008) and uteroglobin (UG) a protein that showed club cells (Rokicki, Rokicki et al. 2016). It resulted that all models presented two compartments, lamina propria out of collagen embedded fibroblasts and epithelium of NHBEC as expected for a full thickness model. There were no significant differences in the applied parameters as NHBEC number, timepoint of airlift performance and cultivation time (**figure 8,** A.1.1- 2.2, B.1.1-.2.2). All showed similar tissue histology. Analysis did not identify characteristic bronchial tissue structure. It did not exhibit basal monolayer and epithelial cells of prismatic morphology as observed in naive human bronchial epithelium (Wang, Lai et al. 2006). Immune fluorescence staining did not show positive signal for goblet and club cells, probably no cell differentiation to characteristic bronchial epithelial cells as goblet and club cells took place. Interestingly, epithelial compartment showed several layers of flat NHBEC. Most epithelial cells were lying in dense layers and cuboidal cells formed basal layer, it reminded to skin histology. Except histology of model with 9 x 10^5 NHBEC (**figure 8**, C). It might show some differentiated NHBEC, also positive signal of mucus and uteroglobin was confirmed after three weeks of cultivation (**figure 8**, C.2.1, C.2.2). It underlined the importance of cell number and the cultivation duration of three weeks emphasized too. Bronchial epithelium morphology was still missing.

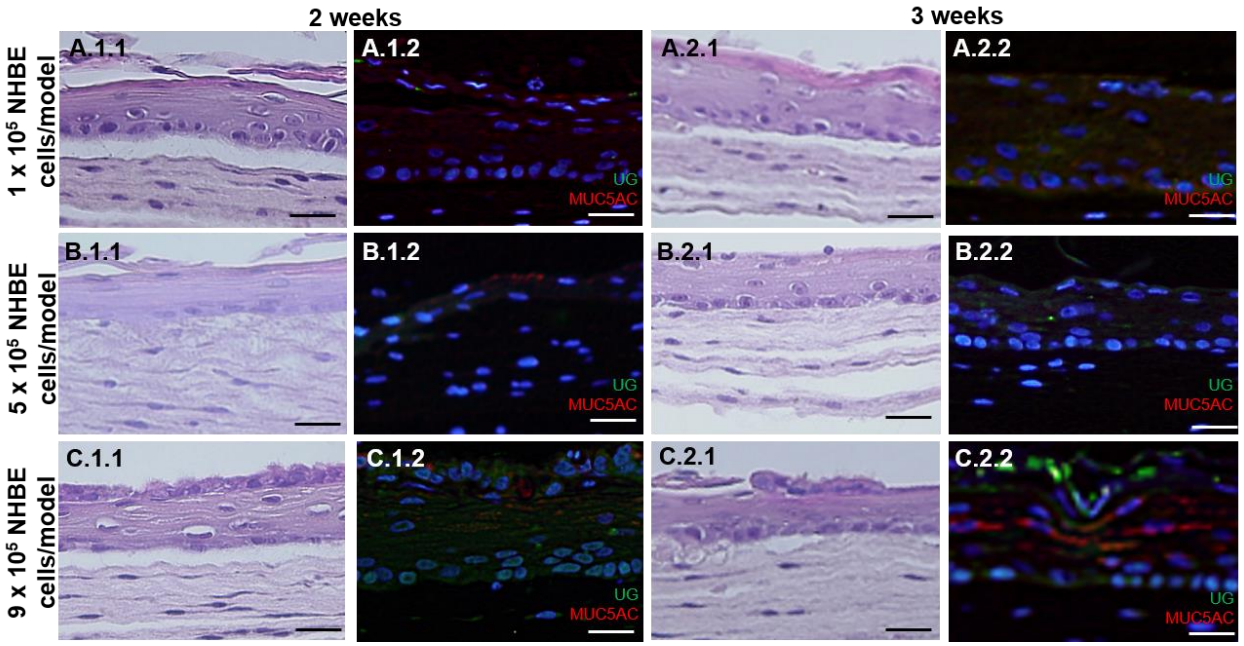

Figure 8. Bronchial epithelial *in vitro* model with NHDF and NHBEC. Development of bronchial epithelium model. with NHBEC and skin fibroblasts and tested different parameter. A.1.1, 1.2, 1 x 10^5 NHBEC were cultivated for 2 weeks. A.2.1, 2.2, 1 x 10^5 NHBEC were cultivated for 3 weeks. Airlift was performed 72 days post seeding. B.1.1, 1.2, 5x10^5 NHBEC were cultivated for 2 weeks. B.2.1, 2.2, 5 x 10^5 NHBEC were cultivated for 3 weeks. C.1.1, 1.2, 9 x 10^5 NHBEC were cultivated for 2 weeks. C.2.1, 2.2, 9x10^5 NHBEC were cultivated for 3 weeks. Airlift was performed 72 days post seeding. Representative histological H&E staining and immunostaining against mucin (MUC5AC), indicates goblet cells and uteroglobin (UG), indicates club cells, scale bar = 100 µm (A, B, C. 1.1 and 2.1), scale bar = 200 µm (A, B, C, 1. 2 and 2. 2). Nuclei were counterstained with DAPI (blue fluorescence). N=2.

The positive impact of the NHBEC number, the tested cultivation time and the timepoint of airlift for bronchial like morphology remained unclear. All models presented a skin like tissue morphology (**figure 8**), probably because of using skin fibroblast. The influence of fibroblasts source was tested in the following part. Skin fibroblasts were exchanged with primary human lung fibroblasts (NHLFb) and previous trials were repeated. The NHBEC number was tested again, 5 x 10^5 and 9 x 10^5 NHBEC were applied and the cultivation time at an air liquid interface for 14- and 21-days was tested. Additionally, different protocols were trialed, as seeding fibroblasts on supportive Alvetex® scaffolds (12-well inserts) (Reprocell, Beltsville, USA). The used scaffolds promised a better cell organization (Marrazzo, Maccari et al. 2016), here inserts were precoated with Puramatrix (BD Falcon) (0,8 mg/ml). The model grown on a scaffold was cultivated for 7 days submerged, then the cultivation continued for 14 and 21 days at an airlift interface. More bronchial epithelium like morphology was desired. The bronchial epithelium is characterized with a basal monolayer, it is attached to prismatic erected epithelial cells (Nichols, Niles et al. 2014). NHBEC differentiation was expected into goblet cells, ciliated and club cells (Wickström, Davies et al. 1998, Rokicki, Rokicki et al. 2016, Bustamante-Marin and Ostrowski 2017).

The histology of scaffold cultured models showed diffuse distributed fibroblasts in the scaffolds independent of cultivation time and NHBEC number (**figure 9**, A.1,2, B.1,2). Further, NHBEC did not show desired prismatic epithelial cell organization by scaffold support. 5 x 10^5 NHBEC presented a thinner epidermal layer than the model with 9 x 10^5 NHBEC independent of cultivation time (**figure 9**, 2.C, 2 D). Immunofluorescence staining showed positive results of a MUC5AC signal just for 9 x 10^5 NHBEC (**figure 9**, 2 C.2, D.2). It indicated goblet cells. The model with an air lift cultivation for 21 days presented soft fluorescence signal was reported (**figure 9**, 2 D.2). Uteroglobin was not detected, probably no club cell was differentiated in any model that was seeded in a scaffold.

In parallel, the previous trial (**figure 9**) was repeated, with lung fibroblasts seeded into a collagen matrix (**figure 10**, 2, E.1-H.2). As before cell number of NHBEC (5 x 10^5, 9 x 10^5) and culture duration for 14 and 21 days at an air liquid interface were tested. **Figure 9**, E.1 and 2 and F.1 and 2 showed models with 5 x 10^5 NHBEC. The epithelial layer was quite thin and NHBEC were not prismatic erected as expected by NHLFb influence independent of the culture duration. NHBEC number seemed to be too little. Immunofluorescence staining showed in both groups a positive signal for MUC5AC. In contrast analyses of models build with 9 x 10^5 NHBEC and NHLFb independent of cultivation time, the morphology (**figure 9**, G.1) presented a prismatic growth of NHBEC and a basal monolayer was recognized in the epithelium. At 21 days a prismatic erected

cell shape of NHBEC was clearly identifiable, as well as basal monolayer (**figure 9,** H.1). Additionally, thick mucus layer was secreted by goblet cells. Goblet cell expression was proofed by strong signals of MUC5AC (**figure 9**, H.2). Even uteroglobin was detected. The research concluded that completely evolved bronchial epithelial tissue needed 21 days of growth, additionally high density of NHBEC as 9 x 10^5 cells and lung fibroblasts to differentiate into characteristic bronchial epithelium cells. All was necessary to develop fully differentiated functional 3D-tissue.

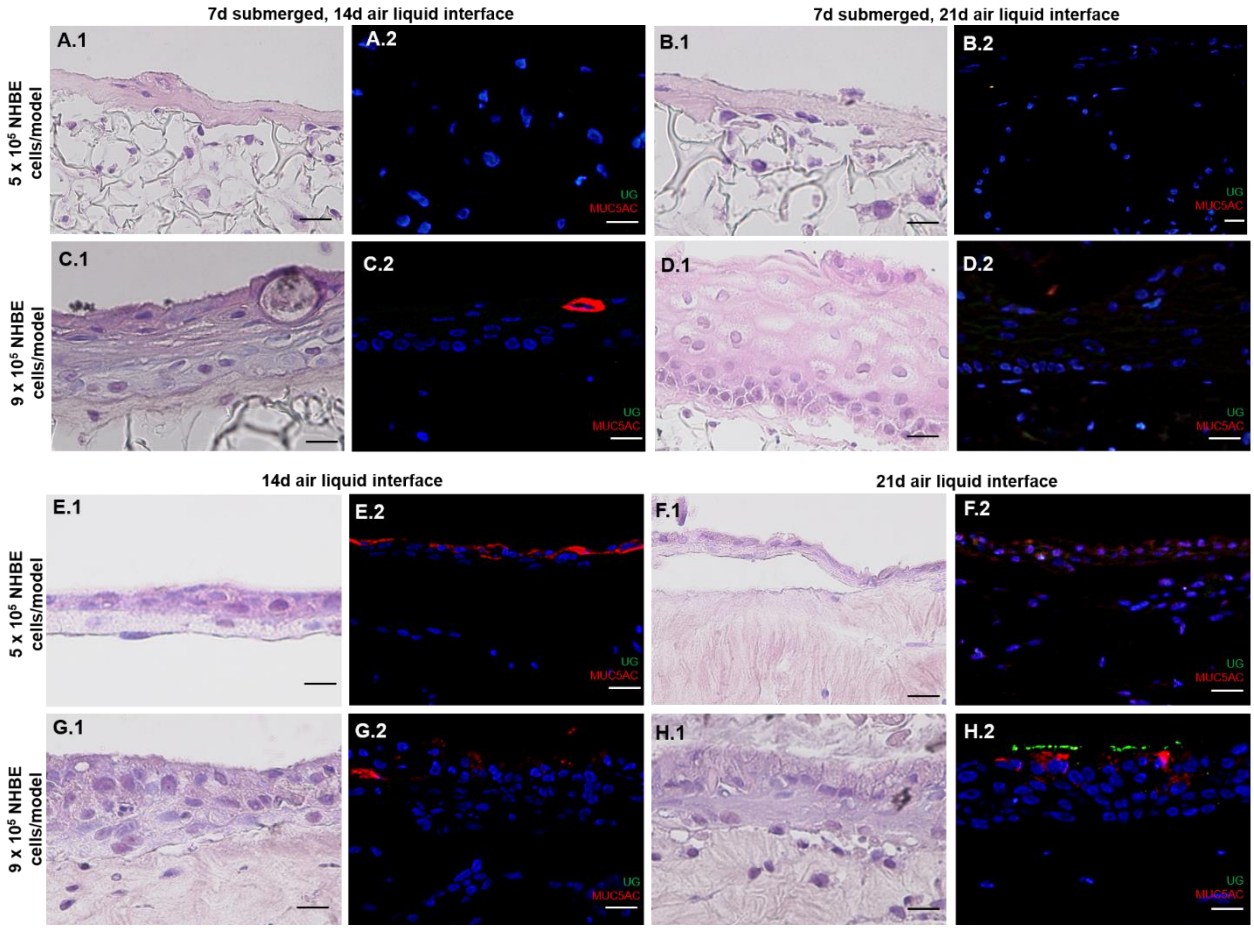

Figure 9. Bronchial epithelial *in vitro* model with NHBEC and NHLFb and different protocols. Representative images were H&E and immune stained against MUC5AC (mucin), indicated goblet cells and UG (uteroglobin), proofed club cells. Nuclei were counterstained with DAPI (blue fluorescence). All models were cultivated with NHLFb and NHBEC. A.-D. 1, 2 models were cultivated on scaffold, air lift was performed 7 days post NHBEC seeding. A.1, 2, 5 x1 0^5 NHBEC were seeded and cultivated for 14 days. B. 1, 2 5 x 10^5 NHBEC were seeded and cultivated for 21 d. C.1, 2 9 x 10^5 NHBEC were seeded and cultivated for 14 days. D.1, 2 9 x 10^5 NHBEC were seeded and cultivated for 21 days. E.-H. 1, 2 models were cultivated on 0.3 µm inserts, air lift was performed 24 hours post NHBEC seeding. E.1, 2 5 x 10^5 NHBEC were seeded and cultivated for 14 days. F.1, 2 5 x 10^5 NHBEC, cultivated for 21 days. G.1, 2 9 x 10^5 NHBEC were seeded and cultivated for 14 days. H. 1, 2 9 x 10^5 NHBEC were seeded and cultivated for 21 days. Scale bar = 100 µm.

The use of human lung fibroblasts (NHLFb), 9 x 10^5 NHBEC and 21 days of cultivation influenced the epithelial differentiation process. Tissue section's morphology presented prismatic erected cells, mucus production through goblet cells, uteroglobin secreted by club cells and probably ciliated cells (**figure 10**, H1, 2). The morphology showed *in vivo* like bronchial epithelium. Proof of characteristic cell structures were tested via staining protocols in following manner. Alcian blue stained acidic glycoproteins blue/green presented produced mucus from goblet cells (Meyerholz, Rodgers et al. 2009). Immunofluorescence maker against acetylated tubulin was applied; it is found in cilia of ciliated cells (Wu, Du et al. 2009). Marker against pan-cytokeratin (keratin 4, 5, 6, 8, 10, 13, and 18) indicated cell differentiation to epithelial tissue, it provides protective stability of cell construct as cytoskeleton (Franke, Schiller et al. 1981, Herrmann, Bär et al. 2007). Zonula occludens-1 is a tight junction protein, it connects cells as peripheral membrane protein (Stevenson, Siliciano et al. 1986, Cleo Leung 2012). These characteristic markers were expected to be detected in tissue sections of the bronchial epithelial *in vitro* model. In parallel I tested the impact of model rinsing to support muco-ciliary clearance. Previous trials showed an immense mucus production (**figure 10**, H). *In vivo* mucus gets transported out of bronchial airway, but *in vitro* model provided closed system and mucus removal through cilia movement alone was not possible. Epithelial cell growth looked hampered through the thick mucus layer, probably rinsing with PBS supports prismatic erect cell shape. Models were built according to last improvements, use of NHLFb embedded in bovine collagen type I, 9 x 10^5 NHBEC seeded on top, airlift performed at 24 hours post seeding and cultivated for 21 days. Models were rinsed gently with PBS; control model was not rinsed (**figure 10**, A. 1-5), model was rinsed twice (**figure 10**, B.1-5) and model was rinsed once (**figure 10**, C. 1-5). For histology analysis H&E, Alcian blue and immune staining was performed.

It resulted that an immense mucus production was observed in the model which was not rinsed, which was visible through green/blue stained mucus on the apical surface (**figure 10**, A.2). Already **figure 10**, A.1 implied the assumption of high mucus secretion during H&E staining. Rinsed models (**figure 10**, B, C) showed mucus reduction, just goblet cells exhibited a mucus reservoir and a thin mucus layer on epithelial surface. Regarding the morphology of the twice rinsed model, it showed down kept epithelial cells (**figure 10**, B.1,2), compared to the once rinsed model (**figure 10**, C.1,2). Its epithelium presented a more prismatic erected epithelial cell shape. Immunostaining indicated for all models ciliated cells with positive signals of acetylated tubulin (**figure 10**, A-C.3). All surfaces were rich in cilia expression. Differentiation to epithelial cells by forming branching cytoskeleton was proven by antibody staining of Pan-Cytokeratin (keratin 4, 5, 6, 8, 10, 13, and

18) (**figure 10**, A-C.4). Also, a response to ZO-1 was positive for all models (**figure 10**, A-C.5). It exhibited that a set of analyses confirmed bronchial epithelial tissue with mucus production, ciliated surface, pan-cytokeratin expression, and ZO-1 detection. Favored epithelial cell shape was observed by the once rinsed model during the last cultivation week, it showed reduced mucus in comparison to the other models, and it exhibited the most erected cell shape. Additionally, in the same model a basal monolayer was detected.

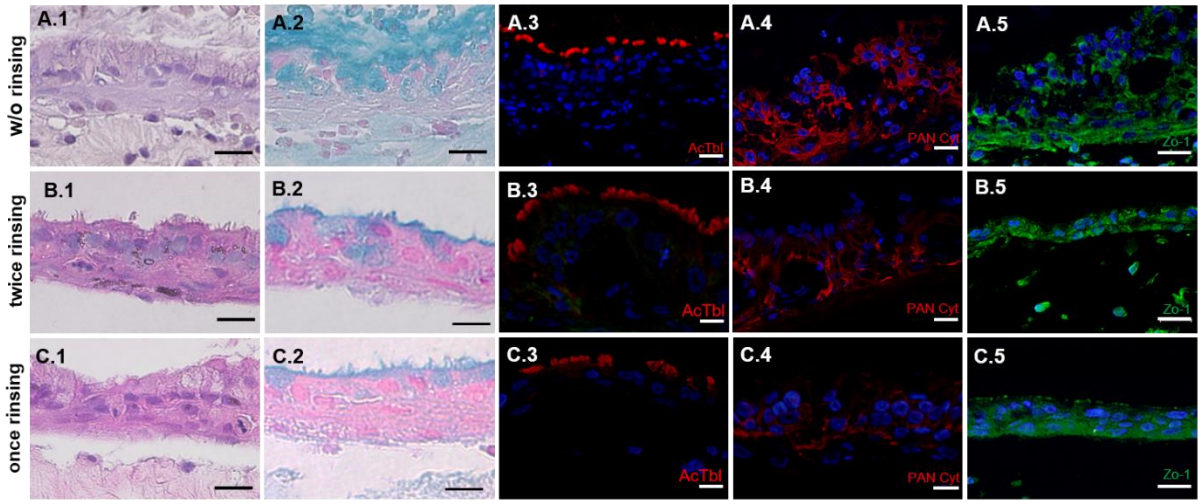

Figure 10. Testing different rinsing times at bronchial epithelial *in vitro* model. Models were cultivated with primary normal human lung fibroblasts (NHLFb), embedded in bovine collagen type 1, 9 x 10^5 NHBEC seeded on top, airlift performed at 24 hours NHBEC post seeding. Scale bar = 100 µm. A.1-5, model was cultivated without rinsing. B. 1-5, model was rinsed twice, from the beginning of second culture week. C.1-5, was rinsed once in last culture week. Representative images show histological analyses H&E (A-C.1), Alcian blue (A-C.2) staining and Immunostaining against acetylated tubulin (Ac Tbl) which indicates ciliated cells (A-C.3), cytokeratin - 4, 5, 6, 8, 10, 13, 18 (PAN Cyt) (A-C.4) and Zonula occludens-1 (ZO-1) (A-C.5). Nuclei were counter stained with DAPI (blue fluorescence). Scale bar = 100 µm.

5.1.1 Ultrastructural analysis of the *in vitro* model of 2- and 3-weeks cultivation

Transmission electron microscopy (TEM) confirmed the results of the model's histological evaluation. To assess ultrastructural morphology differences of both models 9 x 10^5 NHBEC with embedded 64.300 NHLFb in bovine collagen I, at 24 hours post NHBEC seeding the air lift was performed and the model was cultivated for two and three weeks. For additional analysis TEM was performed.

The two weeks cultivated model showed a single kinetosome, which was detected close to a cilia tube (**figure 11**, A, arrow), also a couple were guessed (**figure 11**, B, arrow). The kinetosome is the basal body of a cilia, it sits underneath a cell membrane of ciliated cells and provides stability to the whole construct for a functional movement. Just little numbers of ciliated cells were detectable (**figure 11,** E, arrow 1). Goblet cells with mucus vesicle were detected (**figure 11**, C, arrow, E, arrow 2). In **figure 11**, D a characteristic basal monolayer cell was analyzed. These tests revealed that the analyzed model was bronchial epithelial tissue, but still on its growing process. Expected characteristics of ciliated cells and goblet cells were proven. However, reduced cilia number than expected were found. Furthermore, the morphology and the cell organization were not analyzable at this state of tissue development e. g. just single cells which formed a basal monolayer orientation were detected.

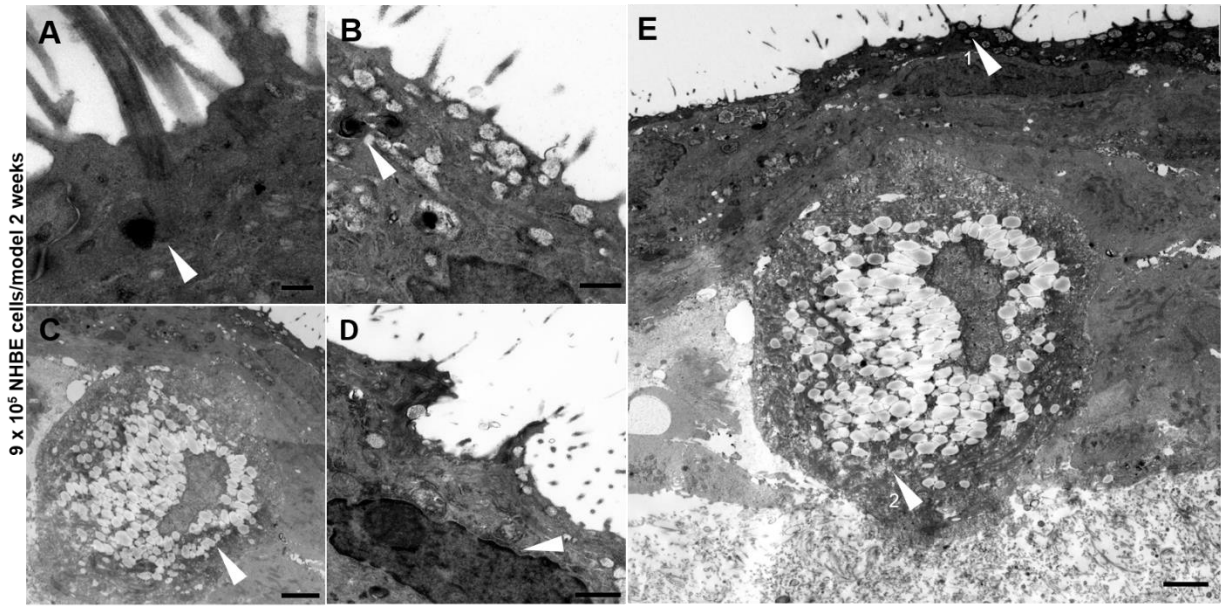

Figure 11. TEM analysis of the bronchial epithelium model cultivated for two weeks. TEM images represented bronchial epithelium model. 64.300 NHLFb embedded in bovine collagen I, 9 x 10^5 NHBEC (self- isolated, USA lung) seeded on top, 24 hours post NHBEC airlift was performed, and 14 days cultivated. Cilia of ciliated cells with a kinetosome (arrow), scale bar 250 nm (A), cross sectional kinetosome pair (arrow), scale bar 100 nm (B), goblet cell with mucus vesicle (arrow), scale bar 500 nm (C), ciliated cell with microtubule and basal cell monolayer (arrow), scale bar 1000 nm (D), overview goblet cell (arrow 2) and ciliated cells (arrow 1), scale bar 2000 nm (E).

The three weeks cultivated model showed the following. Analysis identified a paired kinetosome (**figure 12**, A, arrow). Significantly, a cross-sectional cilium image showed the characteristic orientation of nine peripheral microtubule doublets-pairs of microtubules and a center complex (**figure 12**, B). In general, the presence of ciliated cells was shown (**figure 12**, C, arrow), ciliated cells were clearly identified. Goblet cells were also verified as indicated by the presence of mucus vesicles; vesicle separation was clearly visible (**figure 12**, D, arrow). The last image (**figure 12**, E) presented a tissue section overview, single differentiated NHBEC were forming a prismatic morphology (arrow 2). Ciliated (arrow 1) and goblet cells (arrow 2) were a lined to each other. A basal monolayer is formed (arrow 3), it is specific for bronchial epithelial tissue. It concluded that the advantage of the three weeks cultivation was detected in TEM images. Characteristic cell differentiation as ciliated cells, goblet cells, basal monolayer forming cells were visible and proven. Three weeks of tissue cultivation were necessary to form a bronchial epithelium.

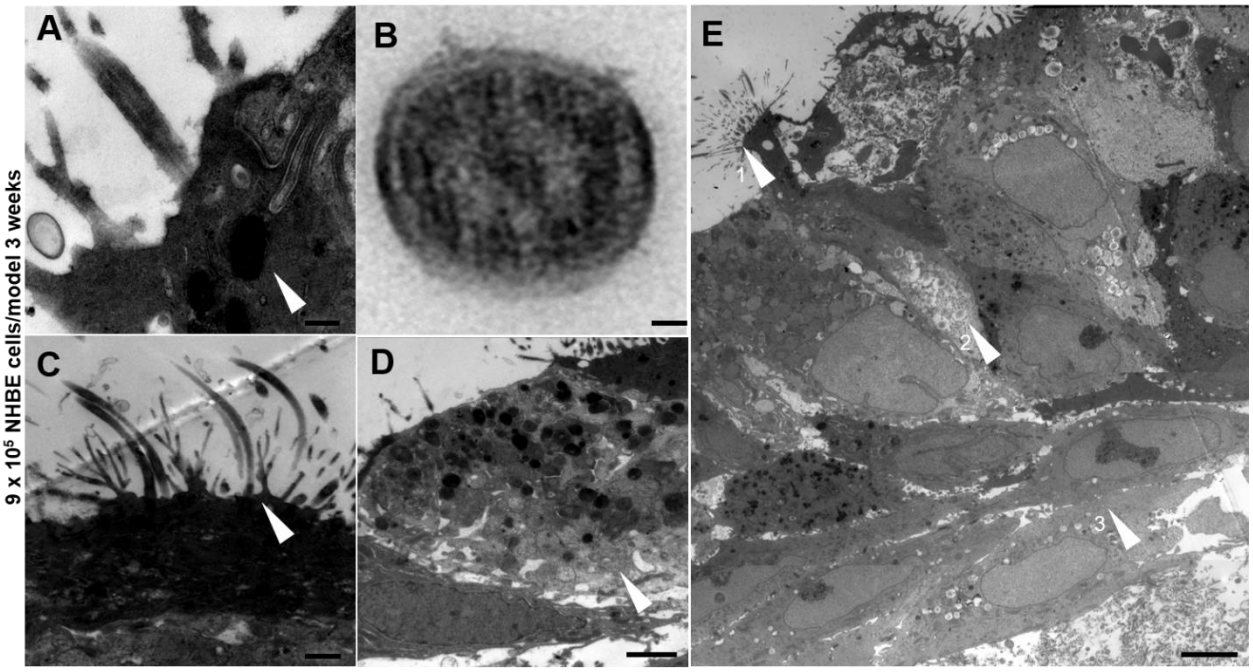

Figure 12. TEM analysis of the bronchial epithelium model cultivated for three weeks. TEM images represented bronchial epithelium model. 64.300 NHLFb embedded in bovine collagen I, 9 x 10^5 NHBEC (self-isolated, USA lung) seeded on top, 24 hours post NHBEC airlift was performed, and 21 days cultivated. Cilia of ciliated cell with kinetosome (arrow), scale bar 250 nm (A), cross sectional cilium, scale bar 50nm (B), ciliated cell with microtubule (arrow), scale bar 1000 nm (C), goblet cell with mucus vesicle (arrow), scale bar 2500 nm (D), overview goblet cell (arrow 2), ciliated cells (arrow 1), basal cell monolayer (arrow 3), scale bar 500 nm (E).

5.2 Bronchial epithelial *in vitro* model modulations

5.2.1.1 ECM enhancement

For a more realistic setting I tried to use a hydrogel of human extra cellular matrix (ECM) along with another approach of self-synthesized ECM instead of the bovine collagen matrix. There is proof that ECM itself influences the cell viability in the phenotype and on genetical level (Hirst, Twort et al. 2000, Hedström, Hallgren et al. 2018). My assumption was to provide the most *in vivo* like environment, to lead to an *in vivo* like bronchial cell differentiation.

For testing this method, NHLFb were embedded into the human matrix hydrogel for 14 days under submersed condition, different ratios of hydrogel and human collagen were combined to find the optimal ECM hydrogel mixture. The control (**figure 13**, A) was cultured according to the established protocol. The control morphology exhibited evenly distributed fibroblasts nuclei-stained deep purple in pinkish stained collagen. **Figure 13**, B contained 1:100 human hydrogel mixed with collagen, many nuclei were detected, and the histology looked comparable to the control. **Figure 13**, C, the 1:20 mixture showed just a single fibroblast nucleus. **Figure 13**, D 1:10 and E 1:3, both did not show any nuclei, only stained collagen. **Figure 13**, F 100 % of hydrogel was used, and only little matrix leftovers were detected, and no NHLFb and no hydrogel were detectable. Unfortunately, the received human matrix hydrogel was from a patient, who was diagnosed with fibrotic lung tissue later. It meant that the desired advantage resulted to be a disfavor for our model. Here, we stopped experimenting with the hydrogel.

Another approach was to cultivate a model with self-synthesized ECM by fibroblast stimulated with ascorbic acid. Ascorbic acid supports ECM synthesis and higher collagen deposition (Marinkovic, Sridharan et al. 2021). Self-synthesized ECM advantages were desired as described before. The protocol for self-synthesized ECM by NHLFb was tested by seeding apically NHLFb on, basal coated and uncoated inserts and submersed cultivated (medium supplemented with 0.1 % ascorbic acid) for 7 days, later the model cultivation was continued according to the established bronchial epithelial *in vitro* model protocol and for analysis the models were stained with H&E. Results presented that uncoated inserts showed 3D grown layer of fibroblasts, pinkish collagen and empty fragments (**figure 13**, G). NHBEC were not visible. Coated inserts (**figure 13**, H, I) presented probably two different cell types because of different pink stains. Both showed a similar unorganized cell distribution, without presenting any cell differentiation of bronchial epithelial cells. All cultivated models did not show a bronchial epithelium like tissue morphology. It concluded that

the use of ascorbic acid alone to stimuli ECM synthesis did not lead to a more realistic bronchial epithelial tissue.

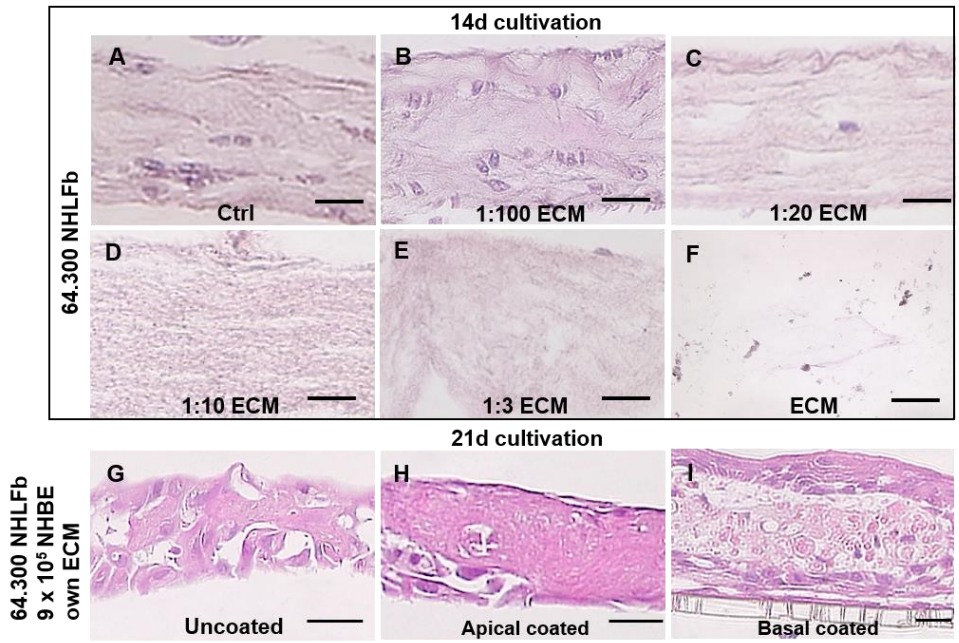

Figure 13. Model modulation - applying human ECM hydrogel and self-assembled ECM. Images presented HE stained tissue sections of 64.300 NHLFb were embedded in human ECM hydrogel in different compositions for 14 days submersed (A-F). 1 x 10^6 NHLFb were stimulated by 0.1 % ascorbic acid to self-synthesize ECM for 7 days during submersed cultivation. Followed by seeding 9 x 10^5 NHBEC on top, 24 hours later air lift was performed, and the model was cultivated for 21 days. All models were fixed in 4 % PFA, embedded in paraffin and cut into tissue sections. A control model, NHLFb embedded in human collagen. B, NHLFb were cultivated in 1:100 (ECM: human collagen). C, cells embedded in 1:20 (ECM: human collagen). D, NHLFb embedded in 1:10 (ECM: human collagen). E, NHLFb embedded in 1:3 (ECM: human collagen). F, NHLFb embedded in ECM. G, insert was uncoated, NHLFb synthesized its own ECM. H, an insert was apically precoated, NHLFb synthesized on its own ECM. I, insert was basal precoated NHLFb synthesized on its own ECM. Scale bar 20 µm (A-F), scale bar 100 µm (G-I).

5.2.2 Teflon® ring to support bronchial epithelium morphology

Different ECM approaches did not support morphology of the *in vitro* bronchial epithelium model. In the following I applied 1 cm diameter Teflon® ring at the bronchial epithelium model to test if it has potential to feature the model morphology. In another tissue engineering protocol, a Teflon® ring was used for culturing an oral skin model, the Teflon® ring was placed on the collagen matrix and keratinocytes were seeded inside the ring to keep the keratinocytes in place (Gronbach, Wolff et al. 2020). Here, the cultivation was supported while seeding NHBEC inside the Teflon® ring. Different applications of the Teflon® ring were tested, it is illustrated in **figure 14**. **Figure 14**, A, the Teflon® ring was applied for 21 days, the air lift was performed at 24 h NHBEC post seeding and the ring was removed after model fixation. **Figure 14**, B the Teflon® ring was applied for 21 days, the air lift was performed at day 7 post NHBEC seeding, and the ring was removed after the model fixation. **Figure 14**, C the proceed was like B, just the ring removal was at day 7 post NHEBC seeding. Histology was analyzed with H&E staining. It resulted in all models being damaged. Epithelial cells were not visible, probably epithelium was fully removed during ring removal or not grown. The thin cell layer remained attached to membrane. No differentiated bronchial epithelial cells were visible. Even in **figure 14**, B image revealed cells cultivated on top and underneath insert membrane. It concluded that the use of a Teflon® ring did not result in an enhancement, no differentiated epithelial cells were noticed and neither prismatic erected epithelial cell shape. Testing ended after these three trials.

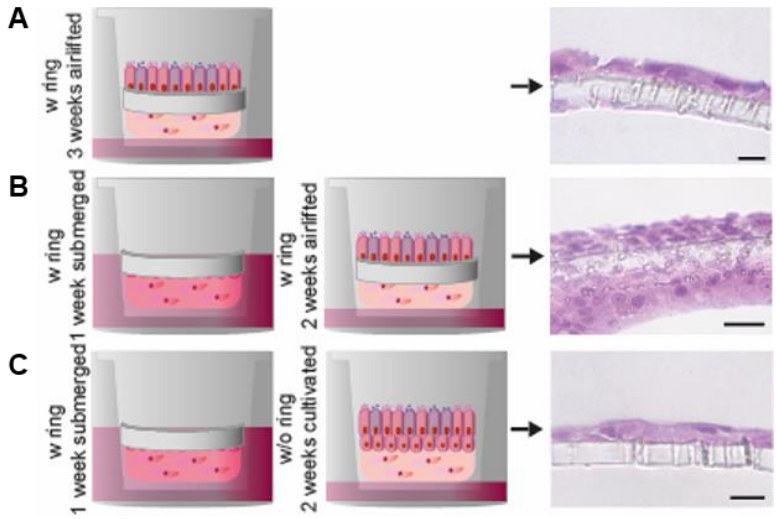

Figure 14. Model modulation - using a Teflon® ring. HE stained tissue sections with illustrations of experimental performance by using Teflon® ring (diameter 1 cm). 64.300 NHLFb embedded in bovine collagen 1, $9x10^5$ NHBEC were seeded on top, followed by Teflon® use varieties. A, model was cultivated for 21 days with ring at an air liquid interface. B, model was cultivated submerged for 7 days and 14 days airlifted with ring support at an air liquid interface. C, model was cultivated submerged for 7 days with ring and 14 days airlifted without ring. Scale bar 20 µm, n=1.

5.2.3 Improving the model cultivation time

A less time-consuming approach was expected while exposing the model to physical stress by applying the *in vitro* model in a perfusion system. In dynamic systems model's medium reservoir exchanges permanently, with an applied perfusion pump at model culture plate. It was expected that medium perfusion speeds up cell differentiation by physical shear forces and has a positive effect on cell membrane barrier function (Chandorkar, Posch et al. 2017). The actual idea of integrating a dynamic system was to reduce the cultivation time, instead of 21 days, 14 days of cultivation time were wanted. A faster model cultivation process was desired to make the use of the *in vitro* model more convenient for e. g. repeating and testing new parameters. Bronchial epithelium model was cultivated for the first week according to the model protocol in static environment, after the static environment was exchanged to a dynamic environment, the model was placed into a cell culture plate connected to a perfusion pump to create a dynamic system. The medium flow rate of 150 µl/min was applied for 7 days. In parallel the control model was cultivated for 21 days under static conditions. The model was fixed, embedded in paraffin, cut and tissue sections were H&E stained. Results showed the control model as expected, it contained prismatic erect epithelial cells, it was lined with cilia on cell surface and underneath the basal monolayer was visible (**figure 15**, A). In contrast the dynamic system exposed model did not show differentiated cells in its epithelium. Instead, a high contraction of collagen matrix with embedded fibroblasts was detected (**figure 15**, B). The diameter of epithelial layer doubled in comparison to matrix layer regarding the dash line. The dash line separated NHLFb embedded in collagen (Fbs+Col) and mucus-cilia-epithelium (Mucucil. Epith.) to visualize multi layers of epithelium compared to control model. Cell trash or distinct cells were flouting above apical side. In conclusion the result showed that applied dynamic system did not show desired advantages, probably implementation needed more fine tuning. Also, reduction of contamination risc was desired, a peristaltic pump was placed outside of the incubator because of its size which connected the perfusion pump with the culture plate.

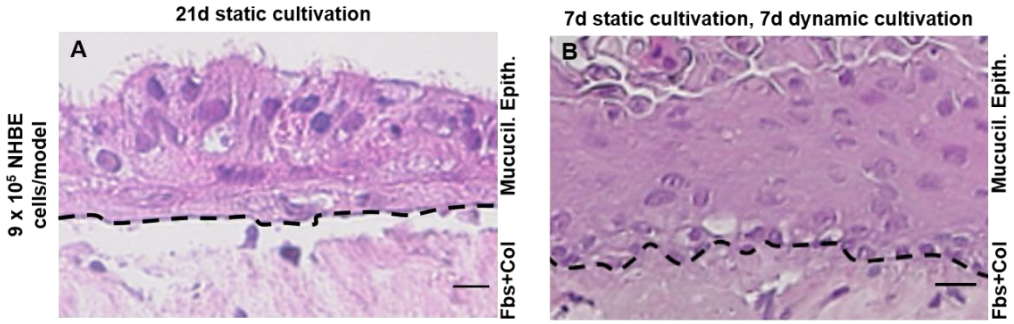

Figure 15. The bronchial epithelium model applied in a perfusion plate. Images represent culturing bronchial epithelial *in vitro* model in dynamic system, culture plate was connected to perfusion pump. Speed up of cell differentiation was expected through shear forces of perfusion system. After the cultivation models were fixed, paraffin embedded, tissue sections were cut, and H&E stained. A, control model, 64.300 NHLFb embedded in bovine collagen I, 9 x 10^5 NHBEC seeded on top, 24 hours post NHBEC seeding air lift was performed and cultured for 21 days. B, model was cultivated 7 days on static stetting according to control model (A) and 7 days in dynamic system by medium flow rate of 150µl/min. The dash line separated NHLFb embedded in collagen (Fbs+Col) and mucus-cilia-epithelium (Mucucil. Epith.) to visualize multi layers of epithelium compared to control model. Scale bar 20 µm, n=2.

5.2.4 Comparison of cell donor, model insert and cell culture medium

In this part I tried to improve the model morphology by testing different cell sources (companies related), cell culture inserts, culture media and collagen batches. The NHBEC were bought from companies as STEMCELL Technologies and Epithelix. Inserts with a pore size of 0.4 µm (Corning) were used in parallel to the established inserts (pore size 3 µm (Corning)) were tested. MucilAir™ (Epithelix) culture medium was compared to common PenumaCult™-ALI Medium (STEMCELL Technologies). Bovine collagen I (Cellsystems) was exchanged by a new collagen batch. Bovine collagen batches can influence model morphology. Model cultivation was according to the model generation protocol and for analysis H&E stained was performed. These tests revealed that the insert pore size of 0.4 µm did not enhance the model growth. Models applied on smaller pore size presented a softer tissue construction, even the model collection resulted difficult (**figure 16**, A, B, C, D). In contrast 3 µm pore sized inserts showed a more stable and straighter matrix and epithelium (**figure 16**, E, F, G, H, I, J). MucilAir™ culture medium did not improve NHBEC differentiation and epithelium morphology (**figure 16**, C, D, G, H), no differentiated cells and prismatic erect cell shape was visual. In contrast PenumaCult™-ALI Medium induced NHBEC prismatic erection and ciliated cells were visible (**figure 16**, E, F, I, J). Different collagen batches did not influence tissue growth (**figure 16**, A-J). NHBEC (STEMCELL Technologies) showed ciliated cells and an erected cell shape (**figure 16**, E, F), in comparison to NHBEC (Epithelix), the number of cilia increased, erected cell shape formed pseudostratified epithelium (**figure 16**, I, J). Concluded exchanged parameter as insert (0.4 µm) and culture medium, did not enhance model morphology and different collagen batches did not show any influence. Interestingly, the NHBEC donor, associated with high viability, showed the best result regarding model morphology, and thus proofed the established parameters of the bronchial epithelial *in vitro* model protocol. The use of established protocol was continued.

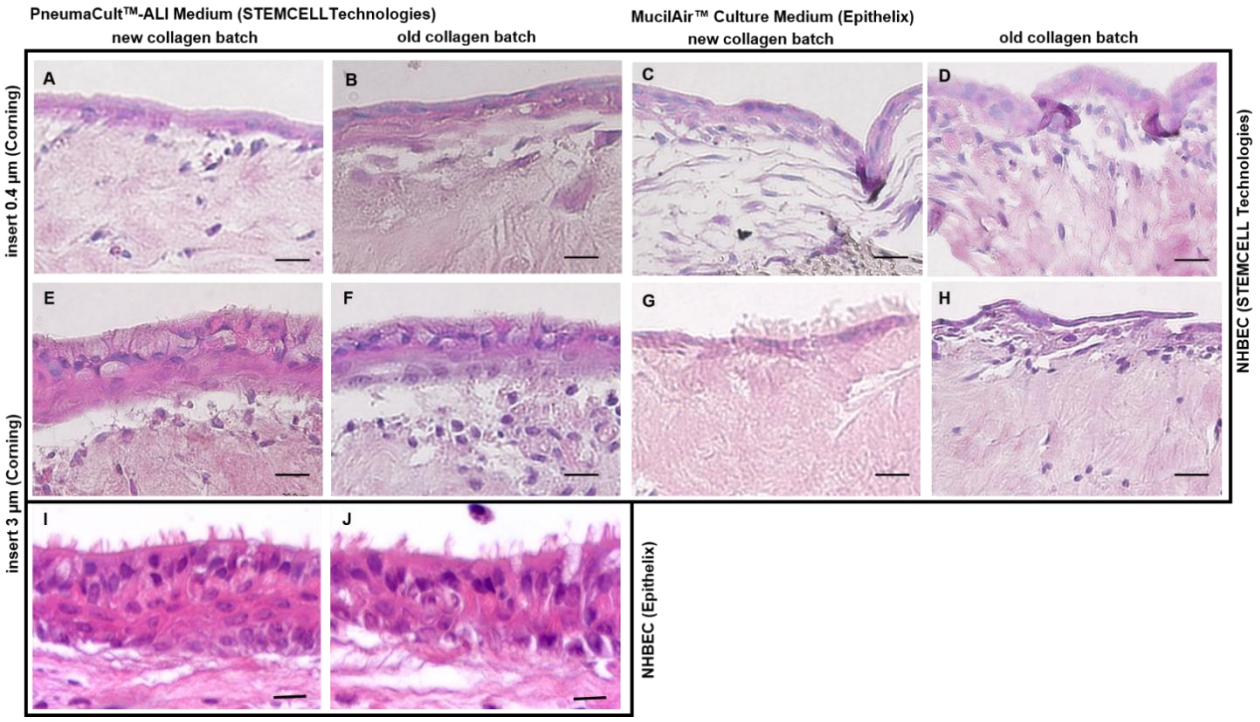

Figure 16. Model modulation by testing different inserts, medium and collagen batches. Presented HE stained tissue sections of model improvement by testing MucilAir™ (Epithelix, Geneva, CH) against PenumaCult™-ALI (STEMCELLTechnologies, Vancouver, CA) culture medium. Inserts 0.4 µm pore size instead of 3 µm (Corning, Amsterdam, NL) and an old and new bovine collagen I batch (Cellsystems, Troisdorf, DE. NHBEC sources from Epithelix and STEMCELL Technologies were tested. 64.300 NHLFb embedded in bovine collagen I, $9x10^5$ NHBEC seeded on top, 24 hours post NHBEC airlift was performed, and 21 days cultivated. (A). PenumaCult™-ALI Medium, insert's pore size 0.4 µm and old collagen (B). MucilAir™, insert's pore size 3 µm and old collagen (C). MucilAir™, insert's pore size 0.4 µm and old collagen (D). Model cultivated with standards consumables and media and new collagen batch (E). PenumaCult™-ALI Medium, insert's pore size 0.4 µm and new collagen (F). MucilAir™, insert's pore size 3 µm and new collagen (G). MucilAir™, insert's pore size 0.4 µm and new collagen (H). Scale bar 20 µm.

5.2.5 Ultrastructural analysis of the *in vitro* model of 3 weeks cultivation and NHBEC donor change

Previous results showed that cell viability respectively to cell donor had a high influence on bronchial epithelial morphology. The basal monolayer contains erected prismatic epithelial cells, ciliated cells, and several goblet cells represented a differentiated *in vivo* like bronchial epithelial tissue (**figure 16**, I, J). The change to NHBEC (Epithelix, Geneva, Switzerland), improved the quality of bronchial epithelium models. Additionally, TEM analysis was applied to ultrastructural morphology, the established protocol to cultivate the *in vitro* bronchial epithelium model was applied. TEM results showed that the cilia number increased, also cell organization became clearer (**figure 17,** A) in comparison to previous analysis (**figure 12**). Cilia were straight-lined shaped and connected to their kinetosome, the kinetosome is located under the cell membrane and grew vertical. Several cilium cross sections were visible, they presented the 9 characteristic microtubule doublet pair organization (**figure 17,** F). Elevated ciliated cell showed a clear cell compartment and a highly ciliated surface (**figure 17,** C). Goblet cells with mucus vesicles were visible (**figure 17,** D). Overview exposure presented a fine defined basal monolayer, there was no second layer visible, and all other cells were prismatic grown to the apical surface (**figure 17,** E). Concluded, that the additional ultrastructural analysis of the *in vitro* model morphology proved the donor influence regarding high cell viability supported cell differentiation and bronchial epithelial morphology.

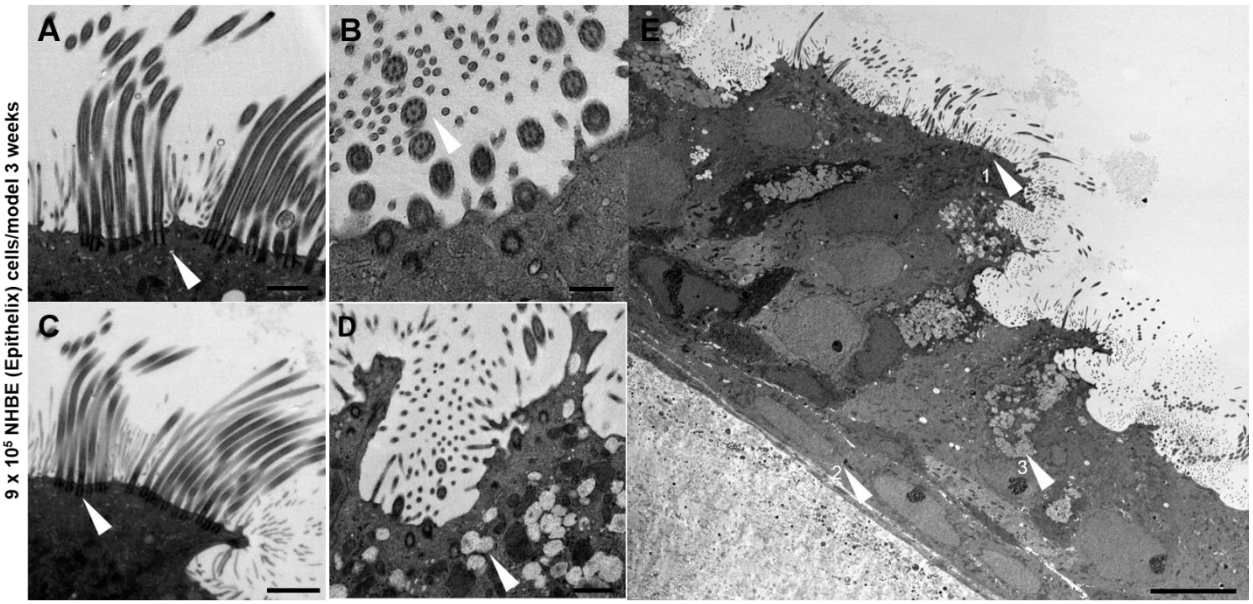

Figure 17. TEM analysis of the bronchial epithelium model with new NHBEC (Epithelix, Geneva, CH) cultivated for three weeks. TEM images represented bronchial epithelium model. 64.300 NHLFb embedded in bovine collagen I, $9x10^5$ NHBEC (Epithelix, Geneva, CH) seeded on top, 24 days post NHBEC airlift was performed, and 21 days cultivated. Cilia of ciliated cells with kinetosomes (arrow), scale bar 1µm (A). Cross sectional cilium (arrow), scale bar 500nm (B), ciliated cell with microtubule (arrow), scale bar 2µm (C), goblet cell with mucus vesicle (arrow), scale bar 1µm (D), Overview image, goblet cell (arrow 3), ciliated cells (arrow 1), basal cells monolayer (arrow 2) were presented, scale bar 10µm (E).

5.2.6 Endothelial cells implemented in human based bronchial epithelial *in vitro* model

To establish a more complex model, I cultivated human based bronchial epithelial *in vitro* model with bronchial endothelial cells (BEC) by self-synthesized ECM. Previous experiment was based on self-synthesized ECM by interplay of ascorbic acid and NHLFb. The recent experiment used coculture feature of vascular BEC and NHLFb. The protocol was developed by Sabine Kaessmeyer (Department of Veterinary Medicine, Institute of Veterinary Epidemiology and Biostatistics, FU Berlin) for skin *in vitro* models (Kaessmeyer 2017). I adapted her protocol for bronchial epithelium models, by exchanging cell culture media for lung cells and cell origin of bronchial epithelial cells and fibroblasts. Self-synthesized ECM was desired for total human based approach and bronchial epithelial *in vivo* like morphology. Desired vascularized system synthesized by the interplay of NHLFb and BEC provides a higher complexity of the *in vitro* tissue. Especially, for further experiments e. g. coculturing of skin and bronchial epithelial tissues, in human body organs are connected though a vascularized system.

For analysis HE, Alcian blue and immune staining was performed. Acetylated tubulin proofed ciliated cells, MUC5AC showed goblet cells and uteroglobin detected club cells. Marker as von Willebrand factor (vWF) was used to characterize vascularized system, it is an expressed protein by endothelial cells and located at vessel's lumen and plays important role in hemostasis (Zanetta, Marcus et al. 2000, Nightingale and Cutler 2013). CD31 was detected as well, also known as platelet endothelial cell adhesion molecule, found among others at endothelial cell surface (Lertkiatmongkol, Liao et al. 2016). TEM was performed as well for ultrastructural analysis to proof tissue histology, the images presented the first trial; another trial was performed during my stay at UBC. Unfortunately, I could not finish the model cultivation as the pandemic situation of COVID-19 became alarming and the UBC decided to close the laboratory.

Following images presented tissue intersections of tissue histology. HE (**figure 18,** A) and Alcian blue (**figure 18,** B) stained images showed ciliated cells, blue colored mucus layer indicated goblet cells. The tissue morphology represented an unorganized differentiated epithelial cell layer; the basal monolayer was not visible. Self-synthesized ECM showed thin cell layer. Immune fluorescence pictures proved presence of ciliated cells, acetylated tubulin showed strong signal and was detected above all epithelial cells (**figure 18,** C). MUC5AC was detected, tissue contained goblet cells and a few club cells, they produced uteroglobin (UG) (**figure 18,** D). **Figure 18**, image E was supposed to prove vascularized tissue with positive signals of von Willebrand

factor (vWF) and CD31. CD31 did not show signals, either vWF showed signals, but it was expected to observe single signals forming a tube, as a vessel proof. TEM analysis confirmed by presenting ciliated cells contained hastate cell shapes (**figure 18,** F, arrow). Also, nuclei indicated the cell organization, but the expected cell arrangement cannot be proven, the basal monolayer was just assumed and only fragments of prismatic epithelial cell shape were present (F). Nevertheless, cilia with several cross sections of the cilium proofed the 9 characteristic microtubule doublet pairs organization (**figure 18**, G, arrow). Also, kinetosome dots were recorded underneath the membrane (**figure 18**, G). However, self-synthesized ECM by NHLFb and BEC presented single fragments with empty spaces in between, the layers seemed thin and unconnected (**figure 18**, H, arrow). Concluded expected vascularized tubes were not detected. Either in TEM analyses, or in immune fluorescence screening. My experiment confirmed cell differentiation of epithelial cells. The coculture of BEC and NHLFb did not show the expected self-synthesized ECM result, probably further experiments are necessary for the model improvement.

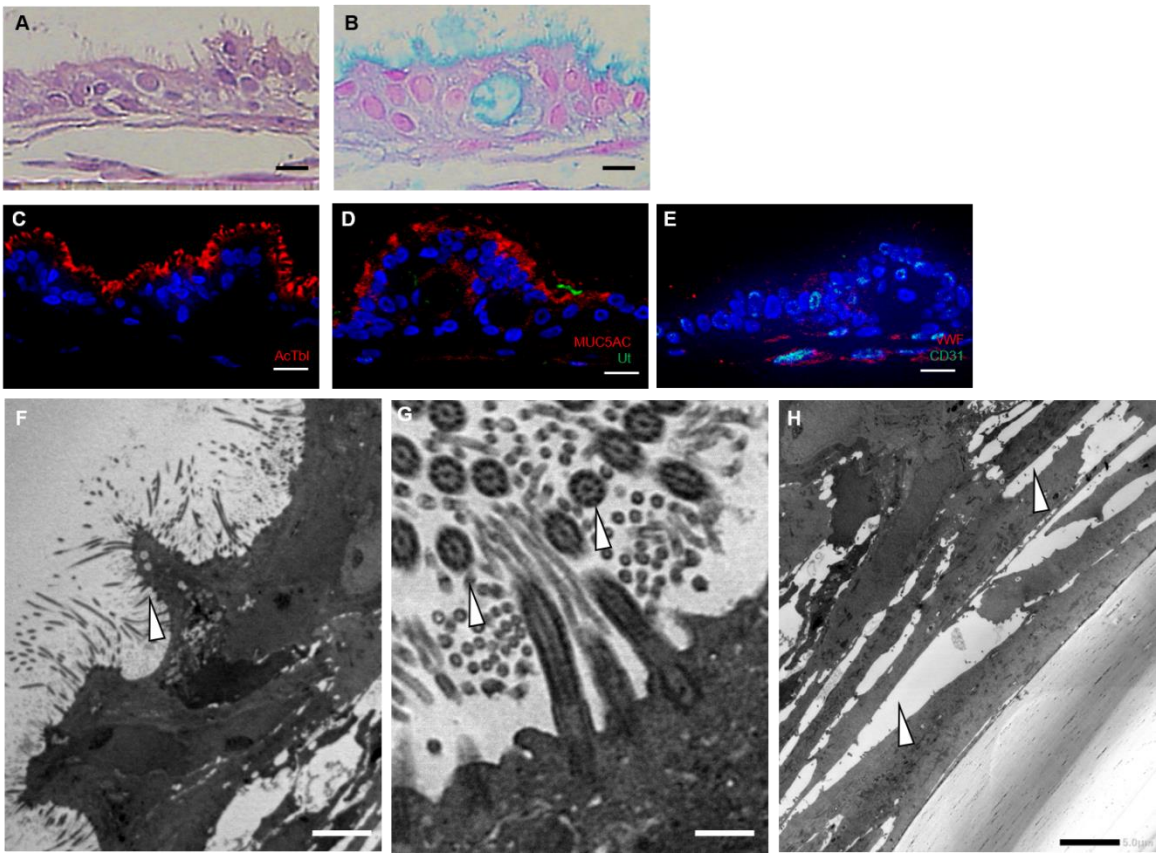

Figure 18. First trial of cultivating a vascularized human based bronchial epithelium model. Images represented first trial of vascularized bronchial epithelium model with self-synthesized ECM by coculture of NHLFb and BEC. 2800 NHLFb and BEC seeded on 0.4 µm pore size inserts, cocultured for 18 days. Day 18, NHBEC seeded on top. Airlift was performed 24 hours NHBEC post seeding and for 21 days cultured, according to protocol. Tissue sections were HE, Alcian blue, immune stained and TEM analysed. Cross sectional HE stained (A) and Alcian blue stained (B) scale bar 20 µm. Tissue section immunological stained acetylated tubulin to visualize the cilia (C). Immunological staining against mucus (MUC5AC) and uteroglobin (Ut) to analyse goblet cells and club cells (D). Von Willebrand factor (vWF) and CD31 to detect vascularized cells (E). Nuclei with DAPI counterstained. Scale bars 20 µm. TEM image ciliated neighboured cells, scale bar 5 µm (F). Ciliated cell with microtubule, scale bar 0.5 µm (G). Base matrix, self-synthesized ECM by BEC and NHLFb, scale bar 5 µm (H).

5.3 The *in vitro* model infection of influenza A virus and the therapeutical use of Zanamivir

Having optimized the *in vitro* culture of the human bronchial epithelium model, next I tested if it can be used for modeling human biology. The human pathogen Influenza A virus (IAV) H3N2 (Chen, Liu et al. 2018) infects human lung epithelial cells leading to cell damage and immune response activation, including the release of cytokines and other cellular factors (Kawai and Akira 2006, Denney and Ho 2018). In clinics, Zanamivir is used as an antiviral drug to block viral replication and treat IAV infection (Elliott 2001, Okomo-Adhiambo, Sleeman et al. 2013). Hence, I investigated whether the *in vitro* model replicated IAV infection and Zanamivir treatment as observed in patients in the clinic.

5.3.1 Establishing an IAV infection protocol

Histology analysis showed clear differences in between virus load and volume used for infection. As expected for the non-infected control tissues submersed in PBS only, the apical layer of pseudostratified columnar epithelium was clearly visible (**figure 19**, A). The lack of cilia in the control tissue is probably related to the submerging protocol, as cilia was present before the infection. All submersed tissues infected independently of MOI showed damaged epithelial cell layer at 24 and 48 hours post infection (**figure 19**, B, C, D, G, H). Cell layers in these tissues were thinner and showed heterogeneous pseudostratified morphology. In contrast, independent of MOI, all spot infected tissues showed similar histology to control at 24 hours post infection (**figure 19**, E, F). Similar results were observed for infections with MOI 0.01 at 48 hours post infection (**figure 19**, J). Interestingly, at 48 hours post infection, tissues infected with MOI 0.1 lacked the epithelium (**figure 19**, I). I concluded that a high virus load of MOI 1 or 0.1 harmed the tissue in submersed and spot infection protocols. Moreover, tissues infected with MOI 0.01 using the spot infection protocol survived for at least 48 hours post infection.

To show that the virus was replicating inside the *in vitro* model cells, I performed a plaque assay on the culture supernatant (**figure 19,** K). For MOI 0.1, independent of the infection volume, virus particles were detected in the supernatant at 1 hour (10^2 PFU/ml), particles concentration increased to 10^{10} PFU/ml at 24 hours and kept constant until 48 hours post infection. No virus particles were detected at 1 hour after spot infection with MOI 0.01 probably due to initial low virus load. This experimental group also showed the lowest virus load at 24 hours (10^5 PFU/ml) and 48 hours (10^8 PFU/ml) post infection. In contrast, submerse infection with the same MOI 0.01 led to higher virus counts, indicating higher infection efficiency with the submersed protocol.

Interestingly, submersed infection with the highest MOI 1 induced a maximum virus particle counts of only 10^5 PFU/ml at 24 hours post infection, likely due to early and widespread epithelial layer damage and cell death (**figure 19 B**), leaving fewer cells for virus replication. Overall, my cultured tissues can be successfully infected, and the virus replicated, as indicated by the exponential increase of viral particles in the supernatant.

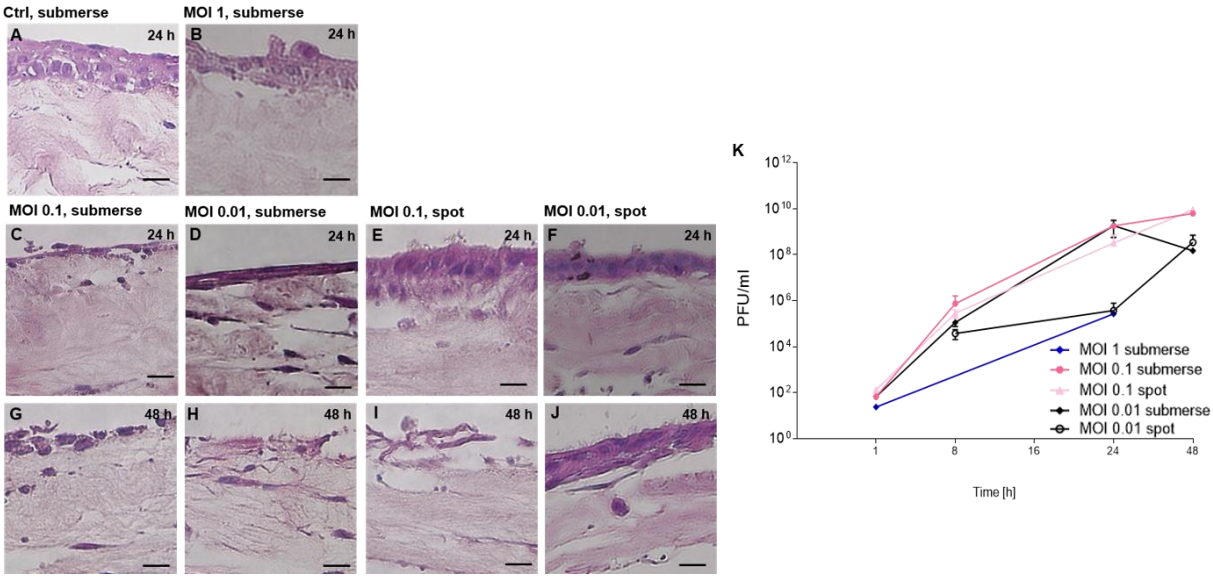

Figure 19. Bronchial epithelial 3D *in vitro* model infection with Influenza A virus. Self-developed 3D model for bronchial epithelial *in vitro* culture was transfected with different amounts of IAV (multiplicities of infection = MOI) and using submersion or spot infection protocols. HE stained tissue sections (A-J) from uninfected control submersed in PBS only (A); 24 hours post infection with submersed protocol using MOI 1 (B), 0.1 (C) or 0.01 (D); 24 hours post infection with spot protocol using MOI 0.1 (E) or 0.01 (F); 48 hours post infection with submersed protocol using MOI 0.1 (G) or 0.01 (H); 48 hours post infection with spot protocol using MOI 0.1 (I) or 0.01 (J). Scale bar 20 µm. Plaque forming unit per ml (PFU/ml) counts of viral particles in the supernatant of cells infected with IAV over time after infection (K). Up to three independent biological replicas were generated for each data point. Data is shown as mean value of biological replicates ± SEM.

Next, I compared the *in vitro* model to a commercially available one, named MucilAir™ (Epithelix, Geneva, CH). MucilAir™ is a 3D *in vitro* model cultured at the air-liquid interface and based on differentiated NHBEC, without NHLFb. Both models were infected with IAV (MOI 0.01, spot infection protocol) for 48 hours. The supernatants were collected as before, and viral particles counted with a plaque assay. Both models showed similar exponentially increasing levels of virus particles in the supernatant over time, suggestive of viral exponential replication (**figure 20**). Therefore, my bronchial epithelial *in vitro* model showed comparable behavior to the commercial 3D model, validating the quality of the self-developed model.

In conclusion, the spot infection protocol with MOI 0.01 is a good working protocol for modeling the virus infection in the *in vitro* model based on the model comparison. From this moment on, I decided to stick with this protocol for further experiments.

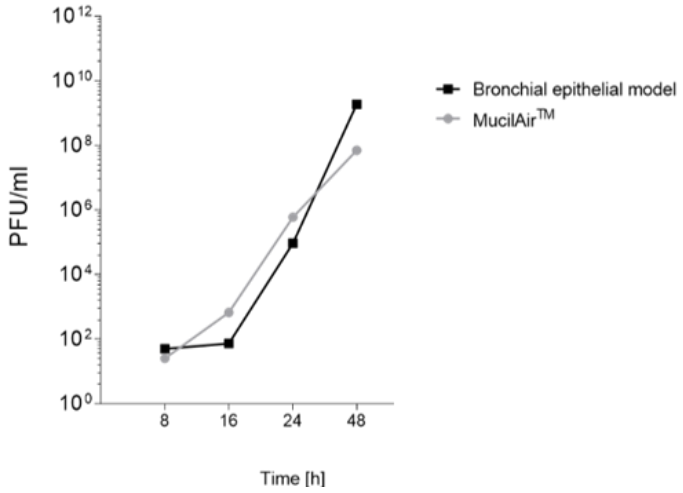

Figure 20. Comparison to commercial tissue culture model infected with Influenza A virus. Plot showed the level of IAV H3N2 (Panama/2007/1999, PANIII) infection in my *in vitro* models of human based bronchial epithelium model and MucilAir™. Both models were infected in parallel (spot infection with MOI 0.01) and plaque assay performed using the culture supernatant 8, 16, 24, 48 hours post infection. A single biological replicate was performed. Data are shown as mean ± SEM. PFU/ml = Plaque forming unit per milliliter.

5.3.2 Zanamivir impact of virus replication and cellular viability in IAV infected tissues

Zanamivir is an anti-viral agent used in the clinic that blocks viral replication. To study the *in vitro* model's response to Zanamivir treatment during IAV infection, cultured tissue was spot infected with MOI 0.01 of influenza A virus and treated with Zanamivir. To create a more realistic setting regarding IAV infection in patients, the infection duration was first extended to 96 hours. The recommended Zanamivir treatment scheme consists of two 5 mg doses per day. To replicate the clinical dosing scheme, I treated infected cells with Zanamivir 1 hour post infection and then every 12 hours during the infection period. Tissues were infected with IAV, treated with Zanamivir, and collected at 8, 24, 36, 48 and 96 hours post infection. Based on previously published studies, I tested three doses of Zanamivir (0.1, 100 and 1000 nM) (Ferraris, Kessler et al. 2005, Memoli, Hrabal et al. 2010, Okomo-Adhiambo, Sleeman et al. 2013).

As an anti-viral reagent that blocks viral replication, I expected lower virus level in IAV infected tissues treated with Zanamivir and associated higher cell viability. First, virus replication was analyzed as before by counting viral particles in the supernatant over time with a plaque assay (**figure 21**, A). In all groups, viral particle counts in the supernatant increased over time in the first 24 hours post infection, indicative of successful cellular replication. Viral particle counts remained constant over several days post infection but strongly decreased at 96 hours after infection, possibly due to cell death. Importantly, viral particles count in the supernatant of infected tissues treated with 1000 nM of Zanamivir were remarkably lower than the non-treated control. These results suggest that while virus replicate in tissues in all groups such replication is inhibited by treatment with 1000 nM Zanamivir.

To evaluate tissue viability at 96 hours post infection, cytotoxicity was accessed in MTT assay (**figure 21**, B). Results from my infected models were compared to the uninfected, untreated control (UTC). A positive control group (PTC) was included by treating uninfected tissues with detergents to induce cell death. As expected, the PTC group showed much lower cell viability compared to UTC, as indicated in the MTT assays by a drop of 75 % in cell viability. Cell viability decreased by about 10 % at 24 hours post infection in infected cells compared to UTC. This viability loss was completely prevented by the treatment with 1000 nM of Zanamivir (**figure 21**, B). Interestingly, cell viability in tissues infected with IAV treated or not with Zanamivir was like the UTC group at 36 and 48 hours post infection. At 96 hours post infection cell viability of the *in vitro*

model dropped by 24 % in the untreated group and only 11 % after Zanamivir treatment, indicating a ~50 % protective effect of the Zanamivir treatment against IAV infection in my *in vitro* model.

In the treatment of patients in the clinics, inhaled Zanamivir crosses the epithelium and reaches the plasma (Cass, Efthymiopoulos et al. 1999, Chairat, Tarning et al. 2013). In analogy to the lung epithelium cellular barrier between the lung lumen and the plasma serum, the epithelium cell layer in my model formed a cellular barrier in between the apical part and the basal medium reservoir. To test Zanamivir permissiveness through the epithelium layer of cells in the *in vitro* model infected with IAV, I added Zanamivir (diluted in PBS) in the apical part and measured concentration over time in the basal medium (**Figure 21**, C). Zanamivir concentration was measure using Mass Spectrometry in collaboration with Dr. Jan Felix Joseph from the Freie Universität Berlin, Germany. Because the apical part was isolated from the basal medium, Zanamivir must diffuse through the epithelium cell barrier. For the experiment, tissues were spot infected with IAV (MOI 0.01, pathogen H3N2, Panama/2007/1999 (PANIII)) and treated with Zanamivir (1000, 100, 0.1 nM, corresponding to 332.31, 33.23 and 0.33 ng/ml of Zanamivir) 2 hours post infection and every 12 hours as before. Basal medium samples (basal, medium reservoir) were collected 0, 2, 24 and 48 hours post treatment during IAV infection.

My results showed that Zanamivir concentration in the basal medium reservoir increased over time. Two hours after the first dose, Zanamivir was already detectable in the basal medium at similar concentrations to the original Zanamivir dose (~300 ng/ml), expect in the experimental group given 0.1 nM (**Figure 21**, C). In fact, Zanamivir could only be detected in the basal medium after 48 hours of the first dose for the group given the lowest amount (0.1 nM). While Zanamivir accumulated in the basal medium until the last time point measured for the group given the maximum amount (1000 nM, or 332.31 ng/ml), it reached an apparent concentration plateau when doses of 100 nM were given. Therefore, Zanamivir was detectable by MS in the basal medium already 2 hours post treatment and accumulated there over time linearly, suggesting that most of it did not rest inside cells nor was metabolized. In vivo, Zanamivir diffuses in the body due to the permanent blood circulation and is metabolized, therefore the concentration does not accumulate over time *in vivo*. However, Zanamivir concentration *in vivo* reaches maximum level already 1 or 2 hours post treatment (this level is then maintained through additional doses) (Cass, Efthymiopoulos et al. 1999). Similarly, we found that Zanamivir concentration in the basal medium reached the given dose after only 2 hours, indicated that my epithelium cell model had similar diffusive properties to the *in vivo* counterpart.

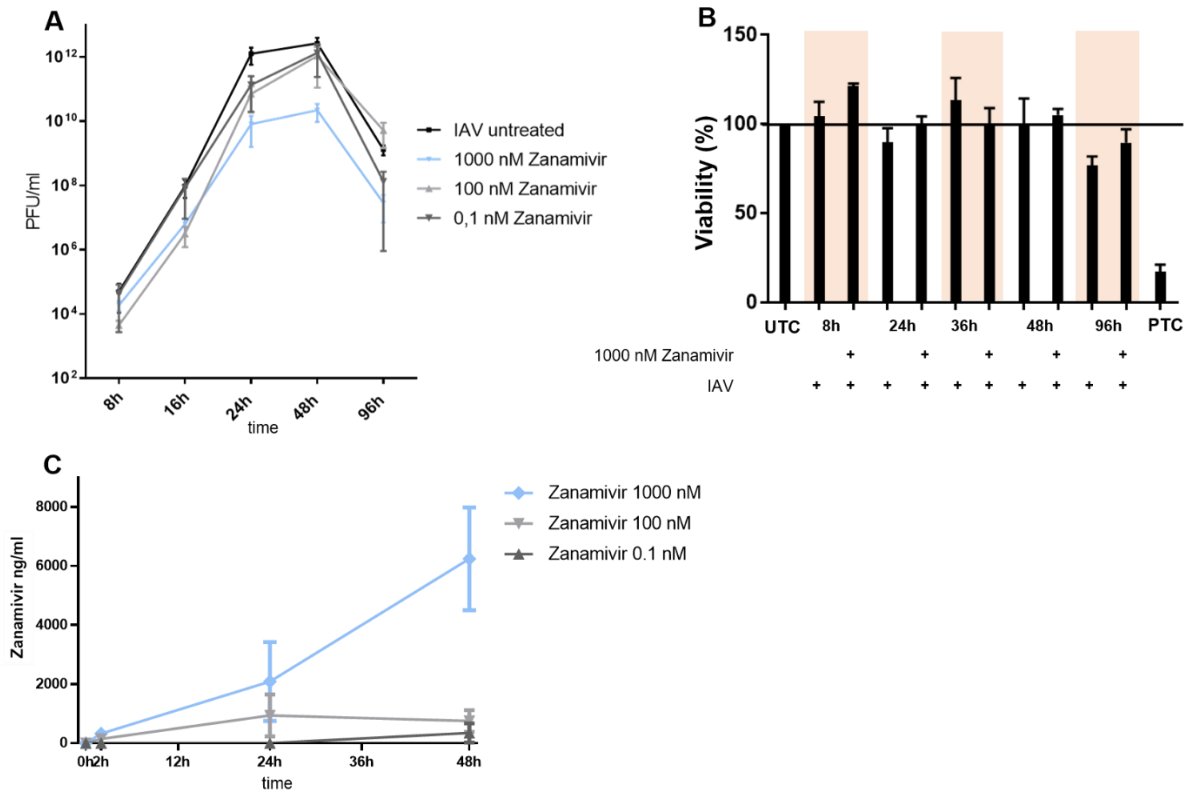

Figure 21. Cell viability, virus replication and Zanamivir concentration assays on my 3D bronchial epithelium model infected with IAV. Tissues were infected with IAV H3N2 (Panama/2007/1999 (PANIII)) (spot infection with MOI 0.01) and treated every 12 hours with 1000 nM Zanamivir, first was given 2 hours after infection. Samples were apically collected 8, 16, 36, 48 and 96 hours and from the basal medium 0, 2, 24 and 48 hours after the first dose of Zanamivir post infection. (A) Plaque assay measuring viral load in the supernatant in plaque forming units per ml (PFU/ml). Three to nine independent biological replicates per time point and Zanamivir treatment. (B) Cellular viability was assessed with MTT assay and normalized to the uninfected, untreated control group (UTC). A positive control group treated with detergents to induce cell death was included (PTC). Three independent biological replicates were generated. (C) Mass spectrometry quantification of Zanamivir concentration in the basal medium at different time points in IAV infected model. Data are shown as mean of biological replicates± SEM.

As before, comparison to a commercial *in vitro* model was performed using the MucilAir^{TM}-HF (Epithelix, Geneva, CH) system. Both models were spot infected (MOI 0.01) in parallel with IAV H3N2 (Panama/2007/1999, PANIII) and treated with 1000 nM Zanamivir every 12 hours. Supernatant was collected at 8, 16, 24, 48, 96 hours post infection and plaque assay analysis were performed. Similarly, as before, the viral particle count in the supernatant increased in the first 24 hours of infection in both tissue culture models, indicating successful IAV infection (**figure 22**). This time, a clear treatment effect was noticeable in both models already at 24 hours post infection. However, while virus level of treated MucilAir^{TM}-HF continued to increase at 48 hours post infection, this was not the case for the self-established *in vitro* model. At 96 hours post infection, viral particles count dropped in all experimental groups. In conclusion, Zanamivir inhibited IAV replication in both tissue culture models.

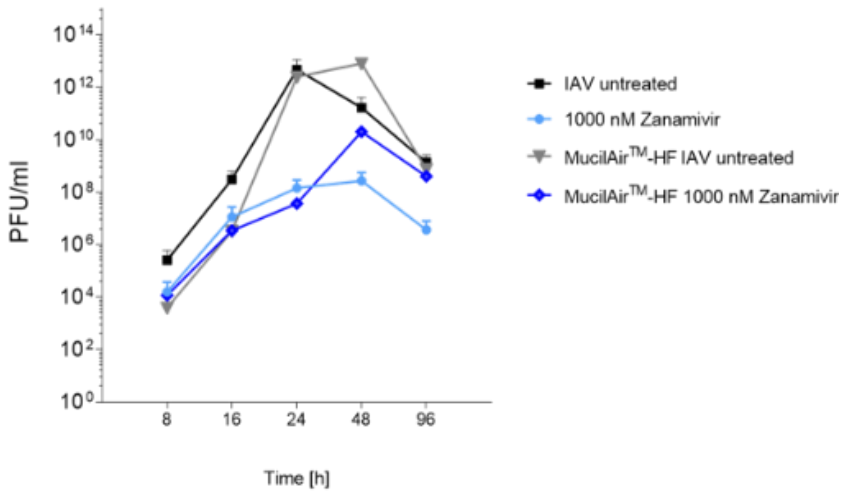

Figure 22. Comparison of different models during an Influenza A virus infection and Zanamivir treatment. Plot showed the level of IAV H3N2 (Panama/2007/1999, PANIII) infection in the supernatant of my *in vitro* models of human based bronchial epithelium model and MucilAir™. Both models were infected in parallel (spot infection with MOI 0.01) and treated with 1000 nM of Zanamivir every 12 hours. Plaque assay was performed using the culture supernatant 8, 16, 24, 48 and 96 hours post infection. One or two biological replicates were performed per experimental group. Data are shown as mean ± SEM. PFU/ml = Plaque forming unit per milliliter.

5.4 Zanamivir inhibits IAV

Next, histology analysis of the infected tissue at 48 and 96 hours post infection were used to visualize tissue morphology. As before, tissues were spot infected (MOI 0.01) with IAV H3N2 (Panama/2007/1999, PANIII) and treated with different Zanamivir concentrations (1000, 100, 0.1 nM). Paraffin-embedded fixed tissues were stained with H&E and Alcian blue. Compared to uninfected control, IAV infection led to no substantial loss of epithelial cells in the first 48 hours independent of Zanamivir treatment (**figure 23,** compare A to B-E, and K to L-O). At this time post infection, epithelial cells still formed the erect prismatic shape found in the untreated control tissues and cell layer was well defined. In contrast, at 96 hours post infection, epithelium layer was damaged in infected tissues not treated with Zanamivir, as well as in tissues treated with 100 or 0.1 nM Zanamivir (**figure 23**, compare F to G-I, and P to Q-S). Although also present, much less damage was visible in tissues infected and treated with 1000 nM Zanamivir 96 hours post infection.

Mucus secretion happened in response to virus infection in the epithelial cell layer. Alcian blue staining was used to visualize the level of secreted mucus. At 48 hours post infection, more secreted mucus was visible in tissues infected with IAV in comparison to the control, while tissues treated with Zanamivir showed similar mucus level comparing to the control (**figure 23**, K- O). After 96 hours in culture, mucus secretion in non-infected tissues was weaker but still visible (**figure 23**, P). At the same time, no secreted mucus was visible in IAV infected tissues (**figure 23**, Q-S), possibly due to the loss of epithelial cells. Remarkably, in tissues treated with 1000 nM of Zanamivir secreted mucus was visible at similar levels as in the control (**figure 23**, compare P and T). Although quantitative analysis of the mucus level was not performed, epithelial cells in the *in vitro* model seemed to respond to viral infection by secreting mucus and Zanamivir sustained such response by protecting epithelial cells from dying.

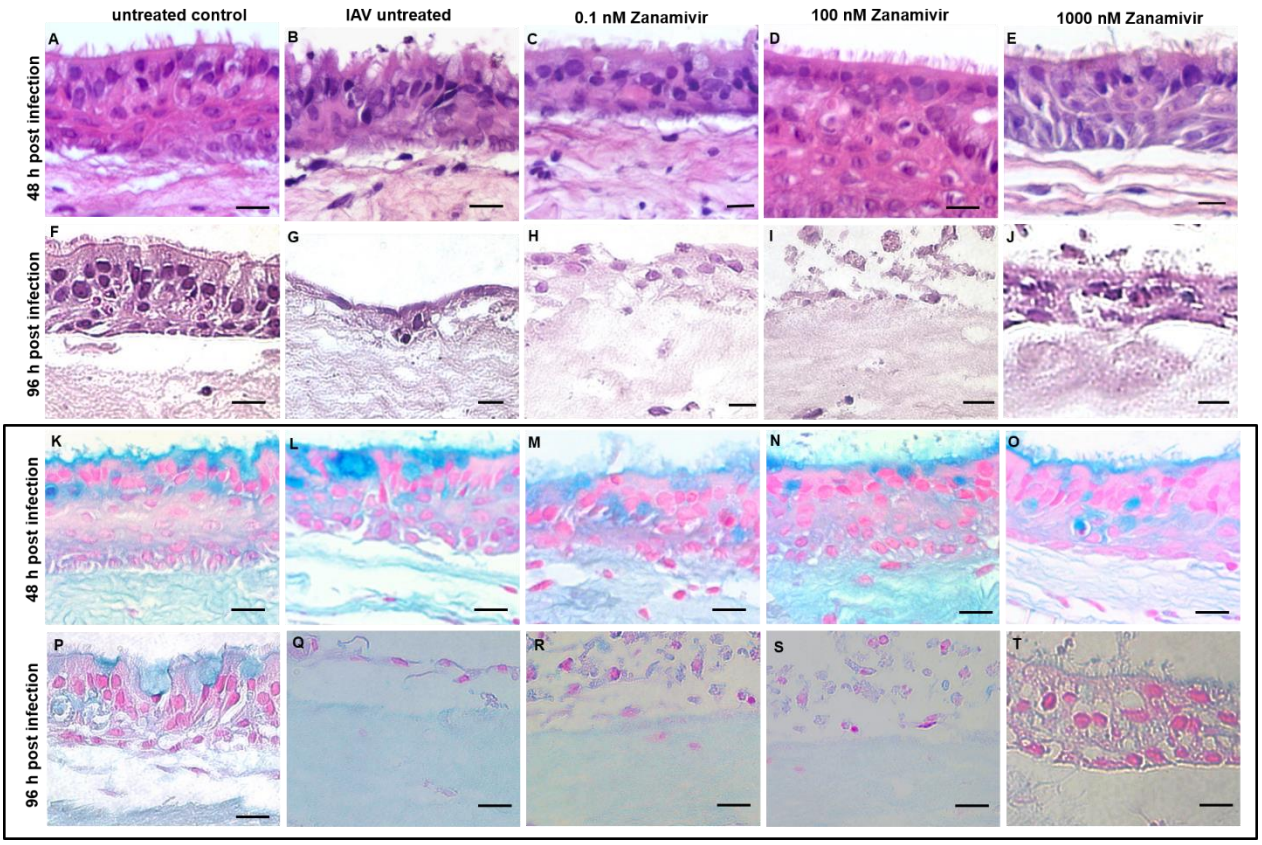

Figure 23. Histology and mucus secretion of the infected tissues infected with IAV and treated with Zanamivir. Histology images of tissue sections from spot infected model with IAV (MOI 0.01), pathogen H3N2 Panama/2007/1999 (PANIII). Sections stained with HE (A-J) and Alcian blue (K-T) were collected from tissues 48 and 96 hours post infection. Tissues were treated with Zanamivir (1000, 100 and 0.1 nM) every 12 hours with Zanamivir. A, F, K and P, untreated, uninfected control. B, G, L and Q, Zanamivir untreated. C, H, M and R, 0.1 nM Zanamivir treated. D, I, N and S, 100 nM Zanamivir treated. E, J, O and T, 1000 nM Zanamivir treated. A-E and K-O 48 hours post infection. and F-J and P-T 96 hours post infection. A-J H & E staining. K-T Alcian blue staining. Scale bar 20 µm.

The effect of Zanamivir in the number of cells in the epithelial layer upon IAV infection can be alternatively explained by cell proliferation instead of cell protection. For testing if Zanamivir (1000, 100, 0.1 nM Zanamivir) and the viral infection itself influenced cell proliferation in the *in vitro* model, tissues were spot infected with IAV H3N2 (Panama/2007/1999 (PANIII), MOI 0.01) and fixed 48 hours later. Tissue slices were immune stained against the protein Ki67 (**figure 24**). Ki67 is a protein specifically expressed in the nucleus of proliferating cells (interphase and mitosis), and therefore used as a cell proliferation marker (Scholzen and Gerdes 2000). Although Ki67 positive cells were detected in all experimental groups, no differences were found in the number of positive cells (**figure 24,** A-E). I conclude that Zanamivir and IAV did not influence cell proliferation at 48 hours post infection.

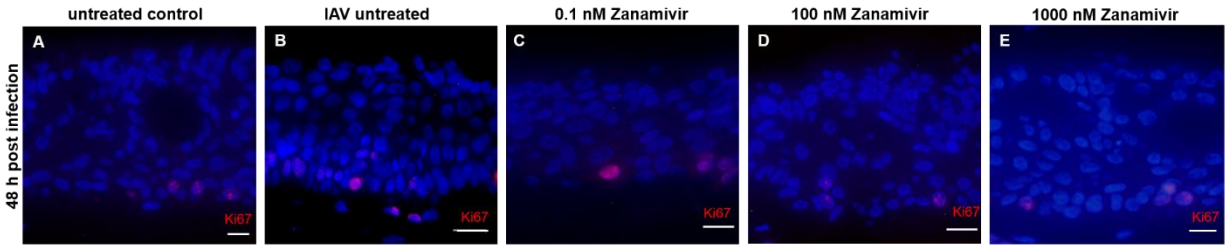

Figure 24. Proliferation assay by Ki67 staining during a IAV infection and Zanamivir treatment. Representative images of tissue sections 48 hours post infection with IAV H3N2, pathogen Panama/2007/1999 (PANIII) (spot infection MOI 0.01) labelled with an antibody against Ki67. A, uninfected and untreated control. B, IAV infected and untreated. C-E, IAV infected and treated with Zanamivir. Tissues were counterstained with DAPI to visualize the nucleus. A single biological replicate was generated. Scale bar = 20 µm.

5.4.1 IAV specifically infects epithelial cells

The results indicated that the IAV virus replicated in the *in vitro* model (figure 22, C). To show that epithelial cells were targeted during infection, I visualized viral particles in infected models using an IAV specific antibody under a confocal microscope. As before, models were infected with IAV (spot infected, MOI 0.01, H3N2, Panama/2007/1999 (PANIII)) for 48 hours and treated with 1000 nM Zanamivir every 12 hours before fixation and antibody staining. As expected, no IAV was detected in the non-infected control group (**figure 25,** A). In contrast, intracellular labeling of viral particles was visible in IAV infected tissues treated or not with 1000 nM Zanamivir (**figure 25**, B and C). No differences in the signal intensity or the number of positive cells in between Zanamivir treated and untreated groups were found. IAV stained cells correspond to infected NHBEC, while no signal was found in lung fibroblasts. These results suggested that IAV specifically infect NHBECs in the *in vitro* tissue culture model independent of Zanamivir treatment.

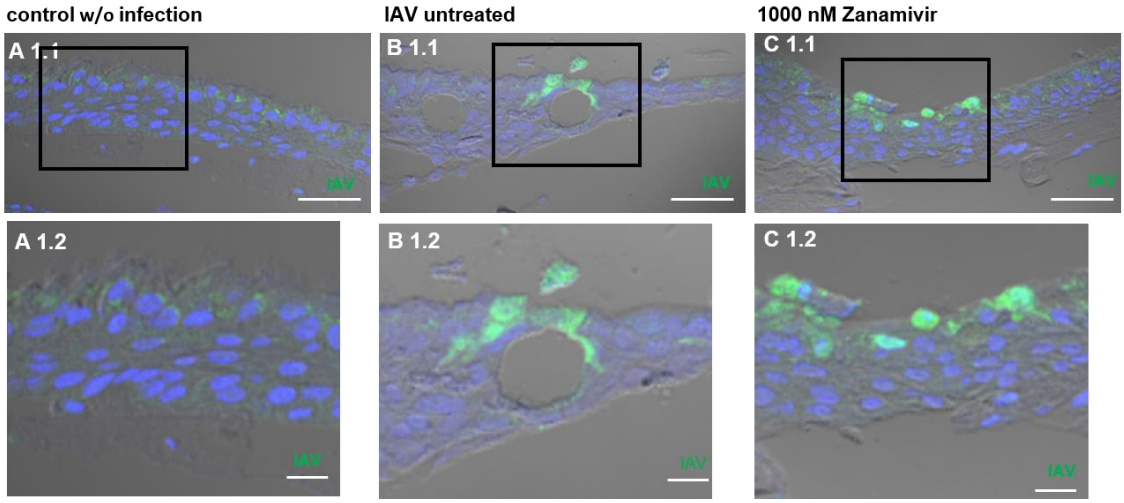

Figure 25. Influenza A virus staining of infected bronchial epithelium models. Representative images of tissue sections 48 hours post infection with IAV H3N2, pathogen Panama/2007/1999 (PANIII) (spot infection MOI 0.01) labelled with an antibody against IAV. Insertions from the regions marked in black squares are also shown. A, uninfected and untreated control. B, IAV infected and untreated. C, IAV infected and treated with Zanamivir. Tissues were counterstained with DAPI to visualize the nucleus. A single biological replicate was generated. Scale bar = 100, 20 µm.

To further explore the Zanamivir effect on IAV infected cells, we analyzed IAV infection throughout the cultured tissue. As before, tissues were infected with IAV (spot infected, MOI 0.01, H3N2, Panama/2007/1999 (PANIII)), treated with 1000 nM of Zanamivir, fixed and immune stained with an IAV-specific antibody. This time, instead of slices, the whole tissue was visualized with a confocal microscope to obtain a better overview. As expected, no IAV was detected in non-infected control group (**Figure 26**, A and D). On the other hand, infected but untreated tissues showed clusters of positive stained cells distributed all over the tissue at 24 hours post infection (**figure 26**, B) while infected tissues treated with 1000 nM Zanamivir showed just a few infected cells (**figure 26**, C). At 48 hours post infection, similar number of positive cells were found in Zanamivir treated and untreated tissues (**figure 26,** E, F). In conclusion, specific IAV signal was detected throughout the tissue. Differences in signal intensity were found in the Zanamivir treated group at 24 hours post infection but not later at 48 hours post infection, possibly due to detachment of dead cells from the epithelium.

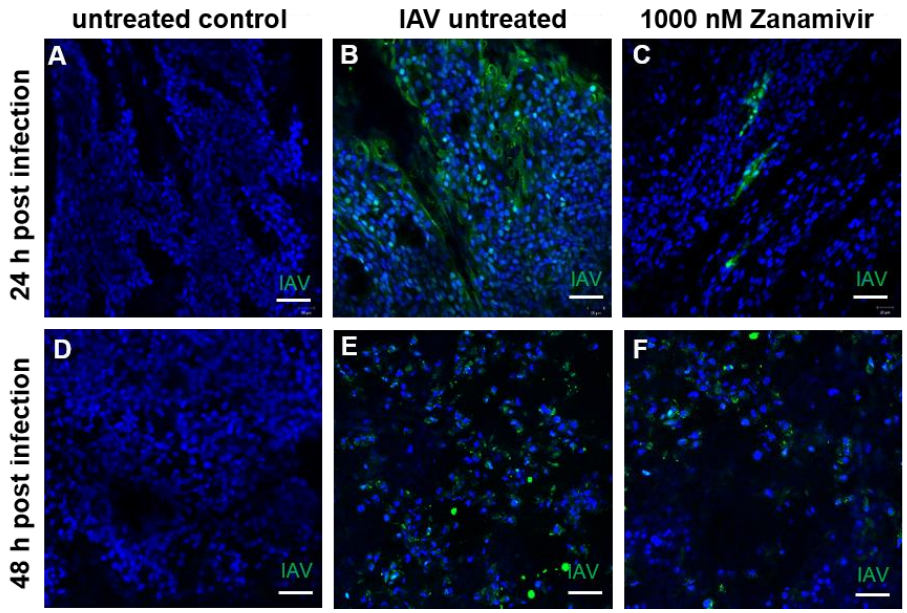

Figure 26. IAV global detection in the bronchial epithelium model. Representative images of tissues 48 hours post infection with IAV H3N2, pathogen Panama/2007/1999 (PANIII) (spot infection MOI 0.01) labelled with an antibody against IAV. A and D, uninfected and untreated control. B and E, IAV infected and untreated. C and F, IAV infected and treated with Zanamivir. Tissues were collected 24 (A-C) or 48 (D-F) hours post-infection. Tissues were counterstained with DAPI to visualize the nucleus. A single biological replicate was generated. Scale bar = 40 µm.

5.4.2 Immunological response during IAV infection

To further characterize the 3D *in vitro* bronchial epithelium model, I evaluated the innate immune response to IAV infection and the impact of Zanamivir treatment. Interferon production and release by infected epithelial and immune cells are primary immune response to IAV infection (Ramos, Smith et al. 2019). Their task is to warn neighbor cells of the infection and to activate antiviral strategies (Ioannidis, Ye et al. 2013). To test the impact of Zanamivir on the immune response to IAV infection in the model, I measured the expression of several interferon genes (from class I, II and III) and interferon stimulated genes (ISG) (**figure 27**). Quantitative RT-PCRs were performed in collaboration with Andreas Hocke lab at Charité (Berlin, Germany). As before, tissues were infected with IAV and treated with Zanamivir. Compared to uninfected controls, IAV infection led to remarkable increase in expression of several interferon genes, especially IFN-α7, IFN-β1, IFN-λ1, IFN-λ2 and IFN-λ3. Importantly, Zanamivir treatment partially reduced the expression boost of interferons suggesting that Zanamivir had a protective effect (**figure 27**, A). These results are in agreement with the cellular response observed *in vivo* (García-Sastre and Biron 2006, Jewell, Cline et al. 2010, Sanders, Doherty et al. 2011).

Strong evidence of immune response to IAV infection and Zanamivir treatment were found in interferon-stimulated gene regulation as well. CXCl10 (C-X-C motif chemokine 10) gene expression is induced by IFN-α and β and has also been shown to respond to H3N2 infection (Préhaud, Mégret et al. 2005, Veckman, Österlund et al. 2006). Accordingly, CXCl10 was highly induced in the infected model and the expression was reduced by ~6-fold in Zanamivir treated tissues (**figure 28**, B). MX1 (MX Dynamin like GTPase), another gene responsive to interferon type I and II during viral infection (Verhelst, Parthoens et al. 2012), was also found to be up-regulated in infected tissues and significant affected by Zanamivir treatment.

In conclusion, quantitative RT-PCR results show that the *in vitro* model tissue responds to IAV infection on the gene level, as expected interferons were up-regulated. Additionally, clear response was observed in the Zanamivir treated group. Therefore, the *in vitro* model shows a comparable immune reaction to *in vivo*.

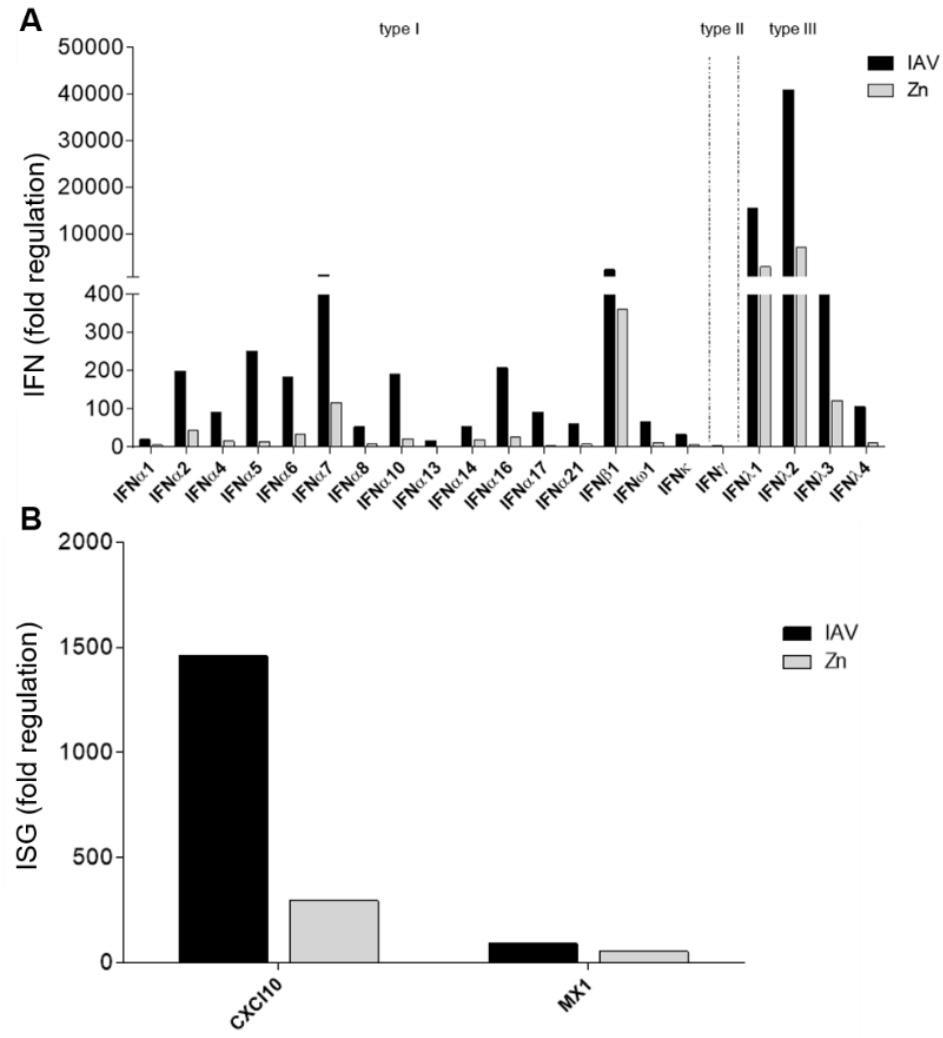

Figure 27. Quantitative RT-PCR of infected bronchial epithelium model untreated and treated with Zanamivir. Quantification of interferon response to IAV infection and Zanamivir treatment in the *in vitro* model. Bronchial epithelium model was spot infected for 24 hours with IAV (MOI 0.01, H3N2, Panama/2007/1999 (PANIII)) and treated with 1000 nM Zanamivir every 12 hours. Gene expression levels are presented as the fold change to uninfected tissues. Several interferon genes (A) and interferon responsive genes (ISG) (B) were quantified. A single biological replicate was generated. Zn = Zanamivir.

To show that gene expression alterations reflect secretion of interferon proteins, ELISA (enzyme-linked immunosorbent assay) was performed against interferons-ß1 and –λ1 (IFN-ß1, –λ1) in the supernatant of tissue cultures after infection with IAV and treatment with Zanamivir (**figure 28**, A and B). Data was normalized to the cell viability results from MTT assays. While IFN-ß1 and IFN-λ1 levels were constant in uninfected tissues in the course of the experiment, it varied in IAV infected groups. Interferon levels were extremely low up to 16 hours post-infection in all experimental groups, increased dramatically 24 hours in the IAV infected group, reaching an expression plateau by 48 hours post-infection and slightly declining 96 hours post infection. Similar increase of expression at 24 hours post infection was not observed for IL-ß1 (**figure 28**, C), a factor associated with microphage response (Lopez-Castejon and Brough 2011).

Infected tissues treated with Zanamivir showed dose response. At 24 hours post infection, increased interferon levels were observed in infected tissues treated with the smallest dose of Zanamivir (0.1nM), but lower than in the untreated group. Tissues treated with the highest dose (100 and 1000 nM) showed no significant increase in interferon protein levels by 24 hours post-infection. However, by 48 hours post-infection, interferon levels reached similar levels to untreated infected control for all doses of Zanamivir except the highest one (1000 nM). Finally, by 96 hours post infection, while the interferon levels slightly decreased for all groups, it showed a slight increase in the infected group treated with 1000 nM of Zanamivir. These results are in strict agreement with the previous results that showed inhibitory effect of Zanamivir in virus proliferation and consequent cellular damage over the course of the infection.

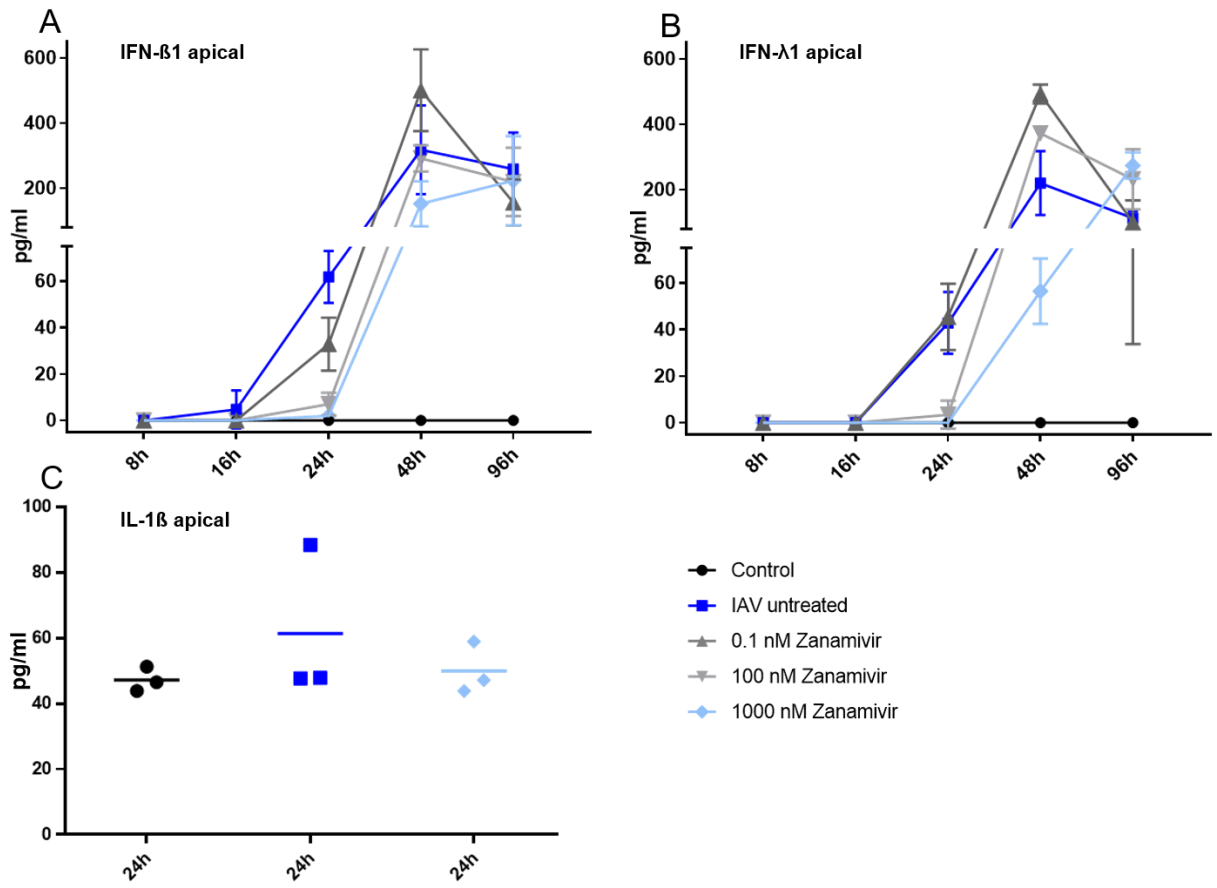

Figure 28. Interferon response in infected bronchial epithelium model tissues treated with Zanamivir. Immune response to IAV infection was assessed by quantifying IFN-ß1, IFN-λ1 and IL- ß1 levels in the culture supernatant by ELISA. Bronchial epithelium model was spot infected with IAV (MOI 0.01, H3N2, Panama/2007/1999 (PANIII)) and treated with Zanamivir every 12 hours. Data is presented as the mean ± SEM of three independent biological replicates.

5.5 Possible applications for the 3D bronchial epithelium *in vitro* model

One key advantage of a human based bronchial epithelium model is to provide a test matrix for viral infections and testing of new drugs. The previous experiments show that the *in vitro* model presents valuable qualities and holds several *in vivo* like features to set a more realistic environment for testing. In this next session, I will show that several recent findings in the literature can be reproduced using the model. The goal is to show that the 3D bronchial epithelia model system can be used for discovery of relevant biology.

5.5.1 Validation of biological markers of IAV infection in the lungs using *in vitro* model

The presence of specific biomarkers of epithelium damage in the lung fluid are useful tools in the clinics for diagnosing and treating patients infected with IAV. A potential biomarker is the club cell specific uteroglobin protein (a.k.a. CC-16), a proinflammatory factor secreted by club cells in the lung epithelia that marks increased permeability of the bronchial epithelia following lung injury (Broeckaert, Arsalane et al. 2000) (Rousseaux, Wallig et al. 2018). As the results indicate that IAV infection damaged epithelial cells in the *in vitro* model, I investigated the level of secreted uteroglobin in the supernatant of the models upon infection and in response to Zanamivir. Tissues were infected as before (spot infection, MOI 0.01, with IAV H3N2, Panama/2007/1999 (PANIII)) and uteroglobin levels were measured in the supernatant with ELISA. To ensure that I was looking at uteroglobin secretion to the corresponding luminal face of the epithelia, supernatant samples were collected from the apical part of the model (**figure 29**, A) and compared to the total amount of uteroglobin collected in both the apical and the basal portions of the model (**figure 29**, B). Protein quantification was corrected by cell viability data from MTT assay in each group.

Surprisingly, the apical levels of uteroglobin in the uninfected control group dropped in the first 24 hours of the experiment, probably in response to the spot infection protocol. Similar behavior was observed in all other experimental groups. However, by 48 hours of the experiment, apical uteroglobin returned to initial levels in uninfected tissues but dropped even lower in tissues infected with IAV and treated with smaller doses of Zanamivir (0.1 and 100 nM). In comparison, the group treated with 1000 nM of Zanamivir showed apical uteroglobin levels similar to the uninfected control by 48 and 96 hours post-infection. While apical uteroglobin was detectable in all experimental groups, lower concentrations were measured in the apical supernatant for infected tissues untreated and treated with smaller doses of Zanamivir (100 and 0.1 nM) but not

with the highest dose (1000 nM), probably reflecting the epithelium damage observed in the previous experiment. Interestingly, the total secreted level of uteroglobin remained constant throughout the experiment with slight increase in the uninfected group and the infected group treated with the highest dose of Zanamivir (**figure 29**, B). This indicate that uteroglobin was specifically secreted in the apical portion of the model.

Additionally, I investigated the cellular expression of uteroglobin by immunohistology of uninfected tissues (**figure 29**, C.1) and infected tissues treated with 1000 nM Zanamivir (**figure 29**, C.2) 96 hours post infection. Infected tissues not treated or treated with smaller doses of Zanamivir were not considered for this analysis because previous histology analysis showed widespread damage to the epithelium (**figure 23**). At 96 hours post infection, untreated and Zanamivir treated tissues were paraffin fixed, cut into sections and specifically labeled with antibody against human uteroglobin. Uteroglobin was detected in the cytosol of cells throughout the tissue in both experimental conditions. Uninfected tissue showed particularly strong uteroglobin signal in cells located on the apical surface of the tissue (**figure 29**, C.1). Besides showing overall lower uteroglobin signal, infected tissues treated with Zanamivir also did not show the specific strong uteroglobin signal in the apical cells. I concluded that IAV infection effects uteroglobin presence in epithelium and Zanamivir treatment only partially reverts this effect.

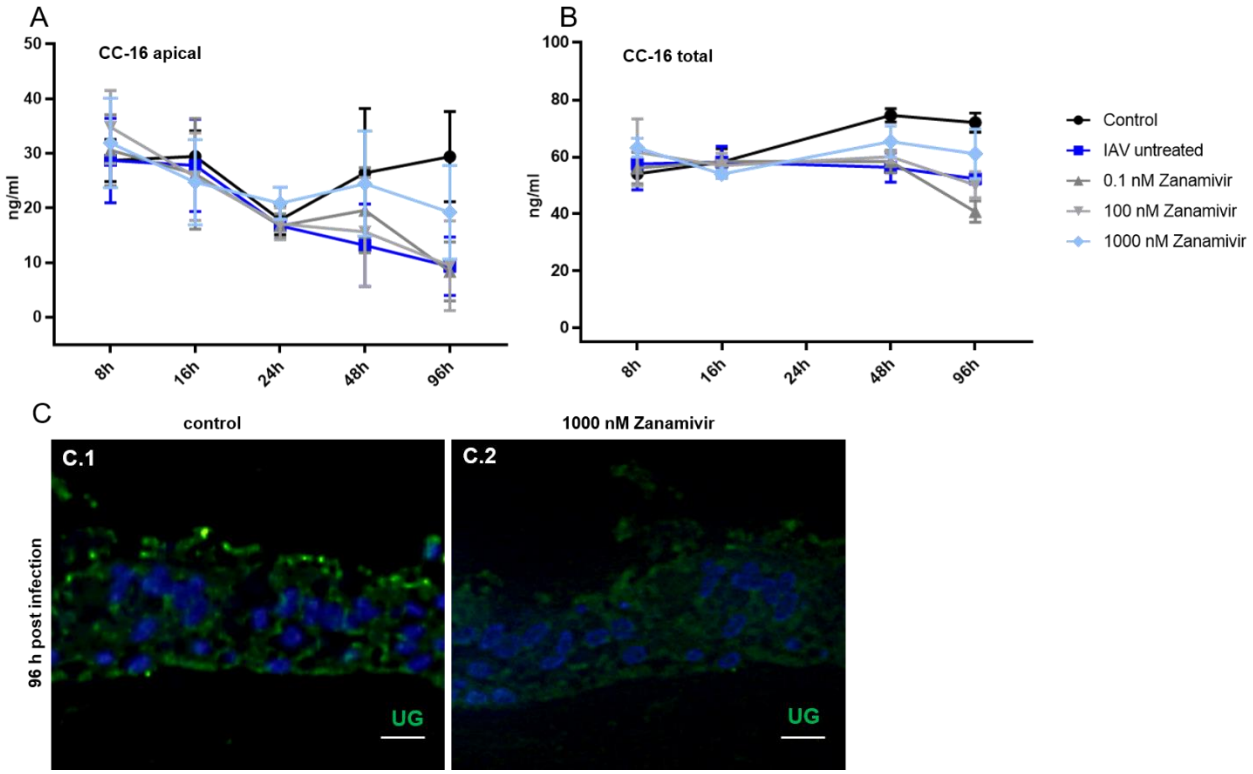

Figure 29. Uteroglobin expression in infected bronchial epithelium model infected with IAV and treated with Zanamivir. Analysis of uteroglobin expression in the bronchial epithelium models following IAV H3N2 infection, pathogen Panama/2007/1999 (PANIII) and treatment with Zanamivir. Apical and basal supernatant samples were collected 8, 16, 24, 48 and 96 hours post infection. A and B, uteroglobin concentration levels were quantified via ELISA. Total concentration of uteroglobin was obtained from the sum of basal and apical uteroglobin. Data is presented as mean ± SEM from 5 and 2 biological replicates for the apical and total values, respectively. Zanamivir 1000 nM to the untreated IAV sample, p = 0.069, one-way Anova, post hoc Dunette. Immunofluorescence images (96 hours post infection) with specific antibody against uteroglobin (UG, green). Tissues were counterstained with DAPI (blue) for visualization of the nucleus. Scale bar = 20 µm.

5.5.2 Validation of a novel candidate treatment for IAV infection in the lungs

Discovery of new treatments for viral infections in the lung is a topic of active research. Next, I tested the antiviral properties of a recently identified potential treatments in the 3D bronchial epithelial *in vitro* model infected with IAV. The bacteriophage capsid – Qß shows host cell-like membrane ligands (like sialic acids α-2,6- and α-2,3) and associates with the viral spike protein, therefore inhibiting viral replication (Weis, Brown et al. 1988, Lauster, Klenk et al. 2020). To test the ability of the Qß capsid to inhibit IAV replication in the tissue culture model, tissues were infected with IAV (spot infection, MOI 0.01, H3N2, pathogen Panama/2007/1999 (PANIII)). Qß capsid were added to the tissue culture 1 and 24 hours post infection (**figure 30**, A). Viral concentration in the supernatant was quantified with plaque assay to test the inhibition of viral replication. Similar virus levels in all experimental groups were found by 8 hours post infection (**figure 30**, A). By 16 hours post infection, treatment with Zanamivir showed reduction of viral particles in the supernatant and this reduced levels of viral persisted throughout the experiment (**figure 30**, B). Similar results were observed for infected tissues treated with Oseltamivir, a drug also used in the clinics, suggesting that the inhibitory effect of viral replication can also be observed with multiple treatments other than Zanamivir.

A small effect on viral particle counts was also observed in the experimental group treated with 10 nM Qß capsid only 24 hours post infection but returned to control levels by 48 hours. In contrast, treatment with 15 nM Qß capsid led to no differences at 24 hours but reduced viral load at 48 hours post infection. This indicates that Qß capsid effect is either limited or delayed in the 3D bronchial epithelium model infected with IAV. Furthermore, the model can be used to study the molecular and cellular mechanisms involved in the Qß capsid inhibition of IAV replication, although a different treatment scheme than used here might be necessary for optimal results.

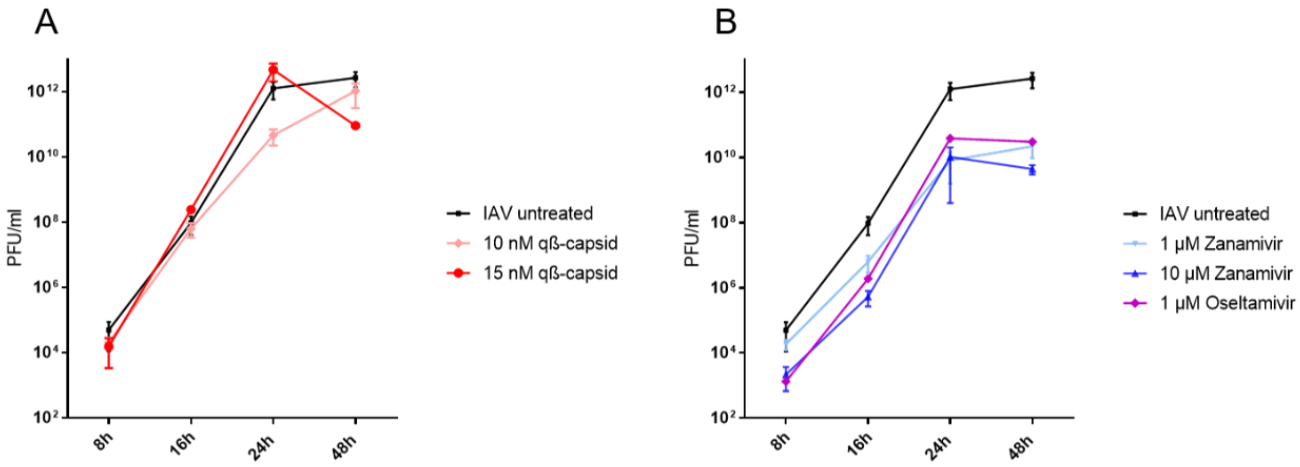

Figure 30. IAV inhibitor trials at the infected bronchial epithelium model. Inhibitory effect of IAV inhibitors on viral replication in the 3D bronchial epithelial tissue model following infection with IAV H3N2, pathogen Panama/2007/1999 (PANIII) (spot infected, MOI 0.01). After infection, tissues were treated with 10 nM, and 15 nM of Qß capsid applied 1 hours and 24 hours post infection (A); or 1 µM and 10 µM Zanamivir, or 1 µM Oseltamivir were applied 2 hours and every 12 hours post infection (B). Data are shown as the mean ± SEM of 1 to 8 independent biological replicates per time point and treatment. IAV untreated control is the same in both plots.

5.5.3 Validation of novel drug delivery tools: nanogels, lipid nanoparticles and curcumin particles

Treatment efficiency depends on successful delivery of drugs to target cells. The presence of luminal mucus and the cilia movement complicates drug delivery in the human lungs. These circumstances demand smart delivery systems. the 3D bronchial epithelial *in vitro* model provides an ideal trial platform for testing new drug delivery systems as it produces mucus and cilia movement is present (**figure 31**, A, B). Therefore, I tested three potential drug delivery systems: nanogels, lipid nanoparticles and synthesized curcumin particle.

Nanogel muco-penetration

Nanogels provide promising delivery features for transmucosal delivery in therapeutical use. In collaboration with the Calderón lab, Polymat - Polymer Chemistry, San Sebastian, I tested the ability of nanogels to penetrate the mucus in the models. Both degradable PNIPMAM-(S-S)-dPG and non-degradable PNIPMAM-dPG nanogels synthesized by Loryn Fecher (Calderón lab, FU Berlin) were applied for 3 to 6 hours to the 3D bronchial epithelial *in vitro* model and compared to PBS treated control (**figure 31**). For detection in histological sections, nanogels were loaded with the fluorescent molecule RhodB. Parts of these experiments were published somewhere else (Charbaji, Kar et al. 2021). Degradable nanogel particles were found in the epithelial layer as early as 3 hours post application (**figure 31**, D, E, H). In contrast, non-degradable nanogel particles were found exclusively in the mucus even after 6 hours post application (**figure 31**, F, I). The higher efficiency in delivery for the degradable nanogel might be due to its ability to form disulfide bonds with mucus proteins, facilitating muco-penetration (Yin, Ding et al. 2009, Nema, Jain et al. 2013).

Of particular interest was to study the effect of the anti-cytokine-TNF antibody Etanercept (ETN) (Zhao, Mysler et al. 2018) in enhancing muco-penetration of nanogel particles. For that, degradable and non-degradable nanogels were loaded with ETN before application to the model. Instead of loading nanogels with RhodB, particles were detected in histological section by the cross-reactivity of ETN to fluorescent secondary antibodies. For degradable nanogels, efficient muco-penetration was visible as before while no nanogel particles were detected in tissues treated with non-degradable nanogel or negative control group treated with PBS. These results show that ETN does not facilitate muco-penetration of non-degradable nanogel particles. Finally, to evaluate the cytotoxicity effect of applying nanogels to the models, I measured level LDH released in the media 6 hours post treatment (**figure 31**, H). Compared to the PBS treated control, LDH levels in

nanogel treated samples were similar or lower, indicating no cellular damage. A control group was included where tissues were treated with detergents to induce cellular damage. In conclusion, degradable nanoparticles penetrate the mucus and enters the cell layer in the model without damaging cells.

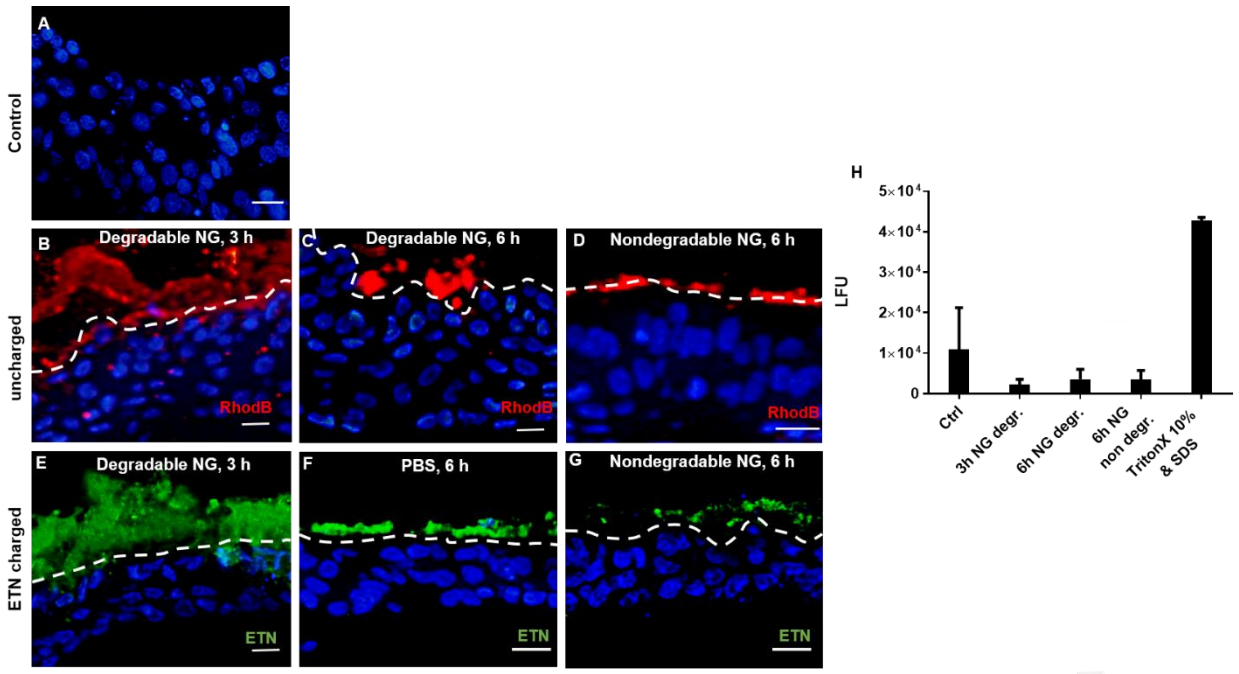

Figure 31. Nanogels penetrate the mucus and enter cellular layer in the 3D bronchial epithelial *in vitro* model. Bronchial epithelium models treated with degradable and non-degradable Nanogels for 3 to 6 hours. Untreated tissues as control (A). Degradable PNIPMAM-(S-S)-dPG and non-degradable PNIPMAM-dPG nanogels were labeled with RhodB (red) for visualization (B-D). Alternatively, ETN loaded nanogels were visualized by cross reactivity with Alexa Fluor®488 fluorescent secondary antibody (E-G). Immune fluorescence images were counterstained with DAPI (blue). Representative images of at least two independent biological replicates are shown for each experimental group. Scale bar 20 µm. Cytotoxicity was measured by quantifying the release of LDH in the media, fluorometric measured in LFU (H). Data are shown as the mean ± SEM of 2 independent biological replicates per treatment. NG = nanogel.

LNP muco-penetration

Lipid nanoparticles (LNPs) are well-studied delivery systems already in use in the clinics (Akinc, Maier et al. 2019, Lamb 2021). LNPs are composed of 4 lipid constituents – ionizable cationic lipids, “helper lipid”, e. g. distearolyphosphatidycholine (DSPC), cholesterol and PEG (polyethylene glycol)-lipids to envelop the genetic material (e. g. siRNA) to be transfected in the target cells (Kulkarni, Myhre et al. 2017). Next, I tested if the epithelial cell layer in the 3D *in vitro* model can be transfected with siRNA delivered via LNPs of different compositions.

First, cultured NHBEC monolayers were used to establish a LNP delivery protocol. Five compositions of LNPs with unique helper lipids were tested: DSPC (1,2-distearoyl-sn-glycero-3-phosphocholine), DOPC (1,2-(cis, cis-9,12-octadecadienoyl)-sn-glycero-3-phosphocholine), DOPE (1,2-dioleoyl-sn-glycero-3-phosphoethanolamine), ES (Egg sphingomyelin) and DSGP (di-stearoyl-phosphatidylglycerol). Distinct proportions of PEG (0.5, 1.5 and 5 %) were also tested as it influences nanoparticles size and thereby transfection potency (Kulkarni, Witzigmann et al. 2019). ApoE is commonly used as a receptor ligand to increase endocytosis and was also tested. Finally, LNPs were load with increasing amounts of siRNA template (0.1, 0.3 and 1 µg/ml). For detection, LNPs were stained with the lipophilic membrane dye Dil (Yektaeian, Mehrabani et al. 2019) and analysis performed with Cellomics Array Scan VTI (Thermo Scientific). LNPs were added to cell cultures for 24 hours and experimental groups compared to PBS-treated control. Transfection efficacy was assessed by high content screening. These experiments were performed in the University of British Columbia.

Arguably, concentration of loaded siRNA showed the strongest impact on transfection efficiency and LNPs with 1 µg/ml siRNA showed highest efficiency in all groups (Two-way ANOVA, multiple comparisons, $p < 0.0001$) (**figure 32**, A). Transfection efficiency was also improved in the majority of experiments where LNPs were combined with ES as “helper lipid”. The proportion of PEG did not seem to impact transfection in most cases, although a small positive effect was observed for LNPs containing DSPC, DOPC or DOPE. On the other hand, presence of ApoE in the LNP composition influenced positively transfection efficiency. Best results were obtained with LNPs composed of ES, containing ApoE, charged with 1 µg/ml siRNA, and with any concentration of PEG.

Transfected cells were also imaged in a confocal microscope (LSM 9, Zeiss) to visualize intracellular LNPs. NHBEC were seeded on 8-well chamber slide and imaged 24 hours post LNPs

treatment. Most favored LNP compositions of DSPC and ES were tested. Images reveal healthy cells with exemplary formed nuclei (**figure 32**, B). While no signal was detected in NHBE cells treated with PBS, cells treated with LNPs showed strong intracellular DiI signal. Importantly, no nuclear nuclear staining was observed.

The next step was to test cell transfection in the 3D bronchial epithelia *in vitro* model. Unfortunately, due to the pandemic situation of COVID-19, the experiments were prematurely interrupted. Nevertheless, I established a protocol for transfection of NHBEC cells *in vitro* that should serve as base for future transfection trials on 3D models of cystic fibrosis (see below).

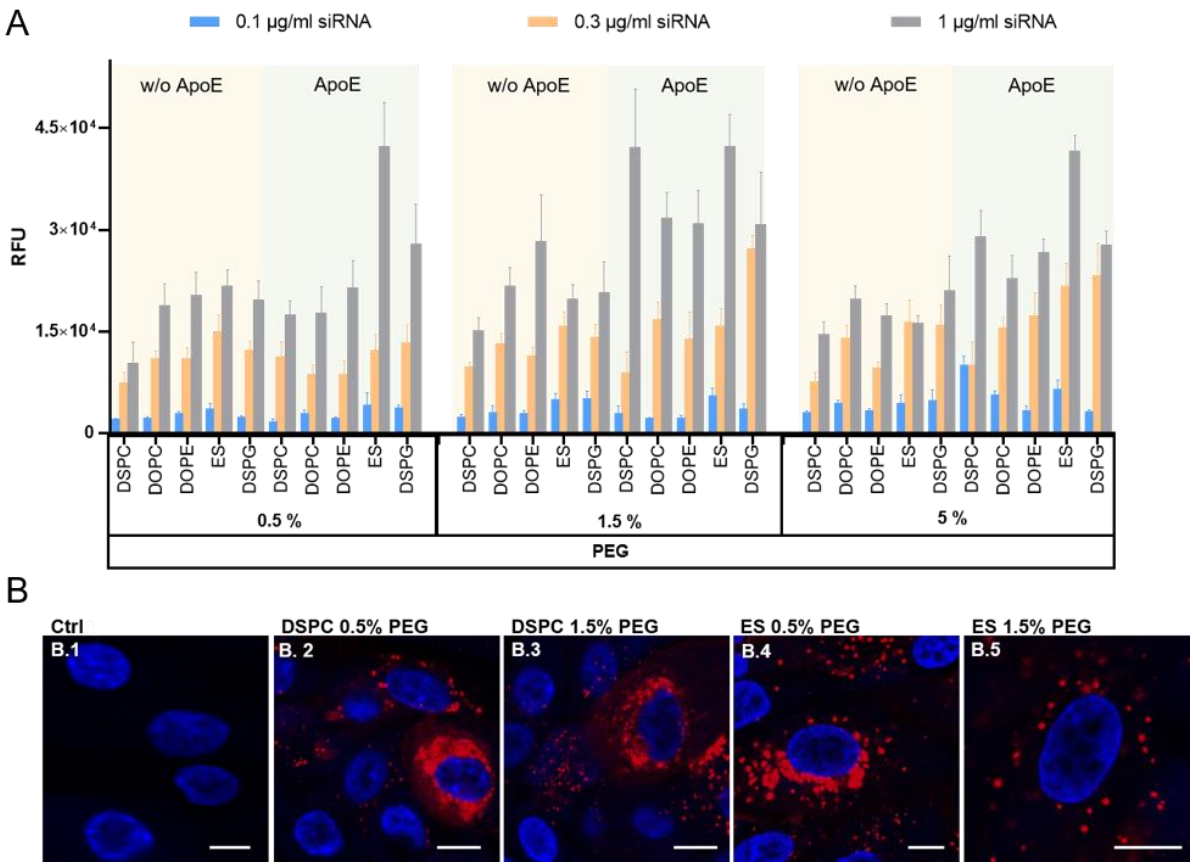

Figure 32. LNP transfection of NHBEC. A, NHBEC monolayers were transfected with different LNPs for 24 hours – DSPC, DOPC, DOPE, ES, DSPG were loaded with distinct siRNA concentrations (0.1 (n=1), 0.3 and 1 µg/ml (n=2)). Additionally, LNPs were combined with 0.5 %, 1.5 % or 5 % PEG and linked to ApoE. LNPs were labeled with Dil (DilC18, 0.2 %) for visualization. Samples were measured by high content screening in a Cellomics Array Scan VTI. B, NHBEC seeded in 8-well chamber slide and treated with LNPs for 24 hours. Nucleus were counterstained with Hoechst 33324 (blue). Scale bar 10 µm. B.1, untreated control. B.2, DSPC linked to 0.5 % PEG, charged with 1 µg/ml and without ApoE. B.3, DSPC linked to 1.5 % PEG, charged with 1 µg/ml and without ApoE. B.4, ES linked to 0.5 % PEG, charged with 1 µg/ml and without ApoE. B.5, ES linked to 1.5 % PEG, charged with 1 µg/ml and without ApoE. LNPs labeled with Dil (DilC18, 0.2 %). Images shown are representative fields from a single biological replicate.

Curcumin delivery

The third type of drug delivery system I tested was synthetic curcumin particles. This work was done in collaboration with the group of Prof. Dr. Shyh-Dar Li at the University of British Columbia, Vancouver, Canada. However, only preliminary results were obtained as work had to be stopped due to the COVID-19 pandemic. For that, the 3D bronchial epithelial *in vitro* model was treated with curcumin particles for 6 and 24 hours. For intracellular detection, particles were labeled with fluorescent markers (DiR) and transfected tissue sections were imaged with fluorescence microscopy. Besides transfection, cytotoxic effects from the curcumin treatment were also evaluated while LDH measured 6 h post treatment. Fluorescent signal was detected on the border of the epithelial cell layer but not inside the cells (**figure 33**, C, F). These results indicated that, at least with the conditions tested, synthetic curcumin particles penetrate the mucus but do not infect bronchial epithelial cells in the model. It is unclear if prolonged exposure would lead to intracellular particle presence in the models. Besides cytotoxicity was not detected 6 h post curcumin treatment (**figure 33**, G).

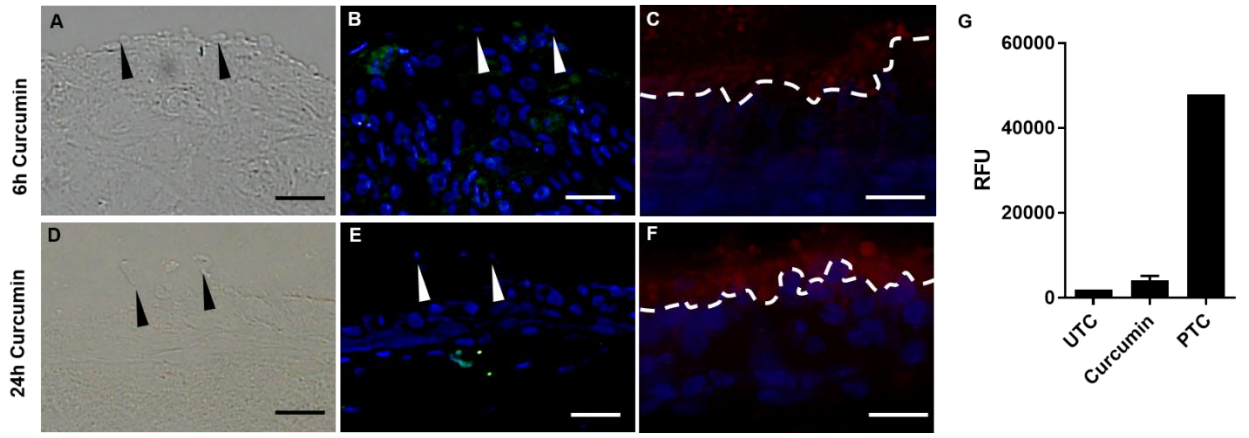

Figure 33. Curcumin treatment on the bronchial epithelium model. Presented images and graph imply results of a curcumin treatment on bronchial epithelium models. All fluorescence images were DAPI counterstained. Bright field image showed treatment with curcumin (first trial). A, at 6 hours post treatment, arrows pointed to apoptotic cells. D, 24 hours post treatment, arrows pointed to apoptotic cells. B, same as image as A with immune fluorescence staining, curcumin treatment (first trail) 6 hours post treatment, arrows pointed to apoptotic cells. E, same as image D with immune fluorescence staining showed treatment with curcumin treatment (first trial) 24 hours post treatment, arrows point to apoptotic cells. C, curcumin treatment (second trial) at 6 hours post treatment, dashed line marks barrier of curcumin solution. F curcumin treatment (second trial) at 24 hours post treatment, dashed line marks barrier of curcumin solution. Scale bar 20 µm, 2 independent replicates. G, graph presented LDH release at 6 hours post treatment, for curcumin 1 and 2 solution. Samples measured against untreated control (UTC) and positive control (PTC) treated with 10 % Triton X, 6 hours post application, n = 2.

5.5.4 Generation of a human cystic fibrosis model system based on the bronchial epithelial *in vitro* model

Besides viral infections and drug delivery systems, a human based 3D *in vitro* models enable safe testing options for studying also gene therapy. Cystic fibrosis (CF) is a relevant genetic disease of the lung caused by the alteration of a single gene, CFTR (Rowe, Miller et al. 2005). Some CF patients carrying insufficient or loss-of-function mutations in CFTR suffer from muco-obstruction due to reduced mucus clearance in the lung lumen (Saint-Criq and Gray 2017). With the discovery of the CRISPR Cas9 gene editing tool (Sternberg, Redding et al. 2014), gene therapy became a promising treatment to increase patient's life quality and possibly curing CF.

Next, I adapted the 3D bronchial epithelial *in vitro* model to study CF. For that, primary human cystic fibrosis bronchial epithelial cells (HCFBEC) were used instead of NHBEC. These HCFBEC contain the most common mutation in the CFTR gene - delta F508 (Cutting 2015). Tissues were cultivated for 21 days as before, paraffin-embedded, cut into tissue sections, and stained with different protocols. Morphologically, CF is characterized by higher amounts of mucus, sticky mucus fragments and smaller cilia (Trinh, Bardou et al. 2012). For morphological analysis, tissues were stained with H&E, and Alcian blue for visualization of the mucus (**figure 34)**. CF models were cultivated with and without rinsing to mimic the clinical scenario by artificial removal of overproduced mucus. As for the model generated with cells from healthy donors, CF models showed two cellular layers, one of NHLFb in collagen matrix and one apical layer of HCFBEC as expected. Increased mucus production could also be observed in CF models. However, cells did not show the characteristic prismatic shape and more diffuse bronchial epithelial cell organization was observed, while CFTR levels were similar in all models (**figure 34** C, F and I). In a second trial, models were rinsed once with PBS in the last week of cultivation, as according to protocol used for cultivation of models generated from healthy cells (**figure 34**, D-F). This time, the histology was more characteristic for bronchial epithelial tissue, by presenting a monolayer of erected epithelial cells. Additionally, mucus production was increased in comparison with control models generated from cells from healthy donors.

In conclusion, the CF *in vitro* model created here partially mirrors characteristics observed *in vivo* in CF patients, like the increased mucus layer. Besides, rising to remove overproduced mucus restored tissue morphology. Therefore, the model was successfully adapted to create a CF model to study the disease *in vitro* using donor patient cells.

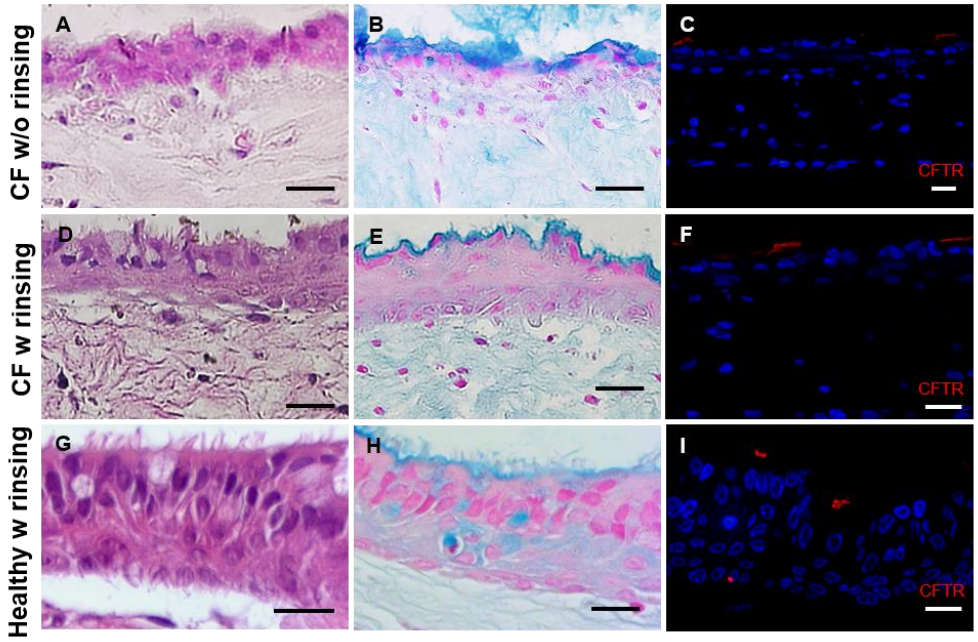

Figure 34. Development of a Cystic fibrosis 3D bronchial epithelial *in vitro* model. Morphological analysis of the CF model. CF models were rinsed (D-F) or not (A-C) once in third week of cultivation with PBS to remove overproduced mucus. Models generated with cells from healthy donors are shown for comparison (G, H, I). Histological sections were stained with H&E (A, D, G) or Alcian blue (B, E, H). Immune fluorescence staining against CFTR (C, F, I). Images are representative fields from two independent biological replicates. Scale bar = 20 µm.

6. Discussion

6.1 Development of the human based 3-D bronchial epithelial *in vitro* model

Cultivation of 3D engineered models is complex and challenging but human tracheal/bronchial, small airway and alveolar 3D models are available on the market. Several of these models contain lung cell lines such as Calu-3, BEAS-2B or 16HBE14o (Hermanns, Freese et al. 2017). The use of cell lines has the advantages as of low costs, long life span and easy handling. However, they differ from primary cells in gene expression, over activated cell cycles and metabolism, and can therefore lead to wrong biological conclusions (Lidington, Moyes et al. 1999, Boerma, Burton et al. 2006, Pan, Kumar et al. 2009). All these disadvantages of cell lines need to be considered and interpreted in all observed results. In comparison primary cells provide *in vivo* like characteristics, they are not modified and are derived from native tissue (Mostafa, Rider et al. 2019), but another not minor fact about desired primary cell cultures is that they are limited, especially the access to healthy bronchial epithelial, endothelial cells or lung fibroblasts. In general, primary lung cells are often obtained during surgeries or biopsies, it can not be excluded that ill tissue parts were collected as well (Annaratone, Marchiò et al. 2013, Huang, Lee et al. 2018). Additionally, old patients are more likely to be the donor, cell proliferation, cell colony forming capacities and even different gene expression and interferon response lowers with aging processes (Maughan, Nigro et al. 2020). Also, donor variations are problematic as seen in histological analyses of the self-generated *in vitro* model as well (**figure 16**). Interestingly, based on the variation problematic, some commercial models contain a pool of NHBEC of several donors to lower the variation (Baxter, Thain et al. 2015, Boda, Benaoudia et al. 2018). A similar benefit offer induced pluripotent stem cells (iPS) cells, they do not have donor specific varieties while using one donor for multiple cell types in one model, here another great advantage is the unlimited source to cells and the cell collection from any healthy organism, 3D *in vitro* model tend to use iPS cells as seen in an alveolar *in vitro* model (van Riet, Ninaber et al. 2020).

In addition, still some low complexity 3D models are composed of a single cell type, in comparison to the several cell types present in the living organ (Cervena, Vrbova et al. 2019). Besides, in some cultures, the medium of 3D tissues contains antibiotics that potentially affect cell proliferation (Llobet, Montoya et al. 2015).

During the studies, I developed a bronchial epithelial 3D *in vitro* model based on primary cells from human donors and presenting *in vivo* like pseudo-stratified epithelium morphology (Tomashefski

and Farver 2008). In the model, bronchial epithelial cells were grown without antibiotics and differentiate into goblet, club and ciliated cells and formed an erect prismatic cell shape with a basal monolayer (**figure 10, 16** I, J), as seen in the *in vivo* airway tissue (Khan and Lynch 2020). The *in vitro* model contains next to the epithelium also embedded fibroblasts in collagen, often commercial models contain just NHBEC as a single layer of differentiated cells (Porotto, Ferren et al. 2019). On one hand, the *in vitro* system is a human based 3D engineered model presenting several benefits for human bronchial tissue studies. On the other hand, I am aware that the *in vitro* model also has limitations.

Initially, the idea was to place the *in vitro* model into a dynamic system to reduce the cultivation time, because best results were obtained when the models were cultivated for 3 weeks (**figure 9,** H.1, H.2). Shorter cultivation times could enhance reproducibility and performance of the bronchial epithelium model as a test matrix. For accelerating the process, models were placed in a dynamic cultivation setting. Dynamic settings promise faster cell differentiation and increased cell connection due to mechanical forces through the media perfusion (Chandorkar, Posch et al. 2017). However, an uncharacteristic double epithelial cell layer formed in the model grown under the dynamic cultivation setting (**figure 15**). A reason for the problematic model growth might have been the missing bronchial endothelial cells (BEC), they are lining the inside of a vascular tube system as arteries and veins, they are in direct contact to the blood stream, here in direct contact to the media stream (Krüger-Genge, Blocki et al. 2019). Previous publications showed successful results of *in vitro* models connected to a fluidic system, all models had in common integrated bronchial endothelial cells (BEC), probably BEC lower sheer stress for the neighbor cells as NHLFb and NHBEC and are essential to obtain benefits from a perfused system (Jeans, Howard et al. 2012, Ataç, Wagner et al. 2013, Box, Livermore et al. 2015). In my study I tried to implement BEC (**figure 18**), more trials need be performed and more praxis in handling is necessary, it will be discussed later (6.1.3 Fibroblasts and ECM). Dynamic systems enable a great advantage, model medium would be permanently exchanged thereby secures nutrient supply, and sheer stress influences even cell morphology, cell proliferation, differentiation metabolism and communication. Observing cell communication in between several *in vitro* models would be possible, while connecting more than one tissue to the system. For studying diseases as the atopic march, the development of an allergic rhinitis or even asthma bronchial triggered by atopic dermatitis during the childhood (Bantz, Zhu et al. 2014), a coculture of a skin and an airway *in vitro* model would be required, to test cell signaling and to study interaction of both tissues.

Furthermore, the perfusion pump had to be placed outside of the incubator (because of its size). The culture medium tubing system went in and outside the incubator to reach the perfusion pump, increasing the risk of contamination. In the future, a micro pump would be of advantage to reduce risk of contamination (Ataç, Wagner et al. 2013) or even companies developed advanced perfusion systems as CULTEX® LTC-C (long term cultivation - continuous) (Cultex Technology, Hannover, Germany) (Aufderheide, Förster et al. 2016). Cultex developed a computer-controlled perfusion system for air-liquid interface cultures, medium volume and perfusion rate can be installed. Dynamic systems allow a more realistic setting and support the advanced application of *in vitro* models.

Scaffolds provide a comparable decellularized ECM structure to embed and to support cell growth for *in vitro* cultures. They build a framework for cells to attach and enhance bronchial tissue morphogenesis (Steinke, Gross et al. 2014, Marrazzo, Maccari et al. 2016). I also tested using scaffolds for tissue assembly. Therefore, the Alvetex® scaffolds tried here did not improve the model quality (**figure 9,** A-D). Alvetex® scaffolds are made of highly porous polystyrene (Knight, Murray et al. 2011), probably the tailored porosity was not ideal for NHLFb and NHBEC, because decellularized ECM of endothelial cells, fibroblast and epithelial cells differ in the airway (Bridge, Aylott et al. 2015, Mao, Hoffman et al. 2017). Tissue specific porous 3D scaffolds can be produced with desired fiber density and structure to support even individual tissue layers of the respiratory tract (Bridge, Aylott et al. 2015). Other publications support the use of scaffolds, seeding smooth airway muscle cells into the scaffold, similar airway ECM proteins as in *in vivo* tissue were detected (Young, Shankar et al. 2017). Also, increased cell proliferation and cell density is promised (Morris, Bridge et al. 2014). Scaffolds can be used as a supportive tool, especially in transplantation research single tissue parts might be replaceable with bioengineered *in vitro* airway tissue on a scaffold (Hamilton, Lee et al. 2020).

Another tool I have been used was a Teflon® ring to limit the epidermal growth area, leading to comparable morphology to the *in vivo* tissue in skin and bronchial models (Harrington, Cato et al. 2014, Gronbach, Wolff et al. 2020). However, use of a Teflon® ring did not improve morphology in the model, especially because tissues were harmed during ring removal (**figure 14**). Contrary to expectations, the use of additional tools for model development was not helpful. Furthermore, these led to increased handling, likely affecting reproduction and the chance of contamination. Another technique to limit epidermal growth area and support cell organization is the usage of bioprinting, as printing individual cell layers of alveolar, bronchial epithelial and endothelial cells for creating alveolar tissue (Ng, Ayi et al. 2021). Application of bioprinting ensures precise cell

seeding and a high reproducibility through the mechanical controlled procedure (Mahfouzi, Safiabadi Tali et al. 2021). Additionally, bioprinting plays a demand role by addressing 4D *in vitro* models, to create a hollow organ (Mahfouzi, Safiabadi Tali et al. 2021). Applying bioprinting in synthesizing an anatomical shaped lung area to grow airway cells, might even allow to connect the individual airway compartments as e. g. bronchos and alveoli in the future.

During the bronchial epithelium model development, it was clear that skin fibroblasts affected the differentiation of NHBECs (**figure 8**). Model morphology was comparable to skin epidermis: cubical cells in the base line and flat cell layers (Löwa, Vogt et al. 2018). In agreement with that, fibroblast heterogeneity (which can depend on the organ of origin) plays a significant role in NHBECs differentiation (Florin, Maas-Szabowski et al. 2005). Fibroblasts produce the extracellular matrix (ECM) composed of collagen, elastin and multiple signaling proteins (Parsonage, Filer et al. 2005). These molecules (for example growth factors) signal to other cells and help coordinating tissue compartmentalization, characterized by different cell morphologies, differentiation, and function (Baptista, Siddiqui et al. 2011). For example, seeding pluripotent stem cells into the ECM-scaffold from decellularized kidney and heart led to formation of a tissue with organ-like morphology (Ullah, Busch et al. 2020). In another example in COPD lung tissues, healthy cells were seeded in healthy and COPD decellularized ECM-scaffold, leading to corresponding gene expression alterations (Hedström, Hallgren et al. 2018). These data highlight fibroblast importance in tissue formation.

ECM can also be produced in the lab with co-cultures of human umbilical venous endothelial cells and human fibroblasts (Chowdhury, Howat et al. 2010, Kaessmeyer 2017, Kreimendahl, Ossenbrink et al. 2019). Morphology in *in vitro* models with this self-synthesized ECM was improved (Kaessmeyer 2017, Kreimendahl, Ossenbrink et al. 2019). Also ascorbic acid has stimulating effects on ECM synthesis (Wu, Puperi et al. 2017). Here, I tested in the *in vitro* model of human bronchial epithelia three different ECM sources obtained from lung biopsies (lung ECM hydrogels), fibroblasts stimulated with ascorbic acid and self-synthesized by co-cultivation of primary, human bronchial endothelial cells and fibroblasts. Lung ECM hydrogels were obtained from fibrotic tissues, which might have led to the poor morphological results observed in the models (**figure 13,** A-F). Even ascorbic acid did not affect ECM production effective (**figure 13**, G-I) From the self-synthesized ECM, I expected models to contain the vascular system on the basal and fibroblasts on apical side, but that was not the case (**figure 18**). However, ECM production might still be further optimized using different combinations of cells and protocols for co-culture, although with increased handling and prolonged protocol.

By exchanging healthy (NHBEC) for CF patient-derived bronchial epithelium cells (CFHBEC), I successfully applied the *in vitro* cultivation protocol to develop a monogenetic diseased CF *in vitro* model. The *in vitro* CF model shared several histological similarities to the tissues in patients, including stickier and solid-looking mucus, irregular cell shapes, and not fully prismatic, erect cellular shape as seen in the healthy tissue (Trinh, Bardou et al. 2012). Interestingly, when comparing CF and healthy models, histology of the epithelial layer differed (**figure 34**). (Li, Sheppard et al. 2004, Moran and Zegarra-Moran 2008). In conclusion, the CF *in vitro* model provides a realistic test platform to enhance CF research. Going further, the *in vitro* CF model could be used for the analysis of CF patient-specific characteristics (like mucus viscosity and clearing rate, chloride level, and cilia movements) in the context of drug treatments.

The bronchial epithelium model is an isolated system and systematic interactions between organs can not be tested. Settings as chips enable multiple organs to exchange information and allow for more complex data interpretation. Platforms with even four organs have been used for testing drug elimination, where nephron and liver play important roles (Ramme, Koenig et al. 2019). Others have established organ on a chip systems with the vascular system connecting bone marrow, liver and kidney, and found similar pharmacokinetic and pharmacodynamics for Cisplatin in patients (Herland, Maoz et al. 2020). Including airway tissues is likely to come in the near future and will be essential for testing inhaled drugs. For example, a co-culture of bronchial epithelium model and liver spheroids on a chip system and tested the effect of aflatoxin B_1 on single and coculture (Schimek, Frentzel et al. 2020).

Another important point is the lack of a robust immune response in the model. Long-term studies are challenging for an *in vitro* setting. Even the “long-term” experiment of 96 hours IAV infection presented here already reflects that. The bronchial epithelium model was not able to remain viable for 96 hours post infection as seen in the MTT assay (**figure 21**, B), while influenza infections in humans last in average for five to seven days (Leekha, Zitterkopf et al. 2007). One possible explanation for the extensive short-term damage observed in the models is the lack of immune response. During infection of the lungs in patients, innate and adaptive host defense are recruited to the infected tissue (Rynda-Apple, Robinson et al. 2015). Indeed, monocytes, macrophages, dendritic cells and neutrophils show an increased presence during influenza infection (Cole and Ho 2017). Dendritic cells and monocytes in particular, play important roles during the immune response to viral infections (Coccia, Severa et al. 2004) and can recognize the virus itself through Toll-like receptors, supporting the viral defense by connecting innate and adaptive immune response (Mailliard 2020). Macrophages also play an important role in the “cut down” of the virus,

by phagocytosis of infected cells (Tumpey, García-Sastre et al. 2005). Furthermore, immune cells drive airway inflammation by releasing cytokines and coordinating the immune response, and are therefore central in chronical infectious diseases (Holtzman, Byers et al. 2014).

Immune cells are present in native bronchial tissue and should not be missing in an *in vitro* model aiming at reproducing the *in vivo* tissue realistically. Still, implementing immune cells into an *in vitro* model is challenging because of allogenic effects in between cell donors or even interactions of immune cells and biomaterials (Mengus, Muraro et al. 2018). One also needs to consider that working with immune cells is demanding. Human immune cells can be isolated from buffy coats, but need to be freshly isolated and the process of isolating immune cells itself takes about a full working day (Nazarpour, Zabihi et al. 2012). That means the primary cultivation of a bronchial epithelium model and parallel immune cell isolation must match timely. Additionally, immune cells are sensitive to small changes in protocol, increasing variability. In conclusion, an *in vitro* model incorporating an immune response is desired but still challenging (Sueki, Matsuda et al. 2014, Hittinger, Janke et al. 2016, Chandorkar, Posch et al. 2017).

6.2 The *in vitro* model infection of influenza A virus and the therapeutical use of Zanamivir

A key result in the thesis is that the bronchial 3D *in vitro* epithelium model can be infected with the IAV H3N2 pathogen (Panama/2007/1999, PANIII) (**figure 19**). Using the spot infection protocol clearly presented advantages over the submersion protocol (**figure 19**), probably because the submerged condition disrupted the air-liquid interface-grown epithelium (**figure 19**, A). Histology analysis of infected models showed viable cells up to 48 hours post infection, confirmed by MTT assay (**figure 21,** B). Effect of Zanamivir treatment on viral replication was also shown (**figure 21**, A, **23**). Furthermore, NHBECs in the model responded to IAV infection by secreting interferons, as measured at both gene and protein levels (**figure 27, 28**). This innate immune response is comparable to the native tissue's response during IAV infection (Denney and Ho 2018). Altogether, these results indicate that IAV infection of the models successfully reproduce the infection in human bronchial epithelia.

One interesting result in the IAV infected models was that tissue viability declines by 96 hours post infection. As mentioned above, the human based bronchial epithelium model is cultivated in isolation from other organs it would interact with in the living body. Then a full immune response was missing, for example recruitment of macrophages, monocytes, and dendritic cells. In particular, bone marrow derived monocytes guided by the chemokine ligand 2 (CCL2) receptors

expressed in infected NHBEC (Herold, von Wulffen et al. 2006). *In vivo*, natural killer cells derived from lymph nodes also limit the virus spread through cytotoxic activity (Guo, Kumar et al. 2011). Therefore, several crucial components of the immune response are not present in the model, explaining the high replication of IAV that likely led to declined cell viability after 96 hours of infection (**figure 19, 20, 21, 22**).

Virus infection levels observed in the *in vitro* model were higher than that observed in other similar models (Weinheimer, Becher et al. 2012). However, comparing infection in different models is difficult due to varying cellular composition and their origin in the lungs. The origin of cells in the lungs is relevant as the distribution of cellular receptors used by the virus to enter target cells differs in between compartments. The IAV haemagglutinin from H3N2 viruses bind to alpha-(2, 6)-linkage sialic acid (α-2,6-SA) receptors predominantly expressed in ciliated cells (in the nasal, trachea, bronchus and bronchiole), in goblet cells (in the trachea and bronchus), and in pneumocytes type I (in the alveoli) (Thompson, Barclay et al. 2006, van Riel, Munster et al. 2007, de Graaf and Fouchier 2014). The α-2,3-SA and α-2,6-SA receptors are equally expressed in the nasal and the trachea tissues, while α-2,3-SA receptor becomes more dominant in the bronchioles and the alveoli (Nicholls, Bourne et al. 2007). Therefore, differences in viral infection and replication were expected in between models according to the origin of bronchial epithelial cells in the lungs. Indeed, viral replication in the model using bronchial epithelial cells was higher than in an *ex vivo* model using alveolar tissue from human lungs sections from thoracic surgeries (Szymanski, Toennies et al. 2012, Hocke, Suttorp et al. 2017). Although the *ex vivo* model tissue might contain infiltrated immune cells that, as discussed above, help limit viral replication. Still, lower viral replication in the ex vivo alveolar tissue can also be explained by the lower expressing of the α-2,6-SA receptors used by IAV to infiltrate target cells.

Here, I compared the model to two commercially available ones: the full-thickness MucilAir™-HF (**figure 22**) and the MucilAir™ (without NHLFb) (**figure 20**). NHBECs in the MucilAir™-HF were isolated from the nasal tissue of donors, while I used cells isolated from the bronchial tissues in the model. Surprisingly, viral replication in all three models reached similar levels (**figure 20 and 22**). However, I did not measure the expression of SA receptors and it is possible that α-2,6-SA receptors levels are similar in all three models. These results make it clear that while comparing results from different models one needs to be cautious, especially if models were developed using different tissue sections in the respiratory tract, as the cellular composition and histology varies a lot.

MucilAir™ models infected with IAV and treated with Oseltamivir showed strong inhibition of IAV replication (Boda, Benaoudia et al. 2018). These authors do not specify the MOI used for infection, so direct comparisons to the results are not possible. In addition, experiments with an *ex vivo* model infected with IAV in similar conditions to the experiments (H3N2, MOI 0.01) and treated with Oseltamivir and Qß-capsid also showed strong reduction of virus replication (Lauster, Klenk et al. 2020). With these results in mind, I tested inhibition of virus replication in the IAV infected models treated with Zanamivir, Oseltamivir or Qß-capsid (**figure 30**). Surprisingly, compared to the above mentioned results, treatment with Zanamivir or Oseltamivir showed only partial reduction of virus replication, while no inhibitory effect for Qß-capsid was detectable (**figure 30**). I speculate that the higher mucus production and cilia presence observed in the *in vitro* models could have prevented the Qß-capsid from reaching the epithelial cells. This hypothesis could be further explored in the future by measuring the Qß-capsid penetrance in the tissue with immune-fluorescence staining.

Another possible explanation for the underwhelming inhibition of viral replication upon Zanamivir treatment of IAV infected models is the treatment protocol setup. During Zanamivir experiments, the working dilution was prepared in PBS and pipetted apically to the model surface (**figure 21, 22**). Manual pipetting does not ensure equal distribution of Zanamivir throughout the tissue. Application of Zanamivir in aerosol form (as in clinical usage) could improve drug distribution on the cultivated tissue (MacConnachie 1999). This could be achieved in the future with a VitroCell® chamber. These chambers enable a “Cloud System” that produces dense droplets by nebulizing the applied substance and assures equal drug distribution and air-liquid interface conditions (Neilson, Mankus et al. 2015, Creager, Zeng et al. 2017, Cao, Coyle et al. 2020). Although alternatives exist, it is not clear whether better application performances of Zanamivir will impact its inhibitory effect on IAV replication in the models.

The models were treated with drugs apically for mimicking the inhaled administration in patients. Zanamivir molecules are zwitterions with protonated guanidine side chains (Lindberg, Fedorova et al. 2015). Similar to carboxy-Oseltamivir (active substance was used, because Oseltamivir is a prodrug, an *in vitro* model has no first pass effect to activate it) (Mazák and Noszál 2020). Having a charged surface is beneficial for several drugs as it influences their pharmacodynamic and pharmacokinetic behavior (Mazák and Noszál 2020). However, the mucus produced in the lung lumen (and by cells in the model) is negatively charged as it is mainly composed of proteins. It is possible that Zanamivir and Oseltamivir attach to the mucus’ surface and fewer molecules reach target cells, leading to lower effective concentration and decreased inhibitory effects on viral

replication. Therefore, it would be interesting in future experiments to study Zanamivir and Oseltamivir location in *in vitro* model, but also to test whether drug delivery in the basal compartment in the model (mimicking other forms of drug delivery in patients) improve viral replication inhibition. Additionally, an attractive question for all substances is if smart delivery systems as nanogels or LNPs could influence drug delivery.

High serum levels of uteroglobin relate to epithelial cell damage and increased epithelium permeability (St Helen, Holland et al. 2013, Laucho-Contreras, Polverino et al. 2016, Rivière, Hua-Huy et al. 2017), followed by high renal clearances. Same effects were seen during asthmatic illness and bronchoilitis, probably caused by epithelium damage (Egron, Labbé et al. 2020). Accordingly, uteroglobin secretion has been proposed is a vitality biomarker of bronchial epithelial tissue, although this has been contested by some (St Helen, Holland et al. 2013).

During IAV infection of the model, secretion of uteroglobin (a. k. a. CC16) was observed (**figure 29**). Interestingly, while the total amount of uteroglobin in models not infected with IAV increased over the duration of the infection, no uteroglobin accumulated in the supernatant of models infected with IAV (**figure 29**, B). Besides the total accumulation of uteroglobin during infection, I also measured the rate of uteroglobin production by cells in the apical compartment in the model (**figure 29**, A). The data indicated that uteroglobin production rate remained constant in models not infected with IAV, while IAV infection led to surprising decrease (and this was reversed by treating infected models with Zanamivir). I speculate that this unexpected result is due to the reduced overall number of viable cells in infected models.

Regarding literature their data leads to a speculation that uteroglobin diffused to model's basal side and increased uteroglobin concentration in medium (serum values) were detectable (Arsalane, Broeckaert et al. 2000). Additionally, images showed higher signals of uteroglobin in healthy control than in infected and 1000 nM Zanamivir treated model at 96 hours post infection (**figure 29,** C). One reason for lower uteroglobin concentration in medium might be missing immune cells, probably they trigger uteroglobin secretion. Another aspect could be *in vitro* model's collagen matrix, that refused viral damage and stayed healthy, and no uteroglobin could differ to basal side (**figure 29**, C).

Interestingly, uteroglobin concentration of 1000 nM Zanamivir treated model recovered at 48 hours post infection (**figure 29**, A) in parallel Zanamivir concentration (basal medium) increased threefold (**figure 21, C**), indicated Zanamivir's protective effect. For lower Zanamivir dosed models, effects were not visible. The low doses might have been more sensitive to small amounts

of adsorbed Zanamivir by e. g. the cell culture plate or even failure by preparing the applied dilution. The graph (**figure 21**, C) is comparable to pharmacokinetic data of clinical study, serum value of Zanamivir concentration was measured (Cass, Efthymiopoulos et al. 1999, Cass, Brown et al. 1999). Data of the *in vitro* model and the clinical study found values in a similar range. The *in vitro* model showed fivefold higher values in comparison to the clinical study at 2 hours post treatment. Increased Zanamivir concentration were caused by Zanamivir application, probands inhaled the drug instead of two times 10 mg, once 20 mg per day, both applications are approved.

Another explanation is that the static system accumulates the drug. Medium was changed at 48 hours post infection, in contrast in human organism blood circulates constantly, resulted diluted drug concentration. Furthermore, earlier and more measure time points would provide a more detailed understanding. Lower dosed models did not detect Zanamivir at early time points, probably Zanamivir concentration was too small to reach medium side (basal) and most of the drug just interacted with target. Either it was not clear how much Zanamivir was absorbed by the model or how much was interacting with the virus or stayed agglomerated with the virus at model surface. Labeled Zanamivir would be interesting to test, for locating Zanamivir at different time points.

Gene expression analysis in the models (**figure 27**, A, B) showed that levels of interferon types I and III increase by 24 hours post infection, while type II interferons did not change. This is in agreement interferon II being released by T-cells (Arra and Abu-Amer 2020) not present in the models. Additionally, a target of the type interferon type II and III signaling (MX1) was also found up-regulated (**figure 27,** B) (Haller, Staeheli et al. 2007, Verhelst, Parthoens et al. 2012, Schattgen, Oguin et al. 2016). Contrary to expectation was the up-regulation of CXCL10, as it is stimulated by the type II interferon IFN-γ (Lu, Masic et al. 2011, Vazirinejad, Ahmadi et al. 2014). Rath-Deschner and collaborators showed up-regulation of CXCL10 induced by mechanical forces (Rath-Deschner, Memmert et al. 2021). Because the protocol involves multiple washing steps, it is likely that CXCL10 expression was induced by sample handling. Still, CXCL10 levels decrease upon treatment with Zanamivir (**figure 27,** B). Different levels of the untreated and treated model might explain that the infected model without treatment got even more affected because of already damaged cells. Remarkably, this correlation was related to active innate immune response of the *in vitro* model.

6.3 Bronchial epithelium model as a test matrix for drug delivery systems

Drug delivery to target epithelial cells in the lungs is hampered by presence of mucus and ciliary movement (Leal, Smyth et al. 2017). Drug delivery systems like thiolated particles facilitate trans-mucosal delivery (Yin, Ding et al. 2009, Nema, Jain et al. 2013, Brar and Kaur 2020) increasing bioavailability of the drug (Winkler, Hochhaus et al. 2004, Kim, Ko et al. 2018). Accordingly, the results using degradable PNIPMAM-(S-S)-dPG nanogels indicate that it passes the mucus layer and reaches epithelial cells in the model (**figure 31,** B, C). The hypothesize that disulphide-containing biodegradable nanogel penetrate mucus by bonding disulfide binds with thiolated mucus terminus functionated, by doing that they penetrated to epithelial cells and passed mucus layer according to the results (**figure 31**, B, C). At the same time, non-degradable nanogels PNIPMAM-dPG without the disulfide linker got stuck to the mucus and could not reach epithelial cell layer (**31**, D, G).

Similarly, the loaded degradable nanogels with Etanercept confirmed the mucus penetration as well. The result pointed out the probability of the drug delivery, histologically speaking images proved successful delivery and no harming cytotoxicity was noticed (**figure 31,** E, F). To further this research, Etanercept charged nanogel application to an inflamed model would be of interest, to observe innate immune response behavior. Additionally, testing established inhalable drugs that must pass mucus and if drug bioavailability increased by testing smart delivery systems, e. g. to study Zanamivir loaded nanogels at an infected model. For Zanamivir it is known that just 10 - 20 % are bioavailable (Cass, Efthymiopoulos et al. 1999).

LNPs provided another type of a delivery system, to minimize toxicity and increased delivery efficiency (Allen and Cullis 2013). In combination with PEG, LNP features their transport by minimizing their size to pass through mucus wire and successful encapsulation with the help of ionizable cationic lipids (Heyes, Hall et al. 2006, Wang, Lai et al. 2008, Suk, Xu et al. 2016). Additionally, some LNP were combined with ApoE for enhanced cell uptake (Johnson, Olsen et al. 2014). LNPs proposed to act as a desired vehicle to transport tools for gene therapy, as they already received an approval for a treatment of polyneuropathies induced by hereditary transthyretin amyloidosis (Akinc, Maier et al. 2019).

Curiously, this first experiment showed different behaviors of the varied LNP compositions while transfecting the NHBEC monolayer (**figure 32,** A). Our experiment found that the quantitative result favored LNP combination with DSPC, it is the same helper lipid that is applied for

transporting Patisiran (Kulkarni, Witzigmann et al. 2019). Positive data presented ES (helper lipid) as well (**figure 32**, A), characteristically it supported the encapsulation by its polarity (Kulkarni, Witzigmann et al. 2019). This was in good agreement with *Veldmann* [2004], the *in vitro* data presented an improved intake by encapsulating the cancer medicament Doxorubicin (Veldman, Zerp et al. 2004). Preferred PEG combinations were about 1.5 % and 5 %, it is in line with previous results from *Belliveau* [2012] (Belliveau, Huft et al. 2012), according to the data the small amount of 1.5 % PEG enhanced the transfection. Further tests carried out that quality data of LNP composition clearly transfected the cytoplasm (**figure 32**, B), *Basha* [2011] published that DSPC combinations presented similar results (Basha, Novobrantseva et al. 2011). Another trial of high content screening was recommended to assure the successful delivery trend of LNP compositions and to reduce statistical variability. Another suggestion for eventual misinterpretation is that LNPs themselves sticked at NHBEC cell surface and thus implicated positive signals. For clarification more fluorescence images of different LNP compositions and negative controls (low delivery property) should be tested. In conclusion more images of all treatments need to be performed, to clarify transfection quality, if ApoE had promising advantages. These tests highlighted the importance of naive tissue as for example for gene therapy by using CRISPR Cas for curing CF. The preliminary results presented a successful NHBEC monolayer transfection. Cell monolayer do not exhibit differentiated NHBEC as ciliated and goblet cells, that means no cilia movement and no mucus to trap LNPs. Especially CF mucus may hamper LNP delivery because patients show high mucus viscosity (Saint-Criq and Gray 2017). These delivery pretrials were important, but successful formulation needs to be tested in a more realistic set up as in a human based 3D bronchial epithelial *in vitro* model.

Curiously, curcumin passiv charged in particle bilayer muco-penetrated to epithelial surface as well. Combination of Chol/Tween80/Curcumin (72,5/25/2,5) was successful in trial two (**figure 33,** C, F). Histology images of the first trial clearly detected apoptotic cells (**figure 33**, A, B, D, E). Irritating data presented LDH analysis, no cytotoxicity was detected (**figure 33**, G). It might be explained by storage failure of LDH samples, LDH is just stable for a couple of hours or LDH test itslef might be to insensitive (Kift, Byrne et al. 2015). Cytotoxicity tests as live/dead staining or FACS could have been more sensitive tests. Optional is that first trial's curcumin particles were not stable, because of the shipment from Canada to Germany. It could have explained no apoptotic effects of second delivery trial with the same curcumin particle composition, here no cell harming was observed (**figure 33**, C, F). A third trial of treatment was performed during my stay

in Canada, unfortunately because of the emerging situation of COVID-19, all experiments were stopped.

Curcumin's properties are anti-inflammatory and anti-oxidative (Hewlings and Kalman 2017) and could provide an enhancement in chronical pulmonary diseases as e. g. COPD, Asthma. These features were observed in animal models (Venkatesan, Punithavathi et al. 2007) but the functionality in a human body is debatable, other publications review contrary results (Lelli, Sahebkar et al. 2017). More of these preclinical trials in an *in vitro* setting are unavoidable.

7. Conclusion

I developed a human based bronchial epithelial *in vitro* model showing important characteristics related to the naïve tissue in humans, including pseudostratified columnar epithelial and basal monolayers. Epithelial cells in the model presented cilia on their surface and high mucus level production associated with goblet cells, highlighting the importance of using a 3D instead of a 2D model when studying lung tissues. Importantly, IAV infection of the model led to responses similar to those observed in patients in the clinics, and this could be treated with drugs given to patients in the clinics. Therefore, the model can be used to study the pathophysiology of influenza infection and possible help in the development of novel therapies. Like the *in vivo* scenario, I was also showed that drug delivery is challenging for bronchial epithelia and smart delivery systems (like degradable nanogels and LNPs) are a relevant option. In that sense, the model serves as a testing and discovery platform for drug delivery systems. Furthermore, I used the protocol to develop an *in vitro* model for cystic fibrosis using primary cells from patients. I hope this model will facilitate investigating gene therapies and provide a safe and efficient testing setup. In conclusion, the model produced here might be useful in studying diverse aspects of preclinical research in the lung pathophysiology and has the potential to decrease the need of animal models during this stage of drug development and discovery.

8. Outlook

The research field of *in vitro* modeling of human tissues moves towards more complex systems that recreate more realistic micro-environment settings. The importance of such developments is already visible for toxicity preclinical trials (Gualtieri, Grollino et al. 2018, Bishop, Haswell et al. 2019). The cell types present in a model and their interactions play an important role and the field trends to using primary and iPS cells (De Servi, Ranzini et al. 2017, van Riet, Ninaber et al. 2020, Marinkovic, Sridharan et al. 2021). More advanced models incorporate several cell types (like fibroblast, endothelial and epithelial cells) to build a vascular system for testing perfusion (Chen, Yu et al. 2019). Alternative advanced models place tissues on a chip connected by micro tubes (Schimek, Frentzel et al. 2020), and therefore facilitate pharmacokinetic and pharmacodynamic studies (Box, Livermore et al. 2015, Herland, Maoz et al. 2020). Furthermore, immune cells (like dendritic cells, macrophages and natural killer cells) restrict and resolve infections *in vivo*, and incorporation of these into in vitro models is desirable (Bahadoran, Lee et al. 2016, Chandorkar, Posch et al. 2017).

Another great advantage of *in vitro* models is the use of patient-derived primary cells in personalized medicine. Close collaborations with hospitals can provide patient's cells and personal bronchial epithelial *in vitro* model for studying individual disease could be created to find the most effective treatments. Personalized models are particularly relevant for diseases like CF, because of the wide variety of CFTR mutations and not every treatment is effective for every patient (Cutting 2015, De Boeck 2020). Other exemplary monogenetic diseases as primary ciliary dyskinesia and hereditary hemorrhagic telangiectasia might benefit from personalized models (Yao and Shen 2017). Also, *in vitro* test models become more relevant for infection trials as relatively quick results can be obtained and with higher reproducibility for a large number of samples, while not requiring manipulating the virus and genetically modifing animals to reproduce the infection (Tan, Ong et al. 2018, Bulitta, Hope et al. 2019, O'Brien and Welch 2019, Chakraborty, Banerjee et al. 2020).

A final aspect worth mentioning is that 3D *in vitro* models provide the ideal platform for testing smart delivery systems in a more realistic setting. Of particular relevant, the need of smart delivery systems increases with the development of genetical therapies for use in the clinics (Doudna 2020). With 3D *in vitro* models, new therapeutic opportunities can be tested ideally in a human based setup.

In summary, creating an *in vitro* model that reproduces human tissues precisely at the morphological and physiological levels remains challenging. Such a model of the airway system, for example, will have to precisely recreate tissue compartments and its physiological and anatomic differences, like in the trachea, bronchus, and alveolus (Sahin-Yilmaz and Naclerio 2011, Verleden, Kirby et al. 2021). The advanced 3D *in vitro* bronchial epithelium model I developed provides a test platform for future studies on human lung pathophysiology, personalized medicine, testing smart delivery systems for novel therapies, and can be further improved by addition of dynamic perfusion systems and incorporation of immune cells.

Acknowledgment

I am happy and grateful for the chance of being part of a research team to develop the *in vitro* model and to work in the field of alternative methods to animal models, here thank you to Prof. Dr. Sarah Hedtrich who offered me this opportunity. She guided me through this process.

Also, a great and appreciated thank you to Prof. Dr. Andreas Hocke, he supervised and helped me during my journey of infection trials. He and his group taught me their lung infection knowledge and enabled me to work on this topic in his lab at Charité.

I would like to thank Prof. Dr. Burkhard Kleuser who accepted to assess my thesis and to be my second reviewer, thank you for your effort, time, and participation.

Thank you to Dr. Sabine Kaessmeyer, who enabled my colleague Dr. Marijana Jevtic and me to continue our work in her lab, we had for a period struggle with recurrent contaminations in our lab.

I am grateful for my lovely colleagues Dr. Marijana Jevtic and Patrick Graff with whom I have spent most of my doctoral student time, thank you for your supporting words and solutional thinking in challenging situations, our adorable time besides work especially during summer at the lake, bouldering after work or just having a drink for a get-together.

Thanks to all sweet people who were part of my time at FU Berlin. Special thanks to Dr. Charlotte Lübow and Judith Bockstiegel, feeling great for having you. Also, I am happy to spend many hours with you in the kitchen or in the lab, dear Dr. Hausi, Tarada, Leonie, Maria, Priscilla, Nan, Rawan, Carola, Petra, Uta, Guy, Kathi and Anna.

And, the Marburg gang who is always with me, wherever I go. Thank you to convincing me to move to Berlin with Dominik Wiggers call meanwhile transporting Christian Zunkers moving boxes to Berlin with Dr. Daniel Ritter. Thank you for a smooth and cheerful arrival to our new home.

Thank you Birte Rath, Manuel Lüke und Ghadah Ismaeel, you are my greatest fans, thank you for creating me to the person who I am.

Thank you, Izabela Megerle, for being my personal strength booster and balancing my life by creating many funny moments with me. I am so happy to have you in my life <3.

Thanks to my greatest support Carlos Vieira e Vieira for spending many hours with me during this process with patience and love for me.

Of course, also a great thanks to my parents, my brother, Sandra and Leonard, I appreciate your unconditional support in any moment of my life. I am glad to have you.

References

(2012). "Ivacaftor (Kalydeco) for cystic fibrosis." Med Lett Drugs Ther **54**(1388): 29-30.

Adam, M., L. Angie, H. Olav, L. Bruno, W. Sylvie van der, S. Brunhilde, O. Matthias, P. John, K. Jan van de, H. Alan and Z. Maria (2009). "Oseltamivir-Resistant Influenza Virus A (H1N1), Europe, 2007–08 Season." Emerging Infectious Disease journal **15**(4): 552.

Adams, J. S. and M. Hewison (2008). "Unexpected actions of vitamin D: new perspectives on the regulation of innate and adaptive immunity." Nature clinical practice. Endocrinology & metabolism **4**(2): 80-90.

Adler, K., M. Tuvim and B. Dickey (2013). "Regulated Mucin Secretion from Airway Epithelial Cells." Frontiers in Endocrinology **4**(129).

Akhtar, A. (2015). "The flaws and human harms of animal experimentation." Cambridge quarterly of healthcare ethics : CQ : the international journal of healthcare ethics committees **24**(4): 407-419.

Akinc, A., M. A. Maier, M. Manoharan, K. Fitzgerald, M. Jayaraman, S. Barros, S. Ansell, X. Du, M. J. Hope, T. D. Madden, B. L. Mui, S. C. Semple, Y. K. Tam, M. Ciufolini, D. Witzigmann, J. A. Kulkarni, R. van der Meel and P. R. Cullis (2019). "The Onpattro story and the clinical translation of nanomedicines containing nucleic acid-based drugs." Nat Nanotechnol **14**(12): 1084-1087.

Allen, T. M. and P. R. Cullis (2013). "Liposomal drug delivery systems: from concept to clinical applications." Adv Drug Deliv Rev **65**(1): 36-48.

Alonso, W. J., C. Viboud, L. Simonsen, E. W. Hirano, L. Z. Daufenbach and M. A. Miller (2007). "Seasonality of influenza in Brazil: a traveling wave from the Amazon to the subtropics." Am J Epidemiol **165**(12): 1434-1442.

Amin, R., P. Subbarao, W. Lou, A. Jabar, S. Balkovec, R. Jensen, S. Kerrigan, P. Gustafsson and F. Ratjen (2011). "The effect of dornase alfa on ventilation inhomogeneity in patients with cystic fibrosis." European Respiratory Journal **37**(4): 806.

Amstad, P., R. R. Reddel, A. Pfeifer, L. Malan-Shibley, G. E. Mark, 3rd and C. C. Harris (1988). "Neoplastic transformation of a human bronchial epithelial cell line by a recombinant retrovirus encoding viral Harvey ras." Mol Carcinog **1**(3): 151-160.

Anczuków, O., M. Akerman, A. Cléry, J. Wu, C. Shen, Nitin H. Shirole, A. Raimer, S. Sun, Mads A. Jensen, Y. Hua, Frédéric H. T. Allain and Adrian R. Krainer (2015). "SRSF1-Regulated Alternative Splicing in Breast Cancer." Molecular Cell **60**(1): 105-117.

Anekthananon, T., S. Pukrittayakamee, W. Ratanasuwan, P. Jittamala, P. Werarak, P. Charunwatthana, S. Suwanagool, S. Lawpoolsri, K. Stepniewska, P. Sapchookul, P. Puthavathana, C. Fukuda, N. Lindegardh, J. Tarning, N. J. White, N. Day and W. R. J. Taylor (2013). "Oseltamivir and inhaled zanamivir as influenza prophylaxis in Thai health workers: a randomized, double-blind, placebo-controlled safety trial over 16 weeks." The Journal of antimicrobial chemotherapy **68**(3): 697-707.

Annaratone, L., C. Marchiò, R. Russo, L. Ciardo, S. M. Rondon-Lagos, M. Goia, M. S. Scalzo, S. Bolla, I. Castellano, L. Verdun di Cantogno, G. Bussolati and A. Sapino (2013). "A collection of

primary tissue cultures of tumors from vacuum packed and cooled surgical specimens: a feasibility study." PloS one **8**(9): e75193-e75193.

Arra, M. and Y. Abu-Amer (2020). Physiologic Role of Inflammatory Cytokines in Bone Homeostasis. Encyclopedia of Bone Biology. M. Zaidi. Oxford, Academic Press**:** 33-44.

Arsalane, K., F. Broeckaert, B. Knoops, M. Wiedig, G. Toubeau and A. Bernard (2000). "Clara Cell Specific Protein (CC16) Expression after Acute Lung Inflammation Induced by Intratracheal Lipopolysaccharide Administration." American journal of respiratory and critical care medicine **161**: 1624-1630.

Ataç, B., I. Wagner, R. Horland, R. Lauster, U. Marx, A. G. Tonevitsky, R. P. Azar and G. Lindner (2013). "Skin and hair on-a-chip: in vitro skin models versus ex vivo tissue maintenance with dynamic perfusion." Lab on a Chip **13**(18): 3555-3561.

Aufderheide, M., C. Förster, M. Beschay, D. Branscheid and M. Emura (2016). "A new computer-controlled air-liquid interface cultivation system for the generation of differentiated cell cultures of the airway epithelium." Exp Toxicol Pathol **68**(1): 77-87.

Bahadoran, A., S. H. Lee, S. M. Wang, R. Manikam, J. Rajarajeswaran, C. S. Raju and S. D. Sekaran (2016). "Immune Responses to Influenza Virus and Its Correlation to Age and Inherited Factors." Frontiers in microbiology **7**: 1841-1841.

Balansin Rigon, R., S. Kaessmeyer, C. Wolff, C. Hausmann, N. Zhang, M. Sochorová, A. Kováčik, R. Haag, K. Vávrová, M. Ulrich, M. Schäfer-Korting and C. Zoschke (2018). "Ultrastructural and Molecular Analysis of Ribose-Induced Glycated Reconstructed Human Skin." International Journal of Molecular Sciences **19**(11): 3521.

Balfour-Lynn, I. M., K. Welch and S. Smith (2019). "Inhaled corticosteroids for cystic fibrosis." Cochrane Database of Systematic Reviews(7).

Bantz, S. K., Z. Zhu and T. Zheng (2014). "The Atopic March: Progression from Atopic Dermatitis to Allergic Rhinitis and Asthma." Journal of clinical & cellular immunology **5**(2): 202.

Bao, L., W. Deng, B. Huang, H. Gao, J. Liu, L. Ren, Q. Wei, P. Yu, Y. Xu, F. Qi, Y. Qu, F. Li, Q. Lv, W. Wang, J. Xue, S. Gong, M. Liu, G. Wang, S. Wang, Z. Song, L. Zhao, P. Liu, L. Zhao, F. Ye, H. Wang, W. Zhou, N. Zhu, W. Zhen, H. Yu, X. Zhang, L. Guo, L. Chen, C. Wang, Y. Wang, X. Wang, Y. Xiao, Q. Sun, H. Liu, F. Zhu, C. Ma, L. Yan, M. Yang, J. Han, W. Xu, W. Tan, X. Peng, Q. Jin, G. Wu and C. Qin (2020). "The Pathogenicity of SARS-CoV-2 in hACE2 Transgenic Mice." bioRxiv: 2020.2002.2007.939389.

Baptista, P. M., M. M. Siddiqui, G. Lozier, S. R. Rodriguez, A. Atala and S. Soker (2011). "The use of whole organ decellularization for the generation of a vascularized liver organoid." Hepatology **53**(2): 604-617.

Barberis, I., P. Myles, S. K. Ault, N. L. Bragazzi and M. Martini (2016). "History and evolution of influenza control through vaccination: from the first monovalent vaccine to universal vaccines." Journal of preventive medicine and hygiene **57**(3): E115-E120.

Barkauskas, C. E., M.-I. Chung, B. Fioret, X. Gao, H. Katsura and B. L. M. Hogan (2017). "Lung organoids: current uses and future promise." Development **144**(6): 986.

Barr, I. G., C. Russell, T. G. Besselaar, N. J. Cox, R. S. Daniels, R. Donis, O. G. Engelhardt, G. Grohmann, S. Itamura, A. Kelso, J. McCauley, T. Odagiri, S. Schultz-Cherry, Y. Shu, D. Smith, M. Tashiro, D. Wang, R. Webby, X. Xu, Z. Ye and W. Zhang (2014). "WHO recommendations for the viruses used in the 2013-2014 Northern Hemisphere influenza vaccine: Epidemiology, antigenic and genetic characteristics of influenza A(H1N1)pdm09, A(H3N2) and B influenza viruses collected from October 2012 to January 2013." Vaccine **32**(37): 4713-4725.

Barrios, R. (2008). Animal Models of Lung Disease. Molecular Pathology of Lung Diseases. D. S. Zander, H. H. Popper, J. Jagirdar et al. New York, NY, Springer New York**:** 144-149.

Basha, G., T. I. Novobrantseva, N. Rosin, Y. Y. C. Tam, I. M. Hafez, M. K. Wong, T. Sugo, V. M. Ruda, J. Qin, B. Klebanov, M. Ciufolini, A. Akinc, Y. K. Tam, M. J. Hope and P. R. Cullis (2011). "Influence of Cationic Lipid Composition on Gene Silencing Properties of Lipid Nanoparticle Formulations of siRNA in Antigen-Presenting Cells." Molecular Therapy **19**(12): 2186-2200.

Bates, J. H. T., M. Rincon and C. G. Irvin (2009). "Animal models of asthma." American journal of physiology. Lung cellular and molecular physiology **297**(3): L401-L410.

Baxter, A., S. Thain, A. Banerjee, L. Haswell, A. Parmar, G. Phillips and E. Minet (2015). "Targeted omics analyses, and metabolic enzyme activity assays demonstrate maintenance of key mucociliary characteristics in long term cultures of reconstituted human airway epithelia." Toxicology in Vitro **29**(5): 864-875.

Bazin, H. (2011). "Vaccination : a history : from Lady Montagu and genetic engineering."

Belliveau, N. M., J. Huft, P. J. Lin, S. Chen, A. K. Leung, T. J. Leaver, A. W. Wild, J. B. Lee, R. J. Taylor, Y. K. Tam, C. L. Hansen and P. R. Cullis (2012). "Microfluidic Synthesis of Highly Potent Limit-size Lipid Nanoparticles for In Vivo Delivery of siRNA." Mol Ther Nucleic Acids **1**(8): e37.

Belser, J. A., X. Lu, T. R. Maines, C. Smith, Y. Li, R. O. Donis, J. M. Katz and T. M. Tumpey (2007). "Pathogenesis of avian influenza (H7) virus infection in mice and ferrets: enhanced virulence of Eurasian H7N7 viruses isolated from humans." J Virol **81**(20): 11139-11147.

Belser, J. A., D. A. Wadford, C. Pappas, K. M. Gustin, T. R. Maines, M. B. Pearce, H. Zeng, D. E. Swayne, M. Pantin-Jackwood, J. M. Katz and T. M. Tumpey (2010). "Pathogenesis of pandemic influenza A (H1N1) and triple-reassortant swine influenza A (H1) viruses in mice." J Virol **84**(9): 4194-4203.

Berdiev, B. K., Y. J. Qadri and D. J. Benos (2009). "Assessment of the CFTR and ENaC association." Molecular bioSystems **5**(2): 123-127.

BéruBé, K., Z. Prytherch, C. Job and T. Hughes (2010). "Human primary bronchial lung cell constructs: The new respiratory models." Toxicology **278**(3): 311-318.

Biere, B., B. Bauer and B. Schweiger (2010). "Differentiation of influenza B virus lineages Yamagata and Victoria by real-time PCR." J Clin Microbiol **48**(4): 1425-1427.

Bishop, E., L. Haswell, J. Adamson, S. Costigan, D. Thorne and M. Gaca (2019). "An approach to testing undiluted e-cigarette aerosol in vitro using 3D reconstituted human airway epithelium." Toxicology in Vitro **54**: 391-401.

Boda, B., S. Benaoudia, S. Huang, R. Bonfante, L. Wiszniewski, E. D. Tseligka, C. Tapparel and S. Constant (2018). "Antiviral drug screening by assessing epithelial functions and innate immune responses in human 3D airway epithelium model." Antiviral research **156**: 72-79.

Boda, B., S. Benaoudia, S. Huang, R. Bonfante, L. Wiszniewski, E. D. Tseligka, C. Tapparel and S. Constant (2018). "Antiviral drug screening by assessing epithelial functions and innate immune responses in human 3D airway epithelium model." Antiviral Res **156**: 72-79.

Boddupalli, B. M., Z. N. K. Mohammed, R. A. Nath and D. Banji (2010). "Mucoadhesive drug delivery system: An overview." Journal of advanced pharmaceutical technology & research **1**(4): 381-387.

Boei, J., S. Vermeulen, B. Klein, P. S. Hiemstra, R. M. Verhoosel, D. G. J. Jennen, A. Lahoz, H. Gmuender and H. Vrieling (2017). "Xenobiotic metabolism in differentiated human bronchial epithelial cells." Arch Toxicol **91**(5): 2093-2105.

Boerma, M., G. R. Burton, J. Wang, L. M. Fink, R. E. McGehee, Jr. and M. Hauer-Jensen (2006). "Comparative expression profiling in primary and immortalized endothelial cells: changes in gene expression in response to hydroxy methylglutaryl-coenzyme A reductase inhibition." Blood Coagulation & Fibrinolysis **17**(3).

Boni, M. F., Y. Zhou, J. K. Taubenberger and E. C. Holmes (2008). "Homologous recombination is very rare or absent in human influenza A virus." Journal of virology **82**(10): 4807-4811.

Bonser, L. R. and D. J. Erle (2019). "Putting Mucins on the Map." American journal of respiratory and critical care medicine **199**(6): 681-682.

Boucher, R. C. (1994). "Human airway ion transport. Part one." Am J Respir Crit Care Med **150**(1): 271-281.

Bouvier, N. M. (2015). "Animal models for influenza virus transmission studies: a historical perspective." Curr Opin Virol **13**: 101-108.

Bouvier, N. M. and A. C. Lowen (2010). "Animal Models for Influenza Virus Pathogenesis and Transmission." Viruses **2**(8): 1530-1563.

Bouvier, N. M. and P. Palese (2008). "The biology of influenza viruses." Vaccine **26 Suppl 4**(Suppl 4): D49-D53.

Box, H., J. Livermore, A. Johnson, L. McEntee, T. W. Felton, S. Whalley, J. Goodwin and W. W. Hope (2015). "Pharmacodynamics of Isavuconazole in a Dynamic In Vitro Model of Invasive Pulmonary Aspergillosis." Antimicrobial agents and chemotherapy **60**(1): 278-287.

Boyle, M. P., S. C. Bell, M. W. Konstan, S. A. McColley, S. M. Rowe, E. Rietschel, X. Huang, D. Waltz, N. R. Patel and D. Rodman (2014). "A CFTR corrector (lumacaftor) and a CFTR potentiator (ivacaftor) for treatment of patients with cystic fibrosis who have a phe508del CFTR mutation: a phase 2 randomised controlled trial." Lancet Respir Med **2**(7): 527-538.

Brand, P. L. (2000). "Bronchodilators in cystic fibrosis." Journal of the Royal Society of Medicine **93 Suppl 38**(Suppl 38): 37-39.

Brar, V. and G. Kaur (2020). "Thiolated okra chitosan nanoparticles: preparation and optimisation as intranasal drug delivery agents." J Microencapsul **37**(8): 624-639.

Brass, A. L., I. C. Huang, Y. Benita, S. P. John, M. N. Krishnan, E. M. Feeley, B. J. Ryan, J. L. Weyer, L. van der Weyden, E. Fikrig, D. J. Adams, R. J. Xavier, M. Farzan and S. J. Elledge (2009). "The IFITM Proteins Mediate Cellular Resistance to Influenza A H1N1 Virus, West Nile Virus, and Dengue Virus." Cell **139**(7): 1243-1254.

Breslin, S. and L. O'Driscoll (2013). "Three-dimensional cell culture: the missing link in drug discovery." Drug Discov Today **18**(5-6): 240-249.

Bridge, J. C., J. W. Aylott, C. E. Brightling, A. M. Ghaemmaghami, A. J. Knox, M. P. Lewis, F. R. A. J. Rose and G. E. Morris (2015). "Adapting the Electrospinning Process to Provide Three Unique Environments for a Tri-layered In Vitro Model of the Airway Wall." Journal of visualized experiments : JoVE(101): e52986-e52986.

Broeckaert, F., K. Arsalane, C. Hermans, E. Bergamaschi, A. Brustolin, A. Mutti and A. Bernard (2000). "Serum clara cell protein: a sensitive biomarker of increased lung epithelium permeability caused by ambient ozone." Environ Health Perspect **108**(6): 533-537.

Brogi, S., T. C. Ramalho, K. Kuca, J. L. Medina-Franco and M. Valko (2020). "Editorial: In silico Methods for Drug Design and Discovery." Frontiers in chemistry **8**: 612-612.

Bulitta, J. B., W. W. Hope, A. E. Eakin, T. Guina, V. H. Tam, A. Louie, G. L. Drusano and J. L. Hoover (2019). "Generating Robust and Informative Nonclinical In Vitro and In Vivo Bacterial Infection Model Efficacy Data To Support Translation to Humans." Antimicrobial agents and chemotherapy **63**(5): e02307-02318.

Bustamante-Marin, X. M. and L. E. Ostrowski (2017). "Cilia and Mucociliary Clearance." Cold Spring Harbor perspectives in biology **9**(4): a028241.

Callaway, E. (2020). "Labs rush to study coronavirus in transgenic animals - some are in short supply." Nature **579**(7798): 183.

Cao, X. (2016). "Self-regulation and cross-regulation of pattern-recognition receptor signalling in health and disease." Nature Reviews Immunology **16**(1): 35-50.

Cao, X., J. P. Coyle, R. Xiong, Y. Wang, R. H. Heflich, B. Ren, W. M. Gwinn, P. Hayden and L. Rojanasakul (2020). "Invited review: human air-liquid-interface organotypic airway tissue models derived from primary tracheobronchial epithelial cells—overview and perspectives." In Vitro Cellular & Developmental Biology - Animal.

Carrington, R., S. Jordan, S. C. Pitchford and C. P. Page (2018). "Use of animal models in IPF research." Pulmonary Pharmacology & Therapeutics **51**: 73-78.

Cass, L. M., C. Efthymiopoulos and A. Bye (1999). "Pharmacokinetics of zanamivir after intravenous, oral, inhaled or intranasal administration to healthy volunteers." Clin Pharmacokinet **36 Suppl 1**: 1-11.

Cass, L. M. R., J. Brown, M. Pickford, S. Fayinka, S. P. Newman, C. J. Johansson and A. Bye (1999). "Pharmacoscintigraphic Evaluation of Lung Deposition of Inhaled Zanamivir in Healthy Volunteers." Clinical Pharmacokinetics **36**(1): 21-31.

Castellani, C., H. Cuppens, M. Macek, Jr., J. J. Cassiman, E. Kerem, P. Durie, E. Tullis, B. M. Assael, C. Bombieri, A. Brown, T. Casals, M. Claustres, G. R. Cutting, E. Dequeker, J. Dodge, I. Doull, P. Farrell, C. Ferec, E. Girodon, M. Johannesson, B. Kerem, M. Knowles, A. Munck, P. F.

Pignatti, D. Radojkovic, P. Rizzotti, M. Schwarz, M. Stuhrmann, M. Tzetis, J. Zielenski and J. S. Elborn (2008). "Consensus on the use and interpretation of cystic fibrosis mutation analysis in clinical practice." J Cyst Fibros **7**(3): 179-196.

Cervena, T., K. Vrbova, A. Rossnerova, J. Topinka and P. Rossner (2019). "Short-term and Long-term Exposure of the MucilAir™ Model to Polycyclic Aromatic Hydrocarbons." Alternatives to Laboratory Animals **47**(1): 9-18.

Chairat, K., J. Tarning, N. J. White and N. Lindegardh (2013). "Pharmacokinetic properties of anti-influenza neuraminidase inhibitors." J Clin Pharmacol **53**(2): 119-139.

Chakraborty, J., I. Banerjee, R. Vaishya and S. Ghosh (2020). "Bioengineered in Vitro Tissue Models to Study SARS-CoV-2 Pathogenesis and Therapeutic Validation." ACS biomaterials science & engineering **6**(12): 6540-6555.

Chandorkar, P., W. Posch, V. Zaderer, M. Blatzer, M. Steger, C. G. Ammann, U. Binder, M. Hermann, P. Hörtnagl, C. Lass-Flörl and D. Wilflingseder (2017). "Fast-track development of an in vitro 3D lung/immune cell model to study Aspergillus infections." Sci Rep **7**(1): 11644.

Charalampidis, C., A. Youroukou, G. Lazaridis, S. Baka, I. Mpoukovinas, V. Karavasilis, I. Kioumis, G. Pitsiou, A. Papaiwannou, A. Karavergou, K. Tsakiridis, N. Katsikogiannis, E. Sarika, K. Kapanidis, L. Sakkas, I. Korantzis, S. Lampaki, K. Zarogoulidis and P. Zarogoulidis (2015). "Pleura space anatomy." Journal of thoracic disease **7**(Suppl 1): S27-S32.

Charbaji, R., M. Kar, L. E. Theune, J. Bergueiro, A. Eichhorst, L. Navarro, P. Graff, F. Stumpff, M. Calderón and S. Hedtrich (2021). "Design and Testing of Efficient Mucus-Penetrating Nanogels—Pitfalls of Preclinical Testing and Lessons Learned." Small **n/a**(n/a): 2007963.

Chatfield, K. and D. Morton (2018). The Use of Non-human Primates in Research. Ethics Dumping: Case Studies from North-South Research Collaborations. D. Schroeder, J. Cook, F. Hirsch, S. Fenet and V. Muthuswamy. Cham, Springer International Publishing**:** 81-90.

Chaudhry R., B. B. (2020). Anatomy, Thorax, Lungs, StatPearls Publishing.

Chen, H., Z. Yu, S. Bai, H. Lu, D. Xu, C. Chen, D. Liu and Y. Zhu (2019). "Microfluidic models of physiological or pathological flow shear stress for cell biology, disease modeling and drug development." TrAC Trends in Analytical Chemistry **117**: 186-199.

Chen, S. N., X. W. Zhang, L. Li, B. Y. Ruan, B. Huang, W. S. Huang, P. F. Zou, J. P. Fu, L. J. Zhao, N. Li and P. Nie (2016). "Evolution of IFN-λ in tetrapod vertebrates and its functional characterization in green anole lizard (Anolis carolinensis)." Developmental & Comparative Immunology **61**: 208-224.

Chen, X., S. Liu, M. U. Goraya, M. Maarouf, S. Huang and J.-L. Chen (2018). "Host Immune Response to Influenza A Virus Infection." Frontiers in Immunology **9**(320).

Cheung, P. P. H., S. J. Watson, K.-T. Choy, S. Fun Sia, D. D. Y. Wong, L. L. M. Poon, P. Kellam, Y. Guan, J. S. Malik Peiris and H.-L. Yen (2014). "Generation and characterization of influenza A viruses with altered polymerase fidelity." Nature communications **5**: 4794-4794.

Chowdhury, F., W. J. Howat, G. J. Phillips and P. M. Lackie (2010). "Interactions between endothelial cells and epithelial cells in a combined cell model of airway mucosa: effects on tight junction permeability." Exp Lung Res **36**(1): 1-11.

Cleo Leung, F. S., Pascal Bernatchez, Tillie-Louise Hackett (2012). "Expression of Myoferlin in Human Airway Epithelium and Its Role in Cell Adhesion and Zonula Occludens-1 Expression." PLOS ONE.

Coccia, E. M., M. Severa, E. Giacomini, D. Monneron, M. E. Remoli, I. Julkunen, M. Cella, R. Lande and G. Uzé (2004). "Viral infection and Toll-like receptor agonists induce a differential expression of type I and λ interferons in human plasmacytoid and monocyte-derived dendritic cells." European Journal of Immunology **34**(3): 796-805.

Coffman, R. L. and E. M. Hessel (2005). "Nonhuman primate models of asthma." The Journal of experimental medicine **201**(12): 1875-1879.

Cohen, M., X.-Q. Zhang, H. P. Senaati, H.-W. Chen, N. M. Varki, R. T. Schooley and P. Gagneux (2013). "Influenza A penetrates host mucus by cleaving sialic acids with neuraminidase." Virology Journal **10**(1): 321.

Cole, Suzanne L. and L.-P. Ho (2017). "Contribution of innate immune cells to pathogenesis of severe influenza virus infection." Clinical Science **131**(4): 269-283.

Condon, T. V., R. T. Sawyer, M. J. Fenton and D. W. Riches (2011). "Lung dendritic cells at the innate-adaptive immune interface." J Leukoc Biol **90**(5): 883-895.

Couceiro, J. N., J. C. Paulson and L. G. Baum (1993). "Influenza virus strains selectively recognize sialyloligosaccharides on human respiratory epithelium; the role of the host cell in selection of hemagglutinin receptor specificity." Virus Res **29**(2): 155-165.

Creager, H. M., H. Zeng, J. A. Pulit-Penaloza, T. R. Maines, T. M. Tumpey and J. A. Belser (2017). "In vitro exposure system for study of aerosolized influenza virus." Virology **500**: 62-70.

Cutting, G. R. (2015). "Cystic fibrosis genetics: from molecular understanding to clinical application." Nature Reviews Genetics **16**(1): 45-56.

Dahl, R. (2006). "Systemic side effects of inhaled corticosteroids in patients with asthma." Respiratory Medicine **100**(8): 1307-1317.

Dao DPD, L. P. (2020). Histology, Goblet Cells, StatPearls Publishing.

De Boeck, K. (2020). "Cystic fibrosis in the year 2020: A disease with a new face." Acta Paediatrica **109**(5): 893-899.

de Graaf, M. and R. A. M. Fouchier (2014). "Role of receptor binding specificity in influenza A virus transmission and pathogenesis." The EMBO journal **33**(8): 823-841.

De Servi, B., F. Ranzini and N. Piqué (2017). "Protective barrier properties of Rhinosectan® spray (containing xyloglucan) on an organotypic 3D airway tissue model (MucilAir): results of an in vitro study." Allergy, Asthma & Clinical Immunology **13**(1): 37.

de Sousa, J. P. and L. David (2006). 14 - Role of Immunohistochemical Expression of MUC5B in Gastric Carcinoma. Handbook of Immunohistochemistry and in Situ Hybridization of Human Carcinomas. M. A. Hayat, Academic Press. **4:** 191-194.

de Weerd, N. A., S. A. Samarajiwa and P. J. Hertzog (2007). "Type I interferon receptors: biochemistry and biological functions." J Biol Chem **282**(28): 20053-20057.

Delamarche, E., N. Tonna, R. D. Lovchik, F. Bianco and M. Matteoli (2013). "Pharmacology on microfluidics: multimodal analysis for studying cell-cell interaction." Curr Opin Pharmacol **13**(5): 821-828.

Denney, L. and L.-P. Ho (2018). "The role of respiratory epithelium in host defence against influenza virus infection." Biomedical journal **41**(4): 218-233.

Denney, L. and L. P. Ho (2018). "The role of respiratory epithelium in host defence against influenza virus infection." Biomed J **41**(4): 218-233.

Despina G. Contopoulos-Ioannidis, M., Evangelia E. Ntzani, MD, John P. A. Ioannidis, MD (2003). "Translation of Highly Promising Basic Science

Research into Clinical Applications." The American Journal of Medicine.

Doudna, J. A. (2020). "The promise and challenge of therapeutic genome editing." Nature **578**(7794): 229-236.

Edmondson, R., J. J. Broglie, A. F. Adcock and L. Yang (2014). "Three-dimensional cell culture systems and their applications in drug discovery and cell-based biosensors." Assay and drug development technologies **12**(4): 207-218.

Egron, C., A. Labbé, E. Rochette, A. Mulliez, A. Bernard and A. Flore (2020). "Urinary club cell protein 16 (CC16): Utility of its assay during acute bronchiolitis." Pediatr Pulmonol **55**(2): 490-495.

Elborn, J. S. (2016). "Cystic fibrosis." The Lancet **388**(10059): 2519-2531.

Elliott, M. (2001). "Zanamivir: from drug design to the clinic." Philos Trans R Soc Lond B Biol Sci **356**(1416): 1885-1893.

Evans, D. T., R. Serra-Moreno, R. K. Singh and J. C. Guatelli (2010). "BST-2/tetherin: a new component of the innate immune response to enveloped viruses." Trends in Microbiology **18**(9): 388-396.

Fatykhova, D., A. Rabes, C. Machnik, K. Guruprasad, F. Pache, J. Berg, M. Toennies, T. T. Bauer, P. Schneider, M. Schimek, S. Eggeling, T. J. Mitchell, A. M. Mitchell, R. Hilker, T. Hain, N. Suttorp, S. Hippenstiel, A. C. Hocke and B. Opitz (2015). "Serotype 1 and 8 Pneumococci Evade Sensing by Inflammasomes in Human Lung Tissue." PLoS One **10**(8): e0137108.

Fauquet, C. M. (2008). "Taxonomy, Classification and Nomenclature of Viruses." Encyclopedia of Virology: 9-23.

Ferraris, O., N. Kessler and B. Lina (2005). "Sensitivity of influenza viruses to zanamivir and oseltamivir: a study performed on viruses circulating in France prior to the introduction of neuraminidase inhibitors in clinical practice." Antiviral Res **68**(1): 43-48.

Florin, L., N. Maas-Szabowski, S. Werner, A. Szabowski and P. Angel (2005). "Increased keratinocyte proliferation by JUN-dependent expression of PTN and SDF-1 in fibroblasts." J Cell Sci **118**(Pt 9): 1981-1989.

Fontoura, J. C., C. Viezzer, F. G. dos Santos, R. A. Ligabue, R. Weinlich, R. D. Puga, D. Antonow, P. Severino and C. Bonorino (2020). "Comparison of 2D and 3D cell culture models for cell growth, gene expression and drug resistance." Materials Science and Engineering: C **107**: 110264.

Forbes, B., A. Shah, G. P. Martin and A. B. Lansley (2003). "The human bronchial epithelial cell line 16HBE14o− as a model system of the airways for studying drug transport." International Journal of Pharmaceutics **257**(1): 161-167.

Franke, W. W., D. L. Schiller, R. Moll, S. Winter, E. Schmid, I. Engelbrecht, H. Denk, R. Krepler and B. Platzer (1981). "Diversity of cytokeratins: Differentiation specific expression of cytokeratin polypeptides in epithelial cells and tissues." Journal of Molecular Biology **153**(4): 933-959.

French, C. A. (2009). Chapter 2 - Respiratory Tract. Cytology (Third Edition). E. S. Cibas and B. S. Ducatman. Philadelphia, W.B. Saunders**:** 65-103.

Gad, H. H., C. Dellgren, O. J. Hamming, S. Vends, S. R. Paludan and R. Hartmann (2009). "Interferon-lambda is functionally an interferon but structurally related to the interleukin-10 family." J Biol Chem **284**(31): 20869-20875.

Galarza, S., H. Kim, N. Atay, S. R. Peyton and J. M. Munson (2019). "2D or 3D? How cell motility measurements are conserved across dimensions in vitro and translate in vivo." Bioengineering & translational medicine **5**(1): e10148-e10148.

Gambotto, A., S. M. Barratt-Boyes, M. D. de Jong, G. Neumann and Y. Kawaoka (2008). "Human infection with highly pathogenic H5N1 influenza virus." The Lancet **371**(9622): 1464-1475.

Gao, H., H. Yao, S. Yang and L. Li (2016). "From SARS to MERS: evidence and speculation." Front Med **10**(4): 377-382.

Gao, R., B. Cao, Y. Hu, Z. Feng, D. Wang, W. Hu, J. Chen, Z. Jie, H. Qiu, K. Xu, X. Xu, H. Lu, W. Zhu, Z. Gao, N. Xiang, Y. Shen, Z. He, Y. Gu, Z. Zhang, Y. Yang, X. Zhao, L. Zhou, X. Li, S. Zou, Y. Zhang, X. Li, L. Yang, J. Guo, J. Dong, Q. Li, L. Dong, Y. Zhu, T. Bai, S. Wang, P. Hao, W. Yang, Y. Zhang, J. Han, H. Yu, D. Li, G. F. Gao, G. Wu, Y. Wang, Z. Yuan and Y. Shu (2013). "Human Infection with a Novel Avian-Origin Influenza A (H7N9) Virus." New England Journal of Medicine **368**(20): 1888-1897.

García-Sastre, A. and C. A. Biron (2006). "Type 1 interferons and the virus-host relationship: a lesson in détente." Science **312**(5775): 879-882.

Glaser, L., G. Conenello, J. Paulson and P. Palese (2007). "Effective replication of human influenza viruses in mice lacking a major alpha2,6 sialyltransferase." Virus Res **126**(1-2): 9-18.

Goldmann, D. A. (2000). "Transmission of viral respiratory infections in the home." Pediatr Infect Dis J **19**(10 Suppl): S97-102.

Grais, R. F., J. H. Ellis, A. Kress and G. E. Glass (2004). "Modeling the Spread of Annual Influenza Epidemics in the U.S.: The Potential Role of Air Travel." Health Care Management Science **7**(2): 127-134.

Grohskopf, L. A., E. Alyanak, K. R. Broder, L. H. Blanton, A. M. Fry, D. B. Jernigan and R. L. Atmar (2020). "Prevention and Control of Seasonal Influenza with Vaccines: Recommendations of the Advisory Committee on Immunization Practices - United States, 2020-21 Influenza Season." MMWR Recomm Rep **69**(8): 1-24.

Gronbach, L., C. Wolff, K. Klinghammer, J. Stellmacher, P. Jurmeister, U. Alexiev, M. Schäfer-Korting, I. Tinhofer, U. Keilholz and C. Zoschke (2020). "A multilayered epithelial mucosa model

of head neck squamous cell carcinoma for analysis of tumor-microenvironment interactions and drug development." Biomaterials **258**: 120277.

Gualtieri, M., M. G. Grollino, C. Consales, F. Costabile, M. Manigrasso, P. Avino, M. Aufderheide, E. Cordelli, L. Di Liberto, E. Petralia, G. Raschellà, M. Stracquadanio, A. Wiedensohler, F. Pacchierotti and G. Zanini (2018). "Is it the time to study air pollution effects under environmental conditions? A case study to support the shift of in vitro toxicology from the bench to the field." Chemosphere **207**: 552-564.

Guilbault, C., Z. Saeed, G. P. Downey and D. Radzioch (2007). "Cystic fibrosis mouse models." Am J Respir Cell Mol Biol **36**(1): 1-7.

Guillot, L., N. Nathan, O. Tabary, G. Thouvenin, P. Le Rouzic, H. Corvol, S. Amselem and A. Clement (2013). "Alveolar epithelial cells: Master regulators of lung homeostasis." The International Journal of Biochemistry & Cell Biology **45**(11): 2568-2573.

Guo, H., P. Kumar and S. Malarkannan (2011). "Evasion of natural killer cells by influenza virus." J Leukoc Biol **89**(2): 189-194.

Halfhide, C., H. J. Evans and J. Couriel (2005). "Inhaled bronchodilators for cystic fibrosis." Cochrane Database Syst Rev(4): Cd003428.

Haller, O., P. Staeheli and G. Kochs (2007). "Interferon-induced Mx proteins in antiviral host defense." Biochimie **89**(6): 812-818.

Hamilton, N. J. I., D. D. H. Lee, K. H. C. Gowers, C. R. Butler, E. F. Maughan, B. Jevans, J. C. Orr, C. J. McCann, A. J. Burns, S. MacNeil, M. A. Birchall, C. Callaghan, R. E. Hynds and S. M. Janes (2020). "Bioengineered airway epithelial grafts with mucociliary function based on collagen IV- and laminin-containing extracellular matrix scaffolds." European Respiratory Journal **55**(6): 1901200.

Harrington, H., P. Cato, F. Salazar, M. Wilkinson, A. Knox, J. W. Haycock, F. Rose, J. W. Aylott and A. M. Ghaemmaghami (2014). "Immunocompetent 3D Model of Human Upper Airway for Disease Modeling and In Vitro Drug Evaluation." Molecular Pharmaceutics **11**(7): 2082-2091.

Hause, B. M., M. Ducatez, E. A. Collin, Z. Ran, R. Liu, Z. Sheng, A. Armien, B. Kaplan, S. Chakravarty, A. D. Hoppe, R. J. Webby, R. R. Simonson and F. Li (2013). "Isolation of a Novel Swine Influenza Virus from Oklahoma in 2011 Which Is Distantly Related to Human Influenza C Viruses." PLOS Pathogens **9**(2): e1003176.

Hay, M., D. W. Thomas, J. L. Craighead, C. Economides and J. Rosenthal (2014). "Clinical development success rates for investigational drugs." Nat Biotechnol **32**(1): 40-51.

Hedström, U., O. Hallgren, L. Öberg, A. DeMicco, O. Vaarala, G. Westergren-Thorsson and X. Zhou (2018). "Bronchial extracellular matrix from COPD patients induces altered gene expression in repopulated primary human bronchial epithelial cells." Scientific Reports **8**(1): 3502.

Heijerman, H. G. M., E. F. McKone, D. G. Downey, E. Van Braeckel, S. M. Rowe, E. Tullis, M. A. Mall, J. J. Welter, B. W. Ramsey, C. M. McKee, G. Marigowda, S. M. Moskowitz, D. Waltz, P. R. Sosnay, C. Simard, N. Ahluwalia, F. Xuan, Y. Zhang, J. L. Taylor-Cousar and K. S. McCoy (2019). "Efficacy and safety of the elexacaftor plus tezacaftor plus ivacaftor combination regimen

in people with cystic fibrosis homozygous for the F508del mutation: a double-blind, randomised, phase 3 trial." Lancet **394**(10212): 1940-1948.

Herland, A., B. M. Maoz, D. Das, M. R. Somayaji, R. Prantil-Baun, R. Novak, M. Cronce, T. Huffstater, S. S. F. Jeanty, M. Ingram, A. Chalkiadaki, D. Benson Chou, S. Marquez, A. Delahanty, S. Jalili-Firoozinezhad, Y. Milton, A. Sontheimer-Phelps, B. Swenor, O. Levy, K. K. Parker, A. Przekwas and D. E. Ingber (2020). "Quantitative prediction of human pharmacokinetic responses to drugs via fluidically coupled vascularized organ chips." Nature Biomedical Engineering **4**(4): 421-436.

Hermanns, M. I., C. Freese, L. Anspach, V. Grützner, C. Pohl, R. E. Unger and C. J. Kirkpatrick (2017). 3.15 Cell Culture Systems for Studying Biomaterial Interactions With Biological Barriers☆. Comprehensive Biomaterials II. P. Ducheyne. Oxford, Elsevier**:** 295-334.

Herold, S., W. von Wulffen, M. Steinmueller, S. Pleschka, W. A. Kuziel, M. Mack, M. Srivastava, W. Seeger, U. A. Maus and J. Lohmeyer (2006). "Alveolar epithelial cells direct monocyte transepithelial migration upon influenza virus infection: impact of chemokines and adhesion molecules." J Immunol **177**(3): 1817-1824.

Herrmann, H., H. Bär, L. Kreplak, S. V. Strelkov and U. Aebi (2007). "Intermediate filaments: from cell architecture to nanomechanics." Nature Reviews Molecular Cell Biology **8**(7): 562-573.

Herszberg, B., D. Ramos-Barbón, M. Tamaoka, J. G. Martin and J. P. Lavoie (2006). "Heaves, an asthma-like equine disease, involves airway smooth muscle remodeling." J Allergy Clin Immunol **118**(2): 382-388.

Hewlings, S. J. and D. S. Kalman (2017). "Curcumin: A Review of Its Effects on Human Health." Foods (Basel, Switzerland) **6**(10): 92.

Heyes, J., K. Hall, V. Tailor, R. Lenz and I. MacLachlan (2006). "Synthesis and characterization of novel poly(ethylene glycol)-lipid conjugates suitable for use in drug delivery." J Control Release **112**(2): 280-290.

Hida, K., S. K. Lai, J. S. Suk, S. Y. Won, M. P. Boyle and J. Hanes (2011). "Common gene therapy viral vectors do not efficiently penetrate sputum from cystic fibrosis patients." PloS one **6**(5): e19919-e19919.

Hill, D. B., P. A. Vasquez, J. Mellnik, S. A. McKinley, A. Vose, F. Mu, A. G. Henderson, S. H. Donaldson, N. E. Alexis, R. C. Boucher and M. G. Forest (2014). "A biophysical basis for mucus solids concentration as a candidate biomarker for airways disease." PloS one **9**(2): e87681-e87681.

Hiller, T., J. Berg, L. Elomaa, V. Röhrs, I. Ullah, K. Schaar, A.-C. Dietrich, M. A. Al-Zeer, A. Kurtz, A. C. Hocke, S. Hippenstiel, H. Fechner, M. Weinhart and J. Kurreck (2018). "Generation of a 3D Liver Model Comprising Human Extracellular Matrix in an Alginate/Gelatin-Based Bioink by Extrusion Bioprinting for Infection and Transduction Studies." International journal of molecular sciences **19**(10): 3129.

Hirst, S. J., C. H. Twort and T. H. Lee (2000). "Differential effects of extracellular matrix proteins on human airway smooth muscle cell proliferation and phenotype." Am J Respir Cell Mol Biol **23**(3): 335-344.

Hiscott, J., R. Lin, P. Nakhaei and S. Paz (2006). "MasterCARD: a priceless link to innate immunity." Trends in Molecular Medicine **12**(2): 53-56.

Hittinger, M., J. Janke, H. Huwer, R. Scherließ, N. Schneider-Daum and C. M. Lehr (2016). "Autologous co-culture of primary human alveolar macrophages and epithelial cells for investigating aerosol medicines. Part I: model characterisation." Altern Lab Anim **44**(4): 337-347.

Hocke, A. C., N. Suttorp and S. Hippenstiel (2017). "Human lung ex vivo infection models." Cell Tissue Res **367**(3): 511-524.

Hocke, A. C., N. Suttorp and S. Hippenstiel (2017). "Human lung ex vivo infection models." Cell and Tissue Research **367**(3): 511-524.

Hogan, B. L. M., C. E. Barkauskas, H. A. Chapman, J. A. Epstein, R. Jain, C. C. W. Hsia, L. Niklason, E. Calle, A. Le, S. H. Randell, J. Rock, M. Snitow, M. Krummel, B. R. Stripp, T. Vu, E. S. White, J. A. Whitsett and E. E. Morrisey (2014). "Repair and regeneration of the respiratory system: complexity, plasticity, and mechanisms of lung stem cell function." Cell stem cell **15**(2): 123-138.

Holtzman, M. J., D. E. Byers, J. Alexander-Brett and X. Wang (2014). "The role of airway epithelial cells and innate immune cells in chronic respiratory disease." Nature Reviews Immunology **14**(10): 686-698.

Hönzke, S., L. Wallmeyer, A. Ostrowski, M. Radbruch, L. Mundhenk, M. Schäfer-Korting and S. Hedtrich (2016). "Influence of Th2 Cytokines on the Cornified Envelope, Tight Junction Proteins, and β-Defensins in Filaggrin-Deficient Skin Equivalents." Journal of Investigative Dermatology **136**(3): 631-639.

Hordvik, N. L., P. H. Sammut, C. G. Judy and J. L. Colombo (2002). "Effectiveness and tolerability of high-dose salmeterol in cystic fibrosis." Pediatr Pulmonol **34**(4): 287-296.

Huang, C.-G., L.-A. Lee, Y.-C. Wu, M.-J. Hsiao, J.-T. Horng, R.-L. Kuo, C.-H. Huang, Y.-C. Lin, K.-C. Tsao, M.-C. Chen, T.-C. Chen and S.-R. Shih (2018). "A pilot study on primary cultures of human respiratory tract epithelial cells to predict patients' responses to H7N9 infection." Oncotarget **9**(18): 14492-14508.

Huch, M. and B. K. Koo (2015). "Modeling mouse and human development using organoid cultures." Development **142**(18): 3113-3125.

Hurley, B. P. and B. A. McCormick (2003). "Translating tissue culture results into animal models: the case of Salmonella typhimurium." Trends Microbiol **11**(12): 562-569.

Hussell, T. and T. J. Bell (2014). "Alveolar macrophages: plasticity in a tissue-specific context." Nature Reviews Immunology **14**(2): 81-93.

Ibricevic, A., A. Pekosz, M. J. Walter, C. Newby, J. T. Battaile, E. G. Brown, M. J. Holtzman and S. L. Brody (2006). "Influenza virus receptor specificity and cell tropism in mouse and human airway epithelial cells." Journal of virology **80**(15): 7469-7480.

Ibricevic, A., A. Pekosz, M. J. Walter, C. Newby, J. T. Battaile, E. G. Brown, M. J. Holtzman and S. L. Brody (2006). "Influenza virus receptor specificity and cell tropism in mouse and human airway epithelial cells." J Virol **80**(15): 7469-7480.

Ioannidis, I., F. Ye, B. McNally, M. Willette and E. Flaño (2013). "Toll-Like Receptor Expression and Induction of Type I and Type III Interferons in Primary Airway Epithelial Cells." Journal of Virology **87**(6): 3261-3270.

Jaks, E., M. Gavutis, G. Uzé, J. Martal and J. Piehler (2007). "Differential Receptor Subunit Affinities of Type I Interferons Govern Differential Signal Activation." Journal of Molecular Biology **366**(2): 525-539.

Jeans, A. R., S. J. Howard, Z. Al-Nakeeb, J. Goodwin, L. Gregson, J. B. Majithiya, C. Lass-Flörl, M. Cuenca-Estrella, M. C. Arendrup, P. A. Warn and W. W. Hope (2012). "Pharmacodynamics of voriconazole in a dynamic in vitro model of invasive pulmonary aspergillosis: implications for in vitro susceptibility breakpoints." J Infect Dis **206**(3): 442-452.

Jefferson, T., M. A. Jones, P. Doshi, C. B. Del Mar, R. Hama, M. Thompson, E. A. Spencer, I. Onakpoya, K. R. Mahtani, D. N. Nunan, J. Howick and C. J. Heneghan (2014). "Neuraminidase inhibitors for preventing and treating influenza in healthy adults and children." Sao Paulo Medical Journal **132**: 256-257.

Jewell, N. A., T. Cline, S. E. Mertz, S. V. Smirnov, E. Flaño, C. Schindler, J. L. Grieves, R. K. Durbin, S. V. Kotenko and J. E. Durbin (2010). "Lambda Interferon Is the Predominant Interferon Induced by Influenza A Virus Infection In Vivo." Journal of Virology **84**(21): 11515-11522.

Johnson, L. A., R. H. J. Olsen, L. S. Merkens, A. DeBarber, R. D. Steiner, P. M. Sullivan, N. Maeda and J. Raber (2014). "Apolipoprotein E-low density lipoprotein receptor interaction affects spatial memory retention and brain ApoE levels in an isoform-dependent manner." Neurobiology of disease **64**: 150-162.

Kaessmeyer, S. S., J.; Khiao In, M.; Merle, R.; Richardson, K.; Plendl, J. (2017). "Subcellular Interactions during Vascular Morphogenesis in 3D Cocultures between Endothelial Cells and Fibroblasts." International Journal of Molecular Sciences **12**: 2590.

Kapałczyńska, M., T. Kolenda, W. Przybyła, M. Zajączkowska, A. Teresiak, V. Filas, M. Ibbs, R. Bliźniak, Ł. Łuczewski and K. Lamperska (2018). "2D and 3D cell cultures - a comparison of different types of cancer cell cultures." Archives of medical science : AMS **14**(4): 910-919.

Kawai, T. and S. Akira (2006). "Innate immune recognition of viral infection." Nature Immunology **7**(2): 131-137.

Kawai, T. and S. Akira (2010). "The role of pattern-recognition receptors in innate immunity: update on Toll-like receptors." Nature Immunology **11**(5): 373-384.

Kerem, B., J. M. Rommens, J. A. Buchanan, D. Markiewicz, T. K. Cox, A. Chakravarti, M. Buchwald and L. C. Tsui (1989). "Identification of the cystic fibrosis gene: genetic analysis." Science **245**(4922): 1073-1080.

Khan, Y. S. and D. T. Lynch (2020). Histology, Lung, StatPearls Publishing, Treasure Island (FL).

Kift, R. L., C. Byrne, R. Liversidge, F. Babbington, C. Knox, J. Binns and J. H. Barth (2015). "The effect of storage conditions on sample stability in the routine clinical laboratory." Ann Clin Biochem **52**(Pt 6): 675-679.

Kim, C. F. B., E. L. Jackson, A. E. Woolfenden, S. Lawrence, I. Babar, S. Vogel, D. Crowley, R. T. Bronson and T. Jacks (2005). "Identification of Bronchioalveolar Stem Cells in Normal Lung and Lung Cancer." Cell **121**(6): 823-835.

Kim, S. N., S. A. Ko, C. G. Park, S. H. Lee, B. K. Huh, Y. H. Park, Y. K. Kim, A. Ha, K. H. Park and Y. B. Choy (2018). "Amino-Functionalized Mesoporous Silica Particles for Ocular Delivery of Brimonidine." Mol Pharm **15**(8): 3143-3152.

Kirby, T. (2018). "Tezacaftor-ivacaftor is safe and efficacious in patients with cystic fibrosis with Phe508del mutations." Lancet Respir Med **6**(1): 13-14.

Klimanskaya, I., E. A. Kimbrel and R. Lanza (2020). Chapter 23 - Embryonic stem cells. Principles of Tissue Engineering (Fifth Edition). R. Lanza, R. Langer, J. P. Vacanti and A. Atala, Academic Press**:** 421-434.

Klimov, A. I., R. Garten, C. Russell, I. G. Barr, T. G. Besselaar, R. Daniels, O. G. Engelhardt, G. Grohmann, S. Itamura, A. Kelso, J. McCauley, T. Odagiri, D. Smith, M. Tashiro, X. Xu, R. Webby, D. Wang, Z. Ye, S. Yuelong, W. Zhang and N. Cox (2012). "WHO recommendations for the viruses to be used in the 2012 Southern Hemisphere Influenza Vaccine: epidemiology, antigenic and genetic characteristics of influenza A(H1N1)pdm09, A(H3N2) and B influenza viruses collected from February to September 2011." Vaccine **30**(45): 6461-6471.

Knight, E., B. Murray, R. Carnachan and S. Przyborski (2011). "Alvetex®: polystyrene scaffold technology for routine three dimensional cell culture." Methods Mol Biol **695**: 323-340.

Knight, E. and S. Przyborski (2015). "Advances in 3D cell culture technologies enabling tissue-like structures to be created in vitro." Journal of Anatomy **227**(6): 746-756.

Kobayashi, Y. and P. R. Tata (2018). "Pulmonary Neuroendocrine Cells: Sensors and Sentinels of the Lung." Developmental Cell **45**(4): 425-426.

Kola, I. and J. Landis (2004). "Can the pharmaceutical industry reduce attrition rates?" Nature Reviews Drug Discovery **3**(8): 711-716.

Konstan, M. W. and F. Ratjen (2012). "Effect of dornase alfa on inflammation and lung function: potential role in the early treatment of cystic fibrosis." J Cyst Fibros **11**(2): 78-83.

Krall, N., F. P. da Cruz, O. Boutureira and G. J. L. Bernardes (2016). "Site-selective protein-modification chemistry for basic biology and drug development." Nature Chemistry **8**(2): 103-113.

Kreimendahl, F., S. Ossenbrink, M. Köpf, M. Westhofen, T. Schmitz-Rode, H. Fischer, S. Jockenhoevel and A. L. Thiebes (2019). "Combination of vascularization and cilia formation for three-dimensional airway tissue engineering." J Biomed Mater Res A **107**(9): 2053-2062.

Krüger-Genge, A., A. Blocki, R.-P. Franke and F. Jung (2019). "Vascular Endothelial Cell Biology: An Update." International journal of molecular sciences **20**(18): 4411.

Küchler, S., D. Henkes, K. M. Eckl, K. Ackermann, J. Plendl, H. C. Korting, H. C. Hennies and M. Schäfer-Korting (2011). "Hallmarks of atopic skin mimicked in vitro by means of a skin disease model based on FLG knock-down." Altern Lab Anim **39**(5): 471-480.

Kulkarni, J. A., J. L. Myhre, S. Chen, Y. Y. C. Tam, A. Danescu, J. M. Richman and P. R. Cullis (2017). "Design of lipid nanoparticles for in vitro and in vivo delivery of plasmid DNA." Nanomedicine **13**(4): 1377-1387.

Kulkarni, J. A., D. Witzigmann, J. Leung, Y. Y. C. Tam and P. R. Cullis (2019). "On the role of helper lipids in lipid nanoparticle formulations of siRNA." Nanoscale **11**(45): 21733-21739.

Lai, S. K., D. E. O'Hanlon, S. Harrold, S. T. Man, Y.-Y. Wang, R. Cone and J. Hanes (2007). "Rapid transport of large polymeric nanoparticles in fresh undiluted human mucus." Proceedings of the National Academy of Sciences of the United States of America **104**(5): 1482-1487.

Lai, S. K., Y.-Y. Wang and J. Hanes (2009). "Mucus-penetrating nanoparticles for drug and gene delivery to mucosal tissues." Advanced drug delivery reviews **61**(2): 158-171.

Lamb, Y. N. (2021). "BNT162b2 mRNA COVID-19 Vaccine: First Approval." Drugs **81**(4): 495-501.

Lancaster, M. A. and M. Huch (2019). "Disease modelling in human organoids." Disease Models & Mechanisms **12**(7): dmm039347.

Lara, P. N., J.-Y. Douillard, K. Nakagawa, J. von Pawel, M. J. McKeage, I. Albert, G. Losonczy, M. Reck, D.-S. Heo, X. Fan, A. Fandi and G. Scagliotti (2011). "Randomized Phase III Placebo-Controlled Trial of Carboplatin and Paclitaxel With or Without the Vascular Disrupting Agent Vadimezan (ASA404) in Advanced Non–Small-Cell Lung Cancer." Journal of Clinical Oncology **29**(22): 2965-2971.

Laucho-Contreras, M. E., F. Polverino, Y. Tesfaigzi, A. Pilon, B. R. Celli and C. A. Owen (2016). "Club Cell Protein 16 (CC16) Augmentation: A Potential Disease-modifying Approach for Chronic Obstructive Pulmonary Disease (COPD)." Expert Opin Ther Targets **20**(7): 869-883.

Lauster, D., S. Klenk, K. Ludwig, S. Nojoumi, S. Behren, L. Adam, M. Stadtmüller, S. Saenger, S. Zimmler, K. Hönzke, L. Yao, U. Hoffmann, M. Bardua, A. Hamann, M. Witzenrath, L. E. Sander, T. Wolff, A. C. Hocke, S. Hippenstiel, S. De Carlo, J. Neudecker, K. Osterrieder, N. Budisa, R. R. Netz, C. Böttcher, S. Liese, A. Herrmann and C. P. R. Hackenberger (2020). "Phage capsid nanoparticles with defined ligand arrangement block influenza virus entry." Nature Nanotechnology **15**(5): 373-379.

Lavoie, T. B., E. Kalie, S. Crisafulli-Cabatu, R. Abramovich, G. DiGioia, K. Moolchan, S. Pestka and G. Schreiber (2011). "Binding and activity of all human alpha interferon subtypes." Cytokine **56**(2): 282-289.

Law, J. X., L. L. Liau, B. S. Aminuddin and B. H. I. Ruszymah (2016). "Tissue-engineered trachea: A review." International Journal of Pediatric Otorhinolaryngology **91**: 55-63.

Leal, J., H. D. C. Smyth and D. Ghosh (2017). "Physicochemical properties of mucus and their impact on transmucosal drug delivery." International Journal of Pharmaceutics **532**(1): 555-572.

Lee, C.-K., D. T. Rao, R. Gertner, R. Gimeno, A. B. Frey and D. E. Levy (2000). "Distinct Requirements for IFNs and STAT1 in NK Cell Function." The Journal of Immunology **165**(7): 3571-3577.

Lee, J., G. D. Lilly, R. C. Doty, P. Podsiadlo and N. A. Kotov (2009). "In vitro toxicity testing of nanoparticles in 3D cell culture." Small **5**(10): 1213-1221.

Leekha, S., N. L. Zitterkopf, M. J. Espy, T. F. Smith, R. L. Thompson and P. Sampathkumar (2007). "Duration of influenza A virus shedding in hospitalized patients and implications for infection control." Infection Control and Hospital Epidemiology **28**(9): 1071-1076.

Lehnert, R., M. Pletz, A. Reuss and T. Schaberg (2016). "Antivirale Arzneimittel bei saisonaler und pandemischer Influenza." Dtsch Arztebl International **113**(47): 799-807.

Lelli, D., A. Sahebkar, T. P. Johnston and C. Pedone (2017). "Curcumin use in pulmonary diseases: State of the art and future perspectives." Pharmacol Res **115**: 133-148.

LeMessurier, K. S., M. Tiwary, N. P. Morin and A. E. Samarasinghe (2020). "Respiratory Barrier as a Safeguard and Regulator of Defense Against Influenza A Virus and Streptococcus pneumoniae." Frontiers in Immunology **11**(3).

Lenz, A. G., E. Karg, E. Brendel, H. Hinze-Heyn, K. L. Maier, O. Eickelberg, T. Stoeger and O. Schmid (2013). "Inflammatory and oxidative stress responses of an alveolar epithelial cell line to airborne zinc oxide nanoparticles at the air-liquid interface: a comparison with conventional, submerged cell-culture conditions." Biomed Res Int **2013**: 652632.

Lertkiatmongkol, P., D. Liao, H. Mei, Y. Hu and P. J. Newman (2016). "Endothelial functions of platelet/endothelial cell adhesion molecule-1 (CD31)." Current opinion in hematology **23**(3): 253-259.

Li, H., D. N. Sheppard and M. J. Hug (2004). "Transepithelial electrical measurements with the Ussing chamber." Journal of Cystic Fibrosis **3**: 123-126.

Lidington, E. A., D. L. Moyes, A. M. McCormack and M. L. Rose (1999). "A comparison of primary endothelial cells and endothelial cell lines for studies of immune interactions." Transplant Immunology **7**(4): 239-246.

Lindberg, R. H., G. Fedorova, K. M. Blum, J. Pulit-Prociak, A. Gillman, J. Järhult, P. Appelblad and H. Söderström (2015). "Online solid phase extraction liquid chromatography using bonded zwitterionic stationary phases and tandem mass spectrometry for rapid environmental trace analysis of highly polar hydrophilic compounds - Application for the antiviral drug Zanamivir." Talanta **141**: 164-169.

Llobet, L., J. Montoya, E. López-Gallardo and E. Ruiz-Pesini (2015). "Side Effects of Culture Media Antibiotics on Cell Differentiation." Tissue Engineering Part C: Methods **21**(11): 1143-1147.

Lopez-Castejon, G. and D. Brough (2011). "Understanding the mechanism of IL-1β secretion." Cytokine & growth factor reviews **22**(4): 189-195.

Löwa, A., A. Vogt, S. Kaessmeyer and S. Hedtrich (2018). "Generation of full-thickness skin equivalents using hair follicle-derived primary human keratinocytes and fibroblasts." Journal of Tissue Engineering and Regenerative Medicine **12**(4): e2134-e2146.

Lowen, A. C., S. Mubareka, J. Steel and P. Palese (2007). "Influenza virus transmission is dependent on relative humidity and temperature." PLoS pathogens **3**(10): 1470-1476.

Lu, X., A. Masic, Q. Liu and Y. Zhou (2011). "Regulation of influenza A virus induced CXCL-10 gene expression requires PI3K/Akt pathway and IRF3 transcription factor." Mol Immunol **48**(12-13): 1417-1423.

Lund, J. M., L. Alexopoulou, A. Sato, M. Karow, N. C. Adams, N. W. Gale, A. Iwasaki and R. A. Flavell (2004). "Recognition of single-stranded RNA viruses by Toll-like receptor 7." Proc Natl Acad Sci U S A **101**(15): 5598-5603.

Lyczak, J. B., C. L. Cannon and G. B. Pier (2002). "Lung infections associated with cystic fibrosis." Clinical microbiology reviews **15**(2): 194-222.

MacConnachie, A. M. (1998). "Dornase-alfa (DNase, Pulmozyme) for cystic fibrosis." Intensive Crit Care Nurs **14**(2): 101-102.

MacConnachie, A. M. (1999). "Zanamivir (Relenza®) — A new treatment for influenza." Intensive and Critical Care Nursing **15**(6): 369-370.

Mahfouzi, S. H., S. H. Safiabadi Tali and G. Amoabediny (2021). "3D bioprinting for lung and tracheal tissue engineering: Criteria, advances, challenges, and future directions." Bioprinting **21**: e00124.

Mailliard, R. B. (2020). "Dendritic Cells and Antiviral Defense." Viruses **12**(10): 1152.

Mall, M., B. R. Grubb, J. R. Harkema, W. K. O'Neal and R. C. Boucher (2004). "Increased airway epithelial Na+ absorption produces cystic fibrosis-like lung disease in mice." Nat Med **10**(5): 487-493.

Mall, M. A. and L. J. Galietta (2015). "Targeting ion channels in cystic fibrosis." J Cyst Fibros **14**(5): 561-570.

Mao, Y., T. Hoffman, A. Wu, R. Goyal and J. Kohn (2017). "Cell type–specific extracellular matrix guided the differentiation of human mesenchymal stem cells in 3D polymeric scaffolds." Journal of Materials Science: Materials in Medicine **28**(7): 100.

Marinkovic, M., R. Sridharan, F. Santarella, A. Smith, J. A. Garlick and C. J. Kearney (2021). "Optimization of extracellular matrix production from human induced pluripotent stem cell-derived fibroblasts for scaffold fabrication for application in wound healing." Journal of Biomedical Materials Research Part A **n/a**(n/a).

Marr, L. C., J. W. Tang, J. Van Mullekom and S. S. Lakdawala (2019). "Mechanistic insights into the effect of humidity on airborne influenza virus survival, transmission and incidence." Journal of the Royal Society, Interface **16**(150): 20180298-20180298.

Marrazzo, P., S. Maccari, A. Taddei, L. Bevan, J. Telford, M. Soriani and A. Pezzicoli (2016). "3D Reconstruction of the Human Airway Mucosa In Vitro as an Experimental Model to Study NTHi Infections." PLOS ONE **11**(4): e0153985.

Martić-Kehl, M. I., R. Schibli and P. A. Schubiger (2012). "Can animal data predict human outcome? Problems and pitfalls of translational animal research." European Journal of Nuclear Medicine and Molecular Imaging **39**(9): 1492-1496.

Martin, K. and A. Helenius (1991). "Nuclear transport of influenza virus ribonucleoproteins: the viral matrix protein (M1) promotes export and inhibits import." Cell **67**(1): 117-130.

Martin, K. and A. Helenius (1991). "Transport of incoming influenza virus nucleocapsids into the nucleus." J Virol **65**(1): 232-244.

Matrosovich, M., T. Matrosovich, J. Uhlendorff, W. Garten and H. D. Klenk (2007). "Avian-virus-like receptor specificity of the hemagglutinin impedes influenza virus replication in cultures of human airway epithelium." Virology **361**(2): 384-390.

Matrosovich, M. N., T. Y. Matrosovich, T. Gray, N. A. Roberts and H. D. Klenk (2004). "Human and avian influenza viruses target different cell types in cultures of human airway epithelium." Proc Natl Acad Sci U S A **101**(13): 4620-4624.

Maughan, E. F., E. Nigro, A. Pennycuick, K. H. C. Gowers, C. Denais, S. Gómez-López, K. A. Lazarus, C. R. Butler, D. D. H. Lee, J. C. Orr, V. H. Teixeira, B. E. Hartley, R. J. Hewitt, C. A. Yaghchi, G. S. Sandhu, M. A. Birchall, C. O'Callaghan, C. M. Smith, P. De Coppi, R. E. Hynds and S. M. Janes (2020). "Cell-intrinsic differences between human airway epithelial cells from children and adults." bioRxiv: 2020.2004.2020.027144.

Mazák, K. and B. Noszál (2020). "Physicochemical Properties of Zwitterionic Drugs in Therapy." ChemMedChem **15**(13): 1102-1110.

McCray, P. B., Jr., L. Pewe, C. Wohlford-Lenane, M. Hickey, L. Manzel, L. Shi, J. Netland, H. P. Jia, C. Halabi, C. D. Sigmund, D. K. Meyerholz, P. Kirby, D. C. Look and S. Perlman (2007). "Lethal infection of K18-hACE2 mice infected with severe acute respiratory syndrome coronavirus." J Virol **81**(2): 813-821.

McDevitt, J. J., S. N. Rudnick and L. J. Radonovich (2012). "Aerosol susceptibility of influenza virus to UV-C light." Applied and environmental microbiology **78**(6): 1666-1669.

Medzhitov, R. and C. A. Janeway, Jr. (1997). "Innate immunity: impact on the adaptive immune response." Curr Opin Immunol **9**(1): 4-9.

Medzhitov, R. and C. A. Janeway Jr (1998). "Innate immune recognition and control of adaptive immune responses." Seminars in Immunology **10**(5): 351-353.

Memoli, M. J., R. J. Hrabal, A. Hassantoufighi, B. W. Jagger, Z.-M. Sheng, M. C. Eichelberger and J. K. Taubenberger (2010). "Rapid selection of a transmissible multidrug-resistant influenza A/H3N2 virus in an immunocompromised host." The Journal of infectious diseases **201**(9): 1397-1403.

Memoli, M. J., R. J. Hrabal, A. Hassantoufighi, B. W. Jagger, Z. M. Sheng, M. C. Eichelberger and J. K. Taubenberger (2010). "Rapid selection of a transmissible multidrug-resistant influenza A/H3N2 virus in an immunocompromised host." J Infect Dis **201**(9): 1397-1403.

Mengus, C., M. G. Muraro, V. Mele, F. Amicarella, C. Manfredonia, F. Foglietta, S. Muenst, S. D. Soysal, G. Iezzi and G. C. Spagnoli (2018). "In Vitro Modeling of Tumor–Immune System Interaction." ACS Biomaterials Science & Engineering **4**(2): 314-323.

Meyerholz, D. K., J. Rodgers, E. M. Castilow and S. M. Varga (2009). "Alcian Blue and Pyronine Y Histochemical Stains Permit Assessment of Multiple Parameters in Pulmonary Disease Models." Veterinary Pathology **46**(2): 325-328.

Middleton, P. G., M. A. Mall, P. Dřevínek, L. C. Lands, E. F. McKone, D. Polineni, B. W. Ramsey, J. L. Taylor-Cousar, E. Tullis, F. Vermeulen, G. Marigowda, C. M. McKee, S. M. Moskowitz, N. Nair, J. Savage, C. Simard, S. Tian, D. Waltz, F. Xuan, S. M. Rowe and R. Jain (2019).

"Elexacaftor–Tezacaftor–Ivacaftor for Cystic Fibrosis with a Single Phe508del Allele." New England Journal of Medicine **381**(19): 1809-1819.

Miknis, Z. J., E. Magracheva, W. Li, A. Zdanov, S. V. Kotenko and A. Wlodawer (2010). "Crystal Structure of Human Interferon-λ1 in Complex with Its High-Affinity Receptor Interferon-λR1." Journal of Molecular Biology **404**(4): 650-664.

Miknis, Z. J., E. Magracheva, W. Li, A. Zdanov, S. V. Kotenko and A. Wlodawer (2010). "Crystal structure of human interferon-λ1 in complex with its high-affinity receptor interferon-λR1." J Mol Biol **404**(4): 650-664.

Miller, A. J., B. R. Dye, D. Ferrer-Torres, D. R. Hill, A. W. Overeem, L. D. Shea and J. R. Spence (2019). "Generation of lung organoids from human pluripotent stem cells in vitro." Nature Protocols **14**(2): 518-540.

Monto, A. S. (2003). "The role of antivirals in the control of influenza." Vaccine **21**(16): 1796-1800.

Monto, A. S., S. Gravenstein, M. Elliott, M. Colopy and J. Schweinle (2000). "Clinical Signs and Symptoms Predicting Influenza Infection." Archives of Internal Medicine **160**(21): 3243-3247.

Moran, O. and O. Zegarra-Moran (2008). "On the measurement of the functional properties of the CFTR." J Cyst Fibros **7**(6): 483-494.

Morens, D. M. and A. S. Fauci (2007). "The 1918 Influenza Pandemic: Insights for the 21st Century." The Journal of Infectious Diseases **195**(7): 1018-1028.

Morris, G. E., J. C. Bridge, L. A. Brace, A. J. Knox, J. W. Aylott, C. E. Brightling, A. M. Ghaemmaghami and F. R. A. J. Rose (2014). "A novel electrospun biphasic scaffold provides optimal three-dimensional topography for in vitro co-culture of airway epithelial and fibroblast cells." Biofabrication **6**(3): 035014.

Mosnier, A., O. Launay, L. Martinez, G. Gavazzi, L. Josset, P. Crepey, C. Hannoun, C. Weil-Olivier and J. Gaillat (2018). "[Quadrivalent influenza vaccine: What is changed and what are the benefits?]." Presse Med **47**(10): 842-853.

Mostafa, A., E. M. Abdelwhab, T. C. Mettenleiter and S. Pleschka (2018). "Zoonotic Potential of Influenza A Viruses: A Comprehensive Overview." Viruses **10**(9): 497.

Mostafa, M. M., C. F. Rider, S. Shah, S. L. Traves, P. M. K. Gordon, A. Miller-Larsson, R. Leigh and R. Newton (2019). "Glucocorticoid-driven transcriptomes in human airway epithelial cells: commonalities, differences and functional insight from cell lines and primary cells." BMC Med Genomics **12**(1): 29.

Mould, J. A., R. G. Paterson, M. Takeda, Y. Ohigashi, P. Venkataraman, R. A. Lamb and L. H. Pinto (2003). "Influenza B virus BM2 protein has ion channel activity that conducts protons across membranes." Dev Cell **5**(1): 175-184.

Müller, L., M. Riediker, P. Wick, M. Mohr, P. Gehr and B. Rothen-Rutishauser (2010). "Oxidative stress and inflammation response after nanoparticle exposure: differences between human lung cell monocultures and an advanced three-dimensional model of the human epithelial airways." J R Soc Interface **7 Suppl 1**(Suppl 1): S27-40.

Muñoz-Fontela, C., W. E. Dowling, S. G. P. Funnell, P.-S. Gsell, A. X. Riveros-Balta, R. A. Albrecht, H. Andersen, R. S. Baric, M. W. Carroll, M. Cavaleri, C. Qin, I. Crozier, K. Dallmeier, L. de Waal, E. de Wit, L. Delang, E. Dohm, W. P. Duprex, D. Falzarano, C. L. Finch, M. B. Frieman, B. S. Graham, L. E. Gralinski, K. Guilfoyle, B. L. Haagmans, G. A. Hamilton, A. L. Hartman, S. Herfst, S. J. F. Kaptein, W. B. Klimstra, I. Knezevic, P. R. Krause, J. H. Kuhn, R. Le Grand, M. G. Lewis, W.-C. Liu, P. Maisonnasse, A. K. McElroy, V. Munster, N. Oreshkova, A. L. Rasmussen, J. Rocha-Pereira, B. Rockx, E. Rodríguez, T. F. Rogers, F. J. Salguero, M. Schotsaert, K. J. Stittelaar, H. J. Thibaut, C.-T. Tseng, J. Vergara-Alert, M. Beer, T. Brasel, J. F. W. Chan, A. García-Sastre, J. Neyts, S. Perlman, D. S. Reed, J. A. Richt, C. J. Roy, J. Segalés, S. S. Vasan, A. M. Henao-Restrepo and D. H. Barouch (2020). "Animal models for COVID-19." Nature **586**(7830): 509-515.

National Center for Biotechnology Information. (2020, 12, 21). "PubChem Compound Summary for CID 60855, Zanamivir." from https://pubchem.ncbi.nlm.nih.gov/compound/Zanamivir.

Nazarpour, R., E. Zabihi, E. Alijanpour, Z. Abedian, H. Mehdizadeh and F. Rahimi (2012). "Optimization of Human Peripheral Blood Mononuclear Cells (PBMCs) Cryopreservation." International journal of molecular and cellular medicine **1**(2): 88-93.

Neilson, L., C. Mankus, D. Thorne, G. Jackson, J. DeBay and C. Meredith (2015). "Development of an in vitro cytotoxicity model for aerosol exposure using 3D reconstructed human airway tissue; application for assessment of e-cigarette aerosol." Toxicol In Vitro **29**(7): 1952-1962.

Nema, T., A. Jain, A. Jain, S. Shilpi, A. Gulbake, P. Hurkat and S. K. Jain (2013). "Insulin delivery through nasal route using thiolated microspheres." Drug Deliv **20**(5): 210-215.

Ng, W. L., T. C. Ayi, Y.-C. Liu, S. L. Sing, W. Y. Yeong and B.-H. Tan (2021). "Fabrication and Characterization of 3D Bioprinted Triple-layered Human Alveolar Lung Models." International journal of bioprinting **7**(2): 332-332.

Nicholls, J. M., A. J. Bourne, H. Chen, Y. Guan and J. S. M. Peiris (2007). "Sialic acid receptor detection in the human respiratory tract: evidence for widespread distribution of potential binding sites for human and avian influenza viruses." Respiratory Research **8**(1): 73.

Nichols, J. E., J. A. Niles, S. P. Vega, L. B. Argueta, A. Eastaway and J. Cortiella (2014). "Modeling the lung: Design and development of tissue engineered macro- and micro-physiologic lung models for research use." Exp Biol Med (Maywood) **239**(9): 1135-1169.

Nightingale, T. and D. Cutler (2013). "The secretion of von Willebrand factor from endothelial cells; an increasingly complicated story." Journal of thrombosis and haemostasis : JTH **11 Suppl 1**(Suppl 1): 192-201.

O'Neal, W. K. and M. R. Knowles (2018). "Cystic Fibrosis Disease Modifiers: Complex Genetics Defines the Phenotypic Diversity in a Monogenic Disease." Annual Review of Genomics and Human Genetics **19**(1): 201-222.

O'Brien, T. J. and M. Welch (2019). "A Continuous-Flow Model for in vitro Cultivation of Mixed Microbial Populations Associated With Cystic Fibrosis Airway Infections." Frontiers in Microbiology **10**(2713).

Okomo-Adhiambo, M., K. Sleeman, C. Lysén, H. T. Nguyen, X. Xu, Y. Li, A. I. Klimov and L. V. Gubareva (2013). "Neuraminidase inhibitor susceptibility surveillance of influenza viruses

circulating worldwide during the 2011 Southern Hemisphere season." Influenza and Other Respiratory Viruses **7**(5): 645-658.

Okomo-Adhiambo, M., K. Sleeman, C. Lysén, H. T. Nguyen, X. Xu, Y. Li, A. I. Klimov and L. V. Gubareva (2013). "Neuraminidase inhibitor susceptibility surveillance of influenza viruses circulating worldwide during the 2011 Southern Hemisphere season." Influenza Other Respir Viruses **7**(5): 645-658.

Olmsted, S. S., J. L. Padgett, A. I. Yudin, K. J. Whaley, T. R. Moench and R. A. Cone (2001). "Diffusion of macromolecules and virus-like particles in human cervical mucus." Biophys J **81**(4): 1930-1937.

Olmsted, S. S., J. L. Padgett, A. I. Yudin, K. J. Whaley, T. R. Moench and R. A. Cone (2001). "Diffusion of Macromolecules and Virus-Like Particles in Human Cervical Mucus." Biophysical Journal **81**(4): 1930-1937.

Ostedgaard, L. S., M. P. Price, K. M. Whitworth, M. H. Abou Alaiwa, A. J. Fischer, A. Warrier, M. Samuel, L. D. Spate, P. D. Allen, B. M. Hilkin, G. S. Romano Ibarra, M. E. Ortiz Bezara, B. J. Goodell, S. E. Mather, L. S. Powers, M. R. Stroik, N. D. Gansemer, C. E. Hippee, K. Zarei, J. A. Goeken, T. R. Businga, E. A. Hoffman, D. K. Meyerholz, R. S. Prather, D. A. Stoltz and M. J. Welsh (2020). "Lack of airway submucosal glands impairs respiratory host defenses." eLife **9**: e59653.

Paget, J., P. Spreeuwenberg, V. Charu, R. J. Taylor, A. D. Iuliano, J. Bresee, L. Simonsen, C. Viboud, N. Global Seasonal Influenza-associated Mortality Collaborator and G. L. C. Teams* (2019). "Global mortality associated with seasonal influenza epidemics: New burden estimates and predictors from the GLaMOR Project." Journal of global health **9**(2): 020421-020421.

Pan, C., C. Kumar, S. Bohl, U. Klingmueller and M. Mann (2009). "Comparative Proteomic Phenotyping of Cell Lines and Primary Cells to Assess Preservation of Cell Type-specific Functions." Molecular & Cellular Proteomics **8**(3): 443-450.

Paolini, R., G. Bernardini, R. Molfetta and A. Santoni (2015). "NK cells and interferons." Cytokine & Growth Factor Reviews **26**(2): 113-120.

Pappas, G., I. J. Kiriaze and M. E. Falagas (2008). "Insights into infectious disease in the era of Hippocrates." Int J Infect Dis **12**(4): 347-350.

Parry, J. (2013). "H7N9 avian flu infects humans for the first time." Bmj **346**: f2151.

Parsonage, G., A. D. Filer, O. Haworth, G. B. Nash, G. E. Rainger, M. Salmon and C. D. Buckley (2005). "A stromal address code defined by fibroblasts." Trends in Immunology **26**(3): 150-156.

Paul, S. M., D. S. Mytelka, C. T. Dunwiddie, C. C. Persinger, B. H. Munos, S. R. Lindborg and A. L. Schacht (2010). "How to improve R&D productivity: the pharmaceutical industry's grand challenge." Nature Reviews Drug Discovery **9**(3): 203-214.

Peake, J. L. and K. E. Pinkerton (2015). Chapter 3 - Gross and Subgross Anatomy of Lungs, Pleura, Connective Tissue Septa, Distal Airways, and Structural Units. Comparative Biology of the Normal Lung (Second Edition). R. A. Parent. San Diego, Academic Press**:** 21-31.

Peteranderl, C., S. Herold and C. Schmoldt (2016). "Human Influenza Virus Infections." Seminars in respiratory and critical care medicine **37**(4): 487-500.

Pezzulo, A. A., T. D. Starner, T. E. Scheetz, G. L. Traver, A. E. Tilley, B.-G. Harvey, R. G. Crystal, J. Paul B. McCray and J. Zabner (2011). "The air-liquid interface and use of primary cell cultures are important to recapitulate the transcriptional profile of in vivo airway epithelia." American Journal of Physiology-Lung Cellular and Molecular Physiology **300**(1): L25-L31.

Pflug, A., M. Lukarska, P. Resa-Infante, S. Reich and S. Cusack (2017). "Structural insights into RNA synthesis by the influenza virus transcription-replication machine." Virus Research **234**: 103-117.

Pierce, R. J. and C. J. Worsnop (1999). "UPPER AIRWAY FUNCTION AND DYSFUNCTION IN RESPIRATION." Clinical and Experimental Pharmacology and Physiology **26**(1): 1-10.

Porotto, M., M. Ferren, Y. W. Chen, Y. Siu, N. Makhsous, B. Rima, T. Briese, A. L. Greninger, H. W. Snoeck and A. Moscona (2019). "Authentic Modeling of Human Respiratory Virus Infection in Human Pluripotent Stem Cell-Derived Lung Organoids." mBio **10**(3): e00723-00719.

Potter, C. W. (2001). "A history of influenza." Journal of Applied Microbiology **91**(4): 572-579.

Préhaud, C., F. Mégret, M. Lafage and M. Lafon (2005). "Virus infection switches TLR-3-positive human neurons to become strong producers of beta interferon." J Virol **79**(20): 12893-12904.

Qin, G., Y. Liu, J. Zheng, Z. Xiang, I. H. Y. Ng, J. S. Malik Peiris, Y.-L. Lau and W. Tu (2012). "Phenotypic and Functional Characterization of Human γδ T-Cell Subsets in Response to Influenza A Viruses." The Journal of Infectious Diseases **205**(11): 1646-1653.

Ramme, A. P., L. Koenig, T. Hasenberg, C. Schwenk, C. Magauer, D. Faust, A. K. Lorenz, A.-C. Krebs, C. Drewell, K. Schirrmann, A. Vladetic, G.-C. Lin, S. Pabinger, W. Neuhaus, F. Bois, R. Lauster, U. Marx and E.-M. Dehne (2019). "Autologous induced pluripotent stem cell-derived four-organ-chip." Future Science OA **5**(8): FSO413.

Ramos, I., G. Smith, F. Ruf-Zamojski, C. Martínez-Romero, M. Fribourg, E. A. Carbajal, B. M. Hartmann, V. D. Nair, N. Marjanovic, P. L. Monteagudo, V. A. DeJesus, T. Mutetwa, M. Zamojski, G. S. Tan, C. Jayaprakash, E. Zaslavsky, R. A. Albrecht, S. C. Sealfon, A. García-Sastre and A. Fernandez-Sesma (2019). "Innate Immune Response to Influenza Virus at Single-Cell Resolution in Human Epithelial Cells Revealed Paracrine Induction of Interferon Lambda 1." J Virol **93**(20).

Randall, R. E. and S. Goodbourn (2008). "Interferons and viruses: an interplay between induction, signalling, antiviral responses and virus countermeasures." Journal of General Virology **89**(1): 1-47.

Rath-Deschner, B., S. Memmert, A. Damanaki, R. S. de Molon, M. Nokhbehsaim, S. Eick, C. Kirschneck, J. A. Cirelli, J. Deschner, A. Jäger and A. V. B. Nogueira (2021). "CXCL5, CXCL8, and CXCL10 regulation by bacteria and mechanical forces in periodontium." Annals of Anatomy - Anatomischer Anzeiger **234**: 151648.

Rau, J. L. (2005). "The Inhalation of Drugs: Advantages and Problems." Respiratory Care **50**(3): 367-382.

Rawlings, J. S., K. M. Rosler and D. A. Harrison (2004). "The JAK/STAT signaling pathway." Journal of Cell Science **117**(8): 1281-1283.

Reid, A. T., E. N. Sutanto, P. Chander-Veerati, K. Looi, N. F. Li, T. Iosifidis, S.-L. Loo, L. W. Garratt and A. Kicic (2019). Chapter 3 - Ground zero—the airway epithelium. Rhinovirus Infections. N. Bartlett, P. Wark and D. Knight, Academic Press**:** 61-98.

Rivière, S., T. Hua-Huy, K. P. Tiev, J. Cabane and A. T. Dinh-Xuan (2017). "High Baseline Serum Clara Cell 16 kDa Predicts Subsequent Lung Disease Worsening in Systemic Sclerosis." The Journal of Rheumatology: jrheum.170440.

Rokicki, W., M. Rokicki, J. Wojtacha and A. Dżeljijli (2016). "The role and importance of club cells (Clara cells) in the pathogenesis of some respiratory diseases." Kardiochirurgia i torakochirurgia polska = Polish journal of cardio-thoracic surgery **13**(1): 26-30.

Rommens, J. M., M. C. Iannuzzi, B. Kerem, M. L. Drumm, G. Melmer, M. Dean, R. Rozmahel, J. L. Cole, D. Kennedy, N. Hidaka and et al. (1989). "Identification of the cystic fibrosis gene: chromosome walking and jumping." Science **245**(4922): 1059-1065.

Ronald Miller, L. E., Lee Fleisher, Jeanine Wiener-Kronish, Neal Cohen, William Young (2014). Miller's Anesthesia, Churchill Livingstone-Elsevier.

Rosen, B. H., M. Chanson, L. R. Gawenis, J. Liu, A. Sofoluwe, A. Zoso and J. F. Engelhardt (2018). "Animal and model systems for studying cystic fibrosis." J Cyst Fibros **17**(2s): S28-s34.

Rossi, G., A. Manfrin and M. P. Lutolf (2018). "Progress and potential in organoid research." Nat Rev Genet **19**(11): 671-687.

Rossi, S., M. C. Bonferoni, F. D'Autilia, G. Sandri, F. Ferrari, C. Caramella, E. Mortara, V. Giannini and F. Gasparri (2014). "Associations of natural polymers to modulate mucoadhesion of vaginal rinse-off and leave-on formulations." Journal of Drug Delivery Science and Technology **24**(5): 496-502.

Rousseaux, C. G., M. A. Wallig, W. M. Haschek and B. Bolon (2018). Chapter 1 - An Overview of Toxicologic Pathology. Fundamentals of Toxicologic Pathology (Third Edition). M. A. Wallig, W. M. Haschek, C. G. Rousseaux and B. Bolon, Academic Press**:** 1-12.

Rowe, S. M., S. Miller and E. J. Sorscher (2005). "Cystic Fibrosis." New England Journal of Medicine **352**(19): 1992-2001.

Rust, M. J., M. Lakadamyali, F. Zhang and X. Zhuang (2004). "Assembly of endocytic machinery around individual influenza viruses during viral entry." Nat Struct Mol Biol **11**(6): 567-573.

Rynda-Apple, A., K. M. Robinson and J. F. Alcorn (2015). "Influenza and Bacterial Superinfection: Illuminating the Immunologic Mechanisms of Disease." Infect Immun **83**(10): 3764-3770.

Sahin-Yilmaz, A. and R. M. Naclerio (2011). "Anatomy and Physiology of the Upper Airway." Proceedings of the American Thoracic Society **8**(1): 31-39.

Saint-Criq, V. and M. A. Gray (2017). "Role of CFTR in epithelial physiology." Cellular and molecular life sciences : CMLS **74**(1): 93-115.

Saltzman, W. M., M. L. Radomsky, K. J. Whaley and R. A. Cone (1994). "Antibody diffusion in human cervical mucus." Biophysical journal **66**(2 Pt 1): 508-515.

Sanders, C. J., P. C. Doherty and P. G. Thomas (2011). "Respiratory epithelial cells in innate immunity to influenza virus infection." Cell Tissue Res **343**(1): 13-21.

Sanne, I., P. Piliero, K. Squires, A. Thiry, S. Schnittman and A. I. C. T. Group (2003). "Results of a Phase 2 Clinical Trial at 48 Weeks (AI424-007): A Dose-Ranging, Safety, and Efficacy Comparative Trial of Atazanavir at Three Doses in Combination with Didanosine and Stavudine in Antiretroviral-Naive Subjects." JAIDS Journal of Acquired Immune Deficiency Syndromes **32**(1).

Sasai, Y. (2013). "Cytosystems dynamics in self-organization of tissue architecture." Nature **493**(7432): 318-326.

Saunders-Hastings, P. R. and D. Krewski (2016). "Reviewing the History of Pandemic Influenza: Understanding Patterns of Emergence and Transmission." Pathogens (Basel, Switzerland) **5**(4): 66.

Schattgen, S. A., T. H. Oguin and P. G. Thomas (2016). "The antiviral molecule Mx1 positively regulates the induction of type I IFN in response to influenza infection." The Journal of Immunology **196**(1 Supplement): 202.207.

Scherzad, A., R. Hagen and S. Hackenberg (2019). "Current Understanding of Nasal Epithelial Cell Mis-Differentiation." Journal of inflammation research **12**: 309-317.

Schimek, K., S. Frentzel, K. Luettich, D. Bovard, I. Rütschle, L. Boden, F. Rambo, H. Erfurth, E.-M. Dehne, A. Winter, U. Marx and J. Hoeng (2020). "Human multi-organ chip co-culture of bronchial lung culture and liver spheroids for substance exposure studies." Scientific Reports **10**(1): 7865.

Schneider, W. M., M. D. Chevillotte and C. M. Rice (2014). "Interferon-Stimulated Genes: A Complex Web of Host Defenses." Annual Review of Immunology **32**(1): 513-545.

Scholzen, T. and J. Gerdes (2000). "The Ki-67 protein: From the known and the unknown." Journal of Cellular Physiology **182**(3): 311-322.

Schulz, O., S. S. Diebold, M. Chen, T. I. Näslund, M. A. Nolte, L. Alexopoulou, Y.-T. Azuma, R. A. Flavell, P. Liljeström and C. Reis e Sousa (2005). "Toll-like receptor 3 promotes cross-priming to virus-infected cells." Nature **433**(7028): 887-892.

Seok, J., H. S. Warren, A. G. Cuenca, M. N. Mindrinos, H. V. Baker, W. Xu, D. R. Richards, G. P. McDonald-Smith, H. Gao, L. Hennessy, C. C. Finnerty, C. M. López, S. Honari, E. E. Moore, J. P. Minei, J. Cuschieri, P. E. Bankey, J. L. Johnson, J. Sperry, A. B. Nathens, T. R. Billiar, M. A. West, M. G. Jeschke, M. B. Klein, R. L. Gamelli, N. S. Gibran, B. H. Brownstein, C. Miller-Graziano, S. E. Calvano, P. H. Mason, J. P. Cobb, L. G. Rahme, S. F. Lowry, R. V. Maier, L. L. Moldawer, D. N. Herndon, R. W. Davis, W. Xiao and R. G. Tompkins (2013). "Genomic responses in mouse models poorly mimic human inflammatory diseases." Proceedings of the National Academy of Sciences **110**(9): 3507-3512.

Sharpless, N. E. and R. A. DePinho (2006). "The mighty mouse: genetically engineered mouse models in cancer drug development." Nature Reviews Drug Discovery **5**(9): 741-754.

Shen, B. Q., W. E. Finkbeiner, J. J. Wine, R. J. Mrsny and J. H. Widdicombe (1994). "Calu-3: a human airway epithelial cell line that shows cAMP-dependent Cl- secretion." American Journal of Physiology-Lung Cellular and Molecular Physiology **266**(5): L493-L501.

Shinya, K., M. Ebina, S. Yamada, M. Ono, N. Kasai and Y. Kawaoka (2006). "Influenza virus receptors in the human airway." Nature **440**(7083): 435-436.

Singh, P. K., M. R. Parsek, E. P. Greenberg and M. J. Welsh (2002). "A component of innate immunity prevents bacterial biofilm development." Nature **417**(6888): 552-555.

Smith, B. T. (1977). "Cell line A549: a model system for the study of alveolar type II cell function." Am Rev Respir Dis **115**(2): 285-293.

Smith, W., C. H. Andrewes and P. P. Laidlaw (1933). "A VIRUS OBTAINED FROM INFLUENZA PATIENTS." The Lancet **222**(5732): 66-68.

Smith, W., C. H. Andrewes and P. P. Laidlaw (1935). "Influenza: Experiments on the Immunization of Ferrets and Mice." British Journal of Experimental Pathology **16**(3): 291-302.

Song, A. S., A. M. Najjar and K. R. Diller (2014). "Thermally Induced Apoptosis, Necrosis, and Heat Shock Protein Expression in Three-Dimensional Culture." Journal of Biomechanical Engineering **136**(7).

St Helen, G., N. T. Holland, J. R. Balmes, D. B. Hall, J. T. Bernert, J. E. Vena, J.-S. Wang and L. P. Naeher (2013). "Utility of urinary Clara cell protein (CC16) to demonstrate increased lung epithelial permeability in non-smokers exposed to outdoor secondhand smoke." Journal of Exposure Science & Environmental Epidemiology **23**(2): 183-189.

Steinhauer, D. A., E. Domingo and J. J. Holland (1992). "Lack of evidence for proofreading mechanisms associated with an RNA virus polymerase." Gene **122**(2): 281-288.

Steinke, M., R. Gross, H. Walles, R. Gangnus, K. Schütze and T. Walles (2014). "An engineered 3D human airway mucosa model based on an SIS scaffold." Biomaterials **35**(26): 7355-7362.

Sternberg, S. H., S. Redding, M. Jinek, E. C. Greene and J. A. Doudna (2014). "DNA interrogation by the CRISPR RNA-guided endonuclease Cas9." Nature **507**(7490): 62-67.

Stevenson, B. R., J. D. Siliciano, M. S. Mooseker and D. A. Goodenough (1986). "Identification of ZO-1: a high molecular weight polypeptide associated with the tight junction (zonula occludens) in a variety of epithelia." Journal of Cell Biology **103**(3): 755-766.

Stewart, C. E., E. E. Torr, N. H. Mohd Jamili, C. Bosquillon and I. Sayers (2012). "Evaluation of differentiated human bronchial epithelial cell culture systems for asthma research." Journal of allergy **2012**: 943982-943982.

Stoltz, D. A., D. K. Meyerholz and M. J. Welsh (2015). "Origins of cystic fibrosis lung disease." N Engl J Med **372**(4): 351-362.

Suarez, D. L. (2016). "Influenza A virus." Animal Influenza: 1-30.

Sueki, A., K. Matsuda, C. Iwashita, C. Taira, N. Ishimine, S. Shigeto, K. Kawasaki, M. Sugano, H. Yamamoto and T. Honda (2014). "Epithelial-mesenchymal transition of A549 cells is enhanced by co-cultured with THP-1 macrophages under hypoxic conditions." Biochem Biophys Res Commun **453**(4): 804-809.

Suk, J. S., Q. Xu, N. Kim, J. Hanes and L. M. Ensign (2016). "PEGylation as a strategy for improving nanoparticle-based drug and gene delivery." Advanced Drug Delivery Reviews **99**: 28-51.

Swearengen, J. R. (2018). "Choosing the right animal model for infectious disease research." Animal Models and Experimental Medicine **1**(2): 100-108.

Swift, D. L. and J. Kesavanathan (1996). "THE ANTERIOR HUMAN NASAL PASSAGE AS A FIBROUS FILTER FOR PARTICLES." Chemical Engineering Communications **151**(1): 65-78.

Szymanski, K. V., M. Toennies, A. Becher, D. Fatykhova, P. D. Guessan, B. Gutbier, F. Klauschen, F. Neuschaefer-Rube, P. Schneider, J. Rueckert, J. Neudecker, T. T. Bauer, K. Dalhoff, D. Drömann, A. D. Gruber, O. Kershaw, B. Temmesfeld-Wollbrueck, N. Suttorp, S. Hippenstiel and A. C. Hocke (2012). "Streptococcus pneumoniae-induced regulation of cyclooxygenase-2 in human lung tissue." European Respiratory Journal **40**(6): 1458.

Tan, K. S., H. H. Ong, Y. Yan, J. Liu, C. Li, Y. K. Ong, K. T. Thong, H. W. Choi, D.-Y. Wang and V. T. Chow (2018). "In Vitro Model of Fully Differentiated Human Nasal Epithelial Cells Infected With Rhinovirus Reveals Epithelium-Initiated Immune Responses." The Journal of Infectious Diseases **217**(6): 906-915.

Teicher, B. A. (2013). Anticancer Drug Development Guide: Preclinical Screening, Clinical Trials, and Approval, Humana Press.

Thompson, C. I., W. S. Barclay, M. C. Zambon and R. J. Pickles (2006). "Infection of human airway epithelium by human and avian strains of influenza a virus." Journal of virology **80**(16): 8060-8068.

Thornton, D. J., K. Rousseau and M. A. McGuckin (2008). "Structure and function of the polymeric mucins in airways mucus." Annu Rev Physiol **70**: 459-486.

Thornton, D. J. and J. K. Sheehan (2004). "From mucins to mucus: toward a more coherent understanding of this essential barrier." Proc Am Thorac Soc **1**(1): 54-61.

Tomashefski, J. F. and C. F. Farver (2008). Anatomy and Histology of the Lung. Dail and Hammar's Pulmonary Pathology: Volume I: Nonneoplastic Lung Disease. J. F. Tomashefski, P. T. Cagle, C. F. Farver and A. E. Fraire. New York, NY, Springer New York**:** 20-48.

Tong, S., X. Zhu, Y. Li, M. Shi, J. Zhang, M. Bourgeois, H. Yang, X. Chen, S. Recuenco, J. Gomez, L.-M. Chen, A. Johnson, Y. Tao, C. Dreyfus, W. Yu, R. McBride, P. J. Carney, A. T. Gilbert, J. Chang, Z. Guo, C. T. Davis, J. C. Paulson, J. Stevens, C. E. Rupprecht, E. C. Holmes, I. A. Wilson and R. O. Donis (2013). "New World Bats Harbor Diverse Influenza A Viruses." PLOS Pathogens **9**(10): e1003657.

Trinh, N. T. N., O. Bardou, A. Privé, E. Maillé, D. Adam, S. Lingée, P. Ferraro, M.-Y. Desrosiers, C. Coraux and E. Brochiero (2012). "Improvement of defective cystic fibrosis airway epithelial wound repair after CFTR rescue." European Respiratory Journal **40**(6): 1390-1400.

Troeger, C. E., B. F. Blacker, I. A. Khalil, S. R. M. Zimsen, S. B. Albertson, D. Abate, J. Abdela, T. B. Adhikari, S. A. Aghayan, S. Agrawal, A. Ahmadi, A. N. Aichour, I. Aichour, M. T. E. Aichour, A. Al-Eyadhy, R. M. Al-Raddadi, F. Alahdab, K. A. Alene, S. M. Aljunid, N. Alvis-Guzman, N. H. Anber, M. Anjomshoa, C. A. T. Antonio, O. Aremu, H. T. Atalay, S. Atique, E. F. Attia, E. F. G. A. Avokpaho, A. Awasthi, A. Babazadeh, H. Badali, A. Badawi, J. A. M. Banoub, A. Barac, Q. Bassat, N. Bedi, A. B. Belachew, D. A. Bennett, K. Bhattacharyya, Z. A. Bhutta, A. Bijani, F. Carvalho, C. A. Castañeda-Orjuela, D. J. Christopher, L. Dandona, R. Dandona, A. K. Dang, A. Daryani, M. G. Degefa, F. M. Demeke, M. Dhimal, S. Djalalinia, D. T. Doku, M. Dubey,

E. Dubljanin, E. E. Duken, D. Edessa, M. El Sayed Zaki, H. Fakhim, E. Fernandes, F. Fischer, L. S. Flor, K. J. Foreman, T. G. Gebremichael, D. Geremew, K. Ghadiri, A. C. Goulart, J. Guo, G. H. Ha, G. B. Hailu, A. Haj-Mirzaian, A. Haj-Mirzaian, S. Hamidi, H. Y. Hassen, C. L. Hoang, N. Horita, M. Hostiuc, S. S. N. Irvani, R. P. Jha, J. B. Jonas, A. Kahsay, A. Karch, A. Kasaeian, T. D. Kassa, A. T. Kefale, Y. S. Khader, E. A. Khan, G. Khan, M. N. Khan, Y.-H. Khang, A. T. Khoja, J. Khubchandani, R. W. Kimokoti, A. Kisa, L. D. Knibbs, S. Kochhar, S. Kosen, P. A. Koul, A. Koyanagi, B. Kuate Defo, G. A. Kumar, D. K. Lal, P. Lamichhane, C. T. Leshargie, M. Levi, S. Li, E. R. K. Macarayan, M. Majdan, V. Mehta, A. Melese, Z. A. Memish, D. T. Mengistu, T. J. Meretoja, T. Mestrovic, B. Miazgowski, G. J. Milne, B. Milosevic, E. M. Mirrakhimov, B. Moazen, K. A. Mohammad, S. Mohammed, L. Monasta, L. Morawska, S. M. Mousavi, O. S. S. Muhammed, S. Murthy, G. Mustafa, A. Naheed, H. L. T. Nguyen, N. B. Nguyen, S. H. Nguyen, T. H. Nguyen, M. I. Nisar, M. R. Nixon, F. A. Ogbo, A. T. Olagunju, T. O. Olagunju, E. Oren, J. R. Ortiz, M. P A, S. Pakhale, S. Patel, D. Paudel, D. M. Pigott, M. J. Postma, M. Qorbani, A. Rafay, A. Rafiei, V. Rahimi-Movaghar, R. K. Rai, M. S. Rezai, N. L. S. Roberts, L. Ronfani, S. Rubino, S. Safari, S. Safiri, Z. Saleem, E. Z. Sambala, A. M. Samy, M. M. Santric Milicevic, B. Sartorius, S. Sarvi, M. Savic, M. Sawhney, S. Saxena, S. Seyedmousavi, M. A. Shaikh, M. Sharif, A. Sheikh, M. Shigematsu, D. L. Smith, R. Somayaji, J. B. Soriano, C. T. Sreeramareddy, M. a. B. Sufiyan, M.-H. Temsah, B. Tessema, M. Teweldemedhin, M. Tortajada-Girbés, B. X. Tran, K. B. Tran, A. G. Tsadik, K. N. Ukwaja, I. Ullah, T. J. Vasankari, G. T. Vu, F. W. Wada, Y. Waheed, T. E. West, C. S. Wiysonge, E. M. Yimer, N. Yonemoto, Z. Zaidi, T. Vos, S. S. Lim, C. J. L. Murray, A. H. Mokdad, S. I. Hay and R. C. Reiner (2019). "Mortality, morbidity, and hospitalisations due to influenza lower respiratory tract infections, 2017: an analysis for the Global Burden of Disease Study 2017." The Lancet Respiratory Medicine **7**(1): 69-89.

Tumpey, T. M., A. García-Sastre, J. K. Taubenberger, P. Palese, D. E. Swayne, M. J. Pantin-Jackwood, S. Schultz-Cherry, A. Solórzano, N. Van Rooijen, J. M. Katz and C. F. Basler (2005). "Pathogenicity of influenza viruses with genes from the 1918 pandemic virus: functional roles of alveolar macrophages and neutrophils in limiting virus replication and mortality in mice." J Virol **79**(23): 14933-14944.

Ullah, I., J. F. Busch, A. Rabien, B. Ergün, C. Stamm, C. Knosalla, S. Hippenstiel, P. Reinke and A. Kurtz (2020). "Adult Tissue Extracellular Matrix Determines Tissue Specification of Human iPSC-Derived Embryonic Stage Mesodermal Precursor Cells." Advanced Science **7**(5): 1901198.

USA, F. a. D. A. (2018). "Step 3: Clinical Research." Retrieved 11.04.2021, 2021, from https://www.fda.gov/patients/drug-development-process/step-3-clinical-research.

Van Goor, F., S. Hadida, P. D. Grootenhuis, B. Burton, D. Cao, T. Neuberger, A. Turnbull, A. Singh, J. Joubran, A. Hazlewood, J. Zhou, J. McCartney, V. Arumugam, C. Decker, J. Yang, C. Young, E. R. Olson, J. J. Wine, R. A. Frizzell, M. Ashlock and P. Negulescu (2009). "Rescue of CF airway epithelial cell function in vitro by a CFTR potentiator, VX-770." Proc Natl Acad Sci U S A **106**(44): 18825-18830.

Van Norman, G. A. (2016). "Drugs, Devices, and the FDA: Part 1: An Overview of Approval Processes for Drugs." JACC: Basic to Translational Science **1**(3): 170-179.

van Riel, D., M. A. den Bakker, L. M. E. Leijten, S. Chutinimitkul, V. J. Munster, E. de Wit, G. F. Rimmelzwaan, R. A. M. Fouchier, A. D. M. E. Osterhaus and T. Kuiken (2010). "Seasonal and

pandemic human influenza viruses attach better to human upper respiratory tract epithelium than avian influenza viruses." The American journal of pathology **176**(4): 1614-1618.

van Riel, D., V. J. Munster, E. de Wit, G. F. Rimmelzwaan, R. A. Fouchier, A. D. Osterhaus and T. Kuiken (2007). "Human and avian influenza viruses target different cells in the lower respiratory tract of humans and other mammals." Am J Pathol **171**(4): 1215-1223.

van Riet, S., D. K. Ninaber, H. M. M. Mikkers, T. D. Tetley, C. R. Jost, A. A. Mulder, T. Pasman, D. Baptista, A. A. Poot, R. Truckenmüller, C. L. Mummery, C. Freund, R. J. Rottier and P. S. Hiemstra (2020). "In vitro modelling of alveolar repair at the air-liquid interface using alveolar epithelial cells derived from human induced pluripotent stem cells." Scientific Reports **10**(1): 5499.

Vazirinejad, R., Z. Ahmadi, M. Kazemi Arababadi, G. Hassanshahi and D. Kennedy (2014). "The biological functions, structure and sources of CXCL10 and its outstanding part in the pathophysiology of multiple sclerosis." Neuroimmunomodulation **21**(6): 322-330.

Veckman, V., P. Österlund, R. Fagerlund, K. Melén, S. Matikainen and I. Julkunen (2006). "TNF-α and IFN-α enhance influenza-A-virus-induced chemokine gene expression in human A549 lung epithelial cells." Virology **345**(1): 96-104.

Veldman, R. J., S. Zerp, W. J. van Blitterswijk and M. Verheij (2004). "N-hexanoyl-sphingomyelin potentiates in vitro doxorubicin cytotoxicity by enhancing its cellular influx." British Journal of Cancer **90**(4): 917-925.

Venkatesan, N., D. Punithavathi and M. Babu (2007). "Protection from acute and chronic lung diseases by curcumin." Adv Exp Med Biol **595**: 379-405.

Verhelst, J., E. Parthoens, B. Schepens, W. Fiers and X. Saelens (2012). "Interferon-inducible protein Mx1 inhibits influenza virus by interfering with functional viral ribonucleoprotein complex assembly." J Virol **86**(24): 13445-13455.

Viboud, C., W. J. Alonso and L. Simonsen (2006). "Influenza in Tropical Regions." PLOS Medicine **3**(4): e89.

von Itzstein, M., W.-Y. Wu, G. B. Kok, M. S. Pegg, J. C. Dyason, B. Jin, T. Van Phan, M. L. Smythe, H. F. White, S. W. Oliver, P. M. Colman, J. N. Varghese, D. M. Ryan, J. M. Woods, R. C. Bethell, V. J. Hotham, J. M. Cameron and C. R. Penn (1993). "Rational design of potent sialidase-based inhibitors of influenza virus replication." Nature **363**(6428): 418-423.

Wang, G. F., M. D. Lai, R. R. Yang, P. H. Chen, Y. Y. Su, B. J. Lv, L. P. Sun, Q. Huang and S. Z. H. Chen (2006). "Histological types and significance of bronchial epithelial dysplasia." Modern Pathology **19**(3): 429-437.

Wang, P., P. Palese and R. E. O'Neill (1997). "The NPI-1/NPI-3 (karyopherin alpha) binding site on the influenza a virus nucleoprotein NP is a nonconventional nuclear localization signal." J Virol **71**(3): 1850-1856.

Wang, S., J. Taaffe, C. Parker, A. Solórzano, H. Cao, A. García-Sastre and S. Lu (2006). "Hemagglutinin (HA) proteins from H1 and H3 serotypes of influenza A viruses require different antigen designs for the induction of optimal protective antibody responses as studied by codon-optimized HA DNA vaccines." J Virol **80**(23): 11628-11637.

Wang, X., X. Zhang, X. Dai, X. Wang, X. Li, J. Diao and T. Xu (2018). "Tumor-like lung cancer model based on 3D bioprinting." 3 Biotech **8**(12): 501.

Wang, Y. Y., S. K. Lai, J. S. Suk, A. Pace, R. Cone and J. Hanes (2008). "Addressing the PEG mucoadhesivity paradox to engineer nanoparticles that "slip" through the human mucus barrier." Angew Chem Int Ed Engl **47**(50): 9726-9729.

Watson, K. K. and M. L. Platt (2012). "Of mice and monkeys: using non-human primate models to bridge mouse- and human-based investigations of autism spectrum disorders." Journal of neurodevelopmental disorders **4**(1): 21-21.

Weinheimer, V. K., A. Becher, M. Tönnies, G. Holland, J. Knepper, T. T. Bauer, P. Schneider, J. Neudecker, J. C. Rückert, K. Szymanski, B. Temmesfeld-Wollbrueck, A. D. Gruber, N. Bannert, N. Suttorp, S. Hippenstiel, T. Wolff and A. C. Hocke (2012). "Influenza A viruses target type II pneumocytes in the human lung." J Infect Dis **206**(11): 1685-1694.

Weis, W., J. H. Brown, S. Cusack, J. C. Paulson, J. J. Skehel and D. C. Wiley (1988). "Structure of the influenza virus haemagglutinin complexed with its receptor, sialic acid." Nature **333**(6172): 426-431.

Westgeest, K. B., C. A. Russell, X. Lin, M. I. Spronken, T. M. Bestebroer, J. Bahl, R. van Beek, E. Skepner, R. A. Halpin, J. C. de Jong, G. F. Rimmelzwaan, A. D. Osterhaus, D. J. Smith, D. E. Wentworth, R. A. Fouchier and M. de Graaf (2014). "Genomewide analysis of reassortment and evolution of human influenza A(H3N2) viruses circulating between 1968 and 2011." J Virol **88**(5): 2844-2857.

White, J., A. Helenius and M.-J. Gething (1982). "Haemagglutinin of influenza virus expressed from a cloned gene promotes membrane fusion." Nature **300**(5893): 658-659.

Whiteley, M., M. G. Bangera, R. E. Bumgarner, M. R. Parsek, G. M. Teitzel, S. Lory and E. P. Greenberg (2001). "Gene expression in Pseudomonas aeruginosa biofilms." Nature **413**(6858): 860-864.

Wickström, C., J. R. Davies, G. V. Eriksen, E. C. Veerman and I. Carlstedt (1998). "MUC5B is a major gel-forming, oligomeric mucin from human salivary gland, respiratory tract and endocervix: identification of glycoforms and C-terminal cleavage." The Biochemical journal **334 (Pt 3)**(Pt 3): 685-693.

Williams, K. and J. Roman (2016). "Studying human respiratory disease in animals--role of induced and naturally occurring models." J Pathol **238**(2): 220-232.

Winkler, J., G. Hochhaus and H. Derendorf (2004). "How the Lung Handles Drugs." Proceedings of the American Thoracic Society **1**(4): 356-363.

Wu, J., H. Du, X. Wang, C. Mei, G. C. Sieck and Q. Qian (2009). "Characterization of Primary Cilia in Human Airway Smooth Muscle Cells." Chest **136**(2): 561-570.

Wu, Y., D. S. Puperi, K. J. Grande-Allen and J. L. West (2017). "Ascorbic acid promotes extracellular matrix deposition while preserving valve interstitial cell quiescence within 3D hydrogel scaffolds." Journal of Tissue Engineering and Regenerative Medicine **11**(7): 1963-1973.

Yángüez, E. and A. Nieto (2011). "So similar, yet so different: selective translation of capped and polyadenylated viral mRNAs in the influenza virus infected cell." Virus Res **156**(1-2): 1-12.

Yao, X., E. M. Gordon, D. M. Figueroa, A. V. Barochia and S. J. Levine (2016). "Emerging Roles of Apolipoprotein E and Apolipoprotein A-I in the Pathogenesis and Treatment of Lung Disease." American journal of respiratory cell and molecular biology **55**(2): 159-169.

Yao, Y. and K. Shen (2017). "Monogenic diseases in respiratory medicine: Clinical perspectives." Pediatric Investigation **1**(1): 27-31.

Yektaeian, N., D. Mehrabani, M. Sepaskhah, S. Zare, I. Jamhiri and G. Hatam (2019). "Lipophilic tracer Dil and fluorescence labeling of acridine orange used for Leishmania major tracing in the fibroblast cells." Heliyon **5**(12): e03073-e03073.

Yin, L., J. Ding, C. He, L. Cui, C. Tang and C. Yin (2009). "Drug permeability and mucoadhesion properties of thiolated trimethyl chitosan nanoparticles in oral insulin delivery." Biomaterials **30**(29): 5691-5700.

Young, B. M., K. Shankar, B. P. Allen, R. A. Pouliot, M. B. Schneck, N. S. Mikhaiel and R. L. Heise (2017). "Electrospun Decellularized Lung Matrix Scaffold for Airway Smooth Muscle Culture." ACS Biomaterials Science & Engineering **3**(12): 3480-3492.

Zambon, M. C. (1999). "Epidemiology and pathogenesis of influenza." Journal of Antimicrobial Chemotherapy **44**(suppl_2): 3-9.

Zanetta, L., S. G. Marcus, J. Vasile, M. Dobryansky, H. Cohen, K. Eng, P. Shamamian and P. Mignatti (2000). "Expression of von Willebrand factor, an endothelial cell marker, is up-regulated by angiogenesis factors: A potential method for objective assessment of tumor angiogenesis." International Journal of Cancer **85**(2): 281-288.

Zhao, S., E. Mysler and R. J. Moots (2018). "Etanercept for the treatment of rheumatoid arthritis." Immunotherapy **10**(6): 433-445.

Ziebach, R., B. Pietsch-Breitfeld, M. Bichler, A. Busch, J. Riethmüller and M. Stern (2001). "Bronchodilatory effects of salbutamol, ipratropium bromide, and their combination: double-blind, placebo-controlled crossover study in cystic fibrosis." Pediatr Pulmonol **31**(6): 431-435.

Eidesstattliche Erklärung

Ich erkläre hiermit, dass ich diese Dissertation selbstständig ohne Hilfe Dritter und ohne Benutzung anderer als der angegebenen Quellen und Hilfsmittel verfasst habe. Alle den benutzten Quellen wörtlich oder sinngemäß entnommenen Stellen sind als solche einzeln kenntlich gemacht.

Diese Arbeit ist bislang keiner anderen Prüfungsbehörde vorgelegt worden und auch nicht veröffentlicht worden.

Ich bin mir bewusst, dass eine falsche Erklärung rechtliche Folgen haben wird.

_____

Ort, Datum, Unterschrift